THE JOURNAL OF

PHYSICAL

CHEMISTRY

Reprints from Chemical & Engineering News

Keeping broadly informed challenges every person today. If you missed these features from recent issues of C&EN, you can still get copies by filling in the coupon below.

Population

A 2-part feature
David M. Kiefer, C&EN
Oct. 7 & 14, 1968   75¢

Mr. Kiefer finds that population is growing unchecked in much of the world, and that U.S. population will expand 50% in the next 30 years or so. Social as well as technological innovation is needed to thwart this advance.   **10148**

Computers in Chemical Education

Dr. Frederick D. Tabbutt
Reed College
Portland, Oregon
January 19, 1970   50¢

A number of experiments with computers in education have been undertaken in the past few years. Some of the approaches to computer-assisted education now show promise as useful adjuncts as surrogate teachers.
                                         11970

Arthritis

A 3-part feature
Howard J. Sanders, C&EN
July 22, 29, & Aug. 12, 1968   75¢

Causes of arthritis are still a mystery, although more and more evidence points to infection as a possible trigger. Mr. Sanders discusses and examines the possible causes and the past, present, and future of treatment.   **07228**

Industrial Research Careers

Howard Reiss
University of California
Los Angeles
June 29, 1970   50¢

A major concern of those beginning careers in science is, of course, where to carry out their careers—in a university, private industry, a foundation or wherever. An industrial research career can be a rewarding one, both professionally and financially.   **62970**

Public Policy and the Environment

February 9, 1970   50¢

Speaking at the 158th ACS National Meeting, Lee DuBridge, Herbert Doan, and Barry Commoner urged cooperation among government, industry, and university in tackling environmental improvement.   **02970**

Pollution Control Instrumentation

Michael Heylin, C&EN
February 15, 1971   50¢

Efforts to control air and water resources intelligently depends on the ability to detect and to monitor pollutants. The challenge to produce better instrumentation for this purpose is now receiving intense attention from industry and government researchers. **21571**

Allergy

Howard J. Sanders, C&EN
May 11, 1970   50¢

Although hay fever, bronchial asthma, and other allergies will not be conquered, they will be better understood and better treated. The expanding study of these diseases in fundamental scientific terms, using the latest research techniques, allergic disorders will yield more and more of their secrets that only a few years ago seemed almost unfathomable.   **51170**

Food Additives

Howard J. Sanders, C&EN
October 10, 1966   75¢

Makers of food additives are keeping their eyes on the spectacular growth of new foods and the shifting moods of regulation-minded Washington. An array of chemicals enhances the wholesomeness, attractiveness, convenience, and nutritional value of American foods.   **10176**

Technology Assessment

David M. Kiefer, C&EN
October 5, 1970   50¢

Technology assessment is an attempt—still halting and uncertain—to establish an early-warning system to control, direct, and, if necessary, restrain technological development so as to maximize the public good while minimizing the public risks.   **10570**

Chemistry and the Atmosphere

Howard J. Sanders, C&EN
March 28, 1966   75¢

The earth's atmosphere is a vast, churning mixture of gases and trace quantities of liquids and solids. Held to the earth by the pull of gravity, it is the transparent envelope without which life on earth would cease to exist.   **32866**

Career Opportunities The New Priorities

March 8, 1971   50¢

C&EN's annual career guide for chemists and chemical engineers. In the search for new priorities, new opportunities are emerging. Here C&EN looks at three such areas—food, shelter, and health.   **03871**

Chaos in Science Teaching

Dr. Conrad E. Ronneberg
Professor Emeritus, Denison University
June 1, 1970   50¢

To many people familiar with the situation in teaching introductory science courses, both in high school and college, the situation is utter chaos. To place attempts to improve science teaching in proper perspective requires a brief review of the progress of science teaching since World II.   **06170**

Artificial Organs

A 2-part feature
Howard J. Sanders, C&EN
April 5 and 12, 1971   75¢

The implanting of a total artificial heart in a human has been the most dramatic single advance to date in the field of artificial organs. In recent years, however, many other artificial organs have also been developed, and scientists foresee a vast increase in the number of body parts that, in the years ahead, will be replaceable by mechanical devices. **04571**

Scientific Societies and Public Affairs

K. M. Reese, C&EN
May 3, 1971   50¢

Scientific and engineering societies for many years have fostered research, published papers, and sponsored meetings without great regard for the world beyond their particular disciplines. Only in the past decade or so have the learned societies edged into the realm of public affairs.   **05371**

1 to 49 copies—single copy price 50 to 299 copies—20% discount

Prices for larger quantities available on request

THE JOURNAL OF
PHYSICAL CHEMISTRY

Notice to Authors last printed in the issue of June 10, 1971

PHOTOCHEMISTRY AND SPECTROSCOPY

By J. P. Simons, *University of Birmingham, England*

This is the first book to explore the common territory between spectroscopy and molecular orbital theory in order to explain the details of the primary photochemical processes. Coverage in this interdisciplinary treatise embraces electromagnetic radiation, molecular orbitals and electronic states, vibrational and rotational states, atomic spectra, decay and deactivation of excited atoms and diatomic molecules, light absorption by atoms, and simple and complex polyatomic molecules.

1971   343 pages   illus. $16.50

SYMMETRY, ORBITALS, AND SPECTRA (S.O.S.)

By Milton Orchin and Hans H. Jaffé, *both of the University of Cincinnati*

Symmetry, Orbitals, and Spectra contains essential, *basic* knowledge concerning quantum mechanics, molecular orbital theory, ultraviolet and infrared absorption spectroscopy, selection rules, group theory, photochemistry, and applications of symmetry. Beginning with a simple treatment of molecular orbital theory which includes a description of the free electron method, the book proceeds to concepts of symmetry and group theory. After they are developed in a nonmathematical form, these concepts are applied to a variety of topics, including the theory of bonding in transition metal complexes; the spectra of inorganic complexes; the fundamentals of infrared absorption spectroscopy; and the basis and application of selection rules in both electronic and vibrational spectra.

1971   396 pages   28 illus. $16.50

REACTIONS OF MOLECULES AT ELECTRODES

By N. S. Hush, *University of Bristol*

This volume shows how electrochemical techniques can be used in the analysis of reaction mechanisms and demonstrates the usefulness of electrochemical methods in preparative chemistry.

CONTENTS: Adsorption of Molecules at Electrodes; Ion Solvation; Theory of Molecular Electrode Kinetics; The Rates of Reactions Involving Only Electron Transfer at Metal Electrodes; Oxidation and Reduction of Aromatic Hydrocarbon Molecules at Electrodes; Reduction Potentials and Orbital Energies of Aza-heteromolecules; Reactions at Organic Semiconductor Electrodes; The Electrode Reactions of Organic Molecules; Redox Reactions and Electron Transfer Chains of Inert Transition Metal Complexes.   1971   498 pages $24.50

ATOMIC AND MOLECULAR RADIATION PHYSICS

By Loucas Georgious Christophorou, *University of Tennessee*

A volume in the series, Monographs in Chemical Physics, edited by J. B. Birks

The differentiated areas of research in atomic and molecular photophysics and atomic and molecular collision processes are integrated in this new work. The author discusses the application of fundamental studies on the atomic and molecular level to radiation science and biology. Exhaustive coverage is given to the available literature, and the volume includes detailed experimental information in tabular or graphical form.

1971   684 pages $29.00

FAR-INFRARED SPECTROSCOPY

By K. D. Möller, *Farleigh-Dickenson University*, and W. G. Rothschild, *Ford Motor Company*

A volume in the Wiley Series in Pure and Applied Optics, edited by Stanley S. Ballard

In this comprehensive volume, far-infrared spectroscopic techniques are applied to a wide variety of phenomena in physical chemistry, solid state physics, and certain areas of molecular biology. The authors thoroughly discuss the major research endeavors in the field, indicating the present "state of the art" and illustrating the types of problems to which far-infrared spectroscopic techniques can be applied.

1971   797 pages   405 illus. $29.95

PRINCIPLES OF ACTIVATION ANALYSIS

By Paul Kruger, *Stanford University*

Here is a comprehensive description of the principles on which the methods of activation analysis are based. Treating activation analysis as a unified subject, the author discusses foundations of basic nuclear science, nuclear reactions, radioisotope production, radiochemical separations, and radiation measurement. Also examined are the practices, limitations, and applications of the method, with specific examples in many disciplines. Finally, selected problems illustrate the quantitative aspects of the various topics covered.

1971   522 pages   168 illus. $25.00

SURFACE AND COLLOID SCIENCE
Volume 4

Edited by Egon Matijević, *Clarkson College of Technology*

Here is the fourth volume in a series consisting of articles written by specialists in the field of colloid and surface science. This book, together with the other volumes in the series, comprises a rigorous, comprehensive treatise of theories, systems, and processes.

Volume 4
CONTENTS: Computer Simulation of Colloidal Systems; Physical Adsorption: The Interaction of Gases with Solids; Convection Diffusion in Laminar and Turbulent Hyperfiltration (Reverse Osmosis) Systems; Bimolecular Lipid Membranes.

1971   464 pages   78 illus. $24.95

WATER AND AQUEOUS SOLUTIONS
Structure, Thermodynamics, and Transport

By R. A. Horne, *JBF Scientific Corporation, Burlington, Massachusetts*

This book is a collection of papers on the structure and properties of water and aqueous solutions and on kindred systems, such as ice and fused salts. The topics range from the surface and transport properties of ice, through the structure, thermodynamics and transport properties of water and aqueous solutions, to the state of water in living cells and tissues. A special feature of the volume is an extended table of ionic molal volumes.   1971   832 pages   172 illus. $37.50

You Are Cordially Invited
To Become
A Charter Subscriber
To The American Chemical Society's
Newest Publication
CHEMICAL TECHNOLOGY

Cutting across all disciplines, the new monthly publication CHEMICAL TECHNOLOGY is written expressly for those charged with industrial innovation. Chemists and chemical engineers in industry will welcome its pragmatic approach.

> Designed to be a highly readable, current awareness magazine, CHEMICAL TECHNOLOGY is a valuable addition to existing ACS publications.
> Its articles range over areas of immediate interest, while monthly features deal with many facets of industrial life through interviews, articles, stories and anecdotes.

To start CHEMICAL TECHNOLOGY on its way to you, just complete and return the form at the right. You'll get a new outlook on the world of industrial chemistry.

THE JOURNAL OF
PHYSICAL CHEMISTRY

NOTES

COMMUNICATIONS TO THE EDITOR

AUTHOR INDEX

In papers with more than one author the name of the author to whom inquiries about the paper should be addressed is marked with an asterisk in the by-line.

ANNOUNCEMENT

On the last two pages of this issue you will find reproduced the table of contents of the October 1971 issue of the *Journal of Chemical and Engineering Data.*

Kinetics of the Shock Wave Pyrolysis of Pentafluoroethane[1a]

by E. Tschuikow-Roux,* G. E. Millward,[1b] and W. J. Quiring[1c]

Department of Chemistry, University of Calgary, Calgary 44, Alberta, Canada   (Received May 3, 1971)

Publication costs borne completely by The Journal of Physical Chemistry

The kinetics of the gas phase decomposition of a dilute mixture of pentafluoroethane in argon has been studied in a single-pulse shock tube in the temperature range 1180–1470°K at total reflected shock pressures of about 2900–4000 Torr. At all temperatures the observed principal product is C_2F_4 and suggests molecular elimination of hydrogen fluoride, $C_2HF_5 \xrightarrow{k_1} C_2F_4 + HF$, with the first-order rate constant given by $\log k_1$ (sec^{-1}) = $13.6 \pm 0.4 - (71,600 \pm 2400)/2.303RT$. At temperatures above ~1350°K significant quantities of C_2HF_3 and smaller amounts of CHF_3, CH_2F_2, C_2F_6, and 1,1,2,2-$C_2H_2F_4$ are also observed. A free-radical mechanism is proposed to explain the formation of these secondary products, which are derived from the homolytic scission of the C–C bond. From a knowledge of k_1 it was possible to evaluate the rate constant for the reaction, $CHF_2-CF_3 \xrightarrow{k_2} CHF_2 + CF_3$, where $\log k_2$ (sec^{-1}) = $16.6 \pm 0.6 - (93,500 \pm 5200)/2.303RT$. The latter provides the first experimental estimate of the bond dissociation energy $D(CHF_2-CF_3)$.

Introduction

The thermal decomposition of simple alkyl and alkenyl fluorides has recently received considerable attention. In particular, a number of studies have dealt with the fluoro derivatives of ethane[2-9] and ethylene.[10-12] Sianesi, Nelli, and Fontanelli[2] were the first to report the pyrolysis of the series $CH_3CH_{3-n}F_n$ (n = 1, 2, 3) in a conventional flow system at temperatures ranging from about 880 to 1070°K. The successful pyrolysis of C_2H_5F in a static system (683–738°K) using a carefully seasoned reaction vessel has been reported by Day and Trotman-Dickenson[3] and by Cadman, et al.,[5] who used a comparative shock-tube technique over the temperature range 1380–1680°K. Another brief communication by Cadman, et al.,[6] on CH_3CHF_2 and CH_3CF_3 has also appeared. In previous communications from this laboratory, Tschuikow-Roux and coworkers reported the single-pulse shock tube (SPST) thermolysis (1040–1450°K) of CH_3CHF_2,[4] CH_3CF_3,[7] and CHF_2CHF_2[8,9] the last being the first high-temperature pyrolysis of an α,β-substituted fluoroethane.

These investigations have shown that, at temperatures at which first product formation occurs, the principal mode of decomposition is *via* molecular elimination of hydrogen fluoride. Furthermore, contrary to the re-

(1) (a) Work supported by the National Research Council of Canada; (b) Postdoctoral Fellow, 1970–1971; (c) Department of Chemistry, Cornell University, Ithaca, N. Y.

(2) D. Sianesi, G. Nelli, and R. Fontanelli, *Chim. Ind. (Milan)*, **50**, 619 (1968).

(3) M. Day and A. F. Trotman-Dickenson, *J. Chem. Soc., A*, 233 (1969).

(4) E. Tschuikow-Roux, W. J. Quiring, and J. M. Simmie, *J. Phys. Chem.*, **74**, 2449 (1970).

(5) P. Cadman, M. Day, and A. F. Trotman-Dickenson, *J. Chem. Soc., A*, 2498 (1970).

(6) P. Cadman, M. Day, A. W. Kirk, and A. F. Trotman-Dickenson, *Chem. Commun.*, 203 (1970).

(7) E. Tschuikow-Roux and W. J. Quiring, *J. Phys. Chem.*, **75**, 295 (1971).

(8) G. E. Millward, R. Hartig, and E. Tschuikow-Roux, *Chem. Commun.*, 465 (1971).

(9) G. E. Millward, R. Hartig, and E. Tschuikow-Roux, *J. Phys. Chem.*, in press.

(10) J. M. Simmie, W. J. Quiring, and E. Tschuikow-Roux, *ibid.*, **74**, 992 (1970).

(11) (a) J. M. Simmie and E. Tschuikow-Roux, *Chem. Commun.*, 773 (1970); (b) *J. Phys. Chem.*, **74**, 4075 (1970).

(12) P. Cadman and W. J. Engelbrecht, *Chem. Commun.*, 453 (1970).

sults of Sianesi, et al.,[2] the shock-tube studies provide clear evidence that the activation energy for the dehydrofluorination reaction increases with additional fluoro substitution, while the preexponential factors change only in a minor way. Therefore, for any given temperature the values of the rate constants decrease with increasing n in the series $C_2H_{6-n}F_n$ ($n = 1-4$). If this trend of increasing activation energy with increasing fluorination continues, then, in relation to the HF elimination, the parallel reaction involving the C–C bond scission should become progressively more important at the elevated temperatures used in shock-tube studies. This should manifest itself by the appearance of products resulting from free-radical reactions. Such products have, in fact, been identified in the case of 1,1,2,2-tetrafluoroethane, and a value of ca. 91 kcal mol^{-1} was found for the C–C bond dissociation energy.[9]

The activation energy *difference* for HF elimination from CHF_2CHF_2 and CH_3CF_3 is notably smaller than the increment found between CH_3CF_3 and CH_3CHF_2. An interesting question which arises is whether this relative abatement is due to the fluorine substituents on the β carbon or simply reflects the higher density of electronegative substituents. A study of the next higher fluoro-substituted member of this series, C_2HF_5, could resolve this question. Such a study should also provide additional evidence for the free-radical contribution to the decomposition kinetics at high temperatures which has been alluded to above.

In this paper we present data on the thermal decomposition of pentafluoroethane, C_2HF_5, in a SPST over the temperature range 1180–1470°K. The results are interpreted in the light of our recent study on the thermolysis of 1,1,2,2,-tetrafluoroethane.[9]

Experimental Section

The modified SPST, the recording devices, and the operating procedure have been described previously.[13,14] Here we note only some changes in the analytical procedure. After each shock the end section of the shock tube was isolated by closure of a rotating ball valve and a sample of the fully mixed gases was withdrawn and subjected to gas chromatographic analysis. The latter was carried out using a Varian 1740 chromatograph with a flame ionization detector, a 3.66-m silica gel column, and helium as a carrier gas at a flow rate of 30 cm^3 min^{-1}. The analyses were carried out using linear temperature programming from 50 to 150° at the rate of 4° min^{-1} to facilitate separation of reaction products.

The gases C_2HF_5, C_2HF_3, CH_2F_2, and 1,1,2,2-$C_2H_2F_4$ were obtained commercially from Peninsular Chemresearch Inc., while C_2F_6 and CHF_3 were obtained from Matheson Co. The tetrafluoroethylene was prepared by heating polytetrafluoroethylene (Teflon) shavings *in vacuo* and was purified by low-temperature distillation. The purity of these gases was determined by gc analysis to be better than 99%. A reaction mixture of

1.0% C_2HF_5 in argon (Matheson, 99.998% purity) was prepared in a stainless steel tank and allowed to mix thoroughly prior to its use. Standard calibration mixtures of reactant and products in argon were also prepared to determine the relative sensitivities of the flame ionization detector. The conversion of C_2HF_5 ranged from 0.2% at 1180°K to 65% at 1470°K.

Results

The pertinent shock parameters, which were calculated from measured incident and reflected shock wave velocities, are given in Table I. The reaction dwell time, t,[13] was calculated from microsecond counter readings and the photographic oscilloscope trace record of the wave history near the end plate.

Except at some of the lowest temperatures, gc analysis of the reaction mixture showed several products. These were identified as C_2F_4, C_2HF_3, CHF_3, CH_2F_2, C_2F_6, and 1,1,2,2-$C_2H_2F_4$. In all of the experiments the major reaction product was C_2F_4, comprising about 90% of the total products exclusive of hydrogen fluoride. The latter was not identified quantitatively because of its reactivity with the walls of the shock tube and the transfer vessel. The major side product was found to be C_2HF_3, which amounted to about 10% of the total C-product formation. The measured quantities of the remaining products were small in comparison to the total product formation and hence could not be investigated in detail. Special considerations apply in the case of C_2F_6 because of its very low sensitivity with respect to the flame ionization detector, and these are discussed below. The product/reactant ratios $r_1 = [C_2F_4]/[C_2HF_5]$ and $r_4 = [C_2HF_3]/[C_2HF_5]$ are set out in Table I.

Kinetic Analysis

The principal primary process in the pyrolysis of fluoroethanes is the molecular elimination of hydrogen fluoride. However, as shown below, under certain conditions there is a significant contribution from the C–C bond rupture. The latter process becomes competitive at high temperatures ($T > 1350$°K) and as the activation energy for HF elimination increases. Previous kinetic studies involving the C–C bond scission in ethane,[15,16] hexafluoroethane,[17] and 1,1,2,2-tetrafluoroethane[9] have been simplified by the symmetry of the molecule. The dissymmetry of the C_2HF_5 molecule complicates the reaction kinetics, since the radicals CHF_2 and CF_3 have their own pathways to extinction. To facilitate the analysis we present a simplified mechanism which is consistent with the observed products.

(13) E. Tschuikow-Roux, J. M. Simmie, and W. J. Quiring, *Astronaut. Acta*, **15**, 511 (1970).

(14) J. M. Simmie, W. J. Quiring, and E. Tschuikow-Roux, *J. Phys. Chem.*, **73**, 3830 (1969).

(15) C. P. Quinn, *Proc. Roy. Soc., Ser. A*, **275**, 190 (1963).

(16) M. C. Lin and M. H. Back, *Can. J. Chem.*, **44**, 505 (1966).

(17) E. Tschuikow-Roux, *J. Chem. Phys.*, **43**, 2251 (1965).

Table I: Experimental Results

Mach. No.		P_2,	T_2,	P_5,	T_5,	t,	Product ratios[a]		k_1,	k_2,
W_{11}	W_{21}	Torr	°K	Torr	°K	μsec	r_1	r_4	sec^{-1}	sec^{-1}
2.209	1.264	878	699	2874	1181	620	0.0020	...	2.20	...
2.235	1.289	899	709	3011	1212	667	0.0042	...	4.51	...
2.259	1.304	920	720	3126	1241	577	0.0048	...	5.96	...
2.283	1.265	940	729	3100	1237	872	0.0090	...	7.91	...
2.267	1.294	926	721	3124	1238	684	0.0112	...	9.99	...
2.305	1.306	959	738	3273	1276	760	0.0323	0.001	32.2	2.0
2.322	1.329	973	748	3389	1306	401	0.0214	...	34.9	...
2.295	1.356	950	734	3373	1294	1000	0.0992	0.006	76.0	9.0
2.385	1.328	1029	774	3592	1353	781	0.140	0.0201	134	38.2
2.433	1.331	1082	799	3798	1401	1055	0.299	0.0481	209	64.1
2.401	1.350	1043	783	3708	1382	631	0.218	0.0328	230	68.5
2.415	1.351	1056	790	3756	1395	637	0.258	0.0398	260	78.6
2.417	1.355	1058	790	3778	1399	736	0.305	0.0489	281	88.5
2.420	1.368	1061	795	3825	1414	333	0.228	0.0338	360	104.0
2.429	1.374	1069	795	3873	1419	926	0.598	0.0900	393	98.4
2.476	1.348	1122	818	3958	1445	1102	0.891	0.135	470	230
2.453	1.360	1091	808	3914	1434	699	0.659	0.0920	517	368
2.455	1.361	1092	808	3921	1434	850	0.791	0.107	556	143
2.457	1.346	1095	807	3886	1425	801	0.765	0.112	577	369
2.458	1.361	1096	812	3933	1442	1075	0.893	0.140	571	180
2.488	1.374	1123	823	4075	1470	859	1.65	0.171	878	...

[a] $r_1 = [C_2F_4]/[C_2HF_5]$; $r_4 = [C_2HF_3]/[C_2HF_5]$.

It should be noted, however, that this mechanism has not been tested for the effects of total pressure, reactant concentration, or inhibitors.

$$CHF_2CF_3 \xrightarrow{k_1} C_2F_4 + HF \qquad (1)$$

$$CHF_2CF_3 \xrightarrow{k_2} CHF_2 + CF_3 \qquad (2)$$

$$CHF_2 + CF_3 \xrightarrow{k_{-2}} CHF_2CF_3 \qquad (-2)$$

$$2CF_3 \xrightarrow{k_{-3}} C_2F_6 \qquad (-3)$$

$$C_2F_6 \xrightarrow{k_3} 2CF_3 \qquad (3)$$

$$2CHF_2 \xrightarrow{k_{-4}} CHF_2CHF_2 \qquad (-4)$$

$$CHF_2CHF_2 \xrightarrow{k_4} 2CHF_2 \qquad (4)$$

$$\xrightarrow{k_5} CHFCF_2 + HF \qquad (5)$$

$$CF_3 + CHF_2CF_3 \xrightarrow{k_6} CHF_3 + C_2F_5 \qquad (6)$$

$$CHF_2 + CHF_2CF_3 \xrightarrow{k_7} CH_2F_2 + C_2F_5 \qquad (7)$$

$$CF_3 + C_2F_5 \xrightarrow{k_8} C_3F_8 \qquad (8)$$

$$CHF_2 + C_2F_5 \xrightarrow{k_9} C_3HF_7 \qquad (9)$$
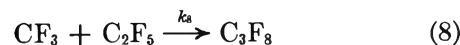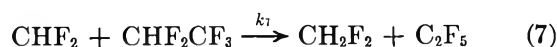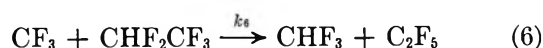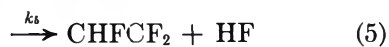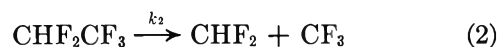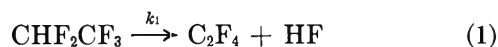
The primary processes in the pyrolysis of the fluoroethanes have been described previously.[9] However, a discussion of the secondary processes in the present scheme is necessary since some possible reactions have been omitted. The disproportionation/combination ratio of CHF_2 radicals has been established[18a] at ~0.17, in the temperature range 297–443°K. However, at the high temperatures of this study the chemically activated adduct formed by the reactive collision of two CHF_2 radicals will contain some 20 kcal mol^{-1} in excess energy over that necessary for HF elimination. Thus, reaction 5 is preferred over the disproportionation reaction

$$2CHF_2 \longrightarrow CH_2F_2 + CF_2$$
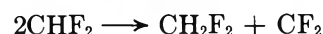
Similarly, the disproportionation/combination ratio for CF_3 and CHF_2 radicals has been found[18b] to be of the order 0.08–0.09 and temperature independent, and for this reason the reaction

$$CF_3 + CHF_2 \longrightarrow CHF_3 + CF_2$$
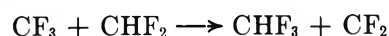
has been omitted from the reaction scheme. To add weight to the arguments against the disproportionation reactions producing CH_2F_2 and CHF_3, it should be noted that only small amounts of these compounds were observed experimentally.

We also note that at high temperatures ($T > 1350°K$) primary radicals combine in preference to H abstraction from the parent molecule, as shown below. Consequently, the concentration of C_2F_5 radicals produced in reactions 6 and 7 will be correspondingly small, and for this reason the combination and disproportionation reactions of two perfluoroethyl radicals

$$2C_2F_5 \longrightarrow C_4F_{10}$$

$$\longrightarrow C_2F_4 + C_2F_6$$
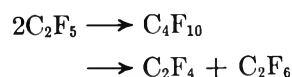
have been omitted from the scheme. In addition, the latter reaction would require a fluorine shift which is

(18) (a) G. O. Pritchard and M. J. Perona, *Int. J. Chem. Kinet.*, **1**, 509 (1969); (b) *ibid.*, **1**, 413 (1969).

unlikely to occur. Similar considerations (as well as experimental evidence since no CF_4 was observed) preclude the reactions

$$CF_3 + C_2F_5 \longrightarrow CF_4 + C_2F_4$$
$$\longrightarrow CF_2 + C_2F_6$$
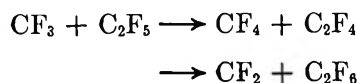
However, the cross-combination reactions 8 and 9 are listed to provide a formal chain termination step. Finally the possible disproportionation

$$CHF_2 + C_2F_5 \longrightarrow CF_2 + C_2HF_5$$
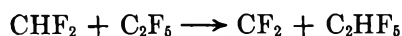
has not been reported in the literature and would, in any event, be less important than reaction 9.

Using the stationary-state equations for the transient species, the theoretical carbon mass balance (neglecting C_3 species, i.e., reactions 8 and 9) can be shown to be given by

$$(A)_0 = (A) + (B) + (C) +$$
$$(D) + (E) + \frac{3}{2}(F) + \frac{3}{2}(G) \quad (I)$$

where for convenience we have set: $(A) = [C_2HF_5]$; $(B) = [C_2F_4]$; $(C) = [C_2F_6]$; $(D) = [CHF_2CHF_2]$; $(E) = [C_2HF_3]$; $(F) = [CHF_3]$; $(G) = [CH_2F_2]$, and $(A)_0$ is the initial concentration of C_2HF_5. To make further analysis possible, the following approximations were made. (i) For mathematical expediency we set $X = [CF_3] \simeq [CHF_2]$. (ii) The concentration of CHF_2 or CF_3 radicals is given approximately by

$$(X)^2 = (k_2/2k_{-2})(A) \quad (II)$$

Equation II results from a consideration of the relative importance of the C_1 radical combination reactions vs. the hydrogen atom abstraction reactions 6 or 7 at high temperatures. Thus, for example, the stationary-state concentration of CHF_2 radicals is given by

$$(X) = [-k_7(A) + [k_7^2(A)^2 +$$
$$8k_2k_{-2}(A)]^{1/2}]/4k_{-2} \quad (III)$$

if we neglect the back reaction 4 as well as reaction 9, and upon setting $k_{-2} \simeq 2k_{-4}$ (since $k_{-2}/k_{-4} = 2(d_{ab}/d_{aa})^2(\mu_{aa}/\mu_{ab})^{1/2} \simeq 2$, where d and μ denote the collision diameter and reduced mass, respectively). If we define ϕ as the rate ratio

$$\phi = |R_{-2} + R_{-4}|/R_7 = 2k_{-2}(X)/k_7(A) \quad (IV)$$

it follows that

$$\phi = \frac{1}{2}([1 + \theta/(A)]^{1/2} - 1) \quad (V)$$

where $\theta = 8k_2k_{-2}/k_7^2$. To evaluate θ, values of the Arrhenius parameters were taken from analogous systems,[17,18a] and it was found that at 1350°K and for $(A) \simeq (A)_0 = 2.6 \times 10^{-7}$ mol cm^{-3} (the most unfavorable case), $\phi = 7$. Hence from eq IV we have the inequality

$$|R_{-2} + R_{-4}| > R_7 \quad (VI)$$

This inequality will in general be favored with (a) the progress of the reaction, i.e., decreasing (A); and (b) increasing temperatures $(T > 1350°K)$, since $\theta \propto \exp[-(E_2 + E_{-2} - 2E_7)/RT]$ and $E_{-2} \simeq 0$, $E_2 > 2E_7$. We thus conclude that at temperatures at which C–C scission becomes significant, the steady-state concentration of CHF_2 radicals is not appreciably perturbed by their removal via the H abstraction reaction 7 and hence eq II follows from eq III. The same arguments and conclusions can be drawn by an analogous consideration of the CF_3 radical.

(iii) We set $(A)_0 \simeq (A) + (B) + (E)$, since from the product analysis it was found that $(A) + (B) + (E) \gg (D) + 3/2(F) + 3/2(G)$ over the entire temperature range and the amount of C_2F_6 formed could not be evaluated.[19] Thus, in terms of product/reactant ratios

$$(A)_0/(A) = 1 + r_1 + r_4 \quad (VII)$$

where $r_1 = (B)/(A)$ and $r_4 = (E)/(A)$ are experimentally determined values.

The depletion of A is given by

$$-d(A)/dt = k_1(A) + k_2(A) -$$
$$k_{-2}(CHF_2)(CF_3) + k_6(CF_3)(A) +$$
$$k_7(CHF_2)(A) \quad (VIII)$$

which in view of the above inequality VI and eq II reduces to a simple first-order rate equation

$$-d(A)/dt = k'(A) \quad (IX)$$

or the integrated form

$$k' = (1/t) \ln (1 + r_1 + r_4) \quad (X)$$

where $k' = (k_1 + \frac{1}{2}k_2)$ and t is the reaction dwell time. Solving for the rate of formation of (B) yields

$$(B) = (k_1/k')(A)_0(1 - e^{-k't}) \quad (XI)$$

Substitution of (X) in (XI), division by (A), and making use of eq VII gives

$$k_1 = r_1 \ln (1 + r_1 + r_4)/t(r_1 + r_4) \quad (XII)$$

or in terms of the first-order rate law corrected for the finite cooling rate of the rarefaction fan[20]

$$k = r_1 \ln (1 + r_1 + r_4)/t(r_1 + r_4)(1 - (\epsilon/t)) \quad (XIII)$$

The values of k_1 obtained from the experimental results are shown in Table I and the temperature dependence is plotted in Figure 1.

(19) It has been shown that the hydrogen abstraction reaction 6 is slow. Thus, the amount of C_2F_6 formed should be equal to the sum of the amounts of CHF_2CHF_2 and C_2HF_3. However, the C_2F_6 peaks had extremely small areas which could not be measured accurately. The small peaks can be ascribed to the fact that the fully fluorinated C_2F_6 was insensitive to the flame ionization detector of the gc; for example C_2F_6 is about 80 times less sensitive than CHF_2CHF_2. For this reason we have neglected, in the mass balance, the amount of C_2F_6 formed. The inclusion of this quantity would affect the Arrhenius parameters to an insignificant degree.
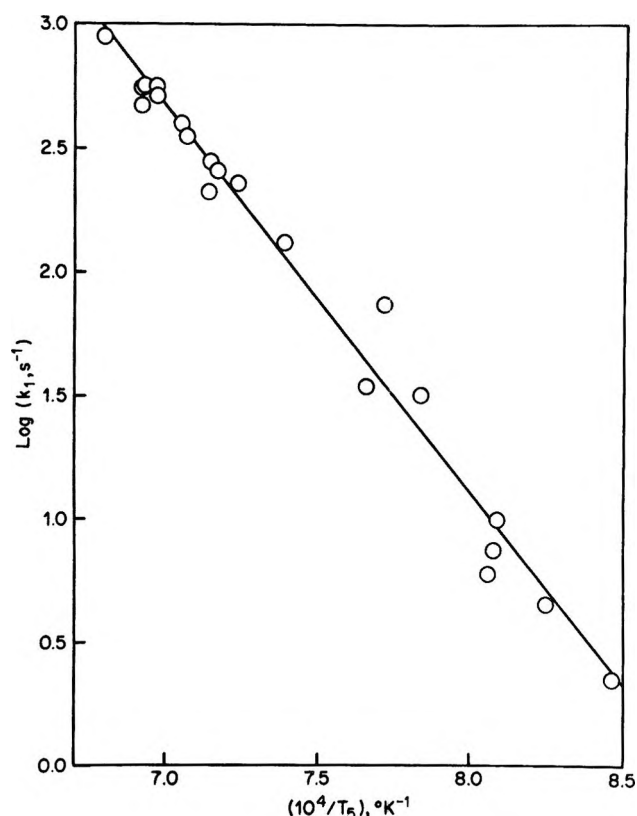
Figure 1. Temperature dependence of the rate constant k_1 for HF elimination from CHF_2CF_3.

Figure 2. Temperature dependence of the rate constant k_2 for C–C bond scission in CHF_2CF_3.

Rearranging the expression for k' we obtain

$$k_2 = 2(k' - k_1) \qquad \text{(XIV)}$$

The values of k_2, corrected for the finite cooling rate of the rarefaction fan[20] (cf. eq XIII) are given in Table I and the temperature dependence is plotted in Figure 2.

Discussion

In the case of C_2H_5F, Day and Trotman-Dickenson[3] found that the rate of HF elimination becomes independent of pressure above 5 Torr and at 425°K. It can be readily shown[4] that under the experimental conditions used in this study the rate is first order and hence the rate constants, k_1, reported in Table I are the high-pressure limiting values. A least-squares analysis of the data of Figure 1 yields an Arrhenius expression

$$k_1 \text{ (sec}^{-1}) = 10^{13.6 \pm 0.4} \exp[-(71{,}600 \pm 2400)/RT]$$

where the indicated error limits are standard deviations. The value of the activation energy fits into the previously observed trend[4-9] of increase in activation energy with increase in fluorination, although the increase is only $\sim 3\%$ over the value observed for $1,1,2,2\text{-}C_2H_2F_4$. As stated earlier, a similar value was found between CH_3CF_3 and CHF_2CHF_2, while that between CH_3CHF_2 and CH_3CF_3 was 11%.

C_2HF_5 may be derived by the substitution of fluorine atoms at the β-carbon position in CH_3CF_3, i.e., CH_3-

$CF_3 \rightarrow CH_2FCF_3 \rightarrow CHF_2CF_3$. The increase in activation energy of CHF_2CF_3 over CH_3CF_3, for the addition of *two* fluorine atoms, is $\sim 4.2\%$. This fact seems to support our earlier postulate[9] that β-fluorine substituents have a regressive effect on increasing the activation energy. However, if C_2HF_5 is considered as being derived from CHF_2CHF_2, in which case the α fluorination is being increased, then one might expect a larger increase in activation energy than the 3% we have obtained. In this case we suggest that the smaller increase in activation energy is due to the higher density of electronegative substituents.

A least-squares analysis of the data of Figure 2 yields an Arrhenius expression

$$k_2 \text{ (sec}^{-1}) = 10^{16.6 \pm 0.6} \exp[-(93{,}500 \pm 5200)/RT]$$

The activation energy for the C–C bond scission of 93.5 kcal mol^{-1} lies in between that obtained for C_2F_6 (94.4 kcal mol^{-1})[17] and $1,1,2,2\text{-}C_2H_2F_4$ (91.4 kcal mol^{-1}),[9] and it shows an increase compared to the latter case. Thus, the substitution of fluorine atoms in the parent species seems to cause a concurrent increase in the C–C bond dissociation energy and the activation energy for HF elimination. The high value of the pre-exponential factor is in agreement with those recorded in previous studies[9,17] and reflects the very loose transition state in reaction 2.

(20) E. Tschuikow-Roux, Phys. Fluids, 8, 821 (1965).

It is of interest to compare the value of the pre-exponential factor for the HF elimination reaction with that calculated by the method of O'Neal and Benson,[21] which was developed for four-center reactions. The entropy of activation, $\Delta S^{\dagger}$, is given by

$$\Delta S^{\dagger} = (S_{tors}{}^{\dagger} - S_{h.i.r.})_{int} + \Delta S_{int}{}^{\dagger} + R \ln g$$

where $(S_{tors}{}^{\dagger} - S_{h.i.r.})_{int}$ is the intrinsic entropy loss of the CHF_2 group in going from the hindered internal rotation of the ground state to the torsional mode of the complex. The moment of inertia of the CHF_2 group about the C–C axis was found to be 62 amu $\overset{\circ}{A}{}^2$, while the reduced moment of inertia[22] was 23 amu $\overset{\circ}{A}{}^2$. Thus, at 1350°K the partition function for free rotation was calculated to be 63.3, from which the entropy contribution for free rotation is 9.24 eu. The barrier to internal rotation for C_2HF_5 is 3.51 kcal mol^{-1},[22] and this value may be used to calculate the entropy decrease from free rotation. The entropy contribution of hindered internal rotation is therefore 9.0 eu. It is possible to assign a value of 350 cm^{-1} to the torsional mode and at 1350°K its entropy contribution is 4.0 eu. Hence, the change for this mode is -5.0 eu. The intrinsic entropy change of the other vibrational modes in going from the ground state to the transition state is given by

$$\Delta S_{int}{}^{\dagger} = \sum_i^{3N-8} S_i{}^{\dagger} - \sum_i^{3N-7} S_i$$

The method used for the assignment of the vibrational frequencies was analogous to that outlined by O'Neal and Benson.[21] Using known values for the bending, twisting, and rocking modes of halocarbons the corresponding modes involving fluorine atoms were calculated from the relationship $\omega_1/\omega_2 = (\mu_2/\mu_1)^{1/2}$ where μ is the reduced mass of the bend $(\overline{A-R-B})$. The vibrational frequencies and their corresponding entropies, at 1350°K, are set out in Table II.

Then, using a reaction path degeneracy of three, for α,β HF elimination, the overall entropy of activation is given by

$$\Delta S^{\dagger} = -5.0 + 0.6 + R \ln 3 = -2.2 \text{ eu}$$

The preexponential factor is then obtained from the transition state theory expression $A = (ekT/h)$ exp-$(\Delta S^{\dagger}/R)$ which yields $\log A$ (sec^{-1}) $= 13.4$. This value is in reasonable agreement with the observed value of 13.6.

Table II: Frequency Assignments for Pentafluoroethane Reaction

Ground state			Activated complex		
Vibrations	Freq., cm^{-1}	Entropies (1350°K), eu	Vibrations	Freq., cm^{-1}	Entropies (1350°K), eu
C /\ 4F F	426	14.4	C /\ 2F F	426	7.2
			C /· F F	294	4.7
			C ·\ F C	236	4.3
C /\ C H	1150	1.7	C /· C H	800	2.4
4 (C–F)	1110	7.2	4 (C–F)	1100	7.2
C–C	1000	1.9	C–̇C	1300	1.5
C /\ 4F C	407	14.8	C /\ 4F C	407	14.8
C /\ F H	708	2.6	C ·\ F H	708	2.6
C–H	3000	0.35	C·H	2200	0.69
C–F	1100	1.8 →	(reaction coordinate)		0.0
		+44.8			+45.4
$\Delta S_{int}{}^{\dagger} = +0.6$ eu					

(21) H. E. O'Neal and S. W. Benson, *J. Phys. Chem.*, **71**, 2903 (1967).

(22) A. B. Tipton, C. O. Britt, and J. E. Boggs, *J. Chem. Phys.*, **46**, 1606 (1967).

Quantum Yields in the 58.4-nm Photolysis of Carbon Dioxide

by J. B. Tellinghuisen, C. A. Winkler,[1a] S. W. Bennett,[1b] and L. F. Phillips*

Chemistry Department, University of Canterbury, Christchurch, New Zealand   (Received June 14, 1971)

Publication costs borne completely by The Journal of Physical Chemistry

Quantum yields have been determined by mass spectrometric analysis and by measurement of the absorption of 58.4-nm radiation by the photolysis products. At pressures near 2 Torr the CO yield is 0.20 ± 0.05. From a comparison with known rates of primary and secondary processes, we deduce that recombination of $C_2O_4^+$ with an electron gives $CO_2 + CO + O$ with 10% probability. At pressures below 200 mTorr, where the electron-ion recombination is predominantly heterogeneous, the measured CO yield is 0.6, which implies that dissociation occurs in 50% of the wall recombination involving CO_2^+. Wall processes which permanently remove oxygen atoms appear to be efficient at low pressures.

Introduction

In the past few years interest in aeronomic processes has inspired numerous studies of photoionization and photoelectron processes initiated by extreme ultraviolet radiation. At the same time problems of handling reactants and products and of interpreting results in windowless systems have hindered efforts to measure quantum yields for photolysis in this spectral region.[2] However, recent developments in the use of thin metal films as windows have made it possible to photolyze gases in static systems using virtually monochromatic He (58.4 nm) or Ne (73.6 and 74.4 nm) resonance radiation;[3] quantum yields at 58.4 nm have been reported for CH_4,[4] for C_3H_8 reacting with Xe^+ and Ar^+,[5] and for production of excited states of CO_2^+.[6]

In this paper we report quantum yields for the stable products formed during 58.4-nm photolysis of CO_2. The results are interpreted in terms of known photofragmentation processes and ion–molecule reactions, together with lesser known electron–ion dissociative recombination processes.

Experimental Section

The photolysis arrangement consisted of a Pyrex cell (volume 120 ml), fitted with copper-wire electrodes and separated from a microwave-powered He discharge lamp by means of a thin-film Al window. This arrangement was described in detail previously,[7] but a few additional points concerning the use of the Al windows are worthy of mention. The few very small (<1 μm across) holes that were often present in our windows generally gave a negligible leak rate. It might be noted that any leaks slow enough to be tolerated must involve effusion rather than mass flow, so pressure differentials cannot prevent mutual contamination of lamp and cell. Traces of He in the cell should not affect the results, because the He atoms absorb a very small fraction of the severely reversed source radiation. However, contamination of the

lamp by the photolysis gas can greatly reduce the 58.4-nm intensity unless the discharge "cleans up" as fast as the gas leaks into the lamp. A number of our windows, purchased as "defective" from the manufacturer, were riddled with tiny (<1 μm) pinholes. We were able to render these windows usable by overdepositing a ~30-nm layer of Al at a rate of 3 nm/sec or greater in a vacuum deposition apparatus maintained at a pressure below 10^{-5} Torr.

Photolysis fluxes of 10^{12}–10^{13} quanta/sec (corresponding to ionization plateau currents of 0.15 to 1.5 μA) were used in these experiments. Although the windows showed the gradual loss in transmissivity noted by Gordon, et al.,[3] the deterioration was negligible over the course of a photolysis run when the flux was maintained below 3×10^{12} quanta/sec. Irradiation times ranged from 1 to 7 hr and were chosen to give a total product conversion $\lesssim 1\%$. The lamp performance was monitored periodically during a run by observing the ion current at a fixed voltage (usually 100 V). Between readings the potential was dropped to a residual value of 2.5 V, which served to inhibit recombination of ions and electrons on the surface of the window. At this voltage the collector current was <1% of the true saturation current. The latter quantity was generally determined at the end of the experiment from the plateau observed with 2–4 Torr H_2 in the cell.

Mass spectrometric analyses were performed with

(1) (a) On leave from the Chemistry Department, McGill University, Montreal, Canada. (b) Department of Chemistry, University of Wisconsin, Madison, Wis.

(2) D. C. Walker and R. A. Back, *J. Chem. Phys.*, **38**, 1526 (1963).

(3) R. Gorden, Jr., R. E. Rebbert, and P. Ausloos, *Nat. Bur. Stand. (U. S.) Tech. Note*, 496 (1969).

(4) (a) R. E. Rebbert and P. Ausloos, *J. Amer. Chem. Soc.*, **90**, 7370 (1968); (b) C. A. Jensen and W. F. Libby, *J. Chem. Phys.*, **49**, 2831 (1968).

(5) S. G. Lias, R. E. Rebbert, and P. Ausloos, *ibid.*, **52**, 773 (1970).

(6) T. S. Wauchop and H. P. Broida, *J. Geophys. Res.*, **76**, 21 (1971).

(7) S. W. Bennett, J. B. Tellinghuisen, and L. F. Phillips, *J. Phys. Chem.*, **75**, 719 (1971).

an A.E.I. Type MS902 high-resolution mass spectrometer, with a Granville-Phillips variable leak to control the flow of sample into the ion source. Gas mixtures were expanded into an evacuated bulb, transferred to the input line on the spectrometer, and analyzed for CO abundance by comparison with a known CO–CO_2 mixture. To reduce the large mass-28 fragmentation peak from the parent CO_2 it was necessary to operate at low (22 V) electron beam potentials. Attempts to measure O_2 production in this way were frustrated by problems of air leaks and background peaks in the spectrometer.

In a number of experiments the buildup of products was followed by using the lamp–cell combination as a sensitive pressure gauge. At intervals the CO_2 was frozen in a side tube cooled with liquid air, and ion current vs. applied voltage data were recorded for the residual gaseous products. Total product concentrations were deduced from these data using eq 1 below.

The gases CO_2, CO, He, and H_2 used in the experiments were Matheson prepurified, high-purity grade or equivalent. The CO_2 was further purified by trap-to-trap distillation. The vacuum line was fitted with a Hitachi two-stage rotary pump capable of evacuating the system to ~ 1 mTorr. Pressures were measured to ± 2 mTorr with a Texas Instruments quartz spiral gauge. In all gas-handling operations the cell, lamp, collection bulbs, etc., were flushed at least twice with 1–5 Torr of the appropriate gas prior to filling.

Results and Discussion

Ionization Current Curves. Typical ion current curves recorded for H_2 and CO_2 are illustrated in Figure 1. Acceptable plateaus were recorded at all fluxes for ~ 4 Torr H_2 (curve a), whereas CO_2 exhibited good saturation behavior only for total fluxes less than 100 nA (curve d). For fluxes greater than 100 nA neither CO_2 nor low pressures (<2 Torr) of H_2 gave true plateaus (curves b and c), although the inflection points in such curves corresponded very nearly to the true saturation currents. Similar characteristics were noted for a number of other gases including O_2, N_2, Ar, H_2O, and NH_3.

Ion current curves recorded for high incident flux and low fractional absorption—the conditions for measuring product concentrations with the CO_2 frozen out—also failed to yield true plateaus. However, the knees of these curves were quite sharp, and we considered that they fixed the true absorption within 10%, which was comparable to other uncertainties in the experiments. With the assumption of stoichiometric production of CO and O_2, total product concentrations n could be calculated using the relation

$$I_a/I_0 = 1 - \exp(-k_{av}xn/n_0) \approx k_{av}xn/n_0 \qquad (1)$$

where I_a is the measured saturation current, I_0 the
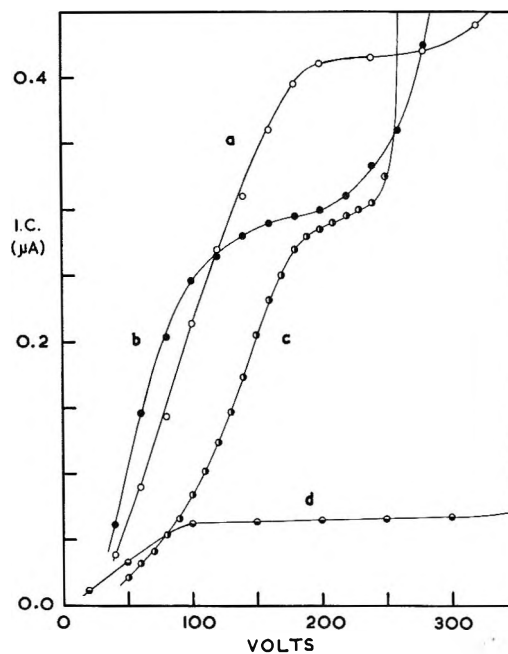
Figure 1. Ionization current vs. applied voltage for (a) 3.63 Torr H_2, $I_0 = 0.415 \pm 0.005$ μA; (b) 1.85 Torr H_2, $I_0 = 0.295 \pm 0.01$ μA; (c) 2.22 Torr CO_2, $I_0 = 0.295 \pm 0.010$ μA; (d) 3.82 Torr CO_2, $I_0 = 0.063 \pm 0.002$ μA. (For curve c the voltage scale is compressed by a factor of 2, i.e., breakdown occurs at 520 V.)

saturation current for total absorption, n_0 the particle concentration at STP ($= 2.69 \times 10^{19}$ cm^{-3}), and x the cell path length ($= 12.0$ cm). Here k_{av} is the average absorption coefficient, given in terms of the ionization yields φ and absorption coefficients k by[7]

$$k_{av} = \frac{2}{3}\varphi_{CO}k_{CO} + \frac{1}{3}\varphi_{O_2}k_{O_2} = 490 \text{ cm}^{-1} \qquad (2)$$

The zero-pressure value of I_a/I_0 was fairly constant from one run to the next and was probably due to photoelectron emission processes involving the window and the electrodes.

Good plateaus are attained in current–voltage curves of the type shown in Figure 1 only when ions and electrons are collected with 100% efficiency at a voltage substantially below that which results in ion multiplication by electron-impact ionization.[8] For voltages below the saturation level ions and electrons are lost through gas phase electron–ion recombination, or through diffusion processes which result in removal of electrons and negative ions at the cathode, positive ions at the anode, or both electrons and ions in wall recombination. With the cylindrical arrangement of our electrodes diffusion losses are likely to be important only at low pressures and/or very low potentials. (See discussion below.) Thus the failure of most gases to display good saturation behavior for high incident flux may be attributed to the great

(8) J. A. R. Samson, "Techniques of Vacuum Ultraviolet Spectroscopy," Wiley, New York, N. Y., 1967.

efficiency of the dissociative recombination processes, for which rates are 10^{-7} cm³/sec or greater.[9] The good performance of H_2 has been attributed to its low absorption coefficient ($k = 175$/cm),[3] but we further suspect that electron–ion recombination is somewhat slower in H_2 than in the other gases. Although calculations predict the rate for $H_2^+ + e^- \rightarrow H + H$ to be about 3×10^{-8} cm³/sec,[10] it is now well known that H_3^+ is the dominant charge carrier in H_2 at pressures around 1 Torr.[11] There appears to be no reliable measurement of the H_3^+ recombination rate.[12] To date the only molecular ion known to recombine with electrons at a rate appreciably slower than 10^{-7} cm³/sec at room temperature is He_2^+,[13] so an accurate determination of the rate for H_3^+ would be of some interest. A more detailed consideration of the nature of these ion current curves will be included in a future report.

58.4-nm Photolysis: General Considerations. Because of the great energy available (21.21 eV), absorption of 58.4-nm radiation initiates a profusion of phenomena, as occurs in high energy radiolysis. The primary process yields ions with practically 100% efficiency, and the ejected electrons have energies ranging up to 21.21 eV minus the ionization potential of the photolysis gas (*i.e.*, 0 to 7.43 eV for CO_2). The positive ions may participate in a variety of ion–molecule reactions in the gas phase and possibly on the cell walls. The electrons can impart translational or internal energy to the neutral gas molecules, or they may attach to give negative ions. The positive ions and electrons (or negative ions) ultimately recombine in the gas phase or on the walls or electrodes to produce neutral molecules and radicals which may themselves retain excitation energy. Finally, the radicals undergo gas phase or wall reactions to yield stable neutral products.

For most small molecules there is now available a body of information on photoionization and ion–molecule reactions. Photofragmentation spectra for CO_2 have been published by Weissler, *et al.*,[14] and more recently by Dibeler and coworkers.[15] From the latter work the processes occurring at 58.4 nm may be represented

$$CO_2 + h\nu \longrightarrow (CO_2^+)^* + e^- \tag{3a}$$

$$(CO_2^+)^* \longrightarrow CO_2^+ + h\nu' \quad (95\%) \tag{3b}$$

$$\longrightarrow O^+ + CO \quad (4\%) \tag{3c}$$

$$\longrightarrow CO^+ + O \quad (1\%) \tag{3d}$$
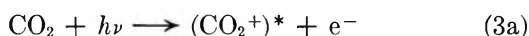
The photoelectron spectra of Turner and May[16] suggest that at least three bound excited states of CO_2^+ are produced in (3a), and visible emission from two of these states has been reported by Wauchop and Broida.[6] Since the transitions involved are fully allowed, the decay (3b) to the ground state ion occurs

rapidly. The O^+ and CO^+ ions formed in (3) are known to undergo the following reactions

$$O^+ + CO_2 \longrightarrow O_2^+ + CO$$
$$k = 1.2 \times 10^{-9} \text{ cm}^3/\text{sec} \tag{4}$$
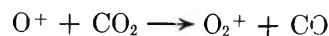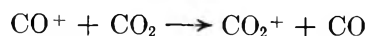
$$CO^+ + CO_2 \longrightarrow CO_2^+ + CO$$
$$k = 2 \times 10^{-9} \text{ cm}^3/\text{sec} \tag{5}$$

In addition $C_2O_4^+$ ions are formed readily in CO_2 at pressures above 200 mTorr, though the mechanism appears to be complicated.[17] The above reactions are an order of magnitude faster than gas kinetic collision rates. Thus, initial processes lead directly to the dominant positive charge carriers O_2^+, CO_2^+, and $C_2O_4^+$. A further charge-transfer reaction[18]
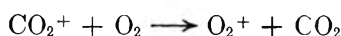
$$CO_2^+ + O_2 \longrightarrow O_2^+ + CO_2$$
$$k = 5 \times 10^{-11} \text{ cm}^3/\text{sec} \tag{6}$$

may become important as the concentration of O_2 builds up in the cell.

Photoelectron spectra[16] of CO_2 indicate that an appreciable fraction of the electrons ejected in photoionization at 58.4 nm have sufficient energy to dissociate CO_2 (5.45 eV[19]). The likelihood of electron-impact dissociation is unfortunately rather difficult to assess, as this excitation process is not yet characterized in great detail.[20] However, because of the sharp resonances and small cross sections ($<10^{16}$ cm²) involved, electron-impact excitation probably cannot contribute significantly to the product yield. Electron attachment is relatively slow in CO_2,[20] so after rapid thermalization through collisions with neutral molecules the electrons must either recombine with positive

$$O_2^+ + e^- \longrightarrow O \text{ atoms}$$
$$\alpha = 2.2 \times 10^{-7} \text{ cm}^3/\text{sec} \tag{7a}$$
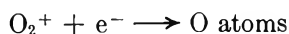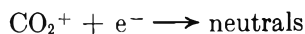
$$CO_2^+ + e^- \longrightarrow \text{neutrals}$$
$$\alpha = 3.8 \times 10^{-7} \text{ cm}^3/\text{sec} \tag{7b}$$

(9) M. A. Biondi, *Can. J. Chem.*, **47**, 1711 (1969).

(10) R. L. Wilkins, *J. Chem. Phys.*, **44**, 1884 (1966).

(11) J. A. Burt, J. L. Dunn, M. J. McEwan, M. M. Sutton, A. E. Roche, and H. I. Schiff, *ibid.*, **52**, 6062 (1970).

(12) H. J. Oskam and V. R. Mittlestadt, *Physica*, **30**, 2021 (1964).

(13) E. E. Ferguson, F. C. Fehsenfeld, and A. L. Schmeltekopf, *Phys. Rev.*, **138A**, 381 (1965).

(14) G. L. Weissler, J. A. R. Samson, H. Ogawa, and G. R. Cook, *J. Opt. Soc. Amer.*, **49**, 338 (1959).

(15) V. H. Dibeler and J. A. Walker, *ibid.*, **57**, 1007 (1967).

(16) D. W. Turner and D. P. May, *J. Chem. Phys.*, **46**, 1156 (1967).

(17) S. M. Shildcrout and J. L. Franklin, *ibid.*, **51**, 4055 (1969).

(18) F. C. Fehsenfeld, D. B. Dunkin, and E. E. Ferguson, *Planet. Space Sci.*, **18**, 1267 (1970).

(19) G. Herzberg, "Electronic Spectra of Polyatomic Molecules," Van Nostrand, Princeton, N. J., 1966.

(20) A. Dalgarno, *Can. J. Chem.*, **47**, 1723 (1969); see also R. D. Hake and A. V. Phelps, *Phys. Rev.*, **158**, 70 (1967). Considering elastic collisions only and assuming a cross section of 10^{-15} cm², most of the ejected electrons will be slowed to thermal velocities in 0.1–0.3 msec (in 1 Torr CO_2), during which time only the most energetic are likely to reach the cell walls.

$$C_2O_4{}^+ + e^- \longrightarrow \text{neutrals} \qquad \alpha = ? \qquad (7c)$$
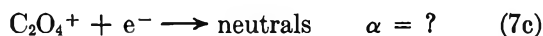
ions in the gas phase or diffuse to the walls and recombine there (ambipolar diffusion). Our calculations for some simplified cell geometries indicate that wall and gas phase recombination have comparable rates at $P = 1$ Torr for a flux of 10^{12} quanta/sec. However, since the diffusion constant is inversely proportional to pressure, and the unit-volume ion-pair production rate is roughly proportional to pressure and flux, gas phase recombination should predominate at pressures >2 Torr and fluxes >2 × 10^{12} quanta/sec.[21] By the same token wall recombination should prevail at pressures <0.3 Torr. The time scale for possible ion–molecule reactions may be compared with τ_D, the characteristic time for ambipolar diffusion, which at $P = 1$ Torr is about 10 msec, or several orders of magnitude longer than the time constants for reactions 4 and 5.

The behavior of neutrals produced in extreme uv photolysis can be predicted from information obtained in vacuum uv work. The fates of radicals formed in CO_2 photolysis at 147 nm are now fairly well understood. Recent studies[22,23] confirm that the CO yield is 1.0 and suggest that the CO_3 intermediate is important only as a short-lived complex in the quenching of $O(^1D)$. The spread in O_2 yields reported through the years is attributed to condition-sensitive wall processes which permanently remove ground-state atoms from the gas phase. Such processes could be important in the present work, as reactions 7 may all yield O atoms. On the other hand, there is little reason to anticipate wall removal of CO; gas phase reactions of CO with O_2 and O atoms are too slow to be significant.[24]

Measured Yields. The mass spectrometric analyses of the products from several runs at 2.0–2.2 torr CO_2 gave a CO yield of 0.19 ± 0.05 with no obvious dependence on lamp flux for the range 3–9 × 10^{12} quanta/ sec. This value was corroborated by independent measurements of product buildup by the absorption method, illustrated in Figure 2. From eq 1 and 2 the slopes of curves c and d give CO yields of 0.25 and 0.15, respectively. Experiments of the latter type are far more sensitive to small product conversions,[25] but unfortunately they are subject to large systematic errors, which propagate as the square of the uncertainty in the quantum flux. The flux was particularly difficult to assess at $P_{CO_2} \approx 2$ Torr, as the monitoring ion current always decreased during the course of the experiment, sometimes by as much as 50%. The decline was usually rapid at first, with a tendency to level off later. For example, in the two runs at ~1.75 Torr presented in Figure 2 the monitoring current dropped about 15% in the initial 20 min, then an additional 5–10% in the remaining photolysis time (30–40 min). Subsequent calibrations of the lamp
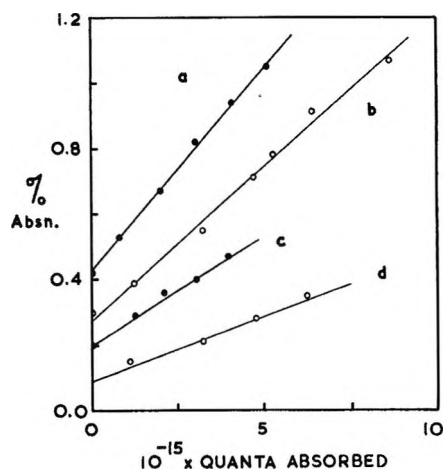
Figure 2. Per cent absorption by photolysis products *vs.* number of quanta absorbed by CO_2. (Data have been shifted on the *y* axis for presentation. Actual zero points lie in range 0.4–0.6% for all plots.) (a) $P_{CO_2} = 122$ mTorr, $I_0 = 0.21$ μA; (b) $P_{CO_2} = 155$ mTorr, $I_0 = 0.21$ μA; (c) $P_{CO_2} = 1.72$ Torr, $I_0 = 0.21$ μA; (d) $P_{CO_2} = 1.75$ Torr, $I_0 = 0.34$ μA.

flux with H_2 in the cell showed a return to the original intensity, and when CO_2 was readmitted to the cell, the initial decline was repeated. These observations suggested an adsorption process, possibly involving O atoms; however, a satisfactory explanation of all aspects of this effect has so far eluded us.

Processes 3–5 account for a CO quantum yield of only 0.09. (The photofragmentation spectra of Weissler and coworkers would allow a yield of 0.16, but are considered less reliable than the later results of Dibeler, *et al.*) Gas phase neutralization of $CO_2{}^+$ presumably occurs to give CO + O with yield unity, but at pressures around 2 Torr the $CO_2{}^+/C_2O_4{}^+$ ratio is very small.[17] Thus the measured CO yield of 0.20 suggests that reaction 7c proceeds to CO_2 + CO + O about 10% of the time, possibly through an unstable excited state of CO_2

$$C_2O_4{}^+ + e^- \longrightarrow CO_2 + CO_2{}^* \qquad (8a)$$

$$CO_2{}^* \longrightarrow CO_2 \ (+ \ h\nu) \qquad (90\%) \qquad (8b)$$

$$CO_2{}^* \longrightarrow CO + O \qquad (10\%) \qquad (8c)$$
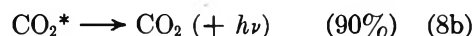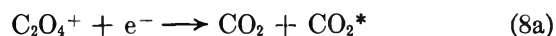
Furthermore, insofar as the product absorption measurements can be accepted as evidence that oxygen is not lost at the cell walls, we may deduce that the reaction

(21) At a pressure of 1 Torr, about 25% of the ion pairs are produced within 3 mm of the window; at 2 Torr, 45%, etc. Thus in the absence of the retarding potential, recombination on the window may be significant even at quite high pressures.

(22) W. B. DeMore and C. Dede, *J. Phys. Chem.*, **74**, 2621 (1970).

(23) T. G. Slanger and G. Black, *J. Chem. Phys.*, **54**, 1889 (1971).

(24) F. Kaufman, *Can. J. Chem.*, **47**, 1917 (1969).

(25) We could measure with precision better than 10% a change of 0.2% absorption, corresponding to the formation of ~1 × 10^{16} product molecules. For conversions greater than this the maximum uncertainty lay in the ±10% reliability of the product absorption plateau and the ±5% stability of the lamp intensity.

$$C_2O_4{}^+ + O_2 \longrightarrow O_2{}^+ + 2CO_2 \qquad (9)$$
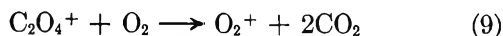
is relatively slow. If, for example, reaction 9 were as fast as (6), it would begin to compete effectively with electron–ion recombination when $[O_2] \approx 2 \times 10^{12}/cm^3$, a value exceeded early in the photolysis. In that case the product yield would decrease to the limiting value of 0.09 predicted by (3)–(5). No such effect was observed.
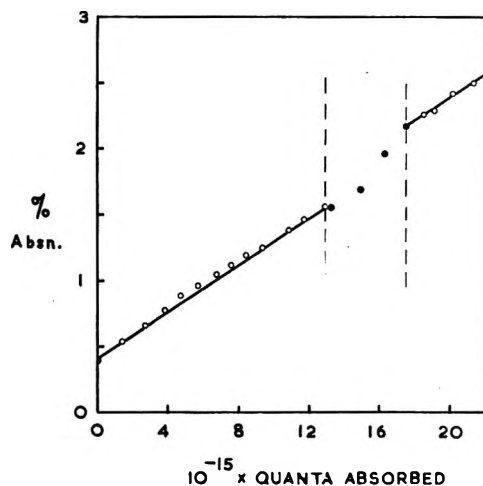
Figure 3. Per cent absorption by photolysis products vs. number of quanta absorbed by 125 mTorr CO_2; $I_0 = 0.31 \mu A$. For period delimited by dashed lines (solid points), roughly two-thirds of the ions were collected at the electrodes at a potential of 100 V.

For CO_2 pressures below 200 mTorr the monitoring ion current could be held constant within 5% for the duration of an experiment; hence, the lamp flux was felt to be similarly well defined. Results of runs in this pressure region (curves a and b of Figure 2) indicate that the CO yield increases by a factor of at least 2 over that at 2 Torr. Since for $P < 200$ mTorr the $C_2O_4{}^+$ concentration is reported to be negligible,[17] the increased yield can be attributed to the neutralization of $CO_2{}^+$. As pointed out above, electron–ion recombination is predominantly heterogeneous at these pressures. If O atoms are not removed quantitatively at the walls, the measured yield should decrease with time, as reaction 6 should compete favorably with the recombination when $k_6[O_2] \approx \tau_D{}^{-1} \approx 10^3/sec$, or when $[O_2] \approx 2 \times 10^{13}/cm^3$. In an attempt to observe this behavior we carried one run at $P = 125$ mTorr to long photolysis times. Although there is some curvature in the resulting data (Figure 3), the change in slope (i.e., the change in the product yield) is so slight as to imply that a substantial fraction of the oxygen is lost in wall processes at these low pressures. The appropriate reassessment of the absorption data gives a CO quantum yield of 0.6, which sug-

gests that dissociation persists in 50% of the wall recombination events

$$CO_2{}^+ + e^- \xrightarrow{\text{wall}} CO_2 \qquad (50\%)$$
$$\xrightarrow{\text{wall}} CO + O \qquad (50\%) \qquad (10)$$
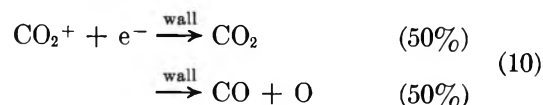
When a potential of 100 V was placed across the electrodes, the yield increased by roughly a factor of 2, as seen in the solid points in Figure 3. This increase is not surprising in view of the ~ 25-eV kinetic energy gained by the positive ions as they impinge on the central cathode, and the likelihood of electron-impact dissociation of neutral CO_2 molecules. As expected, the yield reverted to its previous value when the potential was returned to the residual 2.5-V level.

Summary

Photolysis at 58.4 nm gives ions with practically 100% efficiency in the primary process; hence it might more properly be termed low-energy radiolysis. A lamp–cell arrangement such as the one used here provides a reasonably well defined and easily controlled radiolysis system, in which, because of the nature of the ionizing radiation, the range of possible secondary phenomena is more limited than in conventional high-energy radiolysis experiments. Product quantum yields can be interpreted on the basis of known ion fragmentation yields and ion–molecule reactions, and lesser understood electron–ion dissociative recombination processes.

For CO_2 irradiated with 58.4-nm light at pressures around 2 Torr, the CO quantum yield is 0.20 ± 0.05, indicating that the $C_2O_4{}^+$ ion recombines with an electron to give a 10% yield of CO and O. At pressures of 120–160 mTorr the CO yield is 0.6, which suggests that dissociation occurs with fair probability even in heterogeneous electron–ion recombination. In addition there is evidence that wall losses of oxygen are more significant at the low CO_2 pressures than at the high. For completeness we note that high-energy radiolysis studies of CO_2 have yielded widely conflicting data, the interpretation of which has been a matter of speculation for many years.[26]

(26) A. R. Anderson and D. A. Dominey, Radiat. Res. Rev., 1, 269 (1968).

Naphthalene-Sensitized Photoaquation of Some

Chromium(III)–Ammine Complex Ions[1]

by E. Zinato,* P. Tulli, and P. Riccieri

Institute of General and Inorganic Chemistry, University of Perugia, 06100 Perugia, Italy   (*Received March 30, 1971*)

Publication costs assisted by the National Research Council of Italy (C.N.R.)

Naphthalene sensitizes ammonia photoaquation in 50% water–ethanol solutions of $Cr(NH_3)_6^{3+}$ and $Cr(NH_3)_5Cl^{2+}$. The absence of fluorescence quenching and the increase of the apparent quantum yields upon removal of oxygen indicate the energy donor level as the lowest triplet state. Competition with dissolved oxygen allows the evaluation of the bimolecular quenching constants which are in the range 10^7–10^8 M^{-1} sec^{-1}. The quantum yields for the sensitized reactions are comparable with those of direct photolysis. The main photoreaction product of chloropentaamminechromium(III) is $cis\text{-}Cr(NH_3)_4(H_2O)Cl^{2+}$. Solvation and ion pairing seem to have a larger effect on the energy transfer process than on the subsequent photochemical reaction.

Introduction

Studies of photosensitized luminescence and/or sensitized photochemical reactions have recently unambiguously established the importance of energy transfer in the quenching of organic triplet states by transition metal complexes. The effect seems to be fairly general: cobalt(III),[2-5] chromium(III),[6-9] as well as platinum(II),[10] systems have been reported to act as energy acceptors.

Photosensitized luminescence appears to have been observed only with chromium(III) complexes and, even then, only in fluid solutions at low temperature[6,8] (with the exception of $Cr(en)_3^{3+}$ which weakly phosphoresces at room temperature).[11] A photosensitized reaction can prove to be a more versatile alternative tool for gathering further information on the role of the excited electronic states in the photochemistry of coordination compounds over a wider range of experimental conditions. Energy transfer also has been reported to occur between two complex ions in the solid state within salts of cationic and anionic chromium(III) complexes,[12-14] and from $Ru(bipy)_3^{2+}$ to $Cr(ox)_3^{3-}$, again in a double salt,[15] although the effect seems to be due to crystal perturbations.[16] It has also been observed in low-temperature fluid solutions between reineckate and hexacyanochromate(III) ions.[17]

The present investigation deals with excitation energy transfer, in water–ethanol solutions at room temperature, from naphthalene to some chromium(III) complexes of well-characterized photochemical behavior, $Cr(NH_3)_6^{3+}$ and $Cr(NH_3)_5Cl^{2+}$.

Naphthalene appears to be a suitable energy donor since (i) its lowest triplet excited state is relatively long-lived even in solution at room temperature, (ii) it does not undergo photochemical reactions of its own, and (iii) there exist many literature data on its photophysical processes.[18]

All chromium(III) complexes on direct irradiation

of the d–d absorption bands ($^4A_{2g} \rightarrow {}^4T_{2g}$ and $^4A_{2g} \rightarrow {}^4T_{1g}$ transitions in O_h symmetry, designated L_1 and L_2, respectively[19]) undergo only substitution or substitution-type (as opposed to redox) photoreactions.[19,20] Thus, $Cr(NH_3)_6^{3+}$ irradiated at 452 nm (L_1), photoaquates ammonia with a quantum yield of 0.26.[21]

(1) Part of this paper was presented at the XIII International Conference on Coordination Chemistry - Cracow - Zakopane, Poland, Sept 1970.

(2) A. Vogler and A. W. Adamson, *J. Amer. Chem. Soc.*, **90**, 5943 (1968).

(3) G. B. Porter, *ibid.*, **91**, 3980 (1969).

(4) M. A. Scandola, F. Scandola, and V. Carassiti, *Mol. Photochem.*, **1**, 403 (1969).

(5) M. A. Scandola and F. Scandola, *J. Amer. Chem. Soc.*, **92**, 7278 (1970).

(6) D. J. Binet, E. L. Goldberg, and L. S. Forster, *J. Phys. Chem.*, **72**, 3017 (1968).

(7) A. W. Adamson, J. E. Martin, and F. D. Camassei, *J. Amer. Chem. Soc.*, **91**, 7530 (1969).

(8) T. Ohno and S. Kato, *Bull. Chem. Soc. Jap.*, **42**, 2285 (1969).

(9) J. E. Martin and A. W. Adamson, *Theor. Chem. Acta*, **20**, 119 (1971).

(10) V. Sastri and C. H. Langford, *J. Amer. Chem. Soc.*, **91**, 7533 (1969).

(11) V. Balzani, R. Ballardini, M. T. Gandolfi, and L. Moggi, *ibid.*, **92**, 339 (1971).

(12) H. Gausmann and H. L. Schläfer, *J. Chem. Phys.*, **48**, 4056 (1968).

(13) H. L. Schläfer, H. Gausmann, and C. N. Möbius, *Inorg. Chem.*, **8**, 1137 (1969).

(14) R. Candori and C. Furlani, *Chem. Phys. Lett.*, **5**, 153 (1970).

(15) I. Fujita and H. Kobayashi, *J. Chem. Phys.*, **52**, 4904 (1970).

(16) A. D. Kirk and H. L. Schläfer, *ibid.*, **52**, 2411 (1970).

(17) S. Chen and G. B. Porter, *J. Amer. Chem. Soc.*, **92**, 3196 (1970).

(18) See, for example, (a) A. A. Lamola in "Energy Transfer and Organic Photochemistry," A. A. Lamola and N. J. Turro, Ed., Interscience, New York, N. Y., 1969, p 17; (b) J. B. Birks, "Photophysics of Aromatic Molecules," Wiley-Interscience, New York, N. Y., 1970.

(19) A. W. Adamson, W. L. Waltz, E. Zinato, D. W. Watts, P. D. Fleischauer, and R. D. Lindholm, *Chem. Rev.*, **68**, 541 (1968).

(20) V. Balzani and V. Carassiti, "Photochemistry of Coordination Compounds," Academic Press, London, 1970.

(21) E. E. Wegner and A. W. Adamson, *J. Amer. Chem. Soc.*, **88**, 394 (1966).

For $Cr(NH_3)_5Cl^{2+}$, in the 525–350-nm region, the ammonia and chloride aquation quantum yields are 0.35 to 0.40,[22] and only 0.005 to 0.007, respectively,[23] while Cl^- is the only ligand to be released thermally.[24]

The purpose of this study was to look for possible qualitative differences between the direct and sensitized photolysis of the chosen complexes and to obtain quantitative data on the energy transfer process.

Experimental Section

Materials. $[Cr(NH_3)_6](NO_3)_3$ was prepared from anhydrous $CrCl_3$ and liquid ammonia by a literature method.[25] $[Cr(NH_3)_6](ClO_4)_3$ was obtained by conversion of the above salt with sodium perchlorate. $[Cr(NH_3)_5Cl](ClO_4)_2$ was obtained *via* the chloride salt by a described procedure[26] starting from $[Cr(NH_3)_5(H_2O)](NO_3)_3 \cdot NH_4NO_3$.[27] $[Cr(NH_3)_5(H_2O)](ClO_4)_3$ was prepared from the same double salt by reprecipitation with sodium perchlorate.

All the complexes were recrystallized until their absorption spectra agreed with those reported in the literature. Hexaamminechromium(III) showed maxima at 462 nm ($\epsilon = 38$) and 350 nm ($\epsilon = 34$) for the L_1 and L_2 bands, respectively.[19] In the nitrate salt a third band was present at 303 nm ($\epsilon = 25$) due to the NO_3^- absorption (see Figure 1). For chloropentaamminechromium(III) the L_1 and L_2 maxima were at 512 nm ($\epsilon = 36$) and 375 nm ($\epsilon = 39$), respectively.

The other chemicals and solvents employed were of reagent grade.

Analytical Procedures. Released ammonia was separated from the reaction mixtures and determined by a reported colorimetric method with sodium phenate–sodium hypochlorite reagent.[28] Separations were accomplished as follows. Aliquots of 3 ml were absorbed on a 4–5 cm × 1 cm column of Permutit Zeo-Karb 225 SRC 13 resin (14–52 mesh) which had previously been washed with 0.7 M perchloric acid. Elution with 50–60 ml of 0.7 M $HClO_4$ (which did not move the di- and tripositively charged complex ions) yielded a solution containing only the ammonium ion. The eluate was nearly neutralized with sodium hydroxide and, after addition of the reagent, the solution was diluted to 100 ml with water. The intensity of the blue color was measured at 610 nm after 50–70 min at room temperature. Standardizations were performed simultaneously with each series of determinations. The complexity of the procedure allowed a reproducibility of 5–10%.

Free chloride was determined by a method involving NCS^- displacement from $Hg(SCN)_2$ by the Cl^- ions, followed by a spectrophotometric determination of the former as the Fe^{3+}–NCS^- complex at 450 nm.[29] In this case a preliminary separation procedure was also necessary. In fact, the amount of free chloride produced at room temperature by the thermal aquation of
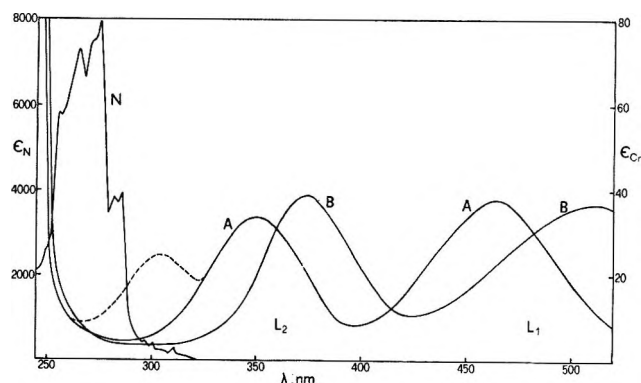
Figure 1. Absorption spectra in 50% water–ethanol: N, naphthalene; A, $Cr(NH_3)_6^{3+}$; B, $Cr(NH_3)_5Cl^{2+}$. Broken line: nitrate ion absorption (three times $\epsilon_{NO_2^-}$). The left- and right-hand scales refer to naphthalene and to the ions, respectively.

$Cr(NH_3)_5Cl^{2+}$, and especially by the subsequent dark reaction of the photoproducts, might be much larger than that of the photoreaction (see ref 23). The extinction coefficient was found to vary with Cl^- concentration and with acidity. Standardization plots showed that, for the concentration (10^{-5} to 10^{-4} M Cl^-) and acidity ranges used, Beer's law was obeyed with $\epsilon = 1.2 \times 10^3$ M^{-1} cm^{-1}. In some experiments the chloride ion was determined by potentiometric titration with silver nitrate.

Photolysis Equipment. The irradiation apparatus is as follows. The light source is an accessory unit of the MPS 50 L Shimadzu multipurpose recording spectrophotometer. It consists of a 500-W compact arc, high-pressure, xenon lamp (Type UXL 500 D) contained in an air-cooled housing and provided with a condenser and a quartz focusing lens system. The lamp is connected to a dc power supply (USHIO Electric Co. Model DSB 501 SS) and aligned on an optical bench with the other parts. The section of the emerging beam is made circular by means of a diaphragm interposed near the focal point, and then, a quartz lens of 40-mm focal length renders the beam parallel with a *ca.* 10-mm diameter.

Monochromatization was accomplished by use of suitable combinations of interference (Bausch and Lomb or Baird Atomic) and blocking (Corning) filters (*vide infra*).

The photolyses were carried out in thermostated,

(22) H. F. Wasgestian and H. L. Schläfer, *Z. Phys. Chem. (Frankfurt am Main)*, **57**, 282 (1968).

(23) H. F. Wasgestian and H. L. Schläfer, *ibid.*, **62**, 127 (1968).

(24) M. A. Levine, T. P. Jones, W. E. Harris, and W. J. Wallace, *J. Amer. Chem. Soc.*, **83**, 2453 (1961).

(25) A. L. Oppegard and J. C. Bailar, Jr., *Inorg. Syn.*, **3**, 153 (1950).

(26) E. Zinato, R. D. Lindholm, and A. W. Adamson, *J. Inorg. Nucl. Chem.*, **31**, 449 (1969).

(27) M. Mori, *Inorg. Syn.*, **5**, 132 (1957).

(28) E. Zinato, R. D. Lindholm, and A. W. Adamson, *J. Amer. Chem. Soc.*, **91**, 1076 (1969).

(29) D. M. Zall, D. Fisher, and M. Q. Garner, *Anal. Chem.*, **28**, 1665 (1956).

standard spectrophotometer cells as specified under Procedures.

Optical densities of solutions were determined with a Beckman DU spectrophotometer, and absorption spectra were recorded with a Beckman DK 1A instrument. Naphthalene fluorescence spectra were measured using a C.G.A. Model DC/3000 spectrophotofluorimeter.

Procedures. Photoaquation quantum yields on direct irradiation of the L_1 band in 50% water–ethanol were determined using solutions 10^{-2} M in complex and 3 × 10^{-2} M in perchloric acid. The solutions photolyzed in conditions of complete light absorption (>99%) in a 10-cm cylindrical spectrophotometer cell (27-ml volume) placed in a thermostated hollow brass holder. The solutions were stirred three to four times during photolysis, and the total reaction did not exceed 10% in order to minimize secondary photolysis and inner filter effects. The absorbed intensity was determined by reineckate actinometry.[21] For $Cr(NH_3)_6^{3+}$ the filter combination BA (349- and 454-nm peaks) + CS-3-73 gave a band centered at 454 nm ($T = 33\%$, 10-nm half-width). For $Cr(NH_3)_5Cl^{2+}$, either the combination BL-500 + CS-3-71 (band centered at 503 nm, $T = 43\%$, 10-nm half-width) or CS-3-71 + CS-4-96 (band centered at 495 nm, $T = 65\%$, 80-nm half-width) was employed.

The sensitization experiments were performed using 50% water–ethanol solutions 2.5 × 10^{-3} M in naphthalene, 3 × 10^{-2} M in perchloric acid and containing the desired concentration of complex. Aliquots of 3 ml were irradiated in a Teflon-stoppered, 1-cm spectrophotometer cell with quartz windows. Before irradiation some of the samples were either deoxygenated or oxygen-saturated by bubbling pure nitrogen or oxygen, respectively, through a capillary tube for 30 min and then quickly stoppering the cells. The cells were kept either at room temperature or thermostated at 18° and stirred periodically. The total reaction was, in most cases, less than 10–15%; only for the lowest complex concentrations did it reach 25–30% because of analytical limitations. The use of a quartz CS-7-54 black filter in combination with a solution filter contained in a cylindrical quartz cell allowed a wavelength selection such that with $Cr(NH_3)_5Cl^{2+}$ the incident light was virtually absorbed only by naphthalene; with $Cr(NH_3)_6^{3+}$ a correction was needed (see below). For chloropentaamminechromium(III) the liquid filters consisted of saturated solutions of the complex to be sensitized and, in the other cases, $[Cr(NH_3)_5(H_2O)]$-$(ClO_4)_3$ was used as a filter because it is more soluble than $[Cr(NH_3)_6](ClO_4)_3$, while its absorption spectrum is similar to that of hexaamminechromium(III) in the wavelength region considered. Light absorption was greater than 99%, but limited to approximately the short wavelength half of the 255–330-nm window. The absorbed intensity (always of the order of magnitude of 10^{-8} einstein/sec) was determined by means of

differential ferrioxalate actinometry.[30] In both types of photolysis an aliquot of the solution under study was kept in the dark at the same temperature; the photolyzed and the "dark" solutions were then simultaneously analyzed in order to allow for any concomitant thermal process.

Results

All the sensitization experiments were carried out in hydroalcoholic medium. Therefore, it seemed advisable to measure some photoaquation quantum yields on direct irradiation of the L_1 band for both complexes in 50% water–ethanol solutions in order to evaluate possible medium change effects on the yields and to check the reliability of the analytical methods. Hexaamminechromium(III) was found to photoaquate ammonia with quantum yields of 0.25 and 0.23 at 18° for the nitrate and the perchlorate salt, respectively, in fair agreement with the literature data.[21] For $Cr(NH_3)_5Cl^{2+}$ (perchlorate salt) the ammonia and chloride photoaquation quantum yields were 0.35 and 0.01, again in agreement with the reported values.[22,23] Thus the presence of 50% ethanol in the solvent seems not to affect the aqueous photochemical behavior.

The absorption spectra of the donor and the acceptor are very different. Figure 1 shows that the intense singlet–singlet (π,π^*) absorption of naphthalene ($\epsilon \sim 4 \times 10^3$) occurs between the charge-transfer absorption and the L_2 band of both complexes. Therefore, in solutions containing one of the two chromium(III) species and naphthalene, light of 250–300 nm is virtually absorbed only by the latter species. Irradiation with such light of 50% water–ethanol solutions, 2.5 × 10^{-3} M in naphthalene and containing the complex to be sensitized in the range 10^{-2} to 10^{-3} M led, in all cases, to a considerable production of free ammonia, much larger than could be accounted for by direct photolysis of the chromium(III) compound which absorbed less than 1% of the incident intensity. The upper and lower limits of complex concentrations were determined by solubility and analytical limitations, respectively, and were 1.5 × 10^{-2} to 2.0 × 10^{-3} M for $[Cr(NH_3)_6]$-$(NO_3)_3$, 5.0 × 10^{-3} to 2.5 × 10^{-3} M for $[Cr(NH_3)_6]$-$(ClO_4)_3$, and 6.6 × 10^{-3} to 1.0 × 10^{-3} M for $[Cr(NH_3)_5$-$Cl](ClO_4)_2$.

Since light of 255–340 nm was employed, a correction was necessary for ammonia produced by direct photolysis in the wavelength range 300–340 nm, where naphthalene does not absorb. In the $Cr(NH_3)_6^{3+}$ case, the amount of extraneous ammonia was estimated by determining the fraction of light absorbed by water–ethanol solutions of complex when an external naphthalene filter, in addition to the filters described above, was interposed in the incident light beam. The average extinction coefficient of the hexaammine was deter-

(30) C. G. Hatchard and C. A. Parker, *Proc. Roy. Soc., Ser. A*, **235**, 518 (1956).

Table I: Results of Sensitization Experiments[a]

Acceptor	a	ϕ_0	b, M^{-1}	$k_q, M^{-1} \sec^{-1}$ [b]
$[Cr(NH_3)_6](NO_3)_3$	8.0 ± 1.5	0.18 ± 0.05	$(10 \pm 2) \times 10^{-2}$	$(3.3 \pm 1.7) \times 10^7$
$[Cr(NH_3)_6](ClO_4)_3$	8.0 ± 1.5	0.18 ± 0.05	$(40 \pm 5) \times 10^{-3}$	$(7.7 \pm 3.6) \times 10^7$
$[Cr(NH_3)_5Cl](ClO_4)_2$	4.0 ± 0.2	0.35 ± 0.05	$(6.5 \pm 0.6) \times 10^{-3}$	2.0×10^8
O_2				$(1.3 \pm 0.4) \times 10^9$

[a] Oxygen concentration in 50% water-ethanol is assumed to be 2.6×10^{-4} M. [b] The bimolecular quenching constants are based on the value for chloropentaamminechromium(III) perchlorate, taken from ref 44.
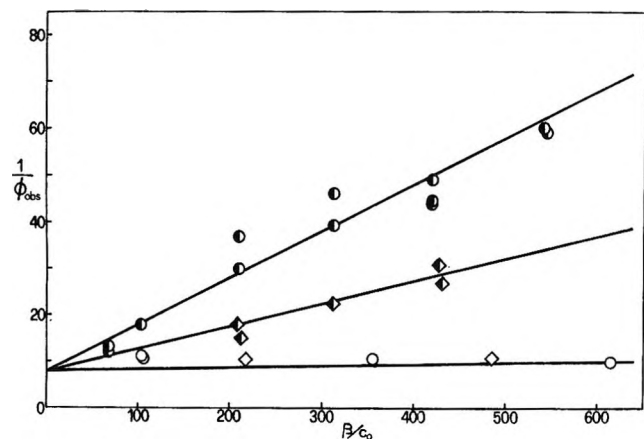
Figure 2. Quantum yields for ammonia aquation of $Cr(NH_3)_6{}^{3+}$ sensitized by naphthalene: ◑, nitrate salt, air-equilibrated; ○, nitrate salt, nitrogen-saturated; ◔, perchlorate salt, air-equilibrated; ◇, perchlorate salt, nitrogen-saturated.
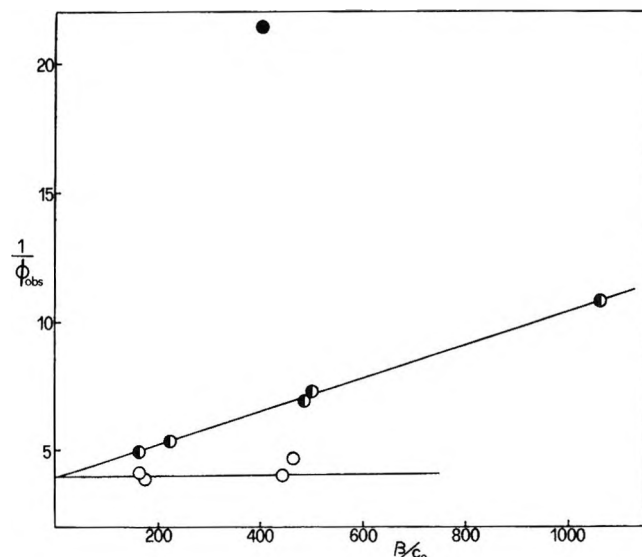
Figure 3. Quantum yields for ammonia aquation of $Cr(NH_3)_5Cl^{2+}$ sensitized by naphthalene: ◑, air-equilibrated solutions; ○, nitrogen-saturated solutions; ●, oxygen-saturated solution.

mined as 8.5, the average ϕ_{NH_3} taken as 0.25. The extraneous ammonia contribution did not exceed 15% of the overall photolysis for the perchlorate and 30% for the nitrate salt. This correction was unnecessary in the case of chloropentaamminechromium(III) due to the congruent spectra of the filter and sample solutions.

Although the liquid filters are themselves made from complex ions, no appreciable change of their absorption features was noticed in the uv region during the photolysis time; almost all the visible light was, in fact, intercepted by the black uv filter.

The corrected ammonia photoaquation quantum yields, ϕ_{obsd}, based on energy absorbed by naphthalene, decrease with decreasing complex concentration in air-equilibrated solutions, whereas in nitrogen-saturated systems they become virtually concentration independent. Figures 2 and 3 show that in all cases ϕ_{obsd} can be plotted according to an equation of the type

$$\frac{1}{\phi_{obsd}} = a + b\frac{\beta}{c_c} \tag{1}$$

which is valid for any photosensitized process governed by acceptor-donor collisions when other paths of deactivation of the donor are competing with the observed reaction and/or luminescence. β allows for disappearance of the acceptor and is given by $(c_0/(c_0 - c))$ ln (c_0/c), where c_0 and c are the initial and final complex concentrations.[2] In all the experiments β was less than 1.2.

For a given concentration, the sensitization effect is larger for $Cr(NH_3)_5Cl^{2+}$ than for $Cr(NH_3)_6{}^{3+}$. Two scale expansions were then needed for the presentation of data, and the scatter of the experimental points is larger for the latter complex (Figure 2). For probably the same reason, the effect of adding oxygen appears to be definite only for chloropentaamminechromium-(III). An additional reason for the scattering might be the presence of slightly different amounts of dissolved oxygen in the air-equilibrated solutions (estimated to be $\sim 2.6 \times 10^{-4}$ M by Henry's law). For both complexes, while the intercept a appears to be oxygen independent, the slope b decreases with decreasing oxygen concentration and becomes very close to zero in the nitrogen-saturated systems. In the case of $Cr(NH_3)_6{}^{3+}$, b, but not a, depends also on the nature of the anion. It is larger for the nitrate than for the perchlorate salt. The values of a and b are reported in Table I.

After irradiation, the absorption spectrum of naphthalene was unchanged even in the faintest details, showing that no consumption of the sensitizer occurred during photolysis.

Fluorescence measurements in the presence of various complex concentrations did not show any quenching effect. No difference was found in naphthalene fluorescent emission between air-equilibrated and oxygen-

saturated solutions. A slight decrease in the luminescence intensity occurred, especially in the presence of $Cr(NH_3)_6^{3+}$. However, this could be completely accounted for by partial light reabsorption by the complex (which was less than 15% in the most unfavorable case), as shown by the fact that it was accompanied by a consistent change in the ratio of the two main fluorescence peaks.

Some additional aspects of the photosensitized aquation of chloropentaamminechromium(III) were investigated, especially to find if chloride was released as in the direct photolysis.[23] In the experimental conditions used, Cl^- ion was found in solution, but it could be accounted for by a secondary thermal aquation reaction of the photoproduced $Cr(NH_3)_4(H_2O)Cl^{2+}$. The chloride aquation rate of the cis isomer in 1 M $HClO_4$, extrapolated at 25°, is 7×10^{-6} sec^{-1} [31] (see also ref 23). Some measurements at 0° showed no difference between the free chloride content of the photosensitized and of the dark samples. The sensitivity of the analytical method allowed us to establish that the ratio of ammonia to chloride photosensitized aquation is certainly not lower than in direct photolysis (ca. 50:1), but we could not establish whether or not it is higher.

It then appeared desirable to determine whether the main (if not the sole) photosensitization product, $Cr(NH_3)_4(H_2O)Cl^{2+}$, was the cis or the trans isomer. The visible absorption spectra of the two species are now well characterized and sufficiently different that even small spectral changes can be highly indicative. The L_1 and L_2 bands of $Cr(NH_3)_5Cl^{2+}$ have absorption maxima at 512 nm ($\epsilon = 36$) and 375 nm ($\epsilon = 39$), respectively.[23,24] cis-Aquochlorotetraamminechromium(III) shows the corresponding maxima at 518 nm ($\epsilon = 41$) and 382 nm ($\epsilon = 34$),[22] whereas for the trans isomer the L_1 band is split into two components at 468 nm ($\epsilon = 18$) and 555 nm ($\epsilon = 20$) and L_2 occurs at 384 nm ($\epsilon = 39$).[32] Absorption spectra were recorded before and after photosensitization at 0° using 5-cm cells in order to gain sensitivity. The definite increase of L_1 (accompanied by a bathochromic shift) and the simultaneous slight decrease of L_2 unambiguously indicated that at least 90% of the product is cis-$Cr(NH_3)_4(H_2O)Cl^{2+}$. Had the photoproduct been the trans isomer, a sharp drop of L_1 and no change in the L_2 intensity would have been observed.

Discussion

The experimental results lead to the conclusion that the observed photosensitized aquation reactions are the consequence of an efficient electronic energy transfer in solution from naphthalene to chromium(III) complex ions.

Chemical quenching, i.e., reaction between excited naphthalene and acceptor is excluded on the grounds that no consumption of the donor occurred, even though its concentration was generally lower than that of the

complex. Naphthalene is known to be photochemically inert towards dissolved oxygen, while heavier aromatic hydrocarbons may not be.[33]

A trivial emission–reabsorption process is not important; a rough, but conservative, estimate places a limit of 10% to its contribution to the reaction, which is within the overall experimental uncertainty. First, naphthalene does not phosphoresce at room temperature and fluoresces with maxima at 327 and 337 nm and quantum yield 0.21 in pure ethanol[34,35] and 0.12 in 95% alcoholic medium,[36] at room temperature, both rather low values. It may be even lower in air-equilibrated solutions and even in nitrogen-saturated samples. One component of naphthalene fluorescence is extremely oxygen sensitive.[37] In nitrogen-saturated solution the concentration of dissolved oxygen (estimated to be 10^{-6} to 10^{-7} M) may have been sufficiently high to produce no difference between the emission of air-equilibrated and deareated samples. Second, while naphthalene fluorescence overlaps only slightly with the short wavelength tail of the L_2 band of $Cr(NH_3)_5$-Cl^{2+}, it is closer to the absorption maximum of $Cr(NH_3)_6^{3+}$. The emission intensity decreases at the maximum but is unchanged in the region where the complex does not absorb. This confirms that no quenching occurs (the decrease is not very large; see Results). Large increase of the apparent quantum yields upon removal of oxygen definitely rules out any appreciable contribution of the trivial process. Little is known of oxygen effects on photoreactions of complexes, but it does not, apparently, affect the emission of chromium(III) complexes in low-temperature fluid systems.[6,8]

The absence of fluorescence quenching and the effect of dissolved oxygen indicate that it is the lowest triplet excited state of the sensitizer which is involved in the energy transfer process.

The results for all the systems examined can be reasonably interpreted by the reaction mechanism

$$^1N + h\nu \xrightarrow{k_1} {}^1N^* \qquad (2)$$

$$^1N^* \xrightarrow{k_2} {}^1N \qquad (3)$$

$$^1N^* \xrightarrow{k_3} {}^1N + h\nu' \qquad (4)$$

$$^1N^* \xrightarrow{k_4} {}^3N^* \qquad (5)$$

$$^3N^* \xrightarrow{k_5} {}^1N \qquad (6)$$

$$^3N^* \xrightarrow{k_6} {}^1N + h\nu'' \qquad (7)$$
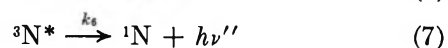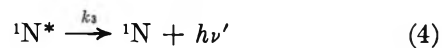
(31) D. W. Hoppenjans, J. B. Hunt, and C. R. Gregoire, Inorg. Chem., 7, 2506 (1968).

(32) D. W. Hoppenjans and J. B. Hunt, ibid., 8, 505 (1969).

(33) E. J. Bowen, Advan. Photochem., 1, 23 (1963).

(34) B. Stevens and M. Thomaz, Chem. Phys. Lett., 1, 549 (1968).

(35) C. A. Parker and T. A. Joyce, Trans. Faraday Soc., 62, 2785 (1966).

(36) B. K. Selinger, Aust. J. Chem., 19, 825 (1966).

(37) I. B. Berlman and T. A. Walter, J. Chem. Phys., 37, 1888 (1962).

$$^3N^* + O_2 \xrightarrow{k_7} {}^1N + O_2 \qquad (8)$$

$$^3N^* + C \xrightarrow{k_8} {}^1N + C^* \qquad (9)$$

$$C^* \xrightarrow{k_9} C \qquad (10)$$

$$C^* \xrightarrow{k_{10}} \text{products} \qquad (11)$$
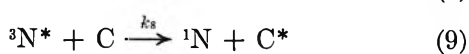
where N denotes naphthalene and C the acceptor complex. In step 9 it is assumed that deactivation by the complex is entirely one of energy transfer. Using the stationary-state concentration for $^3N^*$, the observed quantum yield for photosensitized ammonia aquation is

$$\phi_{obsd} = \frac{k_8\phi_{st}\phi_c[C]}{k_5 + k_6 + k_7[O_2] + k_8[C]} \qquad (12)$$

where $\phi_{st} = k_4/(k_2 + k_3 + k_4)$ represents the quantum yield for intersystem crossing of naphthalene, and $\phi_c = k_{10}/(k_9 + k_{10})$ is the aquation quantum yield for the reactive excited state populated by energy transfer. As shown in Figures 2 and 3 the experimental data fit the above relation in the form

$$\frac{1}{\phi_{obsd}} = \frac{1}{\phi_{st}\phi_c} + \frac{k_5 + k_6 + k_7[O_2]}{\phi_{st}\phi_c k_8} \frac{1}{[C]} \qquad (13)$$

where $[C] = c_0/\beta$. ϕ_{st} is reported to range between 0.65 and 0.80 in ethanol solution at room temperature.[38-40] With $\phi_{st} = 0.72 \pm 0.08$ and assuming that it is not affected either by the hydroalcoholic medium or by the presence of the paramagnetic chromium(III) ions, the values of ϕ_c can be calculated. These are reported in Table I and are comparable with the quantum yields of direct photolysis for both complex ions. The sum of the rate constants ($k_5 + k_6$) represents the spontaneous triplet decay in the absence of any extraneous quencher and is, at 20°, 7.5 × 10³ sec⁻¹ in water[41] and 1.7 × 10⁴ sec⁻¹ in ethanol.[42] In any case it is sufficiently smaller (by a factor of approximately 100) than the product $k_7[O_2]$, to be reasonably neglected. The order of magnitude of the bimolecular quenching constant for oxygen is, in fact, expected to be that of the diffusion-controlled processes. Also, any bimolecular self-quenching of naphthalene can be safely neglected in the range of concentration and light intensity used. The bimolecular annihilation constants for naphthalene in water at 20° are 4 × 10⁹ M^{-1} sec⁻¹ for the ($^3N^* + {}^3N^*$) process[41] and less than 10⁶ M^{-1} sec⁻¹ for ($^3N^* + {}^1N$).[43] Thus, in air-equilibrated solutions, the slope of eq 1 is virtually determined by the competition of two bimolecular quenching processes: by oxygen and by the chromium(III) complex. It is sufficient that the oxygen content be decreased by a factor of 100 for the slope to become unappreciable within our precision limits. Now, more than 99% of naphthalene triplets are quenched by the complex ions, but it is not possible to determine k_8 because of the absence of comparable competition of dissolved oxygen. In air-equilibrated solutions

it is then possible to evaluate k_8, provided k_7 is known. Unfortunately, reliable data for water-ethanol have not been reported and calculated k_8 values are imprecise due to multiplication of quantities themselves having errors (see eq 13), although their ratios would not be subject to so great an error. Very recently, several bimolecular quenching constants of organic triplets by chromium(III) complexes have been determined by flash spectroscopy[44] and one of the systems studied was precisely naphthalene-Cr(NH₃)₅-Cl²⁺ in 50% water-ethanol. Using this datum and still assuming that the quenching process corresponds entirely to energy transfer, the rate constants for the other acceptors and for O_2 can be determined. They are reported in Table I. k_7 is found to be somewhat smaller than the diffusion-controlled rate constant ($k_d = 6 \times 10^9$ M^{-1} sec⁻¹ in 50% water-ethanol at 20°), but this is in agreement with the known behavior in hexane solution (where the oxygen quenching constant is $k_q = 4 \times 10^9$ M^{-1} sec⁻¹,[41] whereas $k_d = 2 \times 10^{10}$ M^{-1} sec⁻¹) or in the gas phase ($k_q = 2 \times 10^9$ M^{-1} sec⁻¹; collision rate = 3 × 10¹¹ M^{-1} sec⁻¹).[45] k_8 is larger for the dipositive chloropenta-amminechromium(III) ion than for the tripositive hexaamminechromium(III). This agrees with the literature findings that, generally, less positively or negatively charged complex ions have larger quenching ability and that neutral species quench organic triplets with a rate close to the diffusion-controlled process.[6,8,44] As has been pointed out,[46] solvation effects play an important role in these phenomena. The thicker the solvation sphere, the less effective the encounter between triplet donor and quencher due to the decrease of their orbital overlap. Ion pairing might have a similar shielding action and could account for the difference between the perchlorate and the nitrate salts. ϕ_c is independent of the nature of the anion, at least for the system examined; thus the energy transfer process is more sensitive to ion pairing than the photochemical reaction which follows.

Energetic requirements and the spin conservation rule allow the transfer of excitation energy from the naphthalene triplet to both the first quartet and doublet excited states of the chromium(III) species,

(38) C. A. Parker and T. A. Joyce, *Chem. Commun.*, 234 (1966).

(39) A. R. Horrocks, T. Medinger, and F. Wilkinson, *ibid.*, 452 (1965).

(40) A. R. Horrocks and F. Wilkinson, *Proc. Roy. Soc., Ser. A*, **306**, 257 (1968).

(41) G. Porter and M. R. Wright, *Discuss. Faraday Soc.*, **27**, 18 (1959).

(42) G. Porter and M. W. Windsor, *Proc. Roy. Soc., Ser. A*, **245**, 238 (1958).

(43) H. Linschitz, C. Steel, and J. A. Bell, *J. Phys. Chem.*, **65**, 2574 (1962).

(44) H. F. Wasgestian and G. S. Hammond, *Theor. Chim. Acta*, **20**, 186 (1971).

(45) G. Porter and P. West, *Proc. Roy. Soc., Ser. A*, **279**, 302 (1964).

(46) H. Linschitz and L. Pekkarinen, *J. Amer. Chem. Soc.*, **82**, 2411 (1960).

whose energy levels are reported in Table II. In view of the quartet state distortion[47] the thermally equilibrated $^4T_{2g}$ state is expected at a lower level than can be deduced from the absorption maxima. For the analogous $Cr(NH_3)_5NCS^{2+}$ ion, the ratio ϕ_{NH_3}/ϕ_{NCS^-} is lower in the doublet than in the quartet region[28] and biacetyl sensitization increases this ratio greatly.[7] It was deduced that only NH_3 photoaquation takes place from the thermally equilibrated quartet state, which photosensitization can populate with "purer" electronic energy.[7] No data are available for the photolysis of $Cr(NH_3)_5Cl^{2+}$ on irradiation of the doublet features, and the small amount of free Cl^- plus the analytical limitations make it impossible to determine the ratio of ammonia to chloride sensitized photoaquation with the desired precision. However, this is at least as high, if not even higher, than in direct photolysis. It is possible that in the present case, as inferred from the similarity of the quantum yields, a smaller difference exists between the direct

Table II: Excited-State Energies (kcal/mol)

Species	Triplet	$^4T_{2g}$	^2E_g
Naphthalene	60.9[a]		
$Cr(NH_3)_6^{3+}$		61.7[b]	43.5[b]
$Cr(NH_3)_5Cl^{2+}$		55.7[b]	42.5[b]

[a] From ref 18b, p 182.   [b] Absorption band maxima.

and the sensitized photoaquation, due to the energy matching between the naphthalene triplet and the quartet states of the complexes (as computed from the band maxima).

(47) A. W. Adamson, *J. Phys. Chem.*, 71, 798 (1967).

Pulse Radiolysis of Aqueous Alkaline Sulfite Solutions

by Z. P. Zagorski, K. Sehested,[*1] and S. O. Nielsen

Accelerator and Chemistry Departments, Danish Atomic Energy Commission, Research Establishment Risö, Roskilde, Denmark   (*Received February 16, 1971*)

Publication costs assisted by the Danish Atomic Energy Commission

$G(-O_2)$ was measured polarographically in 1 N sodium hydroxide solutions with different concentrations of sulfite and oxygen and at different dose rates. A mechanism for the chain oxidation of sulfite is proposed. The SO_3^- radical formed in the reaction $O^- + SO_3^{2-}$ reacts with oxygen and forms a radical SO_5^-, which reacts with sulfite and yields sulfate and O^-. The O^- radical is the chain carrier. The study showed that O_2^- does not react with sulfite, but O_3^- does, and the rate constant was determined to be $k(SO_3^{2-} + O_3^-) = (3.5 \pm 1.0) \times 10^4\ M^{-1}\ sec^{-1}$. The spectrum of the SO_3^- radical was obtained in a N_2O-saturated solution giving a λ_{max} 260 nm and a molar absorptivity $\epsilon_{260} = 1300 \pm 200\ M^{-1}\ cm^{-1}$. The rate constant of the O^- reaction with sulfite was determined from the competition with oxygen. On the basis of $k(O^- + O_2) = 3 \times 10^9\ M^{-1}\ sec^{-1}$, we obtained $k(O^- + SO_3^{2-}) = (2.5 \pm 0.5) \times 10^8\ M^{-1}\ sec^{-1}$. Also in N_2O solutions a chain oxidation of sulfite took place yielding G values of several thousands. This means that SO_3^- reacts with N_2O, yielding O^-, and the rate constant was found to be $k(SO_3^- + N_2O) = (3.5 \pm 1.0) \times 10^7\ M^{-1}\ sec^{-1}$. The e_{aq}^- reacts with sulfite in Ar-saturated solutions with a rate constant $k(e_{aq}^- + SO_3^{2-}) \leq 1.5 \times 10^6\ M^{-1}\ sec^{-1}$.

Introduction

In contradistinction to acid and neutral media, strongly alkaline solutions of sulfites react only slowly with oxygen and thus permit a study of these thermodynamically unstable systems. Zagorski reported in 1961 that γ irradiation causes the reaction $2SO_3^{2-} + O_2 \rightarrow 2SO_4^{2-}$ to proceed with G values reaching 1000.[2] When the reaction was followed polarographically in the radiation field, it was found to proceed stoichiometrically with the production of sulfate. For aerated as well as deaerated solutions hydrogen is produced at a constant yield of $G(H_2) = 0.44 \pm 0.02$.

The influence of CO_3^{2-}, Cl^-, or of varying concentrations of SO_3^{2-} was found to be negligible, but the presence of H_2O_2 and some organics shortened the chain. If organic substances are present in concentrations comparable to that of oxygen, the G value of oxygen consumption is reduced to a few units. The reaction mechanism proposed at that time is not adequate today.

Schönherr, *et al.*,[3] have reported a $G(SO_3) = 2.8$

(1) To whom correspondence should be addressed at Danish Atomic Energy Commission, Research Establishment Risö, DK-4000 Roskilde, Denmark.

(2) Z. P. Zagorski, *Nukleonika* (*Warsaw*), 6, 587 (1961).

in liquid SO_2 saturated with O_2, but with addition of water the G increases above 8, corresponding to a short-chain reaction. Chantry, et al.,[4] have examined single crystals of dithionate and of salts containing the $-SO_3^-$ group after γ irradiation and have found a single esr line with an isotropic g factor of 2.004 and a corresponding ultraviolet absorption at 270 and 240 nm. The esr and uv spectra have been assigned to the SO_3^- radical. Adams and Boag[5] have found a transient with maximum absorption about 720 nm in an oxygen-saturated solution of 0.5 M SO_3^{2-}. They have attributed this absorption to an electron adduct, HSO_3^{2-}. Dogliotti and Hayon[6] have investigated sulfite and dithionate solutions at neutral pH using photochemical methods and have found the same transient, λ_{max} 720 nm decaying with first-order kinetics, both when oxygen was present and absent, but not in N_2O solutions. Furthermore they have found a transient absorption with λ_{max} 275 nm, which they attributed to the SO_3^- radical. The decay was second order with $2k/\epsilon = 2.0 \times 10^6$ cm sec^{-1} for sulfite and $2k/\epsilon = 3.5 \times 10^6$ cm sec^{-1} for dithionate solution. The existence of a chain reaction and a rapid thermal reaction between sulfite and oxygen have not been taken into account. Haber and Wansbrough-Jones[7] have postulated from the photochemistry of sulfite in absence of oxygen the reaction $SO_3^- + SO_3^-$ $\rightarrow S_2O_6^{2-}$, but because of the very low quantum yield (0.07) of dithionate, they suggested the possibility of the "back reaction" $SO_3^- + H \rightarrow HSO_3^-$. Anbar and Hart[8] have measured the rate constant of the reaction between the hydrated electron and sulfite to be less than 1.3×10^6 M^{-1} sec^{-1}. In the present work we describe an investigation of the sulfite oxidation in strongly alkaline solutions, 1 N NaOH. Sulfite is oxidized in a chain reaction, and the chain length was determined by the disappearance of oxygen measured polarographically. To determine the reaction mechanism, solutions with and without oxygen were studied by pulse radiolysis using spectrophotometric monitoring. Some of the important rate constants were determined, and a reaction mechanism is proposed.

Experimental Section

In the polarographic spectrum only O_2 and H_2O_2 can be followed. The polarographic activity of N_2O does not interfere with the determination of O_2 or H_2O_2. The time resolution of the polarographic method is, however, at the present stage low and can only follow phenomena lasting longer than 0.1 sec (or down to 10 msec with oscillographic techniques).[9] Therefore polarography was only used for determination of the O_2 concentration before and after the pulse, permitting a calculation of $G(-O_2)$.

Spectrophotometry has excellent time resolution but cannot be used for determination of the oxygen

concentration. The wavelength region available for measurement of intermediates in the uv is limited by OH^- absorption; if sulfite is present, the limitation is even greater. The sulfite ion does not show any absorption maximum, but the absorption curve increases steeply in uv. Absorption of HO_2^- appears from 350 nm and downward. The molar absorptivity of HO_2^- (Jortner and Stein[10] and Landolt-Börnstein[11]) is 180 M^{-1} cm^{-1} at 260 nm.

Known methods for the determination of low SO_3^{2-} concentrations in strongly alkaline solutions are not very reliable. The concentrations were measured by determining the wavelength at which the absorption equals 1.00. A Cary 15 spectrophotometer was used, and the accuracy is comparable with that of other methods and even superior at concentrations of 1–10 mM SO_3^{2-}. SO_4^{2-} did not interfere with the determinations.

The results from the polarographic and the spectrophotometric measurements supplement each other. Application of pulsed spectroscopy and polarography simultaneously was not attempted in the present setup. Therefore parallel determinations were performed, the polarographic measurement giving the $G(-O_2)$ value and the spectrophotometric determinations giving the absorption of intermediates.

Polarographic Measurement. A PO4 polarograph (Radiometer, Copenhagen) was used, with a conventional dropping mercury electrode. Currents obtained with various electrode characteristics were normalized on the basis of a linear relationship of the O_2 diffusion current and the constant solubility of O_2 in solutions at fixed NaOH concentration and well-defined temperature and oxygen pressure.

Two kinds of vessels were used. The conventional radiometer, Type E69, was used for purity test, O_2 current measurements, and for determination of the "dark" reaction between oxygen and sulfite. A special vessel was designed to obtain the same geometry and dimensions as those of the optical cell used in the spectrophotometric measurements. The polarographic cell was emptied by opening of a magnetic valve at the bottom of the vessel, thus draining the solution and the

(3) S. Schönherr, R. Schrader, and P. Mahlitz, *Z. Anorg. Allg. Chem.*, **365**, 262 (1969).

(4) G. W. Chantry, A. Horsfield, J. R. Morton, J. R. Rowlands, and D. H. Whiffen, *Mol. Phys.*, **5**, 233 (1962).

(5) G. E. Adams and J. W. Boag, *Proc. Chem. Soc.*, 112 (1964); G. E. Adams, J. W. Boag, and B. D. Michael, *Trans. Faraday Soc.*, **61**, 1674 (1965).

(6) L. Dogliotti and E. Hayon, *J. Phys. Chem.*, **72**, 1800 (1968); L. Dogliotti and E. Hayon, *Nature (London)*, **218**, 949 (1968).

(7) F. Haber and O. H. Wansbrough-Jones, *Z. Phys. Chem. (Leipzig)*, **18B**, 103 (1932).

(8) M. Anbar and E. J. Hart, *Advan. Chem. Ser.*, **No. 81**, 79 (1968).

(9) Z. P. Zagorski and K. Sehested, Risö Report No. 114 (1965).

(10) J. Jortner and G. Stein, *Bull. Res. Council Israel, Sect. A*, **6**, 239 (1957).

(11) Landolt-Börnstein, "Zahlenwerte und Funktionen aus Naturwissenschaften und Technik," Springer, Berlin, 1964.

mercury, while at the same time the cell was filled with an appropriate gas.

Both polarographic cells were equipped with a sintered-glass diaphragm and a bridge connecting the solutions with the saturated calomel reference electrode. The sce had a large working area (approx. 30 cm²) making it possible to work for several hours with currents up to tens of microamperes without resulting in changes of potential.[12] The total electrical resistance of the cell was below 100 ohms; corrections for potential drop are then unnecessary at constant potential measurements.[13] The electrode potential was kept at -0.65 V (sce) for O_2 measurements. At this potential the O_2 current is not affected by O_2 maximum, electrocapillary zero phenomena, or the second oxygen wave. At sulfite concentrations lower than 100 mM there is no influence of SO_3^{2-} on the polarographic wave.

Pulse Radiolysis. The equipment has been described by Christensen, *et al.*[14] Throughout the work a two-pass cell (light path 5.2 cm) with the optical axis coinciding with the electron beam was used. As in the case of the polarographic measurements, the syringes were usually without gas phase. In systems showing rapid thermal reaction between SO_3^{2-} and O_2 (*i.e.*, at SO_3^{2-} concentrations of more than 20 mM) the solution in the syringe was continuously saturated with O_2.

Spectra and kinetic studies at longer wavelengths were recorded using a Jena filter WG7 which practically cut off all light below 300 nm. In the short-wave region we prepared a sulfite solution "filter" in a 5-mm quartz cell filled with a concentration of Na_2SO_3 at least ten times greater than that of the solution investigated. This filter gave complete protection against photolysis and had a very sharp cut-off in the region 230–270 nm.

The Varian linear accelerator[15] gives an electron pulse with a rise and fall time of 0.2 μsec. The electron energy is 10 MeV. The peak current in the pulse is 250 mA, and the pulse length was usually 0.5 μsec except for some dose rate measurements in which it was varied from 0.25 to 4 μsec. The dose was 3–4 krads/pulse in a 0.5-μsec pulse.

The dosimetry in the polarographic experiments was performed with the "Super-Fricke" dosimeter.[16] After irradiation the solution was transferred to a Cary 15 spectrophotometer; in some cases a direct polarographic measurement of the Fe^{III} current was used. In the pulse radiolysis measurements a solution of 10^{-3} M $K_4Fe(CN)_6$ saturated with N_2O and equilibrated with 5 ml of air per 100 ml of solution was used.[17] A WG6 optical filter was applied, and ϵ of $Fe(CN)_6^{3-}$ was taken to be 1000 at 420 nm and $G = 5.3$.

All solutions were prepared directly in the syringes. Transfer of a solution into another syringe was only done to achieve desired concentrations of two gases
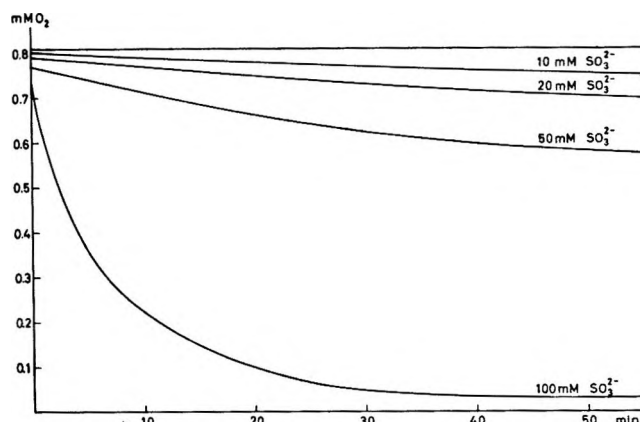
Figure 1. Disappearance (thermal reaction) of oxygen at different sulfite concentrations. All curves recalculated from continuous records on the polarograph of the O_2 current.

(*e.g.*, $O_2 + N_2O$). Different brands of sodium hydroxide were tested, and Merck (item 6498) was found to be the best for our purpose in spite of a 1% content of carbonate. $Ba(OH)_2$ could not be used because of the radiolytic production of sulfate. The following reagent grade chemicals (Merck) were used without further purification: Na_2SO_3, Na_2SO_4, and Na_2O_2. The N_2O was in some cases purified by bubbling through an alkaline pyrogallol solution, and no oxygen could be detected by polarography. The water was purified by conventional three-stage distillation, and all glassware was prebaked at 500°. A cleaning mixture of sodium hydroxide (1–5 M) and Na_2O_2 was used. The temperature during irradiation was kept at 25 ± 3°.

The computations were carried out on the Risö GIER computer with a fifth-order Runge-Kutta method for solving of the differential equations representing the course of the radiolytic reactions in aqueous solutions.[18]

Results

The thermal ("dark") reaction, $SO_3^{2-} + O_2$, was measured by constant potential polarography at -0.65 V (sce) after saturation with oxygen, air, O_2–Ar, or O_2–N_2O. We did not study the nature of this reaction; the measurements were only performed to find the limits of concentrations that could be used.

(12) Z. P. Zagorski, *Advan. Polarography*, **3**, 1132 (1960).

(13) Z. P. Zagorski, "Analiza Polarograficzna," Polarographic Analysis, 2nd ed, PWN, Warsaw, 1970, and Z. P. Zagorski, "Proceedings of the Third International Congress on Polarography," McMillan, London, 1966, pp 653–660.

(14) H. C. Christensen, G. Nilsson, P. Pagsberg, and S. O. Nielsen, *Rev. Sci. Instrum.*, **40**, 786 (1969).

(15) A. Brynjolfsson, N. W. Holm, G. Thärup, and K. Sehested, "Industrial Uses of Large Radiation Sources," Proceedings, Salzburg, May 27–31, 1963, **2** (IAEA, Vienna, 1963), pp 281–295.

(16) K. Sehested in "Manual on Radiation Dosimetry," N. W. Holm and R. J. Berry, Ed., Marcel Dekker, New York, N. Y., 1970, pp 313–317.

(17) J. Rabani and M. S. Matheson, *J. Phys. Chem.*, **70**, 761 (1966).

(18) K. Sehested, E. Bjergbakke, O. L. Rasmussen, and H. Fricke, *J. Chem. Phys.*, **51**, 3159 (1969).
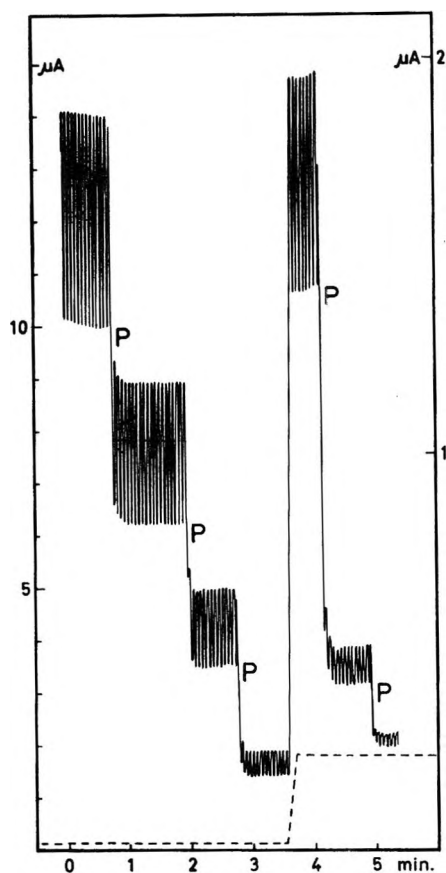
Figure 2. Polarographic record of the O_2 current in pulsed
irradiation. System: 1 N NaOH, 10 mM SO_3^{2-},
oxygen-saturated, 4.3 krads/pulse. After the third pulse
the sensitivity was increased 7.5 times.

Figure 3. $G(-O_2)$ in the first pulse as function of dose per pulse.
System: 1 N NaOH, 20 mM SO_3^{2-}, 0.5 mM O_2 as initial
concentration. Pulse length 0.5–4 μsec.

Figure 1 shows the rate of O_2 disappearance at different
SO_3^{2-} concentrations. The results did not differ
appreciably from what had been obtained previously.[2]
We are not able to offer an explanation of the results
in 100 mM solutions, because the mechanism of the
reaction is not known in detail.[19] Lower concentra-
tions of OH^- increased the rate, whereas lower con-
centrations of oxygen and lower temperature decreased
the rate. The O_2 consumption was enhanced by uv
light and initiated by intermediate products of the
electrode O_2 reactions. This took place only at
-1.0 to -1.5 V (sce) potentials and high SO_3^{2-}
concentrations. Neither this effect nor the presence
of the mercury electrode changed the measured radia-
tion yields. This was proved by an indirect determina-
tion of the chain length. The appearance of the elec-
tron absorption in spectrophotometric measurements
after a few pulses showed O_2 disappearance with G
values corresponding to those measured by polarog-
raphy.

In the polarographic measurements the O_2 current
was continuously recorded before every pulse. The
pulse caused a very sharp drop of the O_2 current,
Figure 2. The current is recalculated into O_2 con-
centration and $G(-O_2)$. The measured G values

were between 10 and 1000 with a precision of $\pm 10\%$.
The O_2 disappearance depended on the SO_3^{2-} and O_2
concentrations. Decreasing of the concentrations de-
creased the G value. Increased dose per pulse also
caused a decrease in $G(-O_2)$, but the change in pulse
length from 0.4 to 4.0 had no influence if the dose was
kept constant. The $G(-O_2)$ in Figure 3 is plotted
$vs.$ the dose/pulse. At low doses the yield approaches
the G value obtained in ^{60}Co γ irradiation for the same
concentrations of SO_3^{2-} and O_2. At doses higher
than 20 krads/pulse the curve seemed to level out with
a G value of about 16.

The influence of N_2O on the $G(-O_2)$ in alkaline
solutions was a drastic increase in the disappearance
of O_2. At equal amounts of O_2 and N_2O the O_2 was
practically consumed after the first pulse. Even
different concentrations (2–20 mM) of sulfite, oxygen,
and N_2O, and different doses exhibited almost the
same result. Without oxygen, N_2O produced a chain
oxidation of sulfite with G values exceeding several
thousand. The hydrogen peroxide caused a decrease
in the O_2 consumption, which has previously been
shown in γ-irradiation experiments. Equal amounts
of HO_2^- and O_2 lowered the $G(-O_2)$ by half, and 10
mM HO_2^- and 1 mM O_2 almost quenched the chain
oxidation of sulfite. H_2 added to the solution before
irradiation had a slight effect on the chain length.
At 0.5 atm H_2 there was a small decrease in $G(-O_2)$.

In oxygen-saturated solutions there were two peaks
in the ultraviolet region: one at 430 nm and one at
250–260 nm. The one at 430 nm was attributed to the
O_3^-.[20] The extinction coefficient was about the same
as that found by Czapski[20] ($\epsilon \simeq 1900$ M^{-1} cm^{-1}).
The half-width was slightly smaller (105 nm). The

(19) R. B. Mason and J. H. Mathews, $J.$ $Phys.$ $Chem.$, 30, 414
(1926).

(20) G. Czapski, "Radiation Chemistry of Aqueous Systems, Pro-
ceedings of the 19th L. Farkas Memorial Symposium, Jerusalem,
Dec 27–29, 1967," G. Stein, Ed., Weizmann Science Press of
Israel, Jerusalem, 1968, pp 211–227.
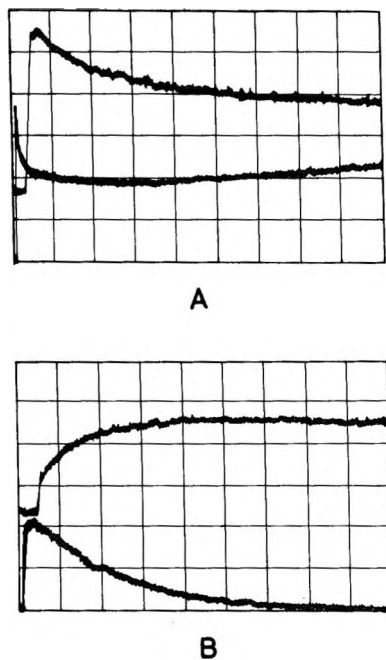
Figure 4.   Optical traces at A, 285 nm; B, 430 nm.   Upper traces in both pictures 20 μsec/div, lower 500 μsec/div. Absorption 2.5%/div.   System: 1 N NaOH, 20 mM SO_3^{2-}, oxygen-saturated, first pulse.

Figure 5.   Absorption spectra of SO_3^- in N_2O-saturated solutions, 1 N NaOH, dose 2 krads, optical path length 5.2 cm.

peak at 260 nm was the same as Dogliotti and Hayon[6] found at 275 nm and assigned to SO_3^-.   The initial optical densities at both peaks depended on the sulfite concentration.   At 260 nm the initial optical density was increased, whereas at 430 nm the optical density decreased by increasing of the sulfite concentration. The absorption at 260 nm decayed in 0.1–1 msec (depending on the sulfite concentration) and it reached a minimum, after which it increased very slowly (Figure 4).   At 430 nm the absorption increased with time until it reached a maximum after 50–100 μsec. It then decayed in the millisecond range.   The build-up kinetics at 430 nm were similar to the fast-decay kinetics at 260 nm.   The kinetics were neither first nor second order.   The absorption at the maximum at 430 nm depended on the sulfite concentration, $i.e.$, high SO_3^{2-} concentration, low absorption.   The decay of O_3^- became pseudo first order with respect to sulfite concentration.   There was no absorption in the visible range at 720 nm where Adams[5] and Dogliotti[6] had found an absorption in the neutral O_2^- and air-saturated solution.   In N_2O-saturated solutions only the peak at 260 nm was observed.   This peak was sulfite concentration dependent, and the maximum was shifted from shorter wavelength to 260 nm when the SO_3^{2-} concentration was increased (Figure 5).   The absorption built up in a few microseconds.   The half-time in 2 mM SO_3^{2-} was 1.5 μsec.   The decay kinetics were of mixed order like the kinetics in O_2 solutions, but in N_2O solutions the species decayed to zero within 100–500 μsec, depending on sulfite concentration.

The absorption without SO_3^{2-} is that of O^-.

After the end of the pulse, this absorption increased in the first 50 μsec due to $e_{aq}^- + N_2O$.   This indicates a relatively long-lived intermediate in the reaction of hydrated electrons with nitrous oxide in strongly alkaline media.

In Ar-saturated solution the hydrated electron absorption was observed at 700 nm, and without sulfite its half-life was 3.5 μsec.   If we increased the sulfite concentration, we increased the half-life of the electron, and the kinetics went into pseudo-first-order kinetics with sulfite.

Discussion

In the oxygen-saturated solution the spectrum of SO_3^- is overlapped by the spectrum of O_2^- produced from e_{aq}^- reacting with O_2.   Furthermore, we have the O_3^- absorption, so a much cleaner spectrum of SO_3^- radical ions is obtained from the N_2O-saturated solution.

In Figure 5 the absorption spectra are presented for different sulfite concentrations from zero to 20 mM in N_2O solution.   The extinction is increased by increasing of the concentration, and the maximum is shifted 10–20 nm.   In this solution we have a chain reaction with $G(-SO_3^{2-})$ of several thousand measured after γ irradiation.   The reactions are assumed to be

$$SO_3^{2-} + O^- \xrightarrow{H_2O} SO_3^- + 2OH^- \qquad (1)$$

$$SO_3^- + N_2O \longrightarrow SO_3 + O^- + N_2 \qquad (2)$$

$$SO_3 + 2OH^- \longrightarrow SO_4^{2-} + H_2O \qquad (3)$$
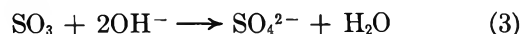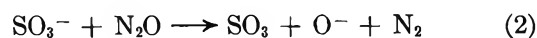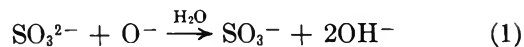
From these three reactions it is seen that SO_3^- and O^- are present at the same time.   By increasing of the sulfite concentrations the reactions are pushed toward SO_3^- radicals only.   The results from 10 and 20 mM sulfite show that 80 to 90% of the total radicals are SO_3^-.   If we take the optical densities for 0, 2, 5, 10, and 20 mM sulfite, calculations show that the extinction of 20 mM sulfite has to be corrected by about 10% for the O^- concentration.   The computations are

based on reactions 1 and 2 and the rate constant $k_1 =$ 2.5 $\times$ 10^8 M^{-1} sec^{-1} (see later). The best fit to the experimental values at 260 nm is obtained with $k_2 =$ (3.5 $\pm$ 1.0) $\times$ 10^7 M^{-1} sec^{-1} and with an extinction coefficient of the SO_3^- radical of $\epsilon_{260} = 1300 \pm 200$ M^{-1} cm^{-1}. The results are shown in Table I. With no corrections for O^- the directly measured extinction equals 1180 M^{-1} cm^{-1}. The rate constant k_1 is calculated from the results from oxygen-saturated solution by using the initial absorptions at 430 nm for different sulfite concentrations. The two competing reactions are reactions 1 and 4

$$O^- + O_2 \longrightarrow O_3^- \qquad k_4 = 3 \times 10^{9\ 20} \qquad (4)$$

The equation for the competition in reactions 1 and 4 is[21]

$$\frac{D_0}{D} = 1 + \frac{k_1[SO_3^{2-}]}{k_4[O_2]}$$

where D_0 is the optical density at 430 nm at a time 1 μsec after the pulse in solutions containing no sulfite ions, and D is the optical density under the same conditions, but with sulfite ions added. The plot of D_0/D as a function of $[SO_3^{2-}]/[O_2]$ gives a straight line with intercept 1 and a slope $k_1/k_4 = 0.083$, which gives a rate constant $k_1 = (2.5 \pm 0.5) \times 10^8$ M^{-1} sec^{-1} (Figure 6).

Table I: Measured and Calculated Optical Absorption at 260 nm, Dose 2 krads, Optical Path Length 5.2 cm

	Measured	Calculated
2 mM SO_3^{2-}	0.0375	0.0383
5 mM SO_3^{2-}	0.0610	0.0624
10 mM SO_3^{2-}	0.0745	0.0713
20 mM SO_3^{2-}	0.0780	0.0785

The buildup in 2 mM SO_3^{2-} N_2O-saturated solution has a half-life of 1.5 μsec corresponding to an estimated $k_1 = 2.2 \times 10^8$ M^{-1} sec^{-1}.

According to Gall and Dorfman[21] O_3^- is in equilibrium with O^- and oxygen, and the rate constant for the dissociation of O_3^- is $k = (3.3 \pm 0.3) \times 10^3$ sec^{-1}. The O_3^- disappeared in a pseudo-first-order reaction with sulfite, which is interpreted as a direct reaction between O_3^- and SO_3^{2-}, because a reaction of O^- with sulfite would reform O_3^- through the reactions 1, 6–8. The direct reaction is assumed to be

$$O_3^- + SO_3^{2-} \longrightarrow SO_4^{2-} + O_2^- \qquad (5)$$
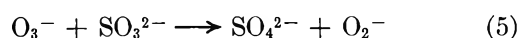
From a first-order plot we obtained the rate constant $k_5 = (3.5 \pm 1.0) \times 10^4$ M^{-1} sec^{-1} (Table II). This rate constant is slightly dependent on OH^- concentration, as Czapski and Dorfman[22] have also found for the rate of O_3^- disappearance in oxygenated alkaline solutions. Reaction 5 is consistent with the slow

Figure 6. Plot of the competition reaction of O^- between O_2 and SO_3^{2-}. Optical density measured 1 μsec after pulse end at 430 nm. Concentration of $O_2 = 0.8$ mM. $k(O^- + O_2) = 3 \times 10^9$ M^{-1} sec^{-1}.[21]

Table II: Rate Constant $k_5(O_3^- + SO_3^{2-})$ M^{-1} sec^{-1} in Solutions of Different Concentrations of SO_3^{2-} and OH^-

	0.1 N OH$^-$	0.5 N OH$^-$	1 N OH$^-$	2 N OH$^-$
10 mM SO_3^{2-}	...	...	4.5 $\times$ 10^4	...
20 mM SO_3^{2-}	2.75 $\times$ 10^4	2.95 $\times$ 10^4	3.6 $\times$ 10^4	4.1 $\times$ 10^4
40 mM SO_3^{2-}	...	...	3.5 $\times$ 10^4	...

(see later). The absorption was stable for minutes, which is consistent with O_2^-, if it does not react with sulfite. Furthermore, it also explains our results in the hydrogen peroxide solutions, where the chain oxidation of SO_3^{2-} is quenched because of the O_2^- formation.

The chain mechanism in the N_2O system is given by reactions 1–3. In the oxygenated system, we can assume that, beginning with reaction 1, a proper selection from the following reaction can be made to describe the buildup of O_3^- and the chain carrier.

increase in optical density at shorter wavelengths in oxygenated solutions (Figure 4). The spectrum from 250 to 300 nm resembles the tail of the O_2^- spectrum and the extinctions are about the same as for O_2^-

$$SO_3^- + O_2 \longrightarrow SO_5^- \quad \text{(Caro acid radical)} \qquad (6)$$
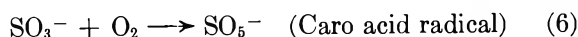
(21) B. L. Gall and L. M. Dorfman, *J. Amer. Chem. Soc.*, **91**, 2199 (1969).

(22) G. Czapski and L. M. Dorfman, *J. Phys. Chem.*, **68**, 1169 (1964).

$$SO_5^- + SO_3^{2-} \xrightarrow{2OH^-} 2SO_4^{2-} + O^- + H_2O \quad (7a)$$

$$SO_5^- + SO_3^{2-} \longrightarrow SO_4^{2-} + SO_4^- \quad (7b)$$

$$SO_4^- + O_2 \xrightarrow{2OH^-} SO_4^{2-} + O_3^- + H_2O \quad (8a)$$

$$SO_4^- + SO_3^{2-} \longrightarrow SO_4^{2-} + SO_3^- \quad (8b)$$
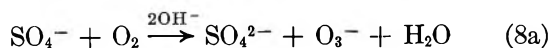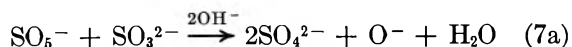
The sulfite radical reacts with oxygen and probably forms a complex (Caro acid radical) rather than causing an electron transfer. An electron transfer would yield O_2^-, which is contradictory to a chain reaction. The radical of Caro acid then reacts with a sulfite ion in the strongly alkaline media, giving sulfate and an O^- radical or an SO_4^- radical (reactions 7a and b). If the chain mechanism consists of 1, 6, and 7a, the O^- radical is the chain carrier as in the N_2O system, and reaction 4 is then responsible for the O_3^- buildup. If the reactions are 1, 6, and 7b, the produced SO_4^- radical must react with both O_2 and SO_3^{2-} (reactions 8a and b) to form O_3^- and SO_3^- radicals. Reaction 8a then explains the buildup of O_3^- and SO_3^- is the chain carrier. The SO_5^- radical has an absorption in the far-ultraviolet, but the extinction is much lower than that of the SO_3^- radical. The SO_4^- radical absorbs in the region 270–500 nm, and the extinction coefficients for the two radicals have been determined by Roebke, et al.,[23] and equals 300 M^{-1} cm^{-1} at 260 nm for SO_3^- and 700 M^{-1} cm^{-1} at 325 nm for SO_4^-.

Under our experimental conditions we cannot prove the existence of the SO_4^- radical, because of the absorption of SO_3^-, O_2^-, and O_3^-. At 325 nm, however, the optical density is very weak and the other radicals (SO_3^-, O_2^-, and O_3^-) are known to contribute to the absorption at that wavelength, and thus the concentration of SO_4^- has to be very low. This may indicate that SO_4^- radicals are not formed or that reactions 8a and b are much faster than the corresponding reactions for SO_3^- and SO_5^- (6 and 7a or b).

Subtracting the absorption at 260 nm of O_2^- formed in the reaction $e_{aq}^- + O_2$ and taking into account the amount of O_3^- formed for different SO_3^{2-} concentrations, we find an extinction coefficient for the SO_3^- radical in oxygenated solutions which is slightly lower than the 1300 M^{-1} cm^{-1} found in N_2O solutions. This is probably due to the lower extinction of the SO_5^- radical as compared to that of the SO_3^- radical. In 20 mM SO_3^{2-} solutions, where 30% of the O^- reacts with O_2, the extinction coefficient is measured to be 1150 M^{-1} cm^{-1}. From this the concentration of SO_5^- radicals present in 20 mM SO_3^{2-} is less than 15%. This means that the rate of reactions 6 and 7a or 6, 7b, 8a, and b is of the same order of magnitude as of reaction 2 in N_2O solutions. It is difficult to say which reaction is the rate-determining step, but reaction 6 is probably faster ($k_6 \sim 10^9$) than the sulfite radical reacting with N_2O (reaction 2).

The chain-terminating reactions are assumed to be

$$O^- + O^- \longrightarrow HO_2^- \text{ or } O_2^{2-} \quad k = 9 \times 10^8 \;{}^{24} \quad (9)$$

$$O^- + SO_3^- \longrightarrow SO_4^{2-} \quad k \simeq 9 \times 10^8 \quad (10)$$

$$O^- + HO_2^- \longrightarrow O_2^- + OH^- \quad k = 7 \times 10^8 \;{}^{24} \quad (11)$$

$$O^- + O_2^- \longrightarrow [O_3^{2-}] \longrightarrow O_2 + O^{2-} \quad k \simeq 10^9 \quad (12)$$

$$SO_3^- + SO_3^- \longrightarrow SO_3^{2-} + SO_3$$
$$k = 2.4 \times 10^9 \;{}^6 \quad (13)$$

$$SO_3^- + HO_2^- \longrightarrow SO_3^{2-} + O_2^- \quad k \simeq 10^8 \quad (14)$$

$$SO_3^- + O_2^- \longrightarrow SO_3^{2-} + O_2 \quad k \simeq 10^9 \quad (15)$$

$$SO_3^- + O_3^- \longrightarrow SO_4^{2-} + O_2 \quad (16)$$
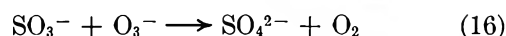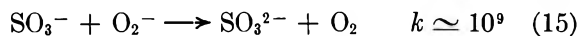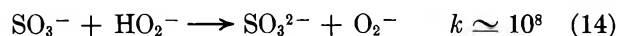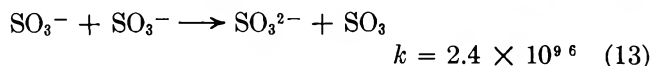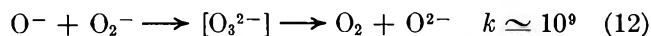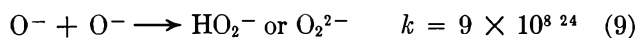
These reactions together with reaction 4 give an explanation of the increase in the measured $G(-O_2)$ values with decrease of dose rate. Computed values for different dose rates and for different concentrations of sulfite and oxygen are in fair agreement with the results for $G(-O_2)$ determined in the polarographic measurements, in spite of the fact that many of the rate constants have to be assumed. Reactions 11 and 14 explain why hydrogen peroxide quenches the sulfite oxidation in solutions where peroxide concentrations are comparable to the sulfite concentration.

Reactions 9, 10, and 13 and, in O_2 solutions, 12 and 15 are the important reactions at high dose rates. Computation shows that variation in pulse lengths from 0.5 to 4 μsec has little effect on the G values. At very high dose rates the G values are very low, but there still seems to be a short-chain reaction, which it is difficult to explain by the reactions proposed. Reaction 15 offers at the same time an explanation of a smaller absorption than expected of O_2^- after SO_3^- and O_3^- have decayed away. From a time 1 msec after the pulse where SO_3^- has disappeared, the increase at 285 nm (Figure 4) is about half of the decrease at 430 nm, which corresponds to $\epsilon_{O_2^-}^{285} \simeq 850$ M^{-1} cm^{-1}, in good agreement with reported values.[25]

Reactions 5 and 16 are responsible for the decay kinetics of the O_3^- radical. At higher concentrations of sulfite, the maximum is lower because of reaction 5. At higher dose rates the maximum is reached more quickly mainly because of reaction 16.

In the γ irradiation, the important reactions in O_2 solutions are 14 and 15, and because of the low concentrations of O_2^- and HO_2^- the chain is very long. In N_2O solutions the chain-breaking mechanism (reactions 9–14) is not very efficient before either N_2O or SO_3^{2-} is almost consumed.

In Ar-saturated solutions the e_{aq}^- reacts with SO_3^{2-}, but very slowly. The half-life of the e_{aq}^- is increased by increasing of the SO_3^{2-} concentration. The half-life in a 20 mM SO_3^{2-} solution is about 10

(23) W. Roebke, M. Renz, and A. Henglein, Int. J. Radiat. Phys. Chem., 1, 39 (1969).

(24) M. Anbar and P. Neta, Int. J. Appl. Radiat. Isotopes, 18, 493 (1967).

(25) J. Rabani and S. O. Nielsen, J. Phys. Chem., 73, 3736 (1969).

μsec, and at higher concentrations the decay kinetics become first order in sulfite. The rate constant for (17)

$$e_{aq}^- + SO_3^{2-} \longrightarrow \text{product} \qquad (17)$$
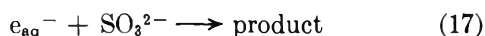
is estimated from the half-life of 9 μsec in 50 mM SO_3^{2-} to $k_{17} \leq 1.5 \times 10^6$ M^{-1} sec^{-1}, which is in agreement with 1.3×10^{-6} M^{-1} sec^{-1} found by Anbar and Hart.[8] The reason for examining e_{aq}^- in Ar-saturated solution was the possible exclusion of the reaction

$$O^- + SO_3^{2-} \longrightarrow SO_4^{2-} + e_{aq}^- \qquad (18)$$
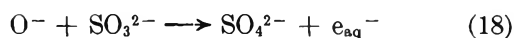
which would replace reaction 1. There are no indications at all at 700 nm of an additional e_{aq}^- production in Ar-saturated solution even with 40 mM SO_3^{2-}, so we are justified in leaving the reaction out of consideration. Furthermore, reaction 18 would be in contradiction to the proposed chain mechanism in O_2 solutions.

We feel confident that the absorption at 700 nm in the Ar-saturated solution is due to e_{aq}^- absorption (measured $\epsilon = 1.5 \times 10^4$ M^{-1} cm^{-1}) and not to the species HSO_3^{2-} (or SO_3^{3-}) as proposed by Adams and Boag[5] as responsible for the absorption at 720 nm in oxygen-saturated solutions. Dogliotti and Hayon[6] have not observed the transient in N_2O-saturated solutions, but, on adding N_2O, they have found an in- crease of more than a factor of 2 over the transient at 275 nm. The reason for the observation in air-saturated solutions is that the thermal oxidation of sulfite with oxygen in neutral media is so fast that the oxygen is consumed immediately. Recalculation of the data in Figure 1 (ref 6) with $\epsilon_{e_{aq}^-} = 1.58 \times 10^4$ M^{-1} cm^{-1} [26] gives an ϵ of about 1000 M^{-1} cm^{-1} for the absorption at 275 nm compared with ours of 1300 M^{-1} cm^{-1} at 260 nm. The first-order rate constant reported $k = 1.9 \times 10^4$ sec^{-1} in 20 mM SO_3^{2-} for the species absorbing at 720 nm, may be recalculated as a pseudo first order giving $k(e_{aq}^- + SO_3^{2-}) = 1 \times 10^6$ M^{-1} sec^{-1} compared with that of Anbar and Hart[8] of 1.3×10^6 M^{-1} sec^{-1} and ours of 1.5×10^6 M^{-1} sec^{-1}. From a competition study in which they used NO_3^- ions, Dogliotti and Hayon[6] have estimated the rate constant $k(e_{aq}^- + SO_3^{2-}) \leq 2 \times 10^6$ M^{-1} sec^{-1}.

(26) E. J. Hart, *Science,* 146, 19 (1964).

Autodetachment Lifetimes, Attachment Cross Sections, and Negative Ions

Formed by Sulfur Hexafluoride and Sulfur Tetrafluoride

by P. W. Harland and J. C. J. Thynne*[1]

Chemistry Department, Edinburgh University, Edinburgh, Scotland (*Received December 21, 1970*)

Publication costs borne completely by The Journal of Physical Chemistry

The formation of long-lived temporary negative ion states in sulfur tetrafluoride and sulfur hexafluoride has been studied. The autodetachment lifetimes of SF_4^{-*} and SF_6^{-*} are 16.3 ± 0.3 and 68 ± 2 μsec, respectively. The measured ratio of the cross sections for electron attachment to SF_6 and SF_4 was 109 ± 6; this leads to a value of $10.7 \pm 0.6 \times 10^{-17}$ cm^2 for the electron attachment cross section of sulfur tetrafluoride. This is some two orders of magnitude smaller than the cross section of the hexafluoride. The SF_3–F bond dissociation energy has been estimated to be ≤ 3.6 eV and a value of 2.9 ± 0.1 eV deduced for the electron affinity of sulfur trifluoride.

Introduction

When an electron interacts with a molecule, one of several processes may occur depending on the energy of the electron and the nature of the molecule. Of these, the processes which lead to negative ion formation are conventionally classified as (i) resonance capture, which occurs with low-energy electrons (usually 0–2 eV)
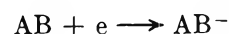
$$AB + e \longrightarrow AB^-$$

(ii) dissociative capture, the relevant electron energy range being $\sim$0–10 eV

$$AB + e \longrightarrow A^- + B$$
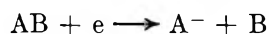
(iii) ion-pair formation which usually occurs with electrons of energies > 10 eV

$$AB + e \longrightarrow A^- + B^+ + e$$

As part of a study of negative ion formation by inorganic fluorides[2,3] we have examined sulfur tetrafluoride and sulfur hexafluoride. The latter molecule has been studied by several workers[4,5] who have noted an abundant parent ion SF_6^- to be formed at 0 eV, and this ion is frequently used to calibrate the electron energy scale. Sulfur tetrafluoride has not been previously examined for negative ion formation.

In electron impact studies, when the electrons are emitted from a heated filament, because of the energy spread of the ionizing electrons uncertainties may arise in the determination of the experimental ionization efficiency curves, the appearance potentials becoming "smeared out." To reduce the effects of this electron energy distribution analytical methods have been developed for positive[6] and negative ion[7] studies.

It has been shown recently that sulfur hexafluoride attaches an electron with a large cross section to form a relatively long-lived metastable ion whose lifetime may be investigated by a time-of-flight technique.[8,9] In preliminary experiments we also observed the formation of a temporary negative ion state with sulfur tetrafluoride, and accordingly we have compared the attachment cross sections and metastable lifetimes of both fluorides.

Experimental Section

The experiments were performed on a Bendix time-of-flight mass spectrometer, Model 3015. Ion source pressures were usually maintained below 5×10^{-6} Torr ($<2 \times 10^{-6}$ Torr for the lifetime studies). The electron energy was measured on a digital voltmeter. Use of two channels of the mass spectrometer analog output scanners enabled two mass peaks to be monitored simultaneously; this was of especial value in energy scale calibration since no switching between peaks was necessary. A small correction to the total SF_4^- current was made when SF_4 and SF_6 were both present in the ion source since electron bombardment of the latter produces some SF_4^-.

The electron current was held constant automatically over the electron energy range studied and ionization efficiency curves usually measured three to five times; the potentials at which the ions appeared were reproducible to ±0.1 eV, often better. The electron energy scale was calibrated at 0 eV using the SF_6^- ion formed by sulfur hexafluoride[4,5] and at higher energies using the appearance of the O^- ion from sulfur dioxide at 4.2 eV.[10,11]

The experimental data for the ionization efficiency curves were analyzed using the deconvolution method described previously.[7] In general it was found that performing 15 smoothing and 20 unfolding iterations on the basic data enabled satisfactory determination of appearance potentials, resonance peak maxima, and peak widths (at half peak height) to be made. The electron energy distribution, which was required to be known for the deconvolution procedure, was measured using the SF_6^- ion formed by sulfur hexafluoride.[4,5]

Lifetime Measurements. The method of Edelson, et al.,[8] was used to determine the mean lifetime of the metastable ions SF_4^{-*} and SF_6^{-*}. For ease of reference an outline of the technique employed is given below.

Negative ions, formed in the ion source as a result of electron capture, are accelerated through a variable electric field (usually 2–3 kV) into a field-free drift region, i.e., a flight tube (200 cm). If, during their passage down this tube, some of the metastable ions undergo autodetachment (i.e., eject electrons) both the remaining ions and the neutral molecules formed will continue moving at the same velocity and they will reach the detector simultaneously. If, however, a retarding potential is applied some time after the ions leave the ion source and enter the drift zone then the ion "packet" will be slowed down and the neutrals will pass on unaffected. The detector will therefore respond to two "packets" separated in time, one being the neutral species resulting from ion decomposition and the other being undecomposed ions. Variation of the ion flight time will cause the relative intensities of the two "packets" to vary and enable conclusions to be drawn regarding the lifetime of the negative ion state.

The ion flight time was measured directly for the various ions by triggering the oscilloscope on the leading edge of the ion draw-out pulse and reading the flight time off the oscilloscope.

It became apparent that the horizontal and vertical deflection plates and the ion lens in the flight tube discriminated substantially between the neutral and the parent ion and could result in quite erroneous lifetimes. As a consequence the focusing electrodes were main-

(2) J. C. J. Thynne, *J. Phys. Chem.*, **73**, 1586 (1969).

(3) (a) K. A. G. MacNeil and J. C. J. Thynne, *Int. J. Mass Spectrosc.*, **3**, 455 (1970); (b) K. A. G. MacNeil and J. C. J. Thynne, *J. Phys. Chem.*, **74**, 2257 (1970).

(4) W. M. Hickam and R. E. Fox, *J. Chem. Phys.*, **25**, 642 (1956).

(5) G. J. Schulz, *J. Appl. Phys.*, **31**, 1134 (1960).

(6) J. D. Morrison, *J. Chem. Phys.*, **39**, 200 (1963).

(7) K. A. G. MacNeil and J. C. J. Thynne, *Int. J. Mass Spectrosc.*, **3**, 35 (1969).

(8) D. Edelson, J. E. Griffiths, and K. B. McAfee, Jr., *J. Chem. Phys.*, **37**, 917 (1962).

(9) R. N. Compton, L. G. Christophorou, G. S. Hurst, and P. W. Reinhardt, *ibid.*, **45**, 4634 (1966).

(10) K. Kraus, *Z. Naturforsch. A*, **16**, 1378 (1961).

(11) J. G. Dillard and J. L. Franklin, *J. Chem. Phys.*, **48**, 2349 (1968).

tained at the drift-tube potential throughout the measurements, and so no preliminary separation near the ion source was employed. The time-of-flight adjust lens (188 cm from the ion source) which was used to separate the neutral and the ion peaks was shown to have a negligible focusing effect by comparing the separated ion currents (lens on) with the total ion current measured with the adjust lens off.

After the sample was leaked into the spectrometer, the apparatus was adjusted so that the resolved charged and neutral peaks were scanned repeatedly (usually about ten times) at 0 eV; the scans were then repeated using 70-V electrons so that the parent ions were formed by resonance capture of the secondary electrons formed during the positive ionization processes.[12] This procedure was repeated for all of the drift potentials consistent with adequate resolution of the peaks. Our measurements showed that, for a wide range of ion source conditions, no difference outside experimental error was noted between the studies made at 0 eV and those at 70 eV; in both cases the results were reproducible and self-consistent. This procedure was developed particularly so that ions of low capture cross-section could be examined under conditions such that the electron current necessary for ion detection was not incompatible with a long filament lifetime. The background to this situation was that in order to obtain sufficient electron current (25 nA) under conditions where the primary electron current at $\sim$0 eV was automatically regulated a relatively high current was required by the tungsten filament. This decreased markedly the filament lifetime. The secondary electron capture method (which required a lower filament current to produce the same electron current) was employed because of the much longer filament lifetimes obtained under these conditions. The fact that no difference was noted between results obtained at low and high electron energies suggests that no additional errors are introduced in the secondary electron capture method.

Autodetachment may be assumed to be a first-order process expressed by the relation

$$N^-(t) = N_0 \exp(-t/\tau)$$

where $N^-(t)$ is the number of ions surviving autodetachment after time t, N_0 is the original number of metastable ions undergoing acceleration = $N^-(t) + N^\circ(t)$, $N^\circ(t)$ is the number of neutrals formed by autodetachment after t, and τ is the mean lifetime of the negative ions. If no process other than autodetachment occurs, equal detection sensitivity of the neutral and the parent ion is assumed, and there is no discrimination due to stray fields or focusing by the time-of-flight ion optics, then the mean ion lifetime may be calculated from the equation

$$-\ln\left(1 - \frac{N^\circ(t)}{N^\circ}\right) = \frac{t}{\tau}$$

Measurements of N_0, $N^\circ(t)$, and t therefore yield the average lifetime of the metastable ion.

The assumption that autodetachment is the exclusive process requires that the following conditions are satisfied. (i) Collisional detachment or charge transfer does not take place in the flight tube. (ii) Detachment by grids in the path of the ion beam is negligible. Compton, et al.,[9] have shown such effects to be unimportant when the pressure in the flight tube region is $\sim$10^{-5} to 10^{-7} Torr. In our work we observed the neutral/parent ion ratio to increase with pressure above 8×10^{-6} Torr for SF$_6$. Since our work was carried out at pressures $<2 \times 10^{-6}$ Torr, this effect may be ignored.

It has been assumed above that the detector has the same sensitivity to charged and neutral particles of the same kinetic energy. Compton, et al.,[9] have suggested that this condition is fulfilled by employing single-pulse counting techniques to detect both the negative ions and the neutral molecules; we have used similar techniques in this work. Agreement between the lifetimes measured over a drift potential range of 2–4 kV[17,24] suggests that the above assumpton is reasonable and that effects resulting from attraction or repulsion of the ion pulse with the target or the contribution of the extra electron to the secondary current are negligible.

Results and Discussion

A. Autodetachment Lifetimes. 1. $C_6H_5NO_2$. As a check on the apparatus and procedure employed, we determined the autodetachment lifetime of $C_6H_5NO_2^{-*}$ since this has been measured previously.[9] The lifetime was measured at three different ion energies and our results are shown in Table I. A mean value of 47 ± 1 μsec was obtained; this may be compared with the results of 38 ±7 μsec previously reported.[9]

Table I: Lifetimes (τ) of Temporary Negative Ions at Various Ion Energies and Cross Sections for Electron Attachment

| Ion | Lifetime, μsec | | | τ_{av} | Cross section ($\times$ 10^{17} cm^2) |
	2 kV	2.5 kV	3 kV		
SF$_6^{-*}$	67.2	67.1	70.0	68 ± 2	1170 (ref 9)
SF$_4^{-*}$	16.1	16.6	...	16.3 ± 0.3	10.7
C$_6$H$_5$NO$_2^{-*}$	46.4	48.3	48.2	47.3 ± 1.0	

2. SF$_6$. Decomposition of the metastable SF$_6^{-*}$ ion was studied at three different ion energies from 2 to 3 kV, and a value of 68 ± 2 μsec was obtained for the mean autodetachment lifetime. Three other values have been reported for the SF$_6^-$ ion lifetime, namely 10,[8] 25,[9] and $\sim$500 μsec.[13] The first two values

(12) J. C. J. Thynne, *Chem. Commun.*, 1975 (1968).

(13) J. M. S. Henis and C. A. Mabie, *J. Chem. Phys.*, **53**, 2999 (1970).

were obtained using a similar technique to that employed in this work; the third value was determined using an ion cyclotron resonance (icr) spectrometer.[13] Regarding the differences between the values obtained by the time-of-flight technique, Compton, et al.,[9] have suggested that autodetachment lifetimes are very dependent on such factors as the different focusing properties of the neutral and charged particle and the prevailing ion source conditions, and in this context Naff[14] considers that differences of 100% in lifetimes are not to be unexpected. It may well be, however, that these differences arise, at least in part, from another source, namely in differences in the total energy of the system. Klots[15] has pointed out that SF_6^- ions, even when formed by monoenergetic electrons, will have a range of energies reflecting the thermal distribution of the original neutral molecules; therefore no unique detachment lifetime can be expected of such an ensemble. His calculations indicate that as the total excess energy of the system increases from 0.01 to 0.1 eV above the threshold, the autodetachment lifetime should change by an order of magnitude. Clearly small changes in the average energy of the attaching electrons could represent substantial changes in the total excess energy of the system and therefore show large changes in the ion lifetimes. This might, at least in part, explain the differences noted between the results of Edelson, et al.,[8] Compton, et al.,[9] and those of this work. The value of ~500 μsec obtained using the icr technique[13] seems difficult to reconcile with any of the time-of-flight values even when the effects of excess energy differences are taken into account. The icr value is very high and, in this respect, it should be noted that Henis and Mabie have reported the lifetime of $C_4F_8^-$ to be ~200 μsec, whereas both Compton[16] and unpublished results from this laboratory[17] have found the mean lifetime of the ion to be approximately 12 μsec. Lifschitz,[18] using a pulsed source magnetic sector mass spectrometer, has observed $C_4F_8^-$ to decay with a half-life of the order of 10–15 μsec. This is in very good agreement with the time-of-flight values. We are unable to explain the large differences with the icr results, and it would seem desirable that the icr technique be applied to other temporary negative ions so that a fuller comparison may be made of the results obtained by both procedures.

3. *SF₄.* The parent ion formed by sulfur tetrafluoride was much less abundant (under comparable ion source conditions) than the SF_6^- ion formed by sulfur hexafluoride. The autodetachment lifetime of SF_4^{-*} was also much shorter than that of SF_6^{-*} and because of such factors as its lower mass and shorter lifetime we were not able to separate the ion and neutral satisfactorily over a wide energy range and so the lifetime was only measured at two ion energies, 2 and 2.5 kV (nominal).

Our results are shown in Table I and indicate that

$\tau_{SF_4} = 16.3 \pm 0.3$ μsec. It will be more convenient to discuss these lifetime results in conjunction with the attachment cross section results reported below.

B. Electron Attachment Cross Sections. The experimental problems and difficulties involved in the measurement of ionization cross sections have been well documented by Kieffer and Dunn.[19] In this work we have attempted to measure the *relative* cross sections for SF_6 and SF_4; this has obviated the need for knowledge of the pressure of the gases in the ion source (only their relative proportions need be known), of the total ionizing electron current and of various ion source and drift tube parameters which are required to be known if measurements are made on only one gas. We have, however, assumed that the SF_4^- and SF_6^- ions have the same collection efficiency; only the parent ion currents were measured. No attempt was made to measure the total ion current at any energy although at 0 eV the parent ions are responsible for virtually all of the ion currents.

$$SF_4 + e \longrightarrow SF_4^- \qquad (1)$$

$$SF_6 + e \longrightarrow SF_6^- \qquad (2)$$
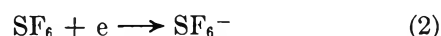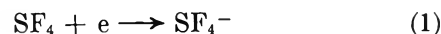
Figure 1 shows typical data obtained for SF_4^- and SF_6^- formation using a mixture of SF_4 and SF_6. "Negative" voltages were obtained by the introduction of a 3-V dry cell into the electron energy circuit. The SF_4^- and SF_6^- ionization curves have been normalized to the same peak height; it is clear that they have very similar electron energy dependences, both reaching a maximum value at the same electron energy. Because of this similar energy dependence, the relative peak heights may be used to evaluate the relative attachment cross sections for reactions 1 and 2. If I_{X^-} is the X^- ion current, (X) the ion source pressure of X, and σ_x the electron attachment cross section of X, then

$$\frac{\sigma_{SF_6}}{\sigma_{SF_4}} = \frac{I_{SF_6^-}}{I_{SF_4^-}} \frac{(SF_4)}{(SF_6)}$$

Our results indicate that $\sigma_{SF_6}/\sigma_{SF_4} = 109 \pm 6$ (the error bars represent the mean deviation of several repeat determinations); if a value for SF_6 is known, we may calculate the attachment cross section of SF_4. Various values[9,20-23] have been reported for the SF_6

(14) W. T. Naft, private communication, 1970.

(15) C. E. Klots, *J. Chem. Phys.*, **46**, 1197 (1967).

(16) R. N. Compton, R. H. Huebner, P. W. Reinhardt, and L. G. Christophorou, *ibid.*, **48**, 901 (1968).

(17) R. MacDonald and J. C. J. Thynne, unpublished results (1969).

(18) C. Lifschitz, private communication, 1970.

(19) L. J. Kieffer and G. H. Dunn, *Rev. Mod. Phys.*, **38**, 1 (1966).

(20) R. K. Asundi and J. D. Craggs, *Proc. Phys. Soc. (London)*, **83**, 611 (1964).

(21) D. Rapp and D. D. Briglia, *J. Chem. Phys.*, **43**, 1480 (1965).

(22) F. C. Fehsenfeld, *ibid.*, **53**, 2000 (1970).

(23) L. G. Christophorou, D. L. McCorkle, and J. G. Carter, *ibid.*, **54**, 253 (1971).
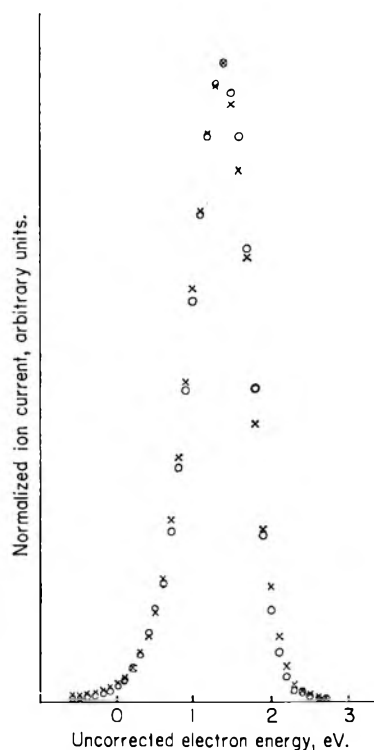
Figure 1. Ion current *vs.* electron accelerating energy: $\times$, SF_6^-; O, SF_4^-. Ion current scale for SF_4^- is 109 times larger than that for SF_6^-.

attachment cross section varying from 3×10^{-20} to 1.17×10^{-14} cm^2. We shall assume the latter value[23] to evaluate σ_{SF_4} but wish to point out that this is an arbitrary assumption. Using this value we find that $\sigma_{SF_4} = 107 \pm 6 \times 10^{-18}$ cm^2. There is no other result with which our value may be compared.

C. Consideration of the Cross Section and Lifetime Results. A semitheoretical model has been suggested[9] to account for the long lifetimes of metastable ions; the ion is represented as an assembly of weakly coupled harmonic oscillators, the captured electron dissipating its energy in the various internal degrees of freedom of the molecule, allowing the ion to exist for some time before the electron is ejected. Such a model would suggest an increase in the negative ion lifetime as the number of atoms in the molecule increases.

Sulfur tetrafluoride and sulfur hexafluoride have 9 and 15 vibrational degrees of freedom, respectively; on the basis of the model described above it is to be expected that SF_4^{-*} will have a shorter autodetachment lifetime than SF_6^{-*}. This is experimentally observed, namely 16.3 μsec compared with 68 μsec. It is apparent that the lifetimes of these temporary negative ion states of fluorosulfur compounds are appreciably longer than those noted for similar sized fluorocarbon anions.[16,17] A ten-atom ion such as $C_4F_6^-$ has a lifetime of about 10 μsec. This presumably reflects the ease with which the captured electron may be accommodated in the unoccupied d orbitals of the sulfur atom.

In view of these long-lived states for SF_4^- and SF_6^- it might have been expected that the attachment cross sections for the two molecules would not be too different. Our results, however, show two order of magnitude difference, the cross section for SF_6 being larger.

It is apparent that, even for relatively similar molecules, the electron attachment cross sections may vary considerably. This view is supported by measurements we have made[24] of the cross sections for a variety of fluorocarbons and suggests that any assumption of similar cross sections for even slightly different molecules should be treated with care.

D. Negative Ion Formation. In Table II we have compared the negative ion mass spectra of SF_4 and SF_6 measured at 70 eV. As might be expected many similar ions are formed by both molecules; surprisingly, however, F^- is the most abundant only in the case of SF_4, the SF_6^- ion being considerably more abundant than F^- in the case of the hexafluoride.

Table II: Negative Ion Mass Spectra of SF_4 and SF_6 at 70 eV

m/e	Ion	SF_4 rel. intensity	SF_6 rel. intensity
19	F^-	1000	160
32	S^-	1.9	3.0
38	F_2^-	2.4	1.0
51	SF^-	1.4	5.6
70	SF_2^-	0.6	0.4
89	SF_3^-	1.8	0.2
108	SF_4^-	45.8	0.2
127	SF_5^-	. . .	13.6
146	SF_6^-	. . .	1000

Table II shows the ratio of SF_5^-/SF_6^- to be 0.014; Fehsenfeld[22] and Chen and Chantry[25] have shown this ratio to be strongly dependent on temperature, Fehsenfeld[22] finding the ratio to vary from 10^{-4} at 0° to 0.04 at 200°. Chen and Chantry report values of 0.06 at 27° and 0.1 at 106° for the ratio. The exact temperature of our ion source was not known, but we estimate it to be around 50°. We did not study the effect of temperature upon the SF_5^-/SF_6^- ratio.

For sulfur tetrafluoride, the relative peak heights of the more abundant ions at their respective resonance maxima were F^- (1000), SF_3^- (2.6), and SF_4^- (6.0). Some F_2^- ion formation was observed at very low energies (~ 0 eV); this must be due to surface ionization on the filament since, assuming $E(F_2) = 2.8$ eV,[7] the minimum enthalpy requirement for the reaction

$$SF_4 + e \longrightarrow F_2^- + SF_2$$
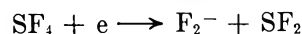
would be ~ 2.6 eV.

(24) P. W. Harland and J. C. J. Thynne, unpublished results, 1969.
(25) C. L. Chen and P. J. Chantry, *Bull. Amer. Phys. Soc.*, 15, 418 (1970).

Table III: Appearance Potentials (A), Resonance Peak Maxima (M), and Peak Widths at Half-Height (PW) for Negative Ions Formed by Sulfur Tetrafluoride and Sulfur Hexafluoride

Ion	A	M	PW	Process
		SF$_4$		
SF$_4^-$	0.00 ± 0.05	0.40 ± 0.03	0.47 ± 0.05	SF$_4 \xrightarrow{e}$ SF$_4^-$
SF$_3^-$	0.70 ± 0.05	1.35 ± 0.05	0.72 ± 0.05	$\longrightarrow$ SF$_3^-$ + F
F$^-$	0.20 ± 0.05	0.89 ± 0.10	0.65 ± 0.05	$\longrightarrow$ F$^-$ + SF$_3$
		SF$_6$ (values taken from ref 29)		
SF$_6^-$	0.0 (calibrant)	0.4 ± 0.1	0.6 ± 0.1	SF$_6 \xrightarrow{e}$ SF$_6^-$
SF$_5^-$	0.1	0.5 ± 0.1	0.8 ± 0.1	$\longrightarrow$ SF$_5^-$ + F
SF$_4^-$	5.0 ± 0.1	6.0 ± 0.1	1.7 ± 0.1	$\longrightarrow$ SF$_4^-$ + 2F
	~ 0			$\longrightarrow$ F$^-$ + SF$_5$
F$^-$	4.3 ± 0.1	5.7 ± 0.1	1.4 ± 0.1	$\longrightarrow$ F$^-$ + F + SF$_4$
	7.8 ± 0.1	9.3 ± 0.1	~ 2	$\longrightarrow$ F$^-$ + SF$_3$ + 2F
	10.5 ± 0.1	11.8 ± 0.1	1.6 ± 0.1	$\longrightarrow$ F$^-$ + SF$_2$ + 3F
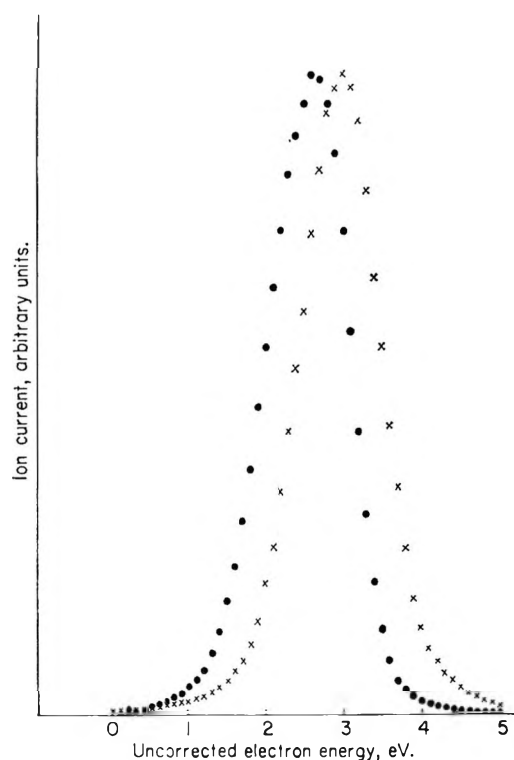
Figure 2. Ionization efficiency curves before deconvolution for F$^-$ and SF$_3^-$ ion formation by SF$_4$: ●, F$^-$; ×, SF$_3^-$.
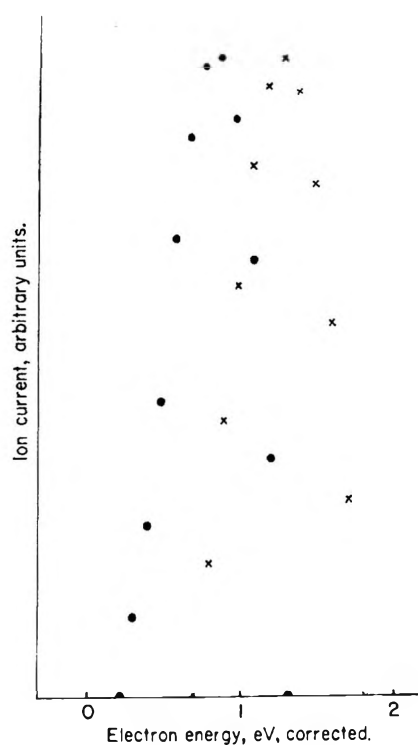
Figure 3. Ionization efficiency curves after deconvolution for F$^-$ and SF$_3^-$ ion formation by SF$_4$: ●, F$^-$; ×, SF$_3^-$.

E. Negative Ions Formed by SF$_4$. *1. SF$_4^-$.* The attachment cross section and the autodetachment lifetime of this ion have been discussed above. The parent ion has an appearance potential at 0 eV and the symmetrical resonance peak reaches a maximum value at 0.40 ± 0.03 eV. The stability of this ion is consistent with the value of 1.2 eV for the electron affinity of SF$_4$ estimated from a study of SF$_4^-$ ion for-formation by SF$_6$.[29]

2. F$^-$. Typical data for this ion before and after deconvolution are shown in Figures 2 and 3, and our results are shown in Table III. It is apparent that, when deconvoluted, a relatively narrow, symmetrical

peak is observed suggesting that the ion is formed with little excess kinetic or excitation energy.

If the process responsible is

$$\text{SF}_4 + \text{e} \longrightarrow \text{F}^- + \text{SF}_3 \qquad (3)$$
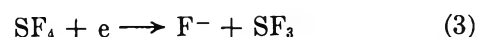
then, using the relation $D(\text{F--SF}_3) \leqslant A(\text{F}^-) + E(\text{F})$, in conjunction with a value of 3.44 eV for the electron affinity of fluorine,[26] we find that $D(\text{F--SF}_3) \leqslant 3.64 \pm 0.05$ eV. Bott,[27] using a shock tube technique, has obtained a value of 3.4 eV for this bond dissociation

(26) R. S. Berry and C. W. Riemann, *J. Chem. Phys.*, **38**, 1540 (1963).

(27) J. F. Bott, *ibid.*, **54**, 181 (1971).

energy. Our data on F^- ion formation from sulfur hexafluoride (Table III) suggest that $D(SF_3-F) \leqslant 3.5$ eV. The primary S–F bond dissociation energy in SF_6 has been reported[28] to be $\leqslant 3.4$ eV; our result for SF_4 suggests that there is little difference between the primary bond dissociation energies of both molecules. It should be noted also that, for both SF_6 and SF_4, the mean bond energies (3.4 and 3.5 eV, respectively) are close to the primary bond strengths.

3. SF_3^-. This ion was also formed by a low energy dissociative capture process. Typical data before and after deconvolution are shown in Figures 2 and 3.

$$SF_4 + e \longrightarrow SF_3^- + F \qquad (4)$$
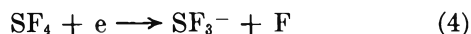
If reaction 4 is responsible for ion formation and we make the assumption that there is zero excess energy associated with reactions 3 and 4, then

$$A(F^-) + E(F) = A(SF_3^-) + E(SF_3)$$

and we may estimate a value for the electron affinity of sulfur trifluoride. Our data yield a value of 2.95 ± 0.05 eV for $E(SF_3)$. In a previous paper[29] dealing with the formation of ions formed by pentafluorsulfur chloride, we measured $A(SF_3^-)$ to be 7.9 eV and suggested the process responsible to be

$$SF_5Cl + e \longrightarrow SF_3^- + 2F + Cl \qquad (5)$$
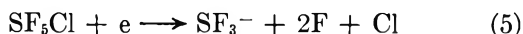
and $E(SF_3)$ to be 0.5 eV. Our result above has led us to reconsider this suggestion, and we now regard the responsible ion formation process in SF_5Cl to be reac-

tion 6. This yields a value of 2.9 ± 0.1 eV for $E(SF_3)$, a result in excellent accord with the value deduced above and with the value of 2.7 eV obtained by Page and Goode[30] using the magnetron technique. We have

$$SF_5Cl + e \longrightarrow SF_3^- + F + FCl \qquad (6)$$
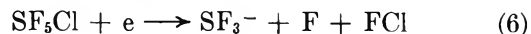
included in Table III appearance potential data obtained[18] for SF_6 for ease of comparison with the SF_4 data.[31]

F. Thermochemical Data. The following values for heats of formation (at 298°K) have been used in our calculations (in electron volts); SF_6, -12.7;[32] SF_5Cl, -10.9;[33] SF_4, -8.0;[32] FCl, -0.6;[34] S, 2.8;[34] F, 0.8.[34]

(28) J. Kay and F. M. Page, *Trans. Faraday Soc.*, **60**, 1042 (1964).

(29) P. W. Harland and J. C. J. Thynne, *J. Phys. Chem.*, **73**, 4031 (1969).

(30) F. M. Page and G. C. Goode, "Negative Ions and the Magnetron," Wiley, New York, N. Y., 1970.

(31) We have used the term "appearance potential" to describe the energy at which the negative ion was detected. It should be noted that D. Rapp and D. D. Briglia[21] have pointed out that the "appearance potential" for an ion showing nonvertical onset behavior is largely a measure of the sensitivity of the experimental arrangement since there is no particular onset energy for such ions only an exponential decrease in cross section. Meaningful results for bond energies and electron affinities may nevertheless be deduced from such negative ion studies; in the absence of a generally accepted term to indicate the electron energy at which ions are detected we have, in common with many other workers in this field, used the term "appearance potential."

(32) P. A. G. O'Hare, J. L. Settle, and W. N. Hubbard, *Trans. Faraday Soc.*, **62**, 558 (1966).

(33) National Bureau of Standards, Technical Note 270-3 (1968).

(34) "JANAF Thermochemica. Tables," Dow Chemical Co., Midland, Mich., 1961.

Reactions of Accelerated Carbon-14 with Benzene.   Degradation

of Toluene and Its Mechanism of Formation[1]

by Tz-Hong Lin and Richard M. Lemmon*

Laboratory of Chemical Biodynamics, Lawrence Radiation Laboratory, University of California, Berkeley, California 94720
(Received May 17, 1971)

We have totally degraded the toluene product obtained from impinging 5000 and 4000 eV $^{14}C^+$ ions on solid benzene at $-196°$. The radioactivity distributions were essentially equivalent to that of toluene obtained in carbon recoil experiments. The ring/methyl activity ratios were also determined for toluenes from irradiations at various energies down to 5 eV. While the yield of toluene decreased drastically below 100 eV, the ring/methyl activity ratio remained constant, changing only when the energy of the incident ions were lowered to 5 eV. It is suggested that bare carbon atoms, as well as CH_2, are important species leading to toluene formation.

Introduction

The present work was undertaken to add to our knowledge of how accelerated carbon ions and atoms interact with benzene to form (among other products) toluene. The first work of this kind, using recoiling ^{14}C atoms, was that of Wolf, *et al.*,[2] who showed that 15% of the activity of the toluene produced from benzene was in the ring of the toluene. A subsequent study by Visser, *et al.*,[3] revealed that the toluene's methyl, C_1, C_2, C_3, and C_4 activities were 85.7, 7.65, 3.68, 2.00, and 0.99%, respectively. Mullen then reported that the toluene-^{14}C from the reaction of kinetically hot $^{14}C^+$ with benzene showed a similar ring/Me activity distribution.[4] Mullen's work was recently repeated and corroborated by us.[5] In reactions of recoiling carbon atoms with organic compounds, hot methylene has usually been postulated as the reactive species for the formation of synthesis products.[6] (A "synthesis" product has one or more carbons than the target molecule.) Since photolytically generated $^{14}CH_2$ gave toluene which was exclusively labeled at the methyl group,[7] it was assumed that, in the recoil-carbon work, a hot methylene must be involved and that a structure such as an excited norcaradiene was responsible for the incorporation of the activity in the aromatic ring.[8]

In the present paper, we report an examination of the above mechanism by total and partial degradations of toluene-^{14}C obtained upon striking solid benzene with $^{14}C^+$ ions of various kinetic energies.

Experimental Section

Toluene-^{14}C was degraded by the two methods shown below.

Method A was essentially that used by Moore and Wolf in the degradation of their ethylbenzenes.[9] The activities in C_{Me} and C_1 were determined by the Schmidt degradation of acetic acid obtained from the Beckmann
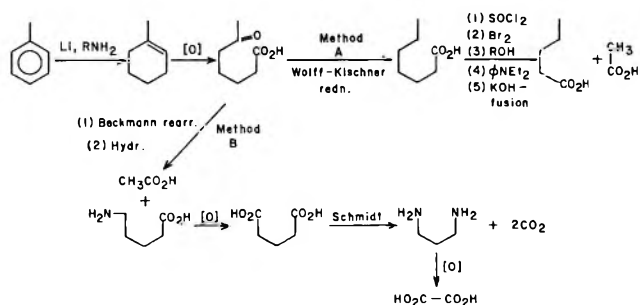
rearrangement of the oxime of 6-ketoheptanoic acid, followed by the hydrolysis of the product. (This is the first step of "method B.") We also found that the alternative method, B, was easier for the total degradation of toluene. Partial degradations (ring/Me activity distributions) were carried out by oxidation to benzoic acid, followed by the Schmidt degradation.

Details of the irradiations, of the separations and purifications of the toluene, and of the degradations are described elsewhere.[5,10,11]

(1) Abstracted in part from the Ph.D. Thesis of T. H. Lin, UCRL-19335, University of California, Berkeley, 1969, and based on work supported by the U. S. Atomic Energy Commission.

(2) A. P. Wolf, B. Gordon, and R. C. Anderson, *J. Amer. Chem. Soc.*, 78, 2657 (1956).

(3) R. Visser, C. R. Redvanly, F. L. J. Sixma, and A. P. Wolf, *Recl. Trav. Chim. Pays-Bas*, 80, 533 (1961).

(4) R. T. Mullen, Ph.D. Thesis, UCRL-9603, University of California, Berkeley, 1961.

(5) H. M. Pohlit, T. H. Lin, W. R. Erwin, and R. M. Lemmon, *J. Amer. Chem. Soc.*, 91, 5421 (1969).

(6) A. P. Wolf, *Advan. Phys. Org. Chem.*, 5, 201 (1964).

(7) R. M. Lemmon and W. Strohmeier, *J. Amer. Chem. Soc.*, 81, 106 (1959).

(8) B. Suryanarayana and A. P. Wolf, *J. Phys. Chem.*, 62, 1369 (1958).

(9) G. G. Moore and A. P. Wolf, *J. Org. Chem.*, 31, 1106 (1966).

(10) H. M. Pohlit, T. H. Lin, and R. M. Lemmon, *J. Amer. Chem. Soc.*, 91, 5425 (1969).

(1) Visser et al.		(2) 5000 eV Method A	(3) 4000 eV Method B
85.7	CH3	85.2	84.3
7.65		7.4	7.9
3.68		5.1	4.6
2.00		2.4	1.2
0.99		1.1	0.6
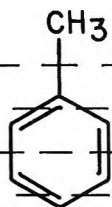
Figure 1. Distributions of radioactivity in toluene-^{14}C formed from benzene and (1) recoiling ^{14}C atoms, (2) 5000-eV ^{14}C ions, and (3) 4000-eV ^{14}C ions. Methods A and B refer to different degradation routes (see text).

Figure 2. The yields of toluene-^{14}C (□) and the toluene ring/Me activity distributions (●), plotted as a function of the kinetic energy of the ^{14}C$^+$.

Results

Toluene-^{14}C from 5000 and 4000 eV ^{14}C$^+$ beams was degraded *via* methods A and B, respectively. The results are shown in Figure 1, along with those from a ^{14}C-recoil experiment (Visser, *et al.*).[3] Close similarity to the latter results is apparent.

As has been previously reported, the partial degradation of toluene-^{14}C obtained from irradiations at various ^{14}C$^+$ energies showed no apparent change in the ring/Me activity ratio at energies above 31 eV.[12] However, a drastic increase in the ring activity was found in 5-eV irradiations. A plot of ring/Me activities *vs.* that of the ion energies is presented in Figure 2. A plot of the toluene-^{14}C yield[5] is also included.

Discussion

The activity distributions reported here (Figure 1), and those reported by Visser and Wolf in their study of the recoil-^{14}C chemistry of benzene, indicate that the hot carbon species that interacts with the benzene is the same in both the recoil-^{14}C and the accelerated ^{14}C$^+$ systems. In addition, it is to be expected, as we have previously inferred from the work of other authors, that our accelerated ions are rapidly neutralized upon entering the benzene matrix;[5] therefore, our system may also be taken as a study of carbon atom reactions.

The formation of toluene from the reactions of recoiling carbon atoms with benzene has been shown to be a hot reaction.[8] Although the involvement of hot methylene is usually postulated in the interpretation of carbon-recoil results,[6,8] there is as yet no direct evidence that indicates at which stage the two hydrogen atoms are picked up, *i.e.*, before or after the carbon's bonding to the benzene. One of the reasons for the assumption of a hot methylene was that the three hexanes (from *n*-pentane and recoiling ^{14}C) and the ethylbenzene and the three xylenes (from toluene and recoiling ^{14}C) were formed in the statistical ratio expected from indiscriminate insertion of CH$_2$ into
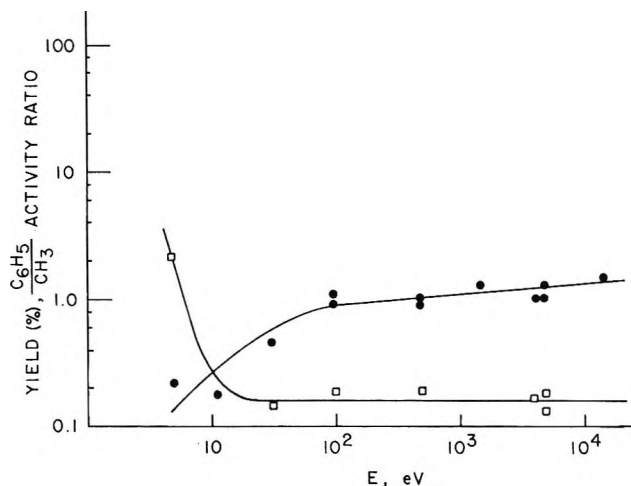
the C–H bonds of the target molecule.[6] The observation that about 15% of the activity of toluene (from benzene and recoiling ^{14}C) was in the ring was believed to have been caused by the excess kinetic energy of the hot methylene intermediate. The more recent study of Williams and Voigt, however, revealed that the products from toluene and xylenes were not statistically distributed,[13] and their work emphasizes the role of bare carbon atoms in the formation, from benzene, of acetylene, ethylene, and higher olefins. The scrambling of activity into an unexpected part of the synthesis product molecule may also be suggestive of the participation of a species other than methylene, *e.g.*, CH or C.

Our finding of a drastic increase in the toluene's ring/Me activity distribution at 5 eV is also suggestive of the involvement of a species other than methylene. Rose, *et al.*,[14] reported that atomic carbon (from ^{11}C recoil) was extremely reactive with benzene. Several stable adducts, including π-bonded configurations, double bond additions, and C–H bond insertions, were postulated. Our recent paper also assumed the formation of benzylidene and cycloheptatrienilidene and/or norcaradienilidene[10] as the precursors for two of our major products, diphenylmethane and phenylcycloheptatriene. It seems reasonable to expect that these precursors would abstract hydrogens from the reaction medium, benzene, to form toluene and cycloheptatriene. In fact, even thermal carbon vapor is reported to give these products with benzene.[15] Skell

(11) T. H. Lin, "The Chemical Interactions of Accelerated Carbon-14 Ions and Atoms with Benzene," Ph.D. Thesis, UCRL-19335, University of California, Berkeley, 1969.

(12) H. M. Pohlit, W. R. Erwin, T. H. Lin, and R. M. Lemmon, *J. Phys. Chem.*, 75, 2555 (1971).

(13) R. L. Williams and A. F. Voigt, *ibid.*, 73, 2538 (1969).

(14) T. Rose, C. Mackay, and R. Wolfgang, *J. Amer. Chem. Soc.*, 89, 1529 (1967).

(15) J. L. Sprung, S. Winstein, and W. F. Libby, *ibid.*, 87, 1812 (1965).

and Engel[16] reported that parent-molecule-plus-CH_2 (i.e., "synthesis") products were obtainable in high yield in the reaction of thermal carbon vapor with hydrocarbons; in their system it was demonstrated that no methylene was involved. To support this mechanism, we have photolytically generated C_6H_5CH: in benzene solution by the photolysis of styrene oxide. The formation of toluene was firmly established by glpc analysis. We therefore believe that bare C atoms, as well as methylene, are reacting directly with benzene.

Another argument that favors the notion that methylene is not the major species involved in the ring labeling of toluene is the following. A methylene route to ring labeling is presumed to involve (after intramolecular hydrogen shifts) such norcaradiene structures as
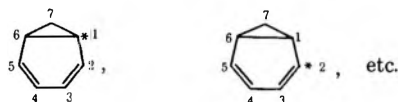
Such structures can only give more C_2-labeled toluene than C_1-labeled. However, the data of Figure 1 show that C_1 is the more highly labeled. These results indicate that a route through methylene is not the principal one in the ring labeling, although it may be for the methyl labeling.

It is possible that the relative populations of the various carbon spin states, the ground state ^1S or the excited ^1D and ^3P states, may decide the yield and radioactivity distributions of the toluene product. However, the high ring/Me activity ratio in the 5-eV experiment is apparently not the result of the $^{14}C^+$ ion reacting with the benzene before the ion becomes neutralized. Recent results in our laboratory, the subject of a forthcoming publication, have (1) confirmed the 5-eV result and (2) shown that, when the irradiating ion's kinetic energy is reduced to 3 or 2 eV, the ring/Me activity ratio diminishes to about 0.1.

(16) P. S. Skell and R. R. Engel, J. Amer. Chem. Soc., 88, 4883 (1966).

Sorption Properties of Activated Carbon

by P. J. Reucroft,

Department of Material Science and Metallurgical Engineering, University of Kentucky, Lexington, Kentucky 40506

W. H. Simpson,

Chemistry Department, The Franklin Institute Research Laboratories, Philadelphia, Pennsylvania 19103

and L. A. Jonas*

Research Laboratories, Edgewood Arsenal, Edgewood Arsenal, Maryland 21010 (Received February 8, 1971)

Publication costs assisted by Edgewood Arsenal

Adsorption–desorption isotherm data were obtained for 15 organic vapors on a BPL grade, PAC, activated carbon. Isotherm data in the form of log W as a function of ϵ^2 for each adsorbate were given to a Univac 1108 computer to determine the characteristic curve equation by means of regression analysis (W = volume of adsorbed vapor, ϵ = adsorption potential). Equations in the form of the Dubinin–Polanyi equation for fine grained carbon were obtained for each adsorbate. Structural constants for the adsorbent and affinity coefficients for the adsorbates were calculated from the coefficients of these equations. Affinity coefficients calculated from the experimental data were then compared to theoretical values in order to test the predictive ability of the characteristic curve equation.

Introduction

Predictive Isotherm Equations. The ability to predict adsorption isotherms for a given adsorbent from a knowledge of the physical properties of the adsorbate has long been an important objective in solid surface–gas interaction research. Kummer in 1946 studied the relation of Polanyi's adsorption potential to molecular

polarizability.[1] In 1947, Dubinin and his coworkers first suggested that the following equations could be used for predicting adsorption isotherms[2]

(1) J. T. Kummer, Ph.D. Thesis, The Johns Hopkins University, Baltimore, Md., 1946.

(2) (a) M. M. Dubinin and E. D. Zaverina, Zh. Fiz. Khim., 23, 1129 (1949); (b) M. M. Dubinin, E. D. Zaverina, and L. V. Radushkevich, ibid., 21, 1351 (1947).

$$\log W = \log W_0 - \frac{B}{2.303}\left[\frac{T}{\beta}\log\frac{P_0}{P}\right]^2 \qquad (1)$$

$$\log W = \log W_0 - \frac{B}{2.303}\left[\frac{T}{\beta}\log\frac{P_0}{P}\right] \qquad (2)$$

Equation 1 was suggested for adsorbents of the "first structural type," that is adsorbents whose pore dimensions are comparable in size to the dimensions of the molecules adsorbed. Equation 2 was suggested for adsorbents with coarse pores, where the pore dimensions are much larger than adsorbate molecule dimensions. In these equations W is the volume of condensed adsorbate; P is the equilibrium pressure of adsorbate vapor; P_0 is the saturated vapor pressure of liquid adsorbate at temperature $T°K$; W_0 and B are constants related to the pore structure of the adsorbent; and β is a constant known as the affinity coefficient, which compares the strength of the adsorptive interaction of the adsorbate in question to that of some reference substance. Thus, if β values are known or can be calculated for several adsorbate vapors, adsorption isotherms can be determined for all the vapors by measuring experimentally the adsorption isotherm of a reference vapor. The problem consists of determining β in a general way so that all types of adsorptive interaction are allowed for.

The equations can also be written in the following form, e.g., for eq 1

$$\log W = \log W_0 - \frac{k'\epsilon^2}{\beta^2} = \log W_0 - k\epsilon^2 \qquad (3)$$

where

$$\epsilon = RT\ln\frac{P_0}{P} \qquad (4)$$

and

$$R = \text{gas constant and } k' = \frac{B}{(2.303)^3 R^2} \qquad (5)$$

Equation 3 is a useful form for comparing adsorption data for several adsorbates on one adsorbent since (1) the equation is not an explicit function of temperature (ϵ is the temperature dependent "adsorption potential" or more rigorously, the change of free energy during the reversible, isothermal transfer of a mole of the adsorbate from bulk liquid to an infinitely large amount of adsorbent) and (2) k depends on the adsorbate parameter β. Thus, if a reference adsorbate is chosen, for which $\beta = 1$, experimental β values can be evaluated for other adsorbates from

$$\beta_{ex} = \left(\frac{k_{REF}}{k}\right)^{1/2} \qquad (6)$$

Experimental procedure will show that except for the first adsorption point, obtained at a P/P_0 of 0.8 to 0.9, all subsequent points were obtained from the desorption

isotherm. This was done because prior unpublished work on the sorption of dimethyl methylphosphonate (DMMP) vapor by this identical gas phase carbon had shown that more reliable and reproducible data were obtained for the desorption rather than the adsorption isotherm, resulting in a better straight line characteristic curve from the Dubinin–Polanyi equations. This was especially true at low pressures because each time a dose of vapor was desorbed the balance system was cleared of air or low boiling impurities. In the study with DMMP vapor the hysteresis loop at 25° formed in a narrow band at a P/P_0 of 0.65 and disappeared at about 0.1. The initial adsorption point in the present study was therefore taken at a P/P_0 of 0.8 and 0.9 since it was expected to be well beyond the hysteresis range and therefore the adsorption and desorption points should coincide.

Experimental β values so evaluated from measured isotherms can then be compared with theoretical β values to assess the predictive ability of the isotherm equation.

Theoretical Affinity Coefficients for Nonpolar Adsorbates. The main problem in using such equations to predict the isotherm for a new adsorbate vapor is to assign a value of β which correctly describes the nature of the adsorptive interaction. The work of Dubinin and coworkers[2,3] has shown that eq 3, 4, and 5 give a good description of adsorption isotherms for systems in which dispersion forces play a dominant role in determining the adsorptive interactions. In this case the adsorptive interaction is strongly dependent on the polarizability (α) of the molecules and β can be expressed in terms of polarizability.

$$\beta = \frac{\alpha}{\alpha_{REF}} \qquad (7)$$

Since the polarizability of a molecule is approximately proportional to the volume of a molecule or molar volume V, the affinity coefficient can also be expressed as[3d]

$$\beta = \frac{V}{V_{REF}} \qquad (8)$$

More precisely, the affinity coefficient can be expressed in terms of the molecular parachor Ω

$$\beta = \frac{\Omega}{\Omega_{REF}} = \frac{\left[\dfrac{\gamma^{1/4}M}{\rho}\right]}{\left[\dfrac{\gamma^{1/4}M}{\rho_{REF}}\right]} \qquad (9)$$

where γ = surface tension, M = molecular weight, and ρ = density of liquid.

(3) (a) M. M. Dubinin, *Chem. Rev.*, **60**, 235 (1960); (b) B. P. Bering, M. M. Dubinin, and V. V. Serpinsky, *J. Coll. Inst. Sci.*, **21**, 378 (1966); (c) M. M. Dubinin, *Izv. Akad. Nauk SSSR Otd. Khim. Nauk*, 1153 (1960); (d) M. M. Dubinin and D. P. Timofeyev, *Zh. Fiz. Khim.*, **22**, 113 (1948).

Theoretical Affinity Coefficients for Polar Adsorbates.
When the adsorbate molecules have polar nature,
i.e., possess a permanent dipole moment, electrostatic
interactions may play a greater role in determining the
total adsorptive interaction which determines the ad-
sorption isotherm. In the case of a nonpolar adsorbent
there will be contributions from dipole–induced dipole
forces.[4] If the adsorbent possesses some polar nature
due to the presence of ionic impurities, there will be an
additional contribution from ion–dipole forces. In the
former case it has been shown that for a dipole moment
of 2 D (2×10^{-18} esu) the electrostatic contribution to
the adsorptive interaction in the case of a conducting
surface is an order of magnitude smaller than the dis-
persion interaction.[5] An upper limit can be set for ion–
dipole force contributions by considering the interaction
between polar molecules and an ionic crystal. In the
case of SO_2 (dipole moment = 1.6 D) adsorbed on
barium fluoride crystals, it has been estimated that the
electrostatic interaction is responsible for 54% of the
total interaction, the remainder being accounted for in
terms of dispersion forces.[6] If a polar molecule having
a dipole moment of 4.0 D is considered, the electro-
static contribution may amount to 70% of the total
interaction. Dipole energy terms usually contain the
dipole moment as a μ^2 term. Thus, when electrostatic
forces play a dominant role in determining the adsorp-
tive interaction energy it might be expected that β
could be expressed as a term in μ^2 such as

$$\beta = \frac{\mu^2}{\mu_{REF}^2} \tag{10}$$

In intermediate situations, empirical expressions of the
type

$$\beta = \frac{(\alpha\mu^2)}{(\alpha\mu^2)_{REF}} \tag{11}$$

may be applicable.

To extend the Dubinin–Polanyi treatment to ad-
sorption situations where interactions other than dis-
persion forces are possible, isotherms have been mea-
sured for a range of organic vapors on a carbon adsor-
bent. The general case of nonpolar, weakly polar
($\mu < 2$ D), and strongly polar vapor ($\mu = 2$–4 D) ad-
sorbed on a carbon adsorbent reported to have little
or no ionic character and having pore dimensions com-
parable to the adsorbate molecule dimensions, has been
investigated. Experimentally determined β values
obtained from isotherm data plotted as log W vs. ϵ^2
(eq 3) have been compared with theoretical β values ob-
tained from eq 7–11.

Experimental Section

The apparatus used for the measurement of isotherms
consisted of two glass vacuum systems. The first
system consisted of a train of traps used for vacuum
distillation of the organic vapor into a storage vessel.

The vapor was prepurified by distillation to greater than
99% before it was introduced into the vacuum system.
A Cahn RG electrobalance and an MKS Baratron[7]
pressure gauge formed the second system. The carbon
sample was suspended from the electrobalance in a
small glass container which had been tared with metal
weights. A change in mass of the carbon due to ad-
sorption was recorded as an electrical signal from the
balance. The pressure changes were recorded as elec-
trical signals due to the change of capacitance between
two electrodes in the pressure heads of the Baratron
gauge. Some instability was noticed at very low
pressures which was attributed to temperature fluctua-
tions in the room. The temperature of the carbon sam-
ple was kept constant by a heat sink constructed at
FIRL to fit the hangdown tubes of the balance.

The system was kept ultraclean by using a General
Electric sorption pump for rough pumping and a Gen-
eral Electric Vac-Ion[7] pump in series with a Veeco
Torgett[7] pump for high vacuums. The system was
capable of pumping down to 10^{-6} Torr and maintaining
this pressure indefinitely. All stopcocks were Teflon
with either silicone or Viton "O" rings. The entire
vacuum system was entirely free of oil and grease.

The purity of the organic vapors was determined by
gas chromatography using a Hewlett-Packard (F & M)
810 chromatograph equipped with dual columns and
flame ionization detectors. The columns used for vpc
analysis were 10% Carbowax on Chromosorb P (6 ft)
and 10% diisodecyl phthalate on Chromosorb P (6 ft).

Before each determination the carbon sample was
heated to 450° for 8 hr under a vacuum of 10^{-5} Torr.
When the sample reached a constant mass, the carbon
was brought to a constant temperature and the organic
vapor was introduced into the system until a P/P_0
of 0.8–0.9 was attained. The system was allowed to
come to equilibrium, and the mass of the material
adsorbed and the pressure were recorded. Subsequent
points were obtained by reducing the pressure of the
adsorbate and recording the decrease in mass of material
adsorbed.

The carbon adsorbent used was a Pittsburgh acti-
vated carbon, Type BPL, 12–30 mesh, which is a com-
mercial adsorbent manufactured from coal for general
gas phase application. The total pore volume has
been determined to be 1058 m^2/g, with 70–75% of this
volume being attributed to pores less than 20 Å in
diameter. The carbon sample used in the balance was
approximately 500 mg.

Treatment of Experimental Data. Isotherm data
were obtained for the 15 vapors on the BPL grade acti-

(4) A. D. Crowell, *J. Chem. Phys.*, **49**, 892 (1968).

(5) D. M. Young and A. D. Crowell, "Physical Adsorption of Gases,"
Butterworths, London, 1962, Chapter 2.

(6) V. A. Crawford and F. C. Tompkins, *Trans. Faraday Soc.*, **44**,
698 (1948).

(7) Registered trademark.

vated carbon. The desorption data, originally obtained as gram adsorbate per gram carbon for various relative pressures, were converted into cubic centimeters of adsorbate per gram of adsorbent (W) for various adsorption potentials. These conversions were made using liquid density values at the test temperatures in accord with the pore volume filling concept of Bering, et al.[3b] Relative pressures in the form P/P_0 were converted into adsorption potential (ϵ) values by means of eq 4, where ϵ is the potential in calories per mole. The adsorption potential represents the work required of an adsorbent surface to compress a vapor at its pressure P to its maximum pressure P_0. Tabulated data in the form of log W as a function of ϵ^2 for each adsorbate were given to a Univac 1108 computer for regression analysis.

The data were expressed in terms of eq 3, the computer print-out providing least mean square values of log W_0 and k. These data are tabulated in Table I. Using eq 5, values of β for the test adsorbate were calculated, compared to the reference vapors, $\beta = 1$, for each polarity group. These values are given in Tables II and IV. CCl_4, $CHCl_3$, and CH_3COCH_3 were reference vapors for the nonpolar, weakly polar, and polar groups, respectively.

Table I: Regression Analysis of Isotherm Data for Organic Vapors

Vapors	Log W_0	$k \times 10^8$	Correlation (R)
CCl_4	−0.37715	1.9839	0.98880
Dioxane	−0.29248	3.838	0.91193
2,2,4-TMP	−0.34277	1.3383	0.76996
Benzene	−0.37202	2.3821	0.99602
Hexane	−0.3425	1.3576	0.99361
$CHCl_3$	−0.35341	2.588	0.99382
Ethyl acetate	−0.37321	2.735	0.98270
Methanol	−0.52407	16.81	0.94757
Fluorobenzene	−0.36121	2.026	0.98749
Tetrachloroethane	−0.48506	1.153	0.89737
Acetone	−0.37472	3.7685	0.98873
Nitromethane	−0.30625	10.465	0.99715
Acetaldehyde	−0.41863	4.4128	0.99183
Acetonitrile	−0.39598	7.4278	0.99132
Propionaldehyde	−0.38171	3.9717	0.99368

In addition to the equation of the line, the computer print-out contained the coefficient of correlation,[8] which is a measure of the degree with which the data points actually show the particular functional relationship constructed by the regression analysis. As can be seen from the tabulated values in Table I, the coefficient of correlation values were very high, ranging between 0.76996 and 0.99715, indicating excellent agreement between the data points and the computer-derived mathematical equations.
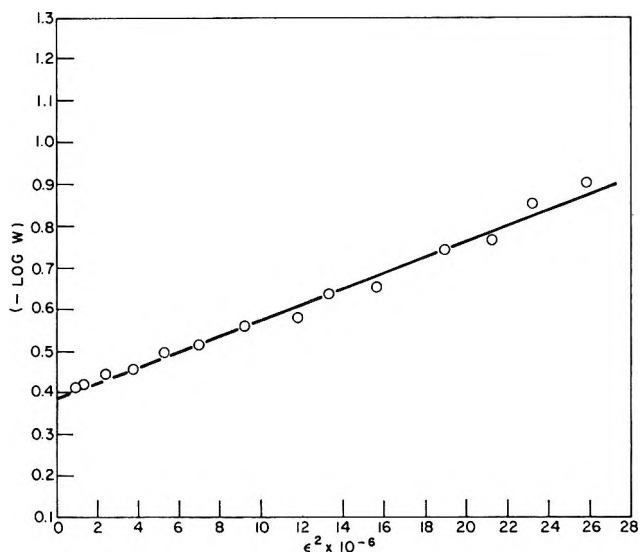
Figure 1. Plot of desorption isotherm data in the form of the Dubinin–Polanyi equation for CCl_4 at 60°.
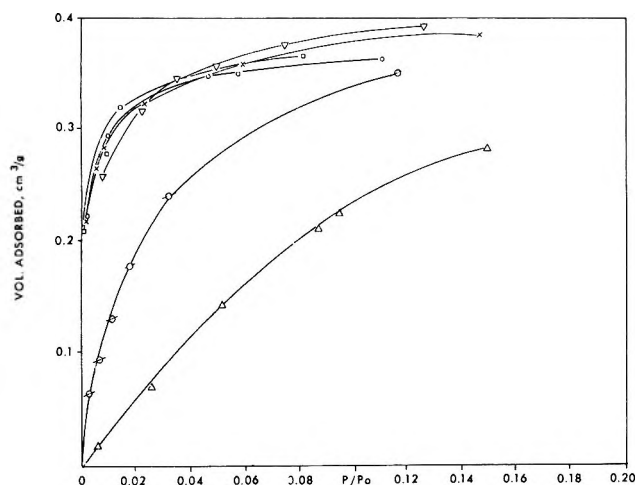
Figure 2. Desorption isotherms on activated carbon, 25°: O, carbon tetrachloride; □, 1,1,2,2-tetrachloroethane; ×, fluorobenzene; ▽, chloroform; ∅, nitromethane; △, methanol.

Results and Discussion

Figure 1 shows a typical plot of log W vs. ϵ^2 for the adsorption isotherm data of carbon tetrachloride at 60°.[9] Figure 2 shows desorption isotherms at 25° for six of the vapors tested and indicates the range of values obtained. Of the 15 organic vapors studied, only 2,2,4-trimethylpentane exhibited a large deviation from straight line behavior when the desorption data were plotted in the form of Dubinin–Polanyi equation. This is obvious from the value of the correlation coefficient (R) for 2,2,4-trimethylpentane listed in Table I.

(8) P. G. Hoel, "Introduction to Mathematical Statistics," Wiley, New York, N. Y., 1954, p 120; M. R. Spiegel, "Statistics," Schaum Publishing Co., New York, N. Y., 1961, p 224.

(9) A comprehensive tabulation of all isotherm data as log W vs. ϵ^2 may be obtained from the Final Report Contract No. DAAA 15-69-C-0712.

Table II: β Values Calculated Using Electronic Polarization

Groups	Vapors	β, experimental			β, theoretical		
		CCl₄	CHCl₃	Acetone	CCl₄	CHCl₃	Acetone
Nonpolar	CCl₄ (ref)	1.00	1.15	1.37	1.00	1.23	1.63
	Dioxane	0.72	0.82	0.99	0.82	1.02	1.35
	2,2,4-TMP	1.22	1.46	1.67	1.48	1.82	2.40
	Benzene	0.92	1.10	1.26	0.98	1.21	1.60
	Hexane	1.20	1.46	1.66	1.15	1.42	1.88
Weakly polar	Chloroform (ref)	0.87	1.00	1.21	0.81	1.00	1.32
$0 < \mu \leq 2$	Ethyl acetate	0.85	0.97	1.17	0.84	1.04	1.38
	Methanol	0.34	0.39	0.47	0.31	0.39	0.51
	Fluorobenzene	0.99	1.13	1.36	0.98	1.21	1.60
	Tetrachloroethane	1.31	1.49	1.81	1.15	1.43	1.88
Strongly polar	Acetone (ref)	0.72	0.83	1.00	0.61	0.76	1.00
$\mu > 2$	Nitromethane	0.43	0.50	0.60	0.48	0.59	0.79
	Acetaldehyde	0.66	0.77	0.92	0.43	0.54	0.70
	Acetonitrile	0.41	0.59	0.71	0.43	0.54	0.70
	Propionaldehyde	0.70	0.81	0.97	0.60	0.75	0.98

This was tentatively attributed to steric hindrance. The regression analysis for the three reference materials—carbon tetrachloride, chloroform, and acetone—included the data taken at 25, 40, and 60° since the temperature dependence over this range was found to be quite small and was taken into account with the T^2 term in the Dubinin–Polanyi equation. Table I also includes the k values for the organic vapors which were used to calculate β_{ex}.

Table II contains the values of β_{ex} calculated from eq 6 and β_{th} calculated from eq 12 for the three reference vapors. Electronic polarization (P_e) is obtained from the Lorenz–Lorentz equation using the following form

$$P_e = \frac{n^2 - 1}{n^2 + 2} \frac{M}{\rho} \qquad (12)$$

The refractive index of the liquid was measured at the sodium D wavelength. The organic vapors are arranged in groups of nonpolar, weakly polar, and strongly polar materials. It is obvious from the per cent deviations listed in Table III that the best agreement between β_{ex} and β_{th} is obtained when a reference compound in each of the groups is used to calculate β. That is, carbon tetrachloride does not serve as a good reference compound in the weakly polar or strongly polar group, but yields good agreement in the nonpolar group of which it is a member.

Table IV contains the values of β_{ex} and β_{th} based on molecular parachor and calculated from eq 9. It is noteworthy that the percentage deviation between the values is greater than that with electronic polarization, especially in the case of the polar compounds. If the dipole moment has a large effect in the adsorbate–adsorbent interaction, the greatest deviation between β_{ex} and β_{th} based on electronic polarization and parachor should occur in the polar group.

A number of empirical equations containing the dipole moment, such as eq 10 and 11, were also used to

Table III: Per Cent Deviation of β_{ex} from β_{th} Based on Electronic Polarization

Vapor	CCl₄	CHCl₃	Acetone
CCl₄ (reference)	...	...	...
Dioxane	12.2	19.5	26.6
2,2,4-TMP	17.6	19.8	30.4
Benzene	6.1	9.1	21.2
Hexane	4.3	2.8	11.7
	Av 10.0	Av 12.3	Av 22.4
Chloroform (reference)	...	...	...
Ethyl acetate	1.2	6.7	15.2
Methanol	9.7	0.0	7.8
Fluorobenzene	1.0	6.6	15.0
Tetrachloroethane	13.9	4.2	3.7
	Av 6.4	Av 4.4	Av 10.4
Acetone (reference)	...	...	...
Nitromethane	10.4	18.0	24.0
Acetaldehyde	53.5	42.5	31.4
Acetonitrile	42.0	9.2	1.4
Propionaldehyde	16.7	8.0	1.0
	Av 30.6	Av 19.4	Av 14.4

calculate theoretical values of β. The agreement between these values and the β_{ex} values, however, was very poor. Total polarization, which includes distortion and orientation polarizations, was calculated from the Debye equation and used to determine values of β_{th} with the equation

$$\beta_{th} = \frac{P}{P_{REF}} \qquad (13)$$

where P denotes the total polarization. Again the agreement between the experimental and theoretical results was poor.

It is interesting to note that all attempts to allow for contributions from permanent dipole forces in the adsorbate–adsorbent interaction by introduction of the

Table IV: Determination of β Using Parachor as Basis

	β, experimental	Ω	β, theoretical	% dev
CCl₄ (reference)	1.00	219	1.00	. . .
Dioxane	0.72	206	0.94	23.4
2,2,4-TMP	1.22	344	1.57	22.2
Benzene	0.92	207	0.94	2.1
Hexane	1.20	272	1.24	3.3
			Av	12.7
Chloroform	1.00	181	1.00	. . .
Ethyl acetate	0.97	216	1.19	18.5
Methanol	0.39	88.5	0.49	20.2
Fluorobenzene	1.13	215	1.19	5.0
Tetrachloroethane	1.49	256	1.36	9.6
			Av	13.3
Acetone	1.00	164	1.00	. . .
Nitromethane	0.60	133	0.81	26.0
Acetaldehyde	0.92	120	0.73	26.0
Acetonitrile	0.71	123	0.75	5.3
Propionaldehyde	0.97	121	0.74	31.0
			Av	22.1

dipole moment into an empirical equation for β_{th} were not successful. Thus it would appear that, in the case of an activated carbon containing only trace ionic impurities, the principal forces involved in the adsorbate–adsorbent interaction are dispersion forces. This appears to be the case for vapors with dipole moments no greater than 4 D. The conclusions follow from the fact that the electronic polarization, which is independent of the dipole moment, gives good agreement between the experimental and theoretical affinity coefficients. Conversely, an isotherm may be predicted for a vapor adsorbed on a carbon adsorbent of the type described from a knowledge of the electronic polarization and a reference vapor isotherm, provided the dipole moment is no greater than 4 D. For optimum predictive ability a reference vapor should be chosen which has similar polarity to the vapor whose isotherm is being predicted. Thus, although the affinity coefficient does not depend explicitly on the dipole moment, there is an implicit dependence of the affinity coefficient calculated from polarizations on the "polarity" of the adsorbate molecule. Allowance can be made for this by appropriate choice of reference vapor. Based upon these results, therefore, it is concluded that the Dubinin–Polanyi equations permit reasonably good predictions (per cent deviations from 4.4 to 14.4) of the adsorbate affinity coefficients for the vapors studied.

A Comparison of C–N Rotational Barriers in Amides,

Thioamides, and Amidinium Ions[1,2]

by Robert C. Neuman, Jr.,* and Violet Jonas

Department of Chemistry, University of California, Riverside, California 92502 (Received March 15, 1971)

Publication costs assisted by the National Institute of General Medical Sciences (PHS)

Rotational barriers about the central C–N bond were determined for N,N-dimethylacetamide-d_3 (E_a, 20.3; log A, 14.1; ΔF^*, 18.5), N,N-dimethylthioacetamide-d_3 (E_a, 25.9; log A, 14.6; ΔF^*, 23.4), N,N-dimethylacetamidinium-d_3 nitrate (E_a, 21.3; log A, 12.7; ΔF^*, 21.5), and N,N-dimethylacetamidinium-d_3 chloride (E_a, 22.8; log A, 13.5; ΔF^*, 21.8) in the solvent DMSO-d_6. These are compared with the results of molecular orbital calculations. Solvation effects are discussed. The conformational preferences for N-methylacetamidinium salts are shown to be essentially the same as those for N-methylacetamide and N-methylthioacetamide.

Several years ago, we set out to determine the barriers to rotation about the central C–N bond in a series of molecules of the general structure **1** including amides (X = O), thioamides (X = S), amidinium ions (X =

$$\delta^- X \quad\quad CH_3$$
$$\overset{\delta^+}{C \text{---} N}$$
$$R \quad\quad CH_3$$

1
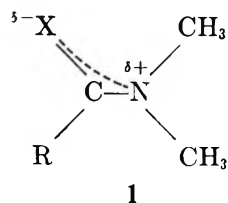
NH_2^+), and amidines (X = NH). Reasoning that variation in the group X could lead to differing degrees of C–N double bond character and that the comparative rotational barriers might reflect such differences, we thought that these data would be useful in other studies of systems in which these heteroatom groups participated in electron delocalization. This study has now been completed using the compounds **2** in the solvent dimethyl sulfoxide-d_6.[3-5]

$$X \quad\quad CH_3$$
$$C \text{---} N$$
$$CD_3 \quad\quad CH_3$$

2
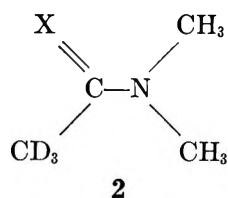
2a, X = O		(DMA-d_3)
2b, X = S		(DMTA-d_3)
2c, X = NH$_2^+$NO$_3^-$		(DMAAN-d_3)
2d, X = NH$_2^+$Cl$^-$		(DMAAC-d_3)

Results and Discussion

The deuterated compounds were synthesized in order to obtain relatively symmetric N(CH$_3$)$_2$ nmr signals amenable to analysis[5c] using the total line shape equations of Gutowsky and Holm.[4a] The Arrhenius plots

of the kinetic data for these systems are shown in Figure 1, and the resultant activation parameters, obtained as outlined in our previous papers,[5] are presented in Table I.[6,7]

We were unable to obtain extensive data for either DMTA-d_3 or DMAAC-d_3 (see Figure 1). In the former case the thioamide reacted slowly with the solvent. In the latter, the nonexchanging chemical shift between the two N(CH$_3$)$_2$ signals decreased to zero with increasing temperature.[6] We have shown that this is the result of ion pairing and a detailed study is reported in a related paper.[8]

(1) (a) This is part VI, Studies of Chemical Exchange by Nuclear Magnetic Resonance; part V: R. C. Neuman, Jr., W. R. Woolfenden, and V. Jonas, *J. Phys. Chem.*, **73**, 3177 (1969). (b) Presented at the Pacific Conference on Chemistry and Spectroscopy, San Francisco, Calif., Oct 6–9, 1970. (c) Taken from the Ph.D. Dissertation of V. Jonas, University of California, Riverside, Calif., Dec 1970.

(2) Support by the U. S. Public Health Service (National Institute of General Medical Sciences) through Grant GM-13342 is gratefully acknowledged.

(3) Since the pioneering work in this area,[4a] an extensive literature has developed.[4b-d] These results are the outgrowth of our previous work[1a,5] in which we established that reliable nmr kinetic data for amide rotation could be obtained *via* total line shape analysis using the complete Gutowsky–Holm equation.

(4) (a) H. S. Gutowsky and C. H. Holm, *J. Chem. Phys.*, **25**, 1228 (1956); (b) W. E. Stewart and T. H. Siddall, III, *Chem. Rev.*, **70**, 517 (1970); (c) M. Kessler, *Angew. Chem., Int. Ed. Engl.*, **9**, 219 (1970); (d) G. Binsch, *Topics Stereochem.*, **3**, 97 (1968).

(5) (a) R. C. Neuman, Jr., and L. B. Young, *J. Phys. Chem.*, **69**, 2570 (1965); (b) R. C. Neuman, Jr., D. N. Roark, and V. Jonas, *J. Amer. Chem. Soc.*, **89**, 3412 (1967); (c) R. C. Neuman, Jr., and V. Jonas, *ibid.*, **90**, 1970 (1968); (d) R. C. Neuman, Jr., W. Snider, and V. Jonas, *J. Phys. Chem.*, **72**, 2469 (1968).

(6) The kinetic and spectral data are given in the Experimental Section (Table IV).

(7) The activation parameters for DMA-d_3 (X = O) reported in Table I are slightly different than those previously reported:[5c] E_a, 20.6 ± 0.3; log A, 14.3 ± 0.3; ΔF^* (25°), 18.6. The values reported here are the result of further refinement of the spectral data.

(8) See related paper in this issue: R. C. Neuman, Jr., and V. Jonas, *J. Phys. Chem.*, **75**, 3550 (1971).

Table I: Activation Parameters for C–N Rotation in $CD_3C(X)N(CH_3)_2$ in DMSO-d_6

X	Concn, mol %	E_a,[a] kcal/mol	log A[a]	ΔF^* (25°),[b] kcal/mol	ΔH^*,[c] kcal/mol	ΔS^*,[d] eu
O	9.5	20.3 ± 0.3	14.1 ± 0.2	18.5	19.7 ± 0.3	+4.1 ± 0.8
S	8.1	25.9 ± 0.9	14.6 ± 0.5	23.4	25.3 ± 0.9	+6.3 ± 2.1
$NH_2^+NO_3^-$	3.1	21.3 ± 0.3	12.7 ± 0.2	21.5	20.7 ± 0.3	−2.6 ± 0.7
$NH_2^+Cl^-$	7.4	22.8 ± 0.7	13.5 ± 0.4	21.8	22.2 ± 0.7	+1.4 ± 1.9

[a] Calculated from a least-squares analysis of the data. [b] $\Delta F^* = E_a + 2.303RT[\log (k'T/h) - \log A]$. [c] $\Delta H^* = E_a - RT$. [d] $\Delta S^* = (\Delta H^* - \Delta F^*)/T$.
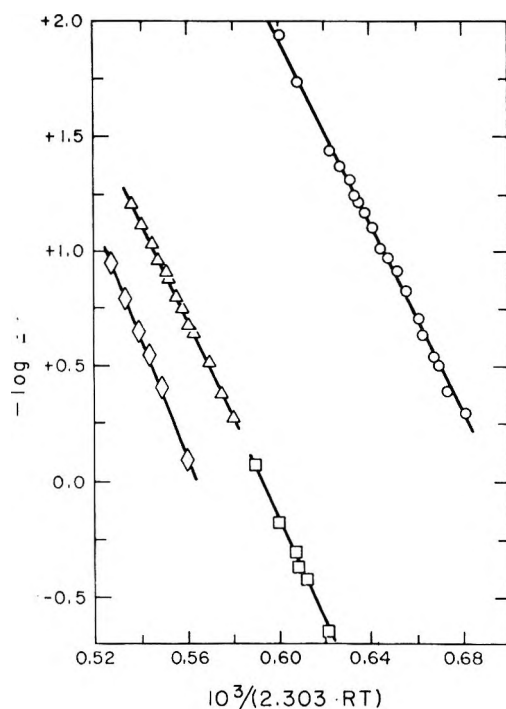
Figure 1. Arrhenius plots of the rate constants for rotation about the central C–N bond in DMA-d_3 (O), DMTA-d_3 (◇), DMAAN-d_3 (△), and DMAAC-d_3 (□) in the solvent DMSO-d_6.

The comparative activation parameters (Table I) indicate that the rotational barriers vary with the heteroatom in X. In the absence of solvation and solute-solute interactions, the values of E_a (or ΔH^*) should reflect differences in electron delocalization. However, DMSO-d_6 must solvate all of these molecules (*vide infra*) and such effects would be included in the values of E_a (or ΔH^*). Since solvation enthalpies and entropies of activation should partially compensate each other, comparative values of ΔF^* may be closer approximations to the true differences between the internal rotational barriers.

Recently, two groups have used molecular orbital theory to calculate properties of systems of the general structure **3** related to rotation about the central C–N bond. Sandström calculated values for the loss in π-electron energy on 90° rotation about the C–N linkage in units of β (ΔE_π), and the π-bond orders for the C–N bonds (pCN), for X = NH, NH_2^+, O, and S (R_1, R_2 =

3
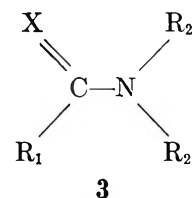
alkyl).[9] Bushweller directly calculated barriers for C–N rotation for X = O, S, and Se (R_1, R_2 = H).[10] Their results are not directly comparable to experimental values of ΔF^*, but Sandström's values of ΔE_π and Bushweller's barriers show the same trends as our values of ΔF^* (Table II).[11]

The π-bond orders do not correlate with ΔF^* values. This is not unreasonable since the former are ground state properties while the latter reflect differences between ground and transition states. However, the values of pCN do correlate with the experimental values of $J(^{13}CH)$ for the $N(CH_3)_2$ groups in these systems (Table II). Haake suggested that values of $J(^{13}CH)$ for N–CH_3 groups would increase with increasing positive charge on nitrogen; he reported the values of 131 and 145 Hz for trimethylamine and tetramethylammonium ion, respectively.[12] Those reported for the compounds in Table II are intermediate, indicating fractional positive charges on the $N(CH_3)_2$ nitrogens. The amount of positive charge on $N(CH_3)_2$ should depend on the π-bond order for the central C–N bond and the agreement between pCN and $J(^{13}CH)$, also a ground state property, provides support for the MO calculations. We suggested that values of $J(^{13}CH)$ might reflect the relative rotational barriers for these systems,[5a] but these results demonstrate that such a general correlation is not valid.

(9) J. Sandström, *J. Phys. Chem.*, **71**, 2318 (1967).

(10) C. H. Bushweller, P. E. Stevenson, J. Golini, and J. W. O'Neil, *ibid.*, **74**, 1155 (1970).

(11) (a) Sandström's values of ΔE_π are in units of β and appear to be related to values of ΔF^* according to the relationship $\Delta F^* = A \Delta E_\pi + B$ where neither constant A or B is known.[9] Bushweller's calculated values of the rotational barriers are about twice as large as experimental values.[10] (b) A rotational barrier for the amidine (X = NH) is not available, but we have reported that the $N(CH_3)_2$ resonance line for $CH_3C(NH)N(CH_3)_2$ is a singlet in chloroform down to the lowest temperature investigated ($-40°$).[5a] The upper limit of 17 kcal/mol (Table II) is based on a $\delta\nu_\infty$ of 1 Hz and a coalescence temperature of $-40°$.

(12) P. Haake, W. B. Miller, and D. A. Tysee, *J. Amer. Chem. Soc.*, **86**, 3577 (1964).

Table II: Comparisons of ΔF^* for C–N Rotation in $CD_3C(X)N(CH_3)_2$ with Results of Molecular Orbital Calculations and ^{13}C–H Coupling Constants

X	ΔF^* $(25°)$,[a] kcal/mol	$\delta_R \Delta F^*$,[b] kcal/mol	$\delta_R \Delta E_\pi$,[c] (β)	δ_R barrier,[d] kcal/mol	pCN[e]	$J(^{13}CH)$[f]
NH	(<17)	(<-1.5)	-0.083		0.363	135
O	18.5	0	0	0	0.422	138
$NH_2{}^+NO_3{}^-$	21.5	$+3.0$	$+0.100$		0.484	141
$NH_2{}^+Cl^-$	21.8	$+3.3$	$+0.100$		0.484	141
S	23.4	$+4.9$	$+0.104$	$+12.0$	0.455	140
Se	23.8	$+5.3$		$+12.6$		

[a] Values for **2a–d** from Table I; value for X = NH is upper limit (ref 11); value for X = Se (solvent, *o*-dichlorobenzene) from K. A. Jensen and J. Sandström, *Acta Chem. Scand.*, **23**, 1911 (1969). [b] $\delta_R \Delta F^* = \Delta F^*(X) - \Delta F^*(X = O)$. [c] $\delta_R \Delta E_\pi = \Delta E_\pi(X) - \Delta E_\pi(X = O)$; $\Delta E_\pi(X = O)$ equals 0.532β; taken from ref 9. [d] $\delta_R$barrier = barrier(X) − barrier(X = O); barrier(X = O) equals 40.8 kcal/mol; taken from ref 10. [e] π-Bond orders; ref 9. [f] ^{13}CH coupling constants for $N(CH_3)_2$ groups; see text. Values for X = NH, O, and $NH_2{}^+Cl^-$ have errors of less than ± 0.5 Hz; those for X = $NH_2{}^+NO_3{}^-$ and S have errors of less than ± 0.2 Hz.

We have shown that both DMA and DMTA form self-association dimers in nonpolar solvents.[5d] The nonexchanging chemical shift between the two NCH_3 signals is sensitive to the association process. From data in CCl_4 (36°), calculated values of $\delta\nu_\infty$ for monomer and dimer DMA are 7.3 and 13.8 Hz, respectively; those for DMTA are 7.1 and 1.8 Hz, respectively.[5d,13] In view of DMA's propensity to self-associate and the polar character of DMSO-d_6, we conclude that it is strongly solvated in this solvent.[5c] This is supported by a relatively temperature-independent value for $\delta\nu_\infty$ of 9.4 Hz (9.5 mol % DMA-d_3 in DMSO-d_6).[5c] The values of $\delta\nu_\infty$ for DMTA-d_3 in DMSO-d_6 (see Experimental Section, Table IV) are smaller than those for monomer DMTA, but larger than expected for the same concentration in CCl_4.[5d] This suggests that DMTA-d_3 is also solvated by DMSO-d_6. The positive values of ΔS^* for **2a** and **2b** agree with these proposals; the transition states should be less polar than the reactants leading to desolvation and values of $S^* > S_{reactant}$.[14]

The entropies of activation for the amidinium ions are smaller than those for the amide and thioamide, and that for DMAAN-d_3 is negative. Since the data for DMAAN-d_3 are more extensive and reliable than those for DMAAC-d_3 (*vide supra*), our discussions of solvation for the amidinium ions will be based on the results for the former system. The negative ΔS^* suggests increased solvation of the rotational transition state. In contrast to the amide and thioamide systems which are presumably solvated by dipolar interaction with DMSO-d_6, solvation of the amidinium ions probably involves hydrogen bonding (**4a** and **4b**). This interaction should be stronger in the transition state (**4b**) than in the planar and charge delocalized ground state (**4a**) in agreement with $\Delta S^* < 0$.

Two additional factors that might influence the rotational barriers for the amidinium ions are (1) the neighboring anion, and (2) steric interaction in the planar ground state between H(A) and CH_3(A) (see **5**).

4a

4b

5
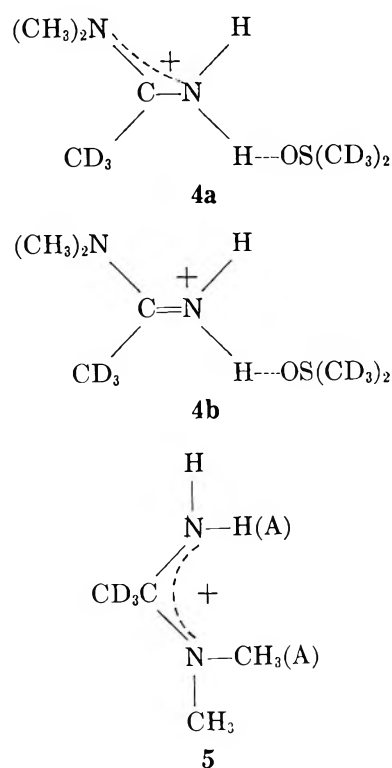
Since the amounts of ion pairing in the chloride and nitrate systems appear to be different,[8] the similarity in the values of ΔF^* (Table I) suggests that the anion and ion pairing do not markedly alter the rotational barriers. To probe the magnitude of the steric interaction between H(A) and CH_3(A) we have synthesized *N*-methylacetamidinium chloride and nitrate and determined the isomer distribution between **6a** and **6b** (X =

(13) The apparent difference in behavior of $\delta\nu_\infty$ for DMA and DMTA is the result of an inversion of the nmr signals for the nonequivalent NCH_3 groups.[5d]

(14) (a) Sandström[9] and Siddall, *et al.*,[14b] have recently reported values of ΔF^* (140°) for DMTA of *ca.* 21.6 and 21.8 kcal/mol, respectively, using the solvent *o*-dichlorobenzene. Our data in DMSO-d_6 (Table I) give a value of ΔF^* (140°) of 22.7 kcal/mol. The difference may be due to a solvent effect. (b) T. H. Siddall, III, W. E. Stewart, and F. D. Knight, *J. Phys. Chem.*, **74**, 3580 (1970).

6a ⇌ **6b**
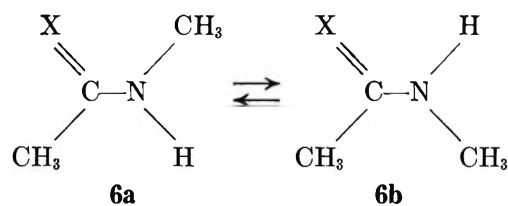
NH$_2$$^+$) in different solvents. These data are compared with those for the analogous amide (X = O) and thioamide (X = S) in Table III.[15,16] The similarity in the isomer distributions for the various X groups suggests that the potential steric interaction (5) is relatively unimportant.

Table III: Isomer Distributions for the Compounds CH$_3$C(X)NHCH$_3$ (**6a** and **6b**) in Solution

X	Solvent	6a, %	6b, %
O	Neat[a]	98	2
	H$_2$O[b]	97	3
S	CCl$_4$[b]	97	3
	C$_6$H$_6$[b]	97	3
NH$_2$$^+Cl^-$	D$_2$O[c]	96	4
NH$_2$$^+NO_3$$^-$	D$_2$O[c]	96	4
	DMSO-d_6[c]	97	3

[a] K. Anderson, unpublished results. [b] J. Sandström and B. Uppström, *Acta Chem. Scand.*, **21**, 2254 (1967). [c] Determined by E. Logue.

Experimental Section

Materials. The solvent DMSO-d_6 was prepared by deuteration of commercial dimethyl sulfoxide[5c] and was also obtained commercially from Diaprep. The synthesis of N,N-dimethylacetamide-d_3 (**2a**) has been described.[5c]

N,N-Dimethylthioacetamide-d_3 (**2b**) was synthesized from DMA-d_3 by treatment with potassium sulfide and phosphorus pentasulfide.[5a] On reaction of 47 g of DMA-d_3 with 87.5 g of K$_2$S and 59 g of P$_2$S$_5$ in 300 ml of xylene, ca. 30 g of crude DMTA-d_3 were obtained. Recrystallization from benzene yielded white crystals of DMTA-d_3; mp 72–74° (mp undeuterated DMTA: 72–73.5°);[5a] nmr: two singlets of equal area at 196.1 and 201.7 cps (reference TMS); ca. 97% deuterated from nmr spectroscopy. Recrystallization was complicated by coprecipitation of bright yellow crystals assumed to be elemental sulfur.

N,N-Dimethylacetamidinium-d_3 chloride (**2d**) was obtained by base-catalyzed deuteration of N,N-dimethylacetamidinium chloride in D$_2$O. An attempt was made to synthesize DMAAC-d_3 from CD$_3$CN (99.5% deuterated) using the conventional amidinium ion synthesis of Pinner;[5a] however, the resulting product was only 33% deuterated in the C–CH$_3$ group. It was shown that deuterium exchange occurred during reaction of the intermediate imino ester hydrochloride

with dimethylamine. The 33% C–CH$_3$ deuterated DMAAC was completely deuterated by the following procedure.

A 5-g quantity of this material was dissolved in 50 g of D$_2$O and immediately reisolated by removal of the solvent. This material was then dissolved in 50 g of D$_2$O saturated with calcium oxide (resulting pD ca. 11) and allowed to stand at room temperature for 15–18 days. About 97% C–CH$_3$ deuteration (by nmr spectroscopy) of DMAAC had occurred, but also ca. 80% hydrolysis to acetamide (by nmr spectroscopy) had taken place. (After 8–9 days 65–68% hydrolysis had occurred while C–CH$_3$ deuteration had proceeded to the extent of 90%.) The reaction mixture was filtered to remove solid calcium oxide and neutralized to pH 6 with concentrated hydrochloric acid. The solvent was removed by evaporation *in vacuo*, and the syrupy residue was dried *in vacuo* over P$_2$O$_5$. The semisolid was washed several times with acetone and dried over P$_2$O$_5$ *in vacuo*. Recrystallization from chloroform yielded 0.16 g of DMAAC-d_3 (ca. 97% C–CH$_3$ deuterated): mp 168.5–169.5° (mp undeuterated DMAAC: 164–166.5°); nmr: two singlets of equal area at 191 and 189 cps (reference TMS, solvent DMSO-d_6). Crude gravimetric chloride analysis yielded 96% of theoretical AgCl.

N,N-Dimethylacetamidinium-d_3 nitrate (**2c**) was prepared by slow addition of an aqueous silver nitrate solution to a stirred equivalent amount of DMAAC-d_3 in water. The mixture was filtered and the water was removed by lyophilization and *in vacuo* over P$_2$O$_5$. A 96.3% yield of DMAAN-d_3 was obtained; mp 150–153° (mp undeuterated DMAAN: 151–153°); nmr: two singlets of equal area at 184.5 and 189.5 cps (reference TMS, solvent DMSO-d_6). *Anal.* Calcd for C$_4$H$_8$D$_3$N$_3$O$_3$: C, 31.57; H (includes D), 7.01; N, 27.61. Found: C, 31.42; H, 7.33; N, 27.11, 27.13.

N-Methylacetamidinium Chloride and Nitrate.[16] The Pinner synthesis of amidinium ions[5a] yielded a mixture of N-methylacetamidinium and N,N'-dimethylacetamidinium[17] chloride when the intermediate imino ester hydrochloride was treated with an equivalent amount of methylamine. Recrystallization from ethanol-ether and subsequently from ethanol-benzene gave pure N-methylacetamidinium chloride; mp 147–149°; nmr (D$_2$O, TPS) partially resolved quartet, 139.2 Hz (area 1.0); partially resolved quartet, 174.6 Hz (area 0.97); broad singlet, 178.4 Hz (area 0.03). *Anal.* Calcd for C$_3$H$_9$N$_2$Cl: Cl, 32.65. Found: Cl, 29.40, 29.89, 28.86. Reaction of an aqueous solution of this chloride

(15) In all cases the NCH$_3$ signals corresponding to **6a** and **b** can be identified with the isomers by the substantially greater CCH$_3$, NCH$_3$ spin-coupling observed in the trans configuration (**6a**).

(16) Ellen Logue synthesized the N-methylacetamidinium salts and determined their nmr spectral data.

(17) G. S. Hammond and R. C. Neuman, Jr., *J. Phys. Chem.*, **67**, 1655 (1963).

Table IV: Kinetic and Spectral Data for C–N Rotation in **2b**, **2c**, and **2d** in DMSO-d_6

Temp, °C	$\delta\nu_\infty$, Hz[a]	2τ, sec[b]	Temp, °C	$\delta\nu_\infty$,[a] Hz	2τ,[b] sec
2b (8.1 mol %)			**2c** (3.1 mol %)		
37.8	5.90		38	5.17	
99.1	6.50		62	4.93	
117.3	6.85	0.818	82	4.73	
124.9	6.95	0.390	103.8	4.35	0.540
128.9	6.95	0.282	107.0	4.35	0.420
132.2	7.05	0.226	110.4	4.35	0.300
137.2	6.95	0.162	115.2	4.35	0.221
141.4	7.10	0.111	116.4	4.30	0.208
			118.4	4.30	0.178
			120.5	4.20	0.159
			122.6	4.25	0.131
2d (7.4 mol %)			123.7	4.05	0.123
37.8	1.8		126.4	4.05	0.109
64.4	1.2		128.3	4.05	0.091
76.7	0.85		131.5	4.05	0.076
78.8	0.85	4.40	134.4	4.05	0.061
83.8	0.85	2.70			
85.7	0.75	2.30			
86.5	0.70	2.04			
91.1	0.60	1.50			
97.2	0.55	0.848			

[a] Nonexchanging chemical shift between the $N(CH_3)_2$ methyl groups. [b] Rotational rate constant k equals $1/(2\tau)$.

with an equivalent amount of aqueous silver nitrate solution gave N-methylacetamidinium nitrate; mp 99–102°; nmr (D_2O, TPS) identical with chloride salt. *Anal.* Calcd for $C_3H_9N_3O_3$: C, 26.67; H, 6.71; N, 31.10. Found: C, 27.18; H, 7.09; N, 29.80, 29.78.

Kinetic Studies. Complete details have been reported.[1a,5] Temperatures were determined using the ethylene glycol standard and the equation $T(°C) = 193.5 - 1.693\delta\nu_e$ where $\delta\nu_e$ is the chemical shift (Hz) between the CH_2 and OH protons. Rate constants for **2a** have been reported[5c] and those for **2b–d** are given in Table IV. All spectra were recorded at 60 MHz.

Thermal Decomposition of DMTA-d_3. Upon heating DMTA-d_3 in DMSO-d_6 at 137° for 1.5 hr, the solution turned brown and 50% of the DMTA-d_3 reacted to form an essentially quantitative yield of DMA-d_3 (by nmr signal position). When undeuterated DMSO was the solvent, a signal corresponding to that expected for $(CH_3)_2S$ developed along with that for DMA-d_3. Because of this reaction it was not possible to obtain more than three or four spectra for any one sample at an elevated temperature, and it was necessary to work with fresh samples of DMTA-d_3 in DMSO-d_6 for each temperature run. By careful pretuning on samples of tetrachloroethane in DMSO-d_6 it was possible to obtain reasonable spectra with less than 10% total decomposition of DMTA-d_3 at the highest temperatures employed.

Anomalous Results with Amidinium Ions. It was found that unusual and erratic spectral behavior of samples of amidinium ions in DMSO-d_6 was caused by trace amounts of the free base N,N-dimethylacetamidine-d_3. Consistent results and spectral behavior were obtained by adding a trace amount of concentrated acid to the solutions.

J(^{13}CH) Values. These values were obtained in the solvent DMSO-d_6 using procedures similar to those previously described.[5a]

Nuclear Magnetic Spin–Lattice Relaxation Times of Phosphorus-31 in Some Organic and Inorganic Compounds

by Stephen W. Dale and Marcus E. Hobbs*

Department of Chemistry, Duke University, Durham, North Carolina 27706 (Received March 22, 1971)

Publication costs assisted by Duke University Special Research Fund No. 393-3206

The spin–lattice relaxation times of phosphorus in 11 liquid compounds investigated over approximately a 100° temperature interval were found to have major relaxation contributions from dipole–dipole, chemical shift anisotropy, and spin–rotation interactions. By means of relaxation times determined at two magnetic field strengths and by the different dependence of the spin–rotation and dipolar interactions on viscosity and temperature, approximately quantitative separations of the several contributions were effected. A rough parallelism was observed between the chemical shift of a particular compound and the chemical shift anisotropy parameter $|\Sigma|$; a similar relation for the spin–rotation parameter was expected but the correlation was considerably poorer. The results of the investigation were taken to indicate that the second-order paramagnetic shielding was dominant for ^{31}P in the compounds investigated and that the approximate relative magnitude of this shielding could be estimated from a study of the spin–lattice relaxation times.

Introduction

Nuclear magnetic resonance studies[1] of the chemical shifts of ^{31}P indicate greater deshielding in phosphites than in phosphates, and in some cases the magnitude and direction of chemical shifts[2] in a series of closely related ^{31}P compounds is difficult to understand. In view of a continuing interest in this laboratory in the chemical shifts of ^{31}P and the relation of chemical shifts to structure, it became of interest to determine if there were shielding contributions from shielding anisotropy and from spin–rotation fields, and, if so, to attempt to relate these fields to the observed chemical shifts.

The most direct way of investigating these matters for liquids seemed to be the determination of spin–lattice relaxation times with the collateral determination of the interaction parameters for the several recognized[3] mechanisms of nuclear spin relaxation. A study of spin–lattice relaxation times, T_1, over a range of temperatures and viscosities and at different external magnetic field intensities allows one, by the temperature study, to differentiate[4] between normal dipolar and the spin–rotation components, and by the magnetic field changes, to determine the chemical shielding anisotropy parameter.[5]

In the present investigation the viscosity and relaxation times at 19.3 MHz as functions of temperature over approximately a 100° range were studied for 11 compounds and, additionally, the relaxation times at 33° were determined at a field strength corresponding to ^{31}P resonance at 40.5 MHz. The compounds investigated were PBr$_3$ (−227); P$_4$O$_6$ (−113); PO(OH)$_3$, 85% (reference); P(OCH$_3$)$_3$ (−140); P(OC$_2$H$_5$)$_3$ (−138); P(O-i-C$_3$H$_7$)$_3$ (−138); P(O-n-C$_4$H$_9$)$_3$ (−138); OP(OCH$_3$)$_3$ (−2); SP(OCH$_3$)$_3$ (−73); OP(OC$_2$H$_5$)$_3$ (+1); OP(O-n-C$_4$H$_9$)$_3$ (+0.5) (−61).

The figures in parentheses are chemical shifts (parts per million) observed in this investigation at 19.3 MHz and
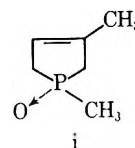
approximately 26° with 85% H$_3$PO$_4$ as an external reference. The cyclic compound is an example from many cyclic phosphines and related oxides on which considerable synthetic work has been done in this laboratory and for which some ^{31}P chemical shift data have been reported;[2,6] chemical shift data and relaxation times for some other ^{31}P ring compounds will be reported elsewhere. The observed chemical shifts of the compounds listed above agree well with previously reported values[1,7] in cases for which a comparison can be made. In the remainder of this paper the various organic groupings will be referred to as follows: −CH$_3$ ≡ Me; −C$_2$H$_5$ ≡ Et, O-i-C$_3$H$_7$ ≡ O-i-Pr, and O-n-C$_4$H$_9$ ≡ OBu.

(1) (a) M. M. Crutchfield, C. H. Dungan, J. H. Letcher, V. Mark, and J. R. Van Wazer, *Top. Phosphorus Chem.*, V, 227 (1967); (b) J. F. Nixon and A. Pidcock, *Ann. Rev. Nmr Spectrosc.*, 2, 345 (1969).

(2) L. D. Quin, J. J. Breen, and D. K. Myers, *J. Org. Chem.*, 36, 1297 (1971).

(3) (a) A. Carrington and A. D. McLachlan, "Introduction to Magnetic Resonance," Harper and Row, New York, N. Y., 1967, Chapter 11; (b) J. A. Pople, W. G. Schneider, and H. J. Bernstein, "High Resolution Nuclear Magnetic Resonance," McGraw-Hill, New York, N. Y., 1959, Chapter 9.

(4) (a) D. K. Green and J. G. Powles, *Proc. Phys. Soc. (London)*, 85, 87 (1965); (b) P. R. Hubbard, *Phys. Rev.*, 131, 1155 (1963).

(5) H. S. Gutowsky and D. E. Woessner, *ibid.*, 104, 843 (1956).

(6) (a) S. W. Dale, M.A. Thesis, Duke University (1966); (b) C. F. Ramirez, C. P. Smith, A. S. Galati, and A. V. Potwardhan, *Tetrahedron Lett.*, No. 26, 3053 (1966).

(7) J. W. Emsley, J. Feeney, and L. H. Sutcliffe, "High Resolution Nuclear Magnetic Resonance Spectroscopy," Vol. 2, Pergamon Press, Elmsford, N. Y., 1966, Appendix F.

Experimental Section

Spin–lattice relaxation times, T_1, of ^{31}P in the several compounds were determined using a Varian HR-60 spectrometer system for measurements at 19.3 MHz (11,200 G) at 0 to 105° and a Varian HA-100 spectrometer system operated[8] in the HR mode for measurements at 40.5 MHz (23,500 G) and 33°. The saturation recovery technique[9] was used for all T_1 determinations, with exceptional care being exercised to ensure negligible saturation during the recovery period. The standard deviation of the average values of T_1 for all neat samples recorded in subsequent tables was in the range of ±2 to ±5%. For the diluted samples and the 85% H_3PO_4 the standard deviation was occasionally as large at ±10%. Chemical shifts of ^{31}P referenced to external 85% H_3PO_4 were determined at 19.3 MHz and 26° using the side band technique[10] employing a carefully calibrated Krohn-Hite Audio Oscillator Model 440-B and either external H_3PO_4 or P_4O_6. The accuracy of the recorded chemical shift values is estimated as ±0.5 ppm. The temperature of the probe was determined by use of a substitute sample tube and a calibrated thermistor element. The temperature was monitored between sample placements in the probe, and recorded temperatures are average values with an average deviation of approximately ±0.5°. It was found that chemical shift determinations and measured relaxation times were not influenced by sample spinning so stationary samples were used so as to minimize noise.
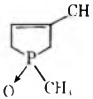
Viscosities of all compounds, excepting P_4O_6 for which the sample was in limited supply, were determined using a dry N_2 atmosphere at 13, 25, 55, and 80° in no. 50 and 100 Ostwald-Fenske viscometers calibrated with carefully purified toluene and aniline, respectively. Densities for all compounds except P_4O_6 were determined at the same temperatures as used for the viscosity measurements so as to allow direct correction of flow times to absolute viscosity. With the exception 85% H_3PO_4 and P_4O_6, diluted samples for T_1 measurements at 25° were prepared by addition of 0.3 ml of $CDCl_3$ to 1.0 ml of the sample; the 85% H_3PO_4 was diluted similarly with $(CD_3)_2CO$. Excepting P_4O_6 and 85% H_3PO_4 all compounds were distilled under dry N_2 and the samples to be examined at 19.3 MHz were sealed in 5-mm o.d. tubes under dry N_2. The samples used for 40.5-MHz nmr examination were obtained as aliquots of the viscosity–density samples and were placed in Type E NMR Specialties 5-mm tubes for relaxation time measurements. In view of this handling of the 40.5-MHz samples the absence of dissolved oxygen, especially in the phosphate samples, is less certain than for the 19.3-MHz samples used for the T_1-temperature study. The viscosity and density samples were stored under dry N_2 until used. The P_4O_6 was obtained from Albright and Wilson, Ltd., London, and contained some solid yellow material which the manufacturers indicated were oxides of phosphorus. Samples with and without the solid

material were found to have the same chemical shift and relaxation time. Other compounds with the exception of the cyclic compound were obtained as the best grades available from chemical supply houses; the cyclic compound was synthesized in this laboratory by Professor L. Quin and coworkers.

Results and Discussion

The values of the ^{31}P spin–lattice relaxation rates found at five temperatures are listed in Table I. The viscosity, η, and the ratio of viscosity to density, η/ρ, found at four temperatures are given in Table II. Except as indicated the results in both tables are for pure liquids. The values of η/T and the dependence of the relaxation rate, $1/T_1$, on this viscosity-temperature ratio will be used later to try to differentiate the relaxation rate attributable to randomly fluctuating dipolar interactions from the relaxation rate attributable to the fluctuating coupling of the nuclear spin of ^{31}P and the field arising from rotation of the molecule, the so-called spin–rotation contribution to relaxation.

Table I: Spin–Lattice Relaxation Rate,[a] $1/T_1$, of ^{31}P in Several Phosphorus Compounds Observed in a Field of 11.2 kG

| Substance | \multicolumn{6}{c}{T, °C} |
| | 0 | 25 | 55 | 80 | 105 | 25 (diluted sample)[b] |
	\multicolumn{6}{c}{$(1/T_1) \times 10^2$, sec^{-1}}
PBr_3	16.7	15.9	18.9	21.2	27.0	19.6
$P(OMe)_3$	10.1	15.6	17.8	21.7	25.0	14.9
$P(OEt)_3$	5.2	8.1	9.5	11.6	11.5	6.2
$P(O\text{-}i\text{-}Pr)_3$	5.1	5.4	6.0	6.3	8.8	5.0
$P(OBu)_3$	9.0	8.5	7.6	6.9	6.8	7.5
$OP(OMe)_3$	11.3	8.6	7.1	8.7	9.8	7.3
$SP(OMe)_3$	6.7	7.0	8.1	10.2	13.0	8.3
$OP(OEt)_3$	6.5	5.5	5.3	6.8	7.6	6.6
$OP(OBu)_3$	16.4	10.8	7.6	6.0	6.5	10.5
$OP(OH)_3$[c]	(20)[c]	(10)[c]	(17)[c]	(9.1)[c]	(13)[c]	(10)[c]
cyclic	40.0	15.6	7.9	9.6	9.9	12.3
P_4O_6[d]	...	5.7	6.3	10.5	13.3	...

[a] All values in the table are the average of four to six separate measurements. With the exception of H_3PO_4 the standard deviation of the average values was generally less than ±5%. [b] The diluted samples were prepared as described in the text. [c] The data for 85% H_3PO_4 are rather uncertain as relaxation times were of the order of 1.0 sec. The recorded rates are × 10 not × 10². [d] The P_4O_6 was solid at 0° and because of short supply no dilutions were made.
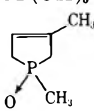
(8) Appreciation is expressed to Dr. C. G. Moreland, of North Carolina State University, Raleigh, N. C., for making available the HA-100 spectrometer.

(9) E. R. Andrew, "Nuclear Magnetic Resonance," Cambridge University Press, New York, N. Y., 1955, p 107 ff.

(10) Reference 3b, p 74.

Table II: Viscosity,[a] η, in Centipoise and the Viscosity–Density Ratio, η/ρ, of Some ³¹P Compounds

						T, °C					
	13		25		55		80		25 (diluted)	
Substance	η	η/ρ	η	η/r	η	η/ρ	η	η/ρ	η^b	η/ρ^b
PBr₃	1.899	0.654	1.667	0.580	1.217	0.435	1.030	0.376	1.288	0.503
P(OMe)₃	0.700	0.660	0.581	0.555	0.470	0.462	0.377	0.384	0.612	0.534
P(OEt)₃	0.746	0.773	0.657	0.689	0.473	0.512	0.375	0.420	0.726	0.675
P(O-i-Pr)₃	1.163	1.277	0.977	1.086	0.645	0.739	0.504	0.595	1.065	1.028
P(OBu)₃	2.172	2.343	1.667	1.926	1.113	1.249	0.833	0.959	1.480	1.412
OP(OMe)₃	2.491	2.038	1.993	1.651	1.236	1.050	0.910	0.793	1.658	1.113
SP(OMe)₃	2.200	1.824	1.749	1.465	1.053	0.908	0.791	0.699	1.262	1.004
OP(OEt)₃	1.872	1.738	1.525	1.433	0.967	0.935	0.722	0.718	1.488	1.293
OP(OBu)₃	4.645	4.725	3.301	3.392	1.751	1.847	1.221	1.320	2.542	2.341
OP(OH)₃[c]	(60.5)	(35.7)	40.6	24.2	15.0	9.03	8.21	5.01	47.2	31.3
(ring structure)	8.90	8.27	5.76	5.41	2.599	2.497	1.683	1.652	4.132	3.568

[a] Average of three measurements with a precision of the average of 1–3%; P₄O₆ not measured as it was in short supply. [b] Results are for diluted samples prepared by addition of 0.3 ml of CHCl₃ to 1.0 ml of sample except for 85% H₃PO₄ for which (CH₃)₂CO was used as diluent. Nominally 85% H₃PO₄ in water solution; the value at 13° was obtained by extrapolation of measurements at 25, 40, 55, and 80°.

Since the dependence of η/T on temperature was of major importance in the interpretation of the applicable mechanisms of relaxation, it was of interest to determine for the compounds investigated if the η–T dependence was well described by normal values of the viscosity activation parameters. In the transition state theory[11] the dependence is given by

$$\eta/\rho = \frac{Nh}{M} e^{\Delta H^{\ddagger}/RT} e^{-\Delta S^{\ddagger}/R} \tag{1a}$$

or in terms of an Arrhenius-type[12] expression the relation is

$$\eta = \eta_0 e^{E_v/RT} \tag{1b}$$
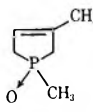
In eq 1a, N is Avogadro's number, M the gram molecular weight, and other symbols have their usual meaning. The relation between E_v and $\Delta H^{\ddagger}$ is given by

$$E_v = \Delta H^{\ddagger} - RT^2 \left(\frac{\partial \ln \rho}{\partial T}\right)_P$$

Since $-RT^2(\partial \ln \rho/\partial T)_P$ for most liquids in the present investigation was of the order of +100 to +300 cal/mol, the values of E_v and $\Delta H^{\ddagger}$ should agree within this difference. The values of $\Delta H^{\ddagger}$ and E_v, along with the value of $\Delta S^{\ddagger}$ calculated using η/ρ at 80°, are given in Table III. The graphs of $\ln \eta/\rho$ vs. $1/T$ and of $\ln \eta$ vs. $1/T$ were straight lines within the estimated experimental errors of the measurements.

The values of the viscosity activation parameters appear normal and predict rather well the observed dependence of η on the temperature. For example, in the best case, P(OBu)₃, using the value of $\Delta H^{\ddagger}$ and from the observed values of η/ρ at 25° the $\Delta S^{\ddagger}$ value calculated is -9.71 cal/(mol °K). This is to be com-

Table III: Activation Parameters for Viscous Flow of Some ³¹P Compounds
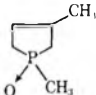
Substance	$\Delta H^{\ddagger}$, kcal mol⁻¹	E_v, kcal mol⁻¹	$\Delta S^{\ddagger}$, cal mol⁻¹ °K⁻¹
PBr₃	1.67	1.82	−10.86
P(OMe)₃	1.63	1.92	−9.45
P(OEt)₃	1.84	2.06	−9.62
P(O-i-Pr)₃	2.15	2.52	−9.88
P(OBu)₃	2.67	2.91	−9.72
OP(OMe)₃	2.84	2.98	−7.73
SP(OMe)₃	2.88	3.11	−7.57
OP(OEt)₃	2.70	3.01	−8.44
OP(OBu)₃	3.87	4.04	−7.09
OP(OH)₃ (85%)	6.01	6.08	−1.68
(ring structure)	4.92	5.06	−3.12

pared with the $\Delta S^{\ddagger}$ value calculated for 80° and shown in Table III as -9.72 cal/(mol °K). In the worst case, the phosphoryl ring compound, the respective values for $\Delta S^{\ddagger}$ were -2.92 and -3.12 cal/(mol °K). For other cases similarly calculated values of $\Delta S^{\ddagger}$ agreed within ±0.04 units in $\Delta S^{\ddagger}$. In later discussion values of η at 0 and 105° are needed and will be obtained by extrapolation of $\ln \eta$ vs. $1/T$ graphs. The consistency of the viscosity activation parameters in predicting the viscosity–temperature dependence allow the indicated extrapolations to be done with confidence.

(11) S. Glasstone, K. J. Laidler, and H. Eyring, "The Theory of Rate Processes," McGraw-Hill, New York, N. Y., 1941, p 480 ff.

(12) E. N. Da C. Andrade, "Viscosity and Plasticity," W. Heffner and Sons, Ltd., Cambridge, 1947, p 23.

Table IV: Comparison of Observed ^{31}P Spin–Lattice Relaxation Rates, $1/T_{1,0}$, at 33° and Calculated Anisotropy Contribution, $1/T_{1,A}$, at Two Magnetic Field Intensities

Substance	$H_1 = 11.2$ kG				$H_2 = 23.5$ kG	
	$(1/T_{1,0})$ $(\times 10^2)$, sec^{-1}	$(1/T_{1,A})$ $(\times 10^2)$, sec^{-1}	$|\Sigma|$ $(\times 10^4)$	σ $(\times 10^4)$	$(1/T_{1,0})$ $(\times 10^2)$, sec^{-1}	$(1/T_{1,A})$ $(\times 10^2)$, sec^{-1}
PBr$_3$	16.7	1.10	3.6	-2.27	20.4	4.79
P(OMe)$_3$	16.7	5.00	3.5	-1.40	33.3	21.70
P(OEt)$_3$	8.7	0.82	3.6	-1.38	11.5	3.61
P(O-i-Pr)$_3$	5.6	3.50	$(5.4)^a$	-1.38	17.6	$(15.4)^a$
P(OBu)$_3$	8.3	1.00	2.0	-1.38	11.8	4.52
OP(OMe)$_3$	7.8	0.26	1.5	-0.02	8.7	1.15
SP(OMe)$_3$	7.3	0.45	1.9	-0.73	8.8	1.96
OP(OEt)$_3$	5.4	0.96	2.6	$+0.01$	8.6	4.24
OP(OBu)$_3$	10.1	1.62	1.8	$+0.05$	15.6	7.14
P$_4$O$_6$	6.3	1.45	3.0	-1.13	11.2	6.37
[ring structure with CH$_3$, P, O, CH$_3$]	12.5	2.72	2.8	-0.67	21.7	11.9

^{a} These values are considered uncertain as the rate observed at high field appears to be in error, though reproducible with the sample of the compound available.

Spin–lattice relaxation rate studies of P$_4$O$_6$ have been reported by Chapman and Mowthorpe[13a] and more recently by Aksnes,[13b] and studies of PBr$_3$ by Winter[14a] and by Rhodes, et al.[14b] It appears that in addition to the above compounds and those reported in the present investigation, the spin–lattice relaxation times of only a few other ^{31}P compounds have been studied.[15] The observed relaxation rates in the present study are thought to arise from dipole–dipole, chemical shift anisotropy, and spin–rotation interactions.[3] In the case of PBr$_3$ the scalar effect observed by Winter[14a] and reported in detail by Abragam[16] and also observed by Rhodes, et al.,[14b] is of little or no consequence in magnetic fields corresponding to resonance frequencies of 19.3 MHz or greater.[17] The scalar effects that might arise from chemical exchange[18] in 85% H$_3$PO$_4$ will not be considered as the relaxation rate data for H$_3$PO$_4$ obtained in the present investigation are of such uncertainty as not to warrant detailed treatment.

The influence on the observed relaxation rate, $1/T_{1,0}$, of changing the magnetic field from 11.2 to 23.5 kG is shown in Table IV. It is apparent that rather large effects are observed in some cases. For the trivalent ^{31}P compounds the presence of O$_2$ is an unlikely explanation of the large differences as O$_2$ is likely to react readily and convert the parent substance into the phosphoryl compound. Measurements with the 23.5-kG field were made at 33° as this was the ambient probe temperature in the available Varian HA-100 instrument. Values of $1/T_{1,0}$ at 33° and a field of 11.2 kG were interpolated from values of $1/T_1$ recorded in Table I.

The values in Table IV under the columns headed by $(1/T_{1,A})$ are the relaxation rate contributions of chemical shift anisotropy to the total relaxation rates, $1/T_{1,0}$, at field H. The values shown were calculated as follows.

Excepting the anisotropic effect, it was assumed all other factors affecting the rate were constant and field independent including the condition that $(\omega\tau_c)^2 \ll 1$, where ω is the Lamor angular frequency and τ_c the tumbling correlation time. If this is the case, the relation of $1/T_{1,0}$ and $1/T_{1,A}$ is given by

$$\left(\frac{1}{T_{1,0}}\right)_{H_1} - \left(\frac{1}{T_{1,0}}\right)_{H_2} = \left(\frac{1}{T_{1,A}}\right)_{H_1} - \left(\frac{1}{T_{1,A}}\right)_{H_2} \quad (2)$$

where $(1/T_{1,A})_H$ is defined[3a] by

$$\frac{1}{T_{1,A}} = (^1/_5)(\gamma_N H)^2(\Sigma_1^2 + \Sigma_2^2 + \Sigma_3^2)\tau_c \quad (3)$$

(13) (a) A. C. Chapman and D. J. Mowthorpe, Mol. Phys., 15, 429 (1968); (b) D. W. Aksnes, Acta Chem. Scand., 23, 1078 (1969).

(14) (a) J. M. Winter, C. R. Acad. Sci., 249, 1346 (1959); (b) M. Rhodes, D. W. Aksnes, and J. H. Strange, Mol. Phys., 15, 541 (1968).

(15) (a) M. Cohn and T. R. Hughes, J. Biol. Chem., 235, 3250 (1960); (b) R. G. Shulman, H. Sternlicht, and B. J. Wyluda, J. Chem. Phys., 43, 3116 (1965); C. H. Stanlicht, R. G. Shulman, and E. W. Anderson, ibid., 43, 3123 (1965); (d) F. Klanberg, J. D. Hunt, and H. W. Dodgen, Naturwissenschaften, 50, 90 (1963); (e) I. T. Salmeen and M. P. Klein, "Spin-Lattice Relaxation Rate of ^{31}P in ATP," 12th Experimental NMR Conference, University of Florida, Gainesville, Fla., Feb 17–20, 1971; (f) D. W. Aksnes, M. Rhodes, and J. G. Powles, Mol. Phys., 14, 333 (1968).

(16) A. Abragam, "The Principles of Nuclear Magnetism," Oxford University Press, London, 1961, p 332.

(17) At frequencies greater than 19 MHz the frequency-dependent term, namely $\tau_c/1 + (\omega\tau_c)^2$, approaches zero as τ_c is the relaxation time of the quadrapole moments of ^{79}Br and ^{81}Br, and these are of the order of 3×10^{-7} sec. If the values of T_1 and frequencies reported by Winter and Abragam are correct, there seems to be some error in the value reported for the coupling constant. Such an error has been noted[14b] by Rhodes, et al., also. Finally it may be noted that the chemical shielding anisotropy contribution to the relaxation of ^{31}P in PBr$_3$ found in the present investigation would make only a 5% contribution to the relaxation rate at 16 MHz, the highest resonance frequency used by Winter and only about a 6% contribution at 18 MHz, the highest frequency used by Rhodes, et al.

(18) Reference 16, p 308 ff.

Here γ_N is the magnetogyric ratio of ^{31}P, H is the external field intensity, and the Σ's are the principal values of the anisotropic part of the chemical shielding tensor. If the fields used in the present investigation are designated as $H_1 = 11.2$ kG and $H_2 = 23.5$ kG, it follows from eq 3 that

$$\left(\frac{1}{T_{1,A}}\right)_{H_1} = 0.227\left(\frac{1}{T_{1,A}}\right)_{H_2} \tag{4}$$

This relation along with experimental values appropriate to eq 2 allow one to obtain the $1/T_{1,A}$ values entered in Table IV.

The only comparison measurements available bearing directly on the anisotropy effect seem to be those made on P_4O_6 at 15 MHz and at 25 MHz by Chapman and Mowthorpe,[13a] presumably at 21°. The values of $1/T_{1,0}$ are reported as $(8.87 \pm 1.20) \times 10^{-2}$ and $(8.55 \pm 0.55) \times 10^{-2}$ sec^{-1}, respectively. These data indicate essentially no field effect and the rates of relaxation reported are approximately 1.5 times faster than was found in the present investigation. In this connection Aksnes[13b] working at 9 MHz with P_4O_6 found a relaxation rate of $\sim(1/17) \equiv 5.9 \times 10^{-2}$ sec^{-1} at 21°; this compares favorably with the rate of $(1/18.7) \equiv 5.4 \times 10^{-2}$ sec^{-1} interpolated for $1/T_{1,0}$ at 19.3 MHz and 21° from the data of Table I. Repeated measurements with the two P_4O_6 samples used in the present investigation confirmed the field effect reported in Table IV. The only suggestions the present authors can make to account for the discrepancies are that Chapman, et al.,[13a] may have had some saturation of the signal during the recovery period and/or paramagnetic impurities may have been present. The effect of a saturation factor, Z, less than unity is to have[19] the approach to steady state characterized by $(1/T',Z)$ rather than by $1/T_1$. This leads to an observed relaxation rate of $1/T_{1,Z}$ which is larger than the proper rate. In the present investigation relaxation time measurements of all samples were checked at several radiofrequency field strengths to make certain that saturation effects were negligible. The observed chemical shift of -113 ppm for the P_4O_6 used in the present investigation agrees well with other[20] reported values, so identity of the compound does not seem in doubt. As a final observation on this matter if one uses the anisotropic relaxation rate-field relation shown in Table IV for P_4O_6, rates of $(1/124)$ and $(1/41)$ sec^{-1} would be calculated for $1/T_{1,A}$ for fields equivalent to the 15 and 25 MHz used by Chapman and Mowthorpe. The difference in these two rates lies approximately within the uncertainty in the difference of the two observed rates reported by these investigators.

The values of $1/T_{1,A}$ in Table IV for P(OMe)$_3$ and P(O-i-Pr)$_3$ at 11.2 kG are about 30 and 60%, respectively, of the values of $1/T_{1,0}$ for these substances, whereas for all other cases the corresponding percentages are 20% or less, and often about 10%. The magnitude of the chemical shift anisotropy effect for

P(O-i-Pr)$_3$ is so large that the results must be taken with reserve, though repeated measurements with different samples did not lead to consistently different results.

In considering the general matter of chemical shift anisotropy in ^{31}P compounds it should be noted that Lucken and Williams[21] have reported the values of $\Delta\sigma$ ($= \sigma_{||} - \sigma_{\perp}$) for ^{31}P in several solid compounds, namely P(CN)$_3$, $\Delta\sigma = 1.38 \times 10^{-4}$; P_4O_{10}, $\Delta\sigma = 3.26 \times 10^{-4}$; and P_4S_{10}, $\Delta\sigma = 1.88 \times 10^{-4}$. The anisotropy was interpreted rather successfully as arising from the second-order paramagnetic term in the theory of chemical shifts. Deverell[22] has examined the relation of the chemical shift anisotropy to the spin-rotation interaction tensor and reports, among values for other ^{31}P compounds, a value of $\Delta\sigma = 2.24 \times 10^{-4}$ for PBr$_3$. This value was adapted from theoretical calculations of Gutowsky and Larmann[23] on several ^{31}PX$_3$-type compounds. The results obtained by Gutowsky and Larmann were based on the theoretical evaluation of the second-order paramagnetic shielding terms for the ^{31}P atom.

An approximate and *relative* value of the chemical shift anisotropy parameter

$$\Sigma = (\Sigma_1^2 + \Sigma_2^2 + \Sigma_3^2)^{1/2} \tag{5}$$

can be determined if one assumes[24] τ_c in eq 3 is given by

$$\tau_c = \frac{4}{3}\frac{\pi a^3}{k}(\eta/T) \tag{6}$$

and if a^3 is expressed in terms of some measurable quantity such as a well-defined function[25] of the molar volume, V. For purposes of comparison it seems sufficient to define the volume to be allocated per molecule as V/N_{Av}, and the value of a^3 by the relation $(2a)^3 = V/N_{Av}$. With these relations in eq 3 and 5 and after introducing appropriate values of constants one obtains the following expression for Σ at 307°K for a field of 11.2 kG

$$\Sigma^2 = 16.4 \times 10^{-6}\frac{\rho}{M\eta T_{1,A}} \tag{7}$$

Here ρ is the density, M the molecular weight, η the viscosity, and $1/T_{1,A}$ the calculated anisotropic shielding contribution to the relaxation rate for the particular ^{31}P compound. Using eq 7, values of $|\Sigma|$ entered in Table IV were calculated; these values should offer, at least as

(19) Reference 9, p 189.

(20) (a) A. C. Chapman, J. Homer, D. J. Mowthorpe, and R. T. Jones, *Chem. Commun.*, 121 (1965); (b) S. I. Shupack and B. Wagner, *ibid.*, 547 (1960).

(21) E. A. C. Lucken and D. F. Williams, *Mol. Phys.*, 16, 17 (1969).

(22) C. Deverell, *ibid.*, 18, 319 (1970).

(23) H. S. Gutowsky and J. Larmann, *J. Amer. Chem. Soc.*, 87, 3815 (1965).

(24) Reference 3a, p 189.

(25) E. A. Moelwyn-Hughes, "Physical Chemistry," 2nd revised ed, Pergamon Press, Elmsford, N. Y., 1965, p 729 ff.

a first approximation, a relative comparison of the anisotropy parameter for the several molecules. The sign of Σ may be negative as it derives primarily from the second-order paramagnetic shielding discussed by Ramsey[26] and used by Saika and Slichter[27] to explain the observed chemical shifts of fluorine in F_2 and in HF, by Gutowsky and Woessner[5] to explain the anisotropy observed in several organofluorine compounds, and by Pople[28] and others[29] in attempting to explain observed chemical shifts.

Examination in Table IV of the values of $|\Sigma|$ and of σ, the observed chemical shift relative to 85% H_3PO_4, shows a moderate correlation of these two parameters. It is far from perfect, and this is to be expected as there are many factors which can influence the detailed value of chemical shifts. Letcher and Van Wazer,[30] using an approach based on the Saika and Slichter[27] and Jameson and Gutowsky[29a] treatments of chemical shifts, have obtained rather successful correlation expressions for the chemical shifts of ^{31}P in its various compounds. The subject of ^{31}P chemical shifts and correlations, including effects of coordination, has been reviewed recently by Nixon and Pidcock.[31] The moderately good correlation of the observed chemical shifts and $|\Sigma|$ shown in Table IV would seem to indicate that the absolute value of the chemical shift anisotropy for the several compounds is closely related to rotational average of the chemical shift components, i.e., $\sigma = \frac{1}{3}(\sigma_{xx} + \sigma_{yy} + \sigma_{zz})$.

The variations of relaxation rates with temperature shown in Table I indicate significant contributions of spin–rotation interactions to the observed rates, especially at the higher temperatures. The significance of this mechanism for the relaxation of P_4O_6 has been reported by Chapman and Mowthorpe[13a] and by Aksnes,[13b] for PBr_3 by Rhodes et al.,[14b] and for a number of organofluorine compounds by several[4a,29e,32] investigators. The paramagnetic shielding arising from spin–rotation fields has been shown by Ramsey[26a] to be of considerable importance in H_2, and by Chan, et al.,[26c] in the case of $^{15}N_2$. The chemical shift is represented by the latter authors as composed of diamagnetic and paramagnetic terms with the average value of the latter, α_p, expressed as

$$\sigma_p = \frac{e^2}{3mc^2}\left[-\sum_i (Z_i/r_i) + \frac{\hbar}{4M_p\mu_N{}^2 g_I}\sum_{\lambda\lambda}(C_{\lambda\lambda}I_{\lambda\lambda}) \right] \quad (8)$$

Here the $I_{\lambda\lambda}$'s are the principal moments of inertia, the $C_{\lambda\lambda}$'s the components of the spin-rotational coupling tensor about the principal axes, M_p is the proton mass, μ_N the nuclear magneton, and g_I the nuclear g factor for the nucleus under consideration. Other symbols have their usual meaning.

The relation of the $C_{\lambda\lambda}$ values to the spin–rotation relaxation rate is given by Hubbard[4b] for the case of spherical top as

$$\frac{1}{T_{1,SR}} = \frac{2IkT}{3\hbar^2}(2C_\perp{}^2 + C_{||}{}^2)\tau_{SR} \quad (9)$$

Equation 9 is a reduced representation of the more general expression given by Green and Powles,[4a] namely

$$\frac{1}{T_{1,SR}} = \frac{2kT}{9\hbar^2}\frac{(I_x + I_y + I_z)(C_{xx}{}^2 + C_{yy}{}^2 + C_{zz}{}^2)\tau_{SR}}{[(1 + (\omega\tau_{SR})^2]} \quad (10)$$

In eq 9 τ_{SR} is a spin–rotation correlation time and, in addition to the specification of a spherical top molecule, it has been assumed $\omega\tau_{SR} \ll 1$. The $C_{||}{}^2$, or $C_{zz}{}^2$, etc., are the principal values of the spin–rotation coupling tensor in radians^2 sec^{-2}.

Hubbard[4b] has shown that for a spherical molecule the relation between τ_{SR} and τ_c is given by

$$\tau_{SR}\tau_c = I_s/6kT \quad (11)$$

where I_s is the characteristic moment of inertia for the spherical molecule. If one uses this relation, defines τ_c by eq 6 as well as defining a^3 by the relation $(2a)^3 = V/N_{Av}$, and assumes that a proper average value of CI is obtained from the expression

$$9(CI)^2 = I_s(I_x + I_y + I_z)(C_{xx}{}^2 + C_{yy}{}^2 + C_{zz}{}^2)$$

then the expression for $(1/T_{1,SR})$, after introduction of appropriate values of the constants in eq 10, is

$$\frac{1}{T_{1,SR}} = 4.76 \times 10^{61}\left(\frac{\rho}{M}\right)(CI)^2\left(\frac{T}{\eta}\right) \quad (12)$$

The observed relaxation rate expressed in terms of the contributions from dipole–dipole, DD, chemical shift anisotropy, A, and spin–rotation, SR, interactions is given by

$$\frac{1}{T_{1,0}} = \frac{1}{T_{1,DD}} + \frac{1}{T_{1,A}} + \frac{1}{T_{1,SR}} \quad (13)$$

(26) (a) N. F. Ramsey, *Phys. Rev.*, **78**, 699 (1950); (b) N. F. Ramsey, *Amer. Scientist*, **49**, 509 (1961); (c) S. I. Chan, M. R. Baker, and N. F. Ramsey, *Phys. Rev. A*, **136**, 1224 (1964).

(27) (a) A. Saika and C. P. Slichter, *J. Chem. Phys.*, **22**, 26 (1954); (b) C. P. Slichter, "Principles of Magnetic Resonance," Harper and Row, New York, N. Y., 1963, Chapter 4.

(28) (a) J. A. Pople, *J. Chem. Phys.*, **38**, 1276 (1963); (b) *Mol. Phys.*, **7**, 301 (1964).

(29) (a) C. J. Jameson and H. S. Gutowsky, *J. Chem. Phys.*, **40**, 1714 (1964); (b) M. Karplus and T. P. Das, *ibid.*, **34**, 1683 (1961); (c) N. Muller, P. C. Lauterbur, and J. Goldenson, *J. Amer. Chem. Soc.*, **78**, 3557 (1956); (d) J. R. Parks, *ibid.*, **79**, 757 (1957); (e) R. H. Faulk and M. Eisner, *J. Chem. Phys.*, **44**, 2926 (1966).

(30) J. H. Letcher and J. R. Van Wazer, *ibid.*, **44**, 815 (1966).

(31) Reference 1b, p 394 ff.

(32) (a) H. S. Gutowsky, I. J. Lawrenson, and K. Shimomura, *Phys. Rev. Lett.*, **6**, 349 (1961); (b) R. C. Brown, H. S. Gutowsky, and K. Shimomura, *J. Chem. Phys.*, **38**, 76 (1963); (c) J. G. Powles, *Ber. Bunsenges. Phys. Chem.*, **67**, 328 (1963); (d) J. H. Rugheimer and P. S. Hubbard, *J. Chem. Phys.*, **39**, 522 (1963); W. R. Hackerman and P. S. Hubbard, *ibid.*, **39**, 2688 (1963).

or, since the correlation time τ_c has been expressed in terms of ρ, M, η, and T, one may write

$$\frac{1}{T_{1,0}} = DD\left(\frac{M}{\rho}\right)_0 \frac{\eta}{T} + A\left(\frac{M}{\rho}\right)_0 \frac{\eta}{T} + SR\left(\frac{\rho}{M}\right)_0 \frac{T}{\eta} \quad (14)$$

Here it has been assumed that the value of the molar volume appropriate to calculating a^3 is the value at $0°$, namely $(M/\rho)_0$, and it has been further assumed that it is not necessary to distinguish between the intra- and intermolecular contributions to the DD term. On multiplication of eq 14 by η/T and by T/η eq 15 and 16 are obtained.

$$\frac{1}{T_{1,0}}\left(\frac{\eta}{T}\right) =$$

$$\left[DD\left(\frac{M}{\rho}\right)_0 + A\left(\frac{M}{\rho}\right)_0\right]\left(\frac{\eta}{T}\right)^2 + \left[SR\left(\frac{\rho}{M}\right)_0\right] \quad (15)$$

$$\frac{1}{T_{1,0}}\left(\frac{T}{\eta}\right) =$$

$$\left[DD\left(\frac{M}{\rho}\right)_0 + A\left(\frac{M}{\rho}\right)_0\right] + \left[SR\left(\frac{\rho}{M}\right)_0\right]\left(\frac{T}{\eta}\right)^2 \quad (16)$$

The form of eq 15 and 16 suggest that by appropriate graphs one should, from slopes and intercepts, obtain values of the two bracketed terms. Figures 1 and 2 illustrate the graphical representations for the cases of PBr$_3$, P(OBu)$_3$, SP(OMe)$_3$, and OP(OBu)$_3$. It is evident that the behavior of the systems is not fully described by eq 15 and 16, but as shown in Table V there is moderately good agreement between the values for the bracketed terms determined from the slope and the intercept for a specific substance. Using values in the last column of Table V and eq 12 and 14 relative values of $|CI|$ for the several compounds can be calculated from the expression

$$|CI| = 1.45 \times 10^{-31}\left[SR\left(\frac{M}{\rho}\right)_0\right]_c^{1/2} \quad (17)$$

The values so calculated are given in Table VI.
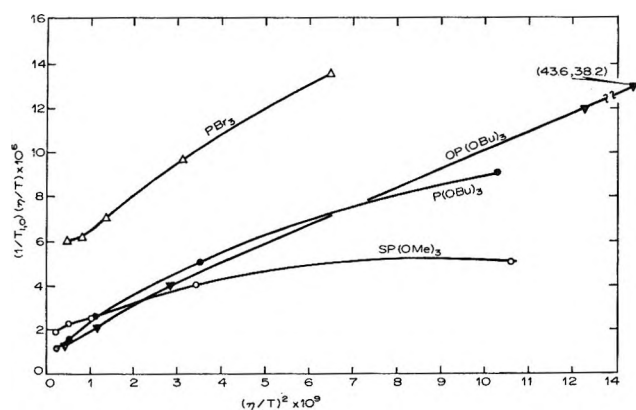
Figure 1. Dependence of the product of the relaxation rate and viscosity–temperature ratio on the square of the viscosity–temperature ratio for a temperature range of 0 to 105°.
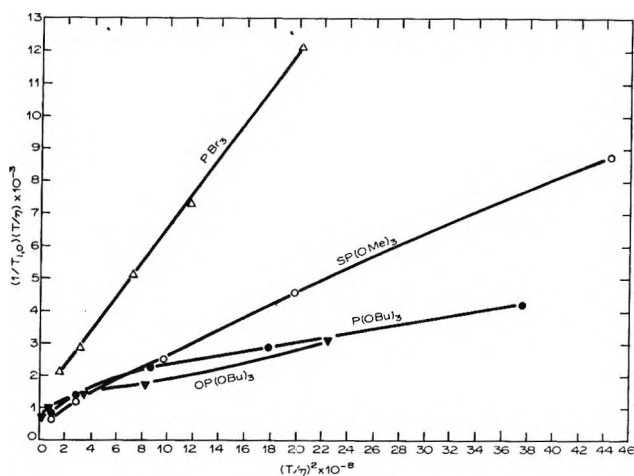
Figure 2. Dependence of the product of the relaxation rate and temperature–viscosity ratio on the square of the temperature–viscosity ratio for a temperature range of 0 to 105°.

Table V: Average Values of Relaxation Rate Factors for Dipole-Anisotropy and Spin–Rotation Interactions

Substance	$[DD-A]_c{}^a$ $\times 10^{-3}$, P^{-1} sec^{-1} °K	$[SR]_c{}^a \times 10^6$, P sec^{-1} °K^{-1}	$\left[SR\left(\dfrac{M}{\rho}\right)_0\right]_c^{1/2}$ $\times 10^2$
PBr$_3$	1.23 ± 0.10	5.39 ± 0.10	2.26
P(OMe)$_3$	$(2.80)^b$	1.80 ± 0.05	1.49
P(OEt)$_3$	$(2.32)^b$	0.70 ± 0.10	1.12
P(O-i-Pr)$_3$	$(0.70)^b$	0.77 ± 0.05	1.35
P(OBu)$_3$	1.15 ± 0.10	0.75 ± 0.05	1.44
OP(OMe)$_3$	0.78 ± 0.15	1.45 ± 0.05	1.32
SP(OMe)$_3$	0.62 ± 0.05	1.90 ± 0.05	1.65
OP(OEt)$_3$	0.56 ± 0.05	1.01 ± 0.10	1.33
OP(OBu)$_3$	0.83 ± 0.10	0.95 ± 0.05	1.62
(structure: P, O, CH$_3$, CH$_3$)	0.80 ± 0.05	1.65 ± 0.35	1.37
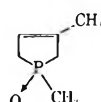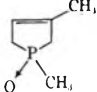
^{a} $[DD-A]_c = \left[DD\left(\dfrac{M}{\rho_0}\right)+ A\left(\dfrac{M}{\rho}\right)_0\right]$; $[SR]_c = \left[SR\left(\dfrac{\rho}{M}\right)_0\right]$.

^{b} Values in parentheses are more uncertain than others in table; only the intercept values derived from eq 16 were used.

Table VI: Values of the Paramagnetic Chemical Shaft Parameter $|CI|$ (radians sec^{-1} g cm^2)

Substance	$|CI|$ $\times 10^{33}$	Substance	$|CI|$ $\times 10^{33}$
PBr$_3$	3.28	OP(OMe)$_3$	1.92
P(OMe)$_3$	2.16	SP(OMe)$_3$	2.40
P(OEt)$_3$	1.64	OP(OEt)$_3$	1.95
P(O-i-Pr)$_3$	1.96	OP(OBu)$_3$	2.35
P(OBu)$_3$	2.09	(structure: P, O, CH$_3$, CH$_3$)	1.98

As noted previously the relaxation rates of ^{31}P in a few compounds have been reported by other authors.

Some of the reports give results from which values of $|CI|$ may be calculated and compared with the results given in Table VI. For P_4O_6 the work of Aksnes[13b] yields a calculated value of $|CI|$ of 3.68×10^{-33} radians sec^{-1} g cm^2. This value is obtained from Aksnes paper as follows

$$I_0 = \text{mean moment of inertia} = 7.88 \times 10^{-33} \text{ g cm}^2$$

$$B = \frac{1}{2\pi}(2C_\perp{}^2 + C_{||}{}^2)^{1/2} =$$

$$13.0 \times 10^3 \text{ Hz for } {}^{31}P \text{ in } P_4O_6$$

The comparison of $|CI|$, as developed in eq 17, and the above data of Aksnes was made by the relation

$$|CI| = \frac{1}{2\pi}(2C_\perp{}^2 + C_{||})^{1/2}\left(\frac{2\pi}{\sqrt{3}}\right)I_0 = 3.6BI_0 \quad .(18)$$

The value of $\bar{C}$ of 19.5×10^3 Hz reported by Chapman and Mowthorpe[13a] for ${}^{31}P$ in P_4O_6 appears to be in error as the comparison value of $|CI|$ in this case is given by $(2\pi)(19.5 \times 10^3)(7.82 \times 10^{-38}) = 9.5 \times 10^{33}$. The apparent error in relaxation rates noted previously in the work of Chapman and Mowthorpe does not account for the large discrepancy, so there appears to be a computational error, also.

The value of $|CI|$ for ${}^{31}P$ in P_4O_6 was not determined in the present investigation as the viscosity–temperature–density relations of this substance were not studied. If, however, one extrapolates a value for $(1/T_{1,\text{SR}}$ at 21° from the data of Tables I and IV by assuming $1/T_1 = 1/T_{1,\text{SR}} + 1/T_{1,\text{A}}$, a value of $1/T_{1,\text{SR}}$ of $(1/24)$ sec^{-1} is obtained. Using the density and viscosity data reported by Aksnes a $|CI|$ value of 2.6×10^{-33} is calculated by eq 12. If one allows for the contribution of chemical shift anisotropy relaxation that was omitted in the Aksnes study, the recalculated Aksnes $|CI|$ value of 2.9×10^{-33} agrees rather well with the 2.6×10^{-33} obtained from the data of the present investigation.

The results of an investigation of PBr_3 by Rhodes, et al.,[14b] yield a calculated value of $|CI| = 2.74 \times 10^{-33}$. This agrees moderately well with the 3.28×10^{-33} shown for PBr_3 in Table VI. Aksnes, Rhodes, and Powles[15f] have investigated the relaxation rates of PCl_3, $OPCl_3$, and OPF_3 and from the reported data the following values of $|CI|$ for ${}^{31}P$ were calculated by eq 18: $|CI|_{PCl_3} = 2.18 \times 10^{-33}$; $|CI|_{OPCl_3} = 3.09 \times 10^{-33}$; and $|CI|_{OPF_3} = 1.56 \times 10^{-33}$. These values along with others cited in the above paragraphs and in Table VI show good concordance as to order of magnitude of $|CI|$ for all ${}^{31}P$ systems for which data are available, and the observed spread in the values, ~1.6 to 3.3×10^{-33}, is not large.

Introduction of the $|CI|$ values into the second term of the Ramsey shielding expression, eq 8, should allow comparisons of calculated and observed chemical shifts, as Chan, et al.,[26c] have found the second

term to be largely determinative in chemical shift differences for a given nucleus. Detailed calculations of this kind for all cases reported in Table VI will serve little purpose as the following sample calculation will show. Assume that the $|CI|$ value for ${}^{31}P$ in 85% H_3PO_4 is 2.0×10^{-33} and that the proper value of $\Sigma_{\lambda\lambda}$-$C_{\lambda\lambda}I_{\lambda\lambda}$ for this case is $3|CI|$. With the indicated values and proper constants, one calculates for the second term, σ_P', of eq 8

$$\sigma_P' = 15.6 \times 10^{-4}$$

If changes in the value of σ_P' were the sole cause of the known range in chemical shifts of ${}^{31}P$ of approximately 5.00×10^{-4}, the value of σ_P' should vary from about 13 to 18×10^{-4} or $|CI|$ values should range from about 1.7 to 2.3×10^{-33}. This $|CI|$ range is very much less than is observed in Table VI. Deverell[22] has taken note of similar discrepancies for ${}^{19}F$ in several fluorine compounds and for ${}^{31}P$ in several other phosphorus compounds.

The calculated value of σ_P' for H_3PO_4 is approximately 15% of the value of δ_0, the reference chemical shift that Letcher and Van Wazer[30] found necessary for H_3PO_4 in their ${}^{31}P$ chemical shift correlation expressions. Also the value of 18.0×10^{-4} calculated, as a proper upper limit of σ_p' is about twice the paramagnetic shift calculated theoretically for PBr_3 by Gutowsky and Larmann.[23] Thus it appears that the $|CI|$ values of Table VI are of the right order of magnitude but details of ${}^{31}P$ chemical shifts are not well accommodated by the observed variations in $|CI|$.

The chemical shift of a variety of systems have been analyzed, and there seems no doubt that the Ramsey[26a] second-order paramagnetic term is mainly responsible for observed variations in chemical shifts of a given nucleus excepting very light atoms. Pople[28b] has examined theoretically the chemical shifts of ${}^{13}C$ is several bonding situations and has calculated chemical shifts that are in exceptionally good agreement with observed values; Van Wazer[1a] and coworkers have achieved rather good correlations of chemical shifts in ${}^{31}P$, primarily by estimating the influence on the paramagnetic term of factors such as ionic character, extent and character of hybridization, bonding angles, nature and extent of d-orbital participation of the ${}^{31}P$ atom, etc.

The poor correlation of the values of $|CI|$ listed in Table VI with the observed chemical shifts in the several compounds needs to be examined to determine, if possible, the basis for this deficiency. First, it should be noted that the range of $|CI|$ values shown in Table VI of 1.64 to 3.28×10^{-33} far exceeds the range required to accommodate the observed chemical shifts, a range of 2.00 to 2.30×10^{-33}. This may indicate gross errors in measurement of $1/T_{1,\text{SR}}$ or some basic flaw in attempting to associate the calculated $|CI|$ values with observed chemical shifts. From

an estimate of reasonable experimental errors the observed range of values cannot be attributed to errors of measurements, especially as $|CI|$ involves taking the square root of measured parameters; further pursuit of this possibility of accounting for the discrepancies seems without merit. An alternative avenue is that the spin-rotation relaxation rate depends on the sum of the squares of $C_{\lambda\lambda}I_{\lambda\lambda}$'s, whereas the chemical shift is dependent on the sum of the first power of the $C_{\lambda\lambda}I_{\lambda\lambda}$'s. Thus not only is a different averaging involved, but variations in sign of the $C_{\lambda\lambda}$'s would affect the chemical shift directly but likely would influence the relaxation rate only by second-order effects such as the chemical shift anisotropy effect.

Finally the above noted discrepancies may result from the use of incorrect values for τ_{SR} in the relaxation rate equation; the direct introduction of the Debye-type correlation expression for τ_c in eq 11 is at best an approximation. If τ_c were smaller by a factor of 5 to 10, the calculated values of $|CI|$ would correlate better, as to magnitude and range, with the observed chemical shifts. Reductions of τ_c by the above factors would require reductions of the coupling constant, $C_{\lambda\lambda}$ from the order of 10×10^3 Hz down to 10^3 or less Hz. This low value of the coupling seems unrealistic when other couplings are found to be mostly in the 1-10-kHz range; e.g., $^{15}N_2 = 22$ kHz[26c]; ^{19}F in C_6H_5F 4 kHz;[4a] ^{19}F in $C_6H_5CF_3 = -25.5$ kHz;[29e] ^{19}F in CF_4 $= -6.0$ kHz;[26b] ^{17}O in OCS $= -4.0$ kHz.[33] On balance, the combination of the different functional dependence of σ and $1/T_{1,SR}$ on $C_{\lambda\lambda}I_{\lambda\lambda}$ and moderate errors in the values used[34] for τ_c for the various compounds seem the most likely explanation of the observed discrepancies in the correlations.

In Figure 3 it is shown graphically that $|\Sigma|$ is much better correlated with σ_{obsd} than is $|CI|$. The reason for this is not clear but a possible explanation is that, for the nearly symmetric top molecules under study, the shielding *changes* are almost exclusively in the parallel component or in the perpendicular component by amounts that correspond approximately to the observed chemical shift changes. Thus the value of $|\Sigma|$ may be determined primarily by the first power of one of the principal chemical shielding components.

The data for diluted samples in Tables I and II were used in conjunction with pure liquid data at the same temperature in an attempt to separate the intra- and intermolecular contribution to the dipole–dipole relaxation rate. The presence of the chemical shift anisotropy and of the relatively large spin–rotation contributions to the relaxation rate necessitated the taking of differences between major relaxation rate terms for the diluted and undiluted samples. The accumulated uncertainties in the differences were such as to make unfeasible the separations of the dipole–dipole intra- and intermolecular terms.
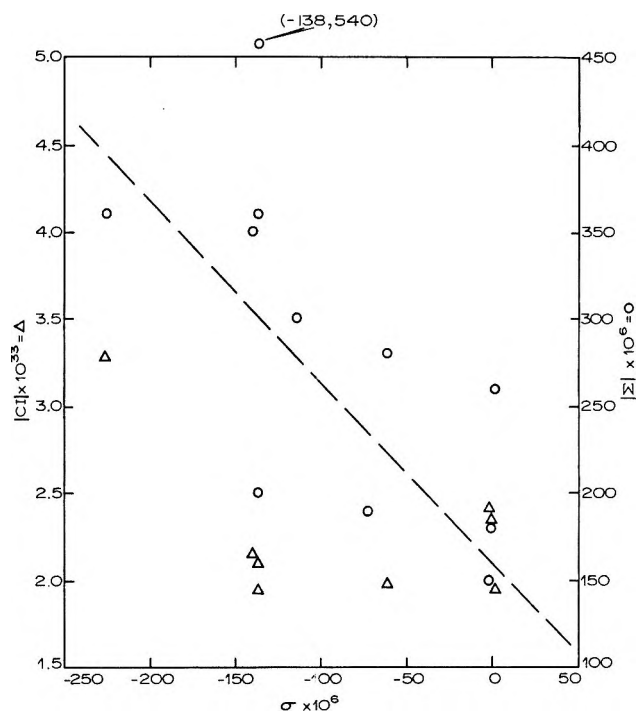
Figure 3. Correlation of the chemical shift anisotropy parameter $|\Sigma|$ and the spin–rotation interaction parameter $|CI|$, in radians sec^{-1} g cm^2 with the observed chemical shift, σ, of some ^{31}P compounds referenced to 85% H_3PO_4.

Although it was not feasible to separate the two components of the DD term of eq 14, it was of interest to separate the $[DD-A]_c$ term recorded in Table V into an anisotropy term, $(A)_c$, and a dipole–dipole term, $(DD)_c$, and to compose a table containing these factors along with the values of $(SR)_c$; from such a table of data one can write the total relaxation rate equation, as

$$\frac{1}{T_{1,0}} = (DD)_c\left(\frac{\eta}{T}\right) + (A)_c\left(\frac{\eta}{T}\right) + (SR)_c\left(\frac{T}{\eta}\right) \quad (19)$$

In Table IV there is listed, for 33° and a field of 11.2 kG, a value of $1/T_{1,A}$ for each of the compounds of interest. Since it was assumed that $(A)_c$ is independent of temperature, its value can be determined from the listed value of $1/T_{1,A}$ at 33° and a value of $\eta_{33°}$ interpolated from a ln η vs. $1/T$ graph. In this manner the values of $(A)_c$ were obtained and with data from Table V one could then complete Table VII with values of $(DD)_c$, $(A)_c$, and $(SR)_c$. As noted in Table VII the values of $(SR)_c$ for all compounds and

(33) C. H. Townes and A. L. Schawlow, "Microwave Spectroscopy," McGraw-Hill, New York, N. Y., 1955, p 215 ff.

(34) As noted by a reviewer the report by A. A. Maryott, T. C. Farrer, and M. S. Malmberg [*J. Chem. Phys.*, **54**, 64 (1971)] on the spin-lattice relaxation time of ClO_3F shows that, in this case, the correlation of τ_c and η/T does not follow the simple Debye formulation. This observation and the further observation that the Hubbard relation for $\tau_c\tau_{SR}$ is not applicable over the range of temperatures investigated strengthens the view that possibly incorrect values of τ_c and thus of τ_{SR} may help account for discrepancies in the correlation of $|CI|$ and σ for ^{31}P in the present investigation.

the $(DD)_c$ and $(A)_c$ values for the phosphoryl compounds are regarded as have considerably less error than the $(DD)_c$ and $(A)_c$ values for several of the trialkoxy phosphines. The data of Table VII show that the spin–rotation contribution clearly dominates the relaxation rate for PBr$_3$, OP(OMe)$_3$, SP(OMe)$_3$, and the cyclic phosphoryl compound over most of the temperature range used in this investigation.

Table VII: Values of the Dipolar, $(DD)_c$, the Anisotropy, $(A)_c$, and the Spin–Rotation, $(SR)_c$, Constants for the Relaxation Rate Equation

Substance	$(DD)_c{}^a$ ($\times 10^{-3}$), P^{-1} sec^{-1} °K		$(A)_c$ ($\times 10^{-3}$), P^{-1} sec^{-1} °K	$(SR)_c$ ($\times 10^6$), P sec^{-1} °K^{-1}
PBr$_3$	1.01		0.22	5.39
P(OMe)$_3$		(2.80)^b		1.80
P(OEt)$_3$		(2.32)^b		0.70
P(O-i-Pr)$_3$		(0.70)^b		0.77
P(OBu)$_3$	0.95		0.20	0.75
OP(OMe)$_3$	0.73		0.05	1.45
SP(OMe)$_3$	0.53		0.09	1.90
OP(OEt)$_3$	0.34		0.22	1.01
OP(OBu)$_3$	0.65		0.18	0.95
(cyclic phosphoryl compound)	0.63		0.17	1.65
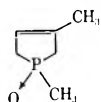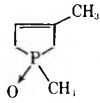
^{a} It was not feasible to separate the DD term into intra- and intercomponents. ^{b} Numbers in parentheses were too uncertain to warrant a breakdown into $(DD)_c$ and $(A)_c$ terms.

From the values of η in Table II and extrapolated values of η at 0 and 105° values of $1/T_1$ were calculated using eq 19. In Table VIII the calculated values of $1/T_1$ are compared with the experimental values $1/T_{1,0}$. The agreement between calculated and observed values is reasonably good, especially since the comparison is between experimental values with standard deviations of $\pm 5\%$ and essentially a smooth curve that has not been adjusted for best fit. The values of the constants of Table VII could certainly be adjusted to give a somewhat better fitting of the calculated and the experimental rate values. This adjustment was thought to be unwarranted as a sim-

plified and certainly in some respects an inadequate model was being used to represent a very complex system. The interesting point is that the simplified approach does yield a quite reasonable fit of theory with experimental findings; specifically, the major mechanisms effective in spin–lattice relaxation were evaluated, the chemical shift parameters obtained from the observed relaxation rates are concordant, and the chemical shift anisotropy parameter was found to be reasonably well correlated with observed chemical shifts.

Table VIII: Comparison of Observed and Calculated Relaxation Rates at Several Temperatures

Substance		T, °C 0	25	55	80	105
		(1/T_1) ($\times 10^2$), sec^{-1}				
PBr$_3$	Obsd	16.8	15.9	18.9	21.2	27.0
	Calcd	16.6	16.5	19.4	22.2	26.9
P(OMe)$_3$	Obsd	10.1	15.5	17.9	21.3	24.9
	Calcd	14.4	14.7	16.5	19.8	24.2
P(OEt)$_3$	Obsd	5.2	8.1	9.6	11.7	11.5
	Calcd	9.7	8.3	8.2	9.0	10.4
P(O-i-Pr)$_3$	Obsd	5.1	5.4	6.0	6.3	9.4
	Calcd	5.1	4.6	5.3	6.4	8.2
P(OBu)$_3$	Obsd	9.0	8.5	7.7	6.8	6.8
	Calcd	12.4	8.1	6.1	5.9	6.5
OP(OMe)$_3$	Obsd	11.3	8.6	7.1	8.7	9.9
	Calcd	10.3	7.4	6.8	7.7	9.5
SP(OMe)$_3$	Obsd	6.7	7.0	8.1	10.2	13.1
	Calcd	8.2	6.9	7.9	9.8	13.6
OP(OEt)$_3$	Obsd	6.5	5.5	5.3	6.8	7.6
	Calcd	6.0	5.8	5.1	6.1	7.9
OP(OBu)$_3$	Obsd	16.3	10.8	7.6	6.0	6.5
	Calcd	19.8	10.1	6.2	5.6	6.3
(cyclic phosphoryl compound)	Obsd	40.0	15.7	7.9	9.6	9.9
	Calcd	39.1	16.4	8.4	7.3	8.5

For the ^{31}P compounds studied it seems unambiguous that spin–rotation interactions are of major importance to the relaxation rate, that chemical shift anisotropy plays a significant role in the relaxation at moderate to high external fields, and that the paramagnetic shielding effects associated with the anisotropy and spin–rotation, in first order, are responsible for the major chemical shifts of the ^{31}P nuclei in the compounds studied.

Effect of P–H Deuterium Substitution on the Phosphorus-31

Nuclear Magnetic Resonance Spectroscopy of Several Dialkyl Phosphonates[1]

by Wojciech J. Stec,[2] Nicholas Goddard, and John R. Van Wazer*[3]

Department of Chemistry, Vanderbilt University, Nashville, Tennessee 37203   (*Received March 31, 1971*)

Publication costs borne completely by The Journal of Physical Chemistry

By means of ^{31}P nuclear magnetic resonance spectroscopy, the coupling constants and chemical shifts have been measured for various dialkyl phosphonates in which the hydrogen bonded to the phosphorus is present as either the normal isotope or deuterium. It is seen that the ratio of the coupling constants $^1J_{PH}/^1J_{PD}$ as well as the isotope shift undergo small but apparently real variations, particularly upon going to a hydrogen-bonding solvent. These variations are ascribed to a difference in hydrogen-bonding capability of the deuterated and nondeuterated species.

Since there are no unusual obstacles in the synthesis of compounds exhibiting bonding of deuterium directly to phosphorus, and since a number of such compounds have been made for other purposes, it is indeed amazing to find no ^{31}P or ^{1}H nuclear magnetic resonance (nmr) data[4] for these compounds even though ^{31}P and ^{1}H nmr spectroscopy of a number of hydrogen analogs have been reported in the literature.[5,6] To rectify this situation we have prepared[7] dimethyl, diethyl, di-*n*-propyl, and diisopropyl phosphonates in which the hydrogen directly bonded to the phosphorus has been substituted by a deuterium atom. This preparation was carried out by the deuterolysis of the corresponding trialkyl phosphites with stoichiometric amounts of deuterium oxide in tetrahydrofuran.

$$(RO)_3P + D_2O \longrightarrow (RO)_2P(O)D + ROD \quad (1)$$

The nmr parameters of these compounds have been measured and are compared with the respective values for their hydrogen analogs, which were redetermined at the same time. The results are shown in Table I.

Coupling Constants

For nuclei in *identical* environments, the relationship[8] between coupling of an atom, X, with hydrogen or deuterium is given by

$$J_{XH}/J_{XD} = \gamma_H/\gamma_D = \mu_H I_D/\mu_D I_H = 6.5145 \quad (2)$$

where γ is the gyromagnetic ratio, μ is the nuclear magnetic moment, and I is the nuclear spin. The value of J_{PH}/J_{PD} from eq 2 should be compared to the respective values given in Table I, from which it can be seen that there is agreement to *ca.* 0.2% between the various numbers.

For the dimethyl and the diethyl phosphonates in Table I, it should be noted that there is a small differ-

ence in the P–H coupling constant depending on whether the compounds are present in the pure state (as the neat liquids) or are mixed with their deuterated analogs. Further there seems to be a small variation in $^1J_{PH}/^1J_{PD}$ upon changing the alkyl group. We believe that these differences are probably real and tentatively ascribe them to small changes in the s-orbital density[9] on the phosphorus due to changes in the phosphoryl P–O bond owing to the differing ability[10] of deuterium to form hydrogen bonds as compared to hydrogen. It is known that dialkyl phosphonates form[11] dimers and larger aggregates, and this is ascribed to intermolecular hydrogen bonding as

(1) This study has been supported by the National Science Foundation under Grant No. GP-9525. The Varian A-60 and XL-100-15 nmr spectrographs were purchased under grants from the National Science Foundation.

(2) On leave of absence for 1970 from the Polish Academy of Science, Lodz.

(3) To whom requests for reprints should be addressed.

(4) A single obviously incorrect value for a P–D coupling constant is reported in ref 5 as a personal communication. This number was probably originally obtained for Dr. R. Wolf of Toulouse by Van Wazer and associates at the Monsanto Co. in the early days of ^{31}P spectroscopy and may have been miscopied in some clerical operation.

(5) M. M. Crutchfield, C. H. Dungan, J. H. Letcher, V. Mark, and J. R. Van Wazer, "P^{31} Nuclear Magnetic Resonance," Vol. 5, Wiley-Interscience, New York, N. Y., 1967.

(6) G. Mavel, "Progress in NMR Spectroscopy," Vol. I, J. W. Emsley, J. Feeney, and L. H. Sutcliffe, Ed., Pergamon Press, Oxford, 1966, Chapter 4, pp 251–373.

(7) G. Aksnes and O. Grahl-Nielson, *Acta Chem. Scand.*, 19, 2373 (1965).

(8) L. M. Jackman and S. Sternhall, "Applications of NMR Spectroscopy in Organic Chemistry," Pergamon Press, Oxford, 1969, p 142.

(9) W. McFarlane, *Quart. Rev. Chem. Soc.*, 2, 187 (1969).

(10) S. Singh and C. N. R. Rao, *Can. J. Chem.*, 44, 2611 (1966).

(11) For example, see J. G. David and H. E. Hallam, *J. Chem. Soc. A*, 1103 (1966), and references cited therein; also see R. Wolf, D. Houalla, and F. Mathis, *Spectrochim. Acta, Part A*, 23, 1641 (1967).

Table I: ^{31}P Nmr Parameters of Deuterated Dialkyl Phosphonates as Neat Liquids

(RO)₂P(O)X	X = deuterium			X = hydrogen				Isotope chemical shift, ppm	¹JPH/¹JPD
	δP,ᵃ ppm	¹JPD, cps	³JPH,ᵇ cps	% of H-phos.	δP, ppm	¹JPH, cps	³JPH, cps		
R = CH₃	−10.8	106.8	12	15ᶜ	−11.2	695.9	12	0.4	6.52
				100	−11.2	695.0	12	0.4	6.51
R = C₂H₅	−6.8	105.7	9	24ᶜ	−7.1	689.3	9	0.3	6.52
				100	−7.1	687.2	9	0.3	6.50
R = n-C₃H₇	−6.9	105.6	9	19ᶜ	−7.3	687.4	9	0.4	6.52
R = i-C₃H₇	−3.4	104.5	9	12ᶜ	−3.8	681.1	9	0.4	6.52

ᵃ δP = chemical shift is reported with respect to "external" 85% H₃PO₄ (values measured from (C₆H₅O)₃P and recalculated from δP[(C₆H₅O)₃P] = δP[H₃PO₄] − 128.1 ppm). ᵇ ³JPH refers to coupling across the chain of atoms HCOP. ᶜ Amount of hydrogen species present after deuteration [i.e., as an impurity in (RO)₂P(O)D].

Table II: Solvent Effects on ^{31}P Nmr Parameters of Dimethyl Phosphonate, (CH₃O)₂P(O)X, Where X = Deuterium or Hydrogen

Molar dilution in solvent	X = deuterium		In mixtureᵇ		Pure		Coupling ratio		Isotope shift	
	δP,ᵃ ppm	¹JPD, cps	δP, ppm	¹JPH, cps	δP,ᵃ ppm	¹JPH, cps	¹JPH-(pure)/ ¹JPD	¹JPH-(mix)/ ¹JPD	δP(H mix) − δP(D), ppm	δP(H pure) −δP(D), ppm
Neat	−10.8	106.8	−11.2	695.9	−11.2	695.0	6.51	6.52	0.4	0.4
1:1 CCl₄	−10.8	106.6	−11.1	694.6	−11.1	693.1	6.50	6.52	0.3	0.3
1:2 CCl₄	−10.5	106.3	−10.8	694.3	−10.7	692.6	6.52	6.53	0.3	0.2
1:5 CCl₄	−10.0	106.2	...ᶜ	...ᶜ	−10.2	691.9	6.51	...	...	0.2
1:1 CHCl₃	−11.2	107.0	−11.5	697.0	−11.5	697.2	6.51	6.51	0.3	0.3
1:2 CHCl₃	−11.1	107.0	−11.4	697.7	−11.4	697.6	6.52	6.52	0.3	0.3
1:5 CHCl₃	−11.0	107.3	...ᶜ	...ᶜ	−11.3	697.2	6.50	...	...	0.3
1:1 CH₃OH	−11.1	107.1	−11.4	702.0	−11.6	703	6.56	6.56	0.3	0.5
1:2 CH₃OH	−11.1	107.5	−11.4	705.5	−12.2	705	6.56	6.56	0.3	1.1
1:5 CH₃OH	−11.1	108.0	...ᶜ	...ᶜ	−12.3	708	6.56	...	...	1.2

ᵃ ^{31}P chemical shift reported with respect to "external" 85% H₃PO₄. ᵇ In mixture refers to the 15% (CH₃O)₂P(O)H impurity in (CH₃O)₂P(O)D. ᶜ Too weak to be measured.

$$
\begin{array}{ccc}
\text{RO} & \text{H}\cdots\text{O} & \text{OR} \\
\diagdown\diagup & \diagdown\diagup & \\
\text{P} & & \text{P} \\
\diagup\diagdown & \diagup\diagdown & \\
\text{RO} & \text{O}\cdots\text{H} & \text{OR}
\end{array}
\qquad (3)
$$
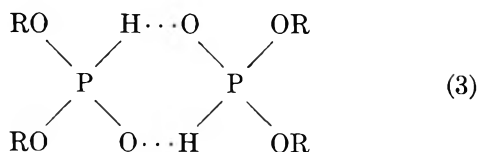
Also, an increase in ¹JPH of the dialkyl phosphonates has been noted[12,13] when these compounds are dissolved in a protonic acid solvent.

From the above information, the value of ¹JPH/¹JPD as measured on a phosphonate would be expected to vary slightly as a function of solvent acidity. The results of putting both the deuterated and the regular forms of dimethyl phosphonate in several solvents are shown in Table II. Of the three solvents studied, only methanol is a strong enough hydrogen donor to interact appreciably with the dimethyl phosphonate through hydrogen bonding with its phosphoryl oxygen,[13] and this shows up as a barely detectable increase in ¹JPH/ ¹JPD. Thus, in methanol, the value of ¹JPH/¹JPD seems to equal 6.56 instead of the standard value of 6.51 to 6.52. Attempts were made to obtain the ^{31}P nmr parameters of deuterated dimethyl phosphonate in a rather strong acid (such as acetic or trifluoroacetic acids) which

would exhibit sufficient hydrogen bonding to the phosphoryl oxygen of the phosphonate to cause a breakup of the dimer shown as (3) to give instead a similar dimer between the dimethyl phosphonate and the solvent acid.[13] However, rapid exchange of the deuterium of the phosphonate for the protonic hydrogen of the acid negated these studies.

Chemical Shifts

In Tables I and II, the changes in ^{31}P chemical shift of the various phosphonates brought about by substitution of P–H by P–D is seen to range from 0.2 to 1.2 ppm, values which are about the same magnitude as those observed for ^{19}F upon deuterium substitution for hydrogen in organic molecules containing fluorine.[14] The observed isotopic shifts are not affected by H/D

(12) L. I. Vinogradov, Yu. Yu. Samitov, E. G. Yarkova, A. A. Muratova, Opt. Spectrosk., 26, 520 (1969).

(13) W. J. Stec, J. R. Van Wazer, and N. Goddard, J. Chem. Soc., submitted.

(14) H. Batiz-Hernandez and R. A. Bernheim, "Progress in Nuclear Magnetic Resonance Spectroscopy," Vol. III, J. W. Emsley, J. Feeney, and L. H. Sutcliffe, Ed., Pergamon Press, Oxford, 1968, pp 63-85.

exchange because the resonances for the two isotopic species are simultaneously observed and do not exhibit noticeable broadening. Explanations of the changes in chemical shift due to isotope substitution have been based on calculations of changes in magnetic shielding which accompany changes in average bond angles and in internuclear distances resulting from the existence of anharmonic components of the vibrational potential.[14] The semiempirical quantum-mechanical theory of ^{31}P nmr chemical shifts developed[5,15,16] by our group several years ago indicates that the ^{31}P chemical shift will be highly sensitive to bond-angle changes and insensitive to small variations in internuclear distances. Using this theory, we can calculate the effect of changes in bond angles on the chemical shift. Thus, upon assuming approximate C_{3v} symmetry for the HPO_3 group of the dialkyl phosphonates, we estimate that a 1° increase in the OPO bond angle of this group leads to a decrease of 4.9 ppm in the chemical shift. Since substitution of a deuterium for the hydrogen of the HPO_3 group causes a positive change in the chemical shift of ca. 0.4 ppm we see that, according to this theory, the change in chemical shift due to isotope substitution is commensurate with a decrease in the OPO bond angle of ca. 0.1° (I ca. 0.1%). This change in average bond angle would be accompanied by a shortening of the average P–H bond length of about 0.3%, as estimated from pertinent experimental data.[17]

Experimental Section

Nmr Experiments. The nmr measurements were carried out on one of the recently introduced Varian XL-100-15 spectrometers at an observed frequency of 40.5 MHz for the phosphorus spectra, using a deuterium lock. Peak positions were obtained by "parking" on the center of the desired resonance, an operation which can be reproduced to ca. 0.1 Hz with this equipment. The resulting frequency was measured with an Eldorado Model 1615 RF frequency counter (standard Varian equipment). The center of the desired resonance was established by passing through the previously charted peak at a slow rate of 0.2 Hz/sec and stopping at the charted maximum in order to measure the frequency. The probe temperature remained at 37° (within 1°) for all measurements.

The samples to be measured were placed in 5-mm high-precision nmr tubes which were centered by polyethylene spacers in 12-mm high-precision nmr tubes, with the spacers being placed so they were not in the "active" region of the tube. The annular space between the 5- and 12-mm tubes contained 6 ml of ace-

tone-d_6, along with 0.2 ml of triphenyl phosphite which was used for "external" ^{31}P chemical shift referencing. Repeated determinations involving filling the 5-mm inner tube with 85% phosphoric acid shows that the chemical shift of triphenyl phosphite with respect to 85% phosphoric acid is −128.1 ppm, a value which corresponds well to the literature reports.[5] This number was used to convert the measured shifts into the usual reference standard of 85% H_3PO_4. Broad-bond decoupling of hydrogen was employed in these referencing experiments to sharpen the triphenyl phosphite resonance.

Nmr observations on the deuterated dialkyl phosphonates had to be carried out very rapidly in methanol to avoid deuterium/hydrogen isotope exchange. For acetic acid and its halo derivatives, the exchange was found to be so rapid that equilibrium was achieved within the shortest time needed to mix the reagents and initiate the nmr measurements. All of the reported data represent two to four replicate measurements each.

Preparation[1] of Deuterated Phosphonates. Into a solution consisting of 0.1 M of commercially available trialkyl phosphite in 50 ml of tetrahydrofuran, a solution of 0.1 M D_2O (allegedly 99.8%) in 5 ml of THF was dropped at a temperature of +5° and stirring was continued for the next 5 hr; at room temperature for compounds 1 and 2 and under reflux for 3 and 4. The solvent was removed under reduced pressure and the compounds were distilled. The boiling points and yields are as follows: (1) $(MeO)_2PD(O)$, bp 57° (12 mm), yield 87%; (2) $(EtO)_2PD(O)$, bp 70–72° (12 mm), yield 82%; (3) $(n\text{-}PrO)_2PD(O)$, bp 112–114° (20 mm), yield 93%; (4) $(i\text{-}PrO)_2PD(O)$, bp 75–78° (12 mm), yield 63%.

According to the ^{31}P nmr spectra, each of these deuterated compounds contained the following mole percentage of its hydrogen analog: 15% for R = CH_3, 24% for R = C_2H_5, 19% for R = $n\text{-}C_3H_7$, and 12% for R = $i\text{-}C_3H_7$ in the $(RO)_2P(O)D$.

(15) J. H. Letcher and J. R. Van Wazer, *J. Chem. Phys.*, **44**, 815 (1966).

(16) J. H. Letcher and J. R. Van Wazer, *ibid.*, **44**, 2916 (1966).

(17) L. E. Sutton, *et al.*, "Tables of Interatomic Distances and Configurations in Molecules and Ions," Supplement 1956–1959, Spec. Publ. 18, The Chemical Society, London, 1965, pp S 1s–S 23s.

Ion Pairing of Amidinium Salts in Dimethyl Sulfoxide[1,2]

by Robert C. Neuman, Jr.,* and Violet Jonas

Department of Chemistry, University of California, Riverside, California 92502 (*Received March 15, 1971*)

Publication costs assisted by the National Institute of General Medical Sciences (PHS)

The nmr signal positions of the proton groups in N,N-dimethylacetamidinium chloride, bromide, iodide, and nitrate are dependent both on concentration and the anion in the solvent DMSO. The data are interpreted in terms of ion-pair interactions between the amidinium ions and the anions. Association constants and limiting chemical shifts have been calculated, and the results are compared to those for similar systems.

During the course of studies on rotational barriers about C–N partial double bonds in amides and related compounds, we found that the positions of the nmr signals of the N,N-dimethylacetamidinium ion (**1**)

$$
\begin{array}{c}
\text{(o)}H \\
\diagdown \\
N\text{—}H^{(i)} \\
CH_3C \quad \vert \quad + \qquad X^- \\
\diagup\diagdown \\
N\text{—}CH_{3(i)} \\
\diagup \\
\text{(o)}CH_3 \\
\mathbf{1}
\end{array}
$$
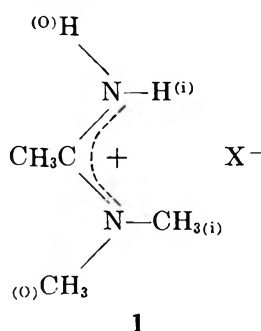
were highly dependent on concentration in the solvent DMSO-d_6 and on the nature of the gegen anion X^-.[1a] This suggested rapid equilibria between solvent separated ions and ion pairs.

We have examined the effects of concentration on the chemical shifts of the proton groups CCH_3, NCH_3(o), NCH_3(i), NH(o), and NH(i) for DMSO solutions of the chloride, bromide, iodide, and nitrate salts of **1**. The data suggest that two types of ion pairs may be present: (1) an ion pair involving a nonspecific electrostatic interaction between the amidinium ion (A^+) and its anion (X^-); and (2) an ion pair resulting from hydrogen bonding between X^- and the NH_2 protons of A^+. Their relative importance seems to vary with the anion.

Results and Discussion

Spectral Assignments. In compounds of the general structure **1**, the highest field proton signal corresponds to the CCH_3 group.[3] The assignments of NCH_3(i) and NCH_3(o) are based on the general observation that trans coupling (CCH_3, NCH_3(i)) is greater than cis coupling (CCH_3, NCH_3(o)) across C–N partial double bonds.[3] Based on precedent, the higher field NH resonance signal has been assigned to NH(i).[3c] The relative assignments of NH(i) and NH(o) are not particularly critical, however, since it will be seen that their resonance lines behave similarly with concentration in each system.

Concentration Dependence of Nmr Signals. The concentration dependences of the resonance lines for the various proton groups (δ_{obsd}) (Table I, Figures 1–3) have been analyzed using a simple ion-pair association model (eq 1).[4] The quantities χ_A and χ_{AX} are the mole

$$
\delta_{obsd} = \chi_A \delta^A + \chi_{AX} \delta^{AX} \tag{1}
$$

fractions ($\chi_{AX} + \chi_A = 1$) of free and ion-paired amidinium ion, respectively, and the corresponding chemical shifts are δ^A and δ^{AX}. This model is suggested by the apparent convergence of the resonance lines for each proton grouping (Figures 1–3) to an anion-independent infinite dilution chemical shift (δ^A).

Best-fit values of the ion-pair association constants (K), and the limiting chemical shifts δ^A and δ^{AX}, were determined for the signals corresponding to CCH_3, NCH_3(i), and NCH_3(o) (Table II) and give the solid lines in Figures 1 and 2.[5] The NCH_3(o) data for the chloride deviated substantially from this model (Figure 2) and could not be analyzed. The values of $\delta_{CCH_3}{}^A$ and $\delta_{NCH_3(i)}{}^A$ for this system also appear to be too high (Table II) compared to those for the other anions. Using arbitrary values of 134.2 and 182.9 Hz for these quantities,[6] the *bracketed* values of K and δ^{AX} were obtained (Table II) and these give the dashed curves in Figures 1 and 2.

The observed values of δ_{NH} (Figure 3, Table I) for the amidinium iodide were virtually concentration inde-

(1) (a) This is part VII, Studies of Chemical Exchange by Nuclear Magnetic Resonance; part VI: R. C. Neuman, Jr., and V. Jonas, *J. Phys. Chem.*, **75**, 3532 (1971). (b) Presented on the Pacific Conference on Chemistry and Spectroscopy, San Francisco, Calif., Oct 6–9, 1970.

(2) Support by the U. S. Public Health Service (National Institute of General Medical Sciences) through Grant GM-13342 is gratefully acknowledged.

(3) See (a) R. C. Neuman, Jr., and L. B. Young, *J. Phys. Chem.*, **69**, 1777 (1965); (b) R. C. Neuman, Jr., and L. B. Young, *ibid.*, **69**, 2570 (1965); (c) G. S. Hammond and R. C. Neuman, Jr., *ibid.*, **67**, 1655 (1963).

(4) See R. L. Buckson and S. G. Smith, *ibid.*, **68**, 1875 (1964).

(5) Computer programs used in this study are outlined in the Ph.D. Dissertation of Violet Jonas, University of California, Riverside, Calif., 1970.

(6) Based on the computed values of $\delta_{CCH_3}{}^A$ and $\delta_{NCH_3(i)}{}^A$ for the bromide, iodide, and nitrate (see Table II).

Table I: Concentration Dependence of the Chemical Shifts of the Proton Groups in 1[a]

Anion	Concn, mol %	δ_{CCH_3}	$\delta_{NCH_3(i)}$	$\delta_{NCH_3(o)}$	$\delta\nu_\infty$[b]	$\delta_{NH(i)}$	$\delta_{NH(o)}$	δ_{NH_2}[c]
NO$_3$$^-$	0.20	134.2	183.0	188.5	5.6	494.8	534.8	...
	0.43	134.5	183.2	188.6	5.5	496.0	536.0	...
	0.85	134.6	183.3	188.6	5.4	498.0	538.0	40.0
	1.68	135.0	183.7	189.0	5.3	499.6	539.6	40.0
	2.37	135.2	183.8	189.0	5.2	500.6	540.6	40.0
	4.80	135.9	184.4	189.5	5.1	501.8	541.8	40.0
	9.09	136.5	185.1	190.0	5.0	502.6	542.6	40.0
	12.65	137.1	185.5	190.2	4.9	502.6	542.6	40.0
	18.83	138.3	186.5	191.3	4.8	503.4	543.4	39.5
I$^-$	0.24	134.4	183.0	188.8	5.7	496.5	534.5	39.0
	0.60	134.9	183.3	189.0	5.7	494.6	534.6	40.0
	1.11	135.5	183.8	189.5	5.8	495.0	535.4	41.0
	2.14	136.2	184.3	190.1	5.8	495.8	536.6	41.0
	3.70	137.6	185.4	191.2	5.9	495.4	536.6	41.0
	7.59	139.5	186.7	192.8	6.1	494.6	536.2	41.5
	13.94	142.2	188.7	194.9	6.3	493.4	534.6	42.0
Br$^-$	0.20	134.6	183.0	188.4	5.3	496.4	538.4	42.0
	0.62	135.6	183.8	188.7	4.9	499.8	541.8	42.0
	1.27	136.3	184.3	189.0	4.6	502.4	544.4	43.0
	2.30	137.5	185.0	189.4	4.3	503.9	547.4	44.3
	4.30	139.5	186.6	190.6	4.0	506.2	551.4	44.8
	8.64	141.8	188.2	192.1	3.9	508.7	554.2	45.5
	15.23	144.5	190.3	194.0	3.7	509.5	554.6	45.5
Cl$^-$	0.06	134.7	183.4	188.3	5.0	...	...	...
	0.12	135.3	183.8	188.1	4.4	507.0	551.0	...
	0.27	135.8	184.1	188.0	3.9	510.0	554.0	45.0
	0.45	...	...	...	...	512.0	560.0	48.5
	0.57	136.6	184.7	188.0	3.3	514.6	564.6	50.0
	0.67	136.7	184.8	188.0	3.2	516.4	565.4	50.0
	0.75	136.8	185.1	188.0	3.0	516.6	566.6	50.5
	0.97	137.2	185.4	188.0	2.9	518.2	568.2	50.5
	1.42	137.5	185.6	187.9	2.5	520.0	572.0	51.5
	2.19	138.6	186.4	188.3	...	...	...	...
	2.80	138.7	186.6	188.4	2.0	525.0	578.0	52.5
	3.88	139.6	187.4	188.9	1.8	527.1	580.1	52.5
	6.15	141.1	188.5	189.8	1.4	530.8	582.8	52.0
	9.85	142.7	189.8	190.9	1.3	532.8	583.8	51.5

[a] Chemical shifts, in hertz, downfield from internal TMS. [b] Separation between signals for NCH$_3$(o) and NCH$_3$(i) (see Experimental Section). [c] Separation between signals for NH(i) and NH(o) (see Experimental Section).

pendent and were not analyzed. Those for the other systems were analyzed assuming a fit to eq 1 and the arbitrary values of 493 and 533 Hz, respectively, for $\delta_{NH(i)}{}^A$ and $\delta_{NH(o)}{}^A$.[7] The resulting values of $\delta_{NH}{}^{AX}$ and K_{NH} (Table II) correspond to the curves shown in Figure 3.

The downfield shifts of the NH resonance signals with increasing concentration (Figure 3) suggest that these protons are involved in hydrogen bonding with the anions. The importance of such a process would be expected to decrease in the order Cl$^-$ > Br$^-$ > I$^-$, and this appears to be the trend (Table II). While the analyses of the data suggest that the hydrogen bonding equilibrium constants for NO$_3$$^-$ are greater than those for Br$^-$, the small values of $\delta^{AX} - \delta^A$ for the nitrates probably make these values relatively uncertain (see Figure 3 and Table II).

The differences observed with anion variation in the concentration dependences of the amidinium nmr resonance signals indicate that the trends (Figures 1–3) cannot be entirely due to changes in the total amidinium ion concentration. This is further supported by the results of a limited study in which the chemical shifts of the various proton groups of 1 were determined as a function of chloride ion concentration at constant amidinium ion concentration (0.53 mol %) in DMSO-d_6 (Figures 4 and 5).[8] The experimental points compare reasonably well with curves (Figures 4 and 5) calculated using the values of K, δ^A, and δ^{AX} obtained for the chloride system by varying the total amidinium salt concen-

(7) These values of δ^A were chosen after visual inspection of the data (Figure 3, Table I).

(8) These data were determined by Kathelyn Steimer.

Table II: Ion-Pair Association Constants and Limiting Chemical Shifts[a]

Signal	Anion	K, mF^{-1}	δ^A, Hz	δ^{AX}, Hz
CCH_3	NO_3^-	10.1	134.1	140.7
	I^-	8.4	134.1	151.9
	Br^-	10.5	134.2	154.9
	Cl^-	10.1 (19.4)	135.3 (134.2)	154.7 (151.4)
$NCH_3(i)$	NO_3^-	8.0	182.9	189.4
	I^-	9.8	182.7	194.6
	Br^-	12.5	182.7	196.6
	Cl^-	11.2 (19.7)	183.7 (182.9)	198.8 (196.6)
$NCH_3(o)$	NO_3^-	5.6	188.4	194.2
	I^-	7.8	188.4	203.1
	Br^-	3.9	188.2	206.6
	Cl^-	...	...	...
$NH(i)$	NO_3^-	119	493	506
	I^-	...	493	...
	Br^-	76	493	516
	Cl^-	226	493	542
$NH(o)$	NO_3^-	119	533	545
	I^-	...	533	...
	Br^-	79	533	564
	Cl^-	355	533	594

[a] Data correspond to the calculated curves in Figures 1–3.

Figure 2. Concentration dependences of the NCH_3 (o) and NCH_3 (i) nmr signals (open and half-solid symbols, respectively) of 1 for DMSO solutions of the chloride (O,◑), bromide (△,▲), iodide (□,◪), and nitrate (◇,◆) salts. Curves are calculated; see text.

Figure 1. Concentration dependence of the CCH_3 nmr signal of 1 for DMSO solutions of the chloride (O), bromide (△), iodide (□), and nitrate (◇) salts. Curves are calculated; see text.
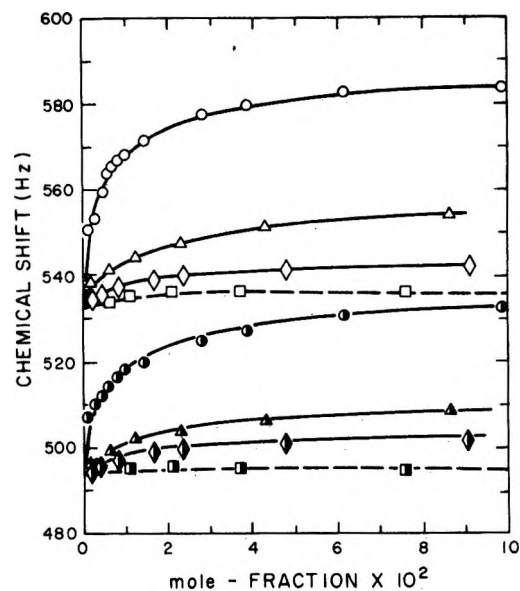
Figure 3. Concentration dependences of the NH(o) and NH(i) nmr signals (open and half-solid symbols, respectively) of 1 for DMSO solutions of the chloride (O, ◑), bromide (△, ▲), iodide (□, ◪), and nitrate (◇, ◆) salts. Curves are calculated; see text.

tration (Table II). Even the unusual behavior of $NCH_3(o)$ (see Figures 2 and 4) is observed in these data.

The values of K derived from the methyl group signals are much smaller than those obtained from the NH data (Table II). The CCH_3 and $NCH_3(i)$ data also show a much smaller spread in K between the various anions. It can be seen from these data, however, that the values increase in the order $I^- < Br^- < Cl^-$. This would be the expected order for the impor-

tance of ion pairing between a positively charged center and these anions in dimethyl sulfoxide. Since the difference between the iodide and chloride systems is much smaller when the CCH_3 and $NCH_3(i)$ groups are used as probes, compared to the data arising from the NH protons, we suggest that these former proton groups are relatively insensitive to the in-plane hydrogen bonding ion-pair equilibria (*vide supra*). Rather
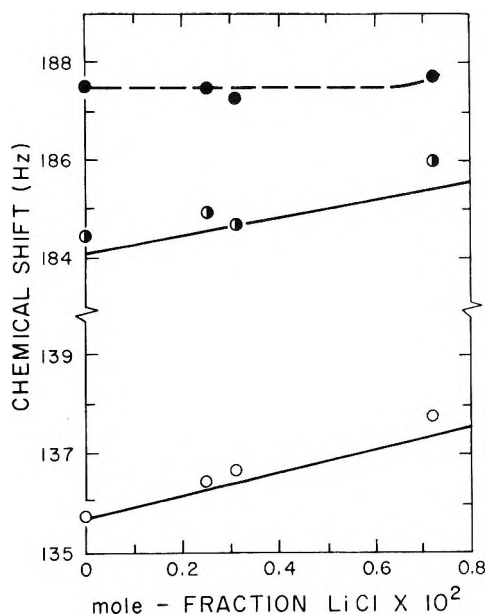
Figure 4. The effect of added LiCl on the chemical shifts of the CCH$_3$ (O), NCH$_3$(i) (◑), and NCH$_3$(o) (●) nmr signals for 0.53 mol % N,N-dimethylacetamidinium chloride in DMSO. Solid curves are calculated; see text.
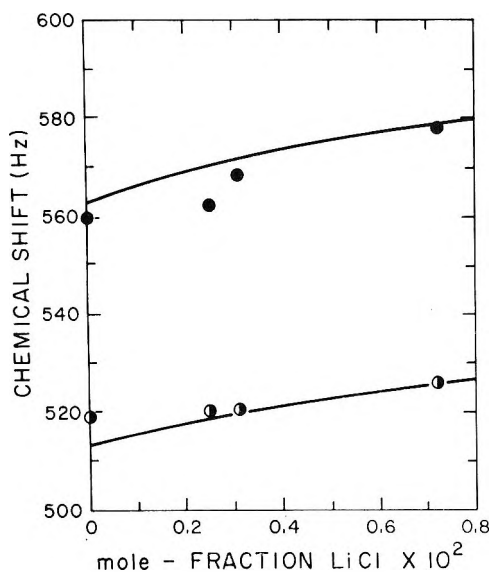
Figure 5. The effect of added LiCl on the chemical shifts of the NH(i) (◑) and NH(o) (●) nmr signals for 0.53 mol % N,N-dimethylacetamidinium chloride in DMSO. Curves are calculated; see text.

we think they reflect a nonspecific ion-pair interaction between the anion and amidinium ion in which the former probably resides above or below the plane of the amidinium ion.

The unusual behavior of the resonance signal for NCH$_3$(o) in the chloride systems (Figures 2 and 5), and the atypical ordering of the other values of K derived from this signal (see Table II), suggest that this proton group is sensitive to the presence of both ion pairs. It also appears that the CCH$_3$ and NCH$_3$(i)

resonance signals are not totally insulated from the effects of a hydrogen-bonded anion. Deviations from the calculated curves are particularly visible in the chloride system (Figures 1 and 2) at concentrations below 0.02 mole fraction where the greatest change in concentration of the hydrogen bonded ion pair occurs (see Figure 3).

These results should be compared with those of other workers. Buckson and Smith[4] found that the N–CH$_2$ proton resonance signal for tetra-n-butylammonium halides shifted downfield with increasing concentration in nitrobenzene. The data fit an ion-pair association model and gave values of the association equilibrium constant (K) equal to 18.9, 25.6, and 37.0 l./mol for the iodide, bromide, and chloride, respectively. Conductance measurements for solutions of tetramethylammonium halides in acetonitrile[9] gave ion-pair association constants of 5, 36, and 56 l./mol. for the iodide, bromide, and chloride, respectively; in DMSO,[10] the values for the iodide and bromide were 2.2 and 4.5 l./mol.

The NH nmr resonance signal of pyridinium halides was found to shift downfield with increasing concentration in the solvents CH$_2$Cl$_2$, CH$_3$CN, and CH$_3$NO$_2$.[11] The shifts increased in the order I < Br < Cl. Similar behavior was observed for the NH protons of p-n-butylanilinium halides in CDCl$_3$.[12]

Experimental Section

N,N-Dimethylacetamidinium chloride was prepared by the method of Pinner;[3b] mp 164–166.5°. Anal. Calcd for C$_4$H$_{11}$N$_2$Cl: Cl, 28.92. Found: Cl, 29.22, 29.04. N,N-Dimethylacetamidinium bromide was prepared from the chloride by ion exchange. A column containing 60 g of Dowex 1, X10 anion-exchange resin (50–100 mesh) was washed with 3 l. of an aqueous solution containing 240 g of potassium bromide. To this column was then added a solution of 2.2 g of the amidinium chloride in 15 ml of H$_2$O. Elution with water, lyophilization, and drying in vacuo over sulfuric acid gave 33% recovery of amidinium bromide; mp 152–153.5°. Anal. Calcd for C$_4$H$_{11}$N$_2$Br: Br, 47.83. Found: Br, 48.85, 49.07. N,N-Dimethylacetamidinium iodide was prepared from the chloride by a procedure analogous to that for preparation of the bromide. Several passes through the ion-exchange column were necessary to bring about complete exchange; mp 215.5–218.5° (dec). Ancl. Calcd for C$_4$H$_{11}$N$_2$I: I, 59.29. Found: I, 59.13, 59.39. N,N-Dimethylacetamidinium nitrate was prepared as previously described from the chloride by treatment with aqueous silver

(9) D. F. Evans, C. Zawoyski, and R. L. Kay, J. Phys. Chem., 69, 3878 (1965).

(10) D. E. Arrington and E. Griswold, ibid., 74, 123 (1970).

(11) G. Kotowycz, T. Schaeffer, and E. Bock, Can. J. Chem., 42, 2541 (1964).

(12) G. Fraenkel and J. P. Kim, J. Amer. Chem. Soc., 88, 4203 (1966).

nitrate;[1a] mp 151.5–153°. *Anal.* Calcd for $C_4H_{11}N_3O_3$: C, 32.21; H, 7.43. Found: C, 32.88; H, 7.89. All of the amidinium salts except for the iodide were noticeably hygroscopic, and great care was taken to keep them dry.

Preparation of Nmr Samples. Samples were prepared by weight; both solvent and solute were carefully dried. The most concentrated solution was prepared first, and samples of decreasing mole fraction solute were prepared by dilution of this master sample. A trace of concentrated sulfuric acid was added to the master solutions to protonate trace amounts of neutral amidine. Addition of acid did not affect nmr signal positions nor did varying trace amounts of acid lead to differences in spectral behavior for a particular amidinium salt.

Determination of Nmr Signal Positions. Spectra were carefully recorded at ambient temperature (40.5°) using a Varian A-60-D nmr spectrometer. The NCH_3 and CCH_3 shifts were determined at a sweep width of 250 Hz using TMS as the internal standard. The N,N-dimethyl peak separation ($\delta\nu_\infty$) was determined at a sweep width of 50 Hz. The NH shifts were determined at a sweep width of 1000 Hz, while the peak separation $\delta(NH_2)$ between these components was determined at a sweep width of 500 Hz. The calibration of all of the sweep widths was checked using the standard described by Jungnickel.[13] Multiple spectra were recorded for each sample and concentration.

(13) J. L. Jungnickel, *Anal. Chem.*, **35**, 1985 (1963).

Micelle Formation by Some Phenothiazine Derivatives. II.[1a] Nuclear Magnetic Resonance Studies in Deuterium Oxide

by A. T. Florence* and R. T. Parfitt[1b]

School of Pharmaceutical Sciences, University of Strathclyde, Glasgow, United Kingdom   (*Received March 19, 1971*)

Publication costs borne completely by The Journal of Physical Chemistry

Nuclear magnetic resonance, pH, and viscosity measurements have been carried out on solutions of promethazine, chlorpromazine, promazine, and thioridazine hydrochlorides in D_2O or H_2O. The positions of the nmr signals of two portions of each molecule were observed as a function of solute concentration above and below the critical micelle concentration. The concentration of monomers above the critical micelle concentration, calculated from the chemical shift data, decreases perceptibly in chlorpromazine and thioridazine solutions. The magnitude of the chemical shifts observed on micelle formation is compatible with a vertical stacking of the phenothiazine rings, probably in an alternating mode in the micelle interior. pH measurements indicated that increased dissociation of the hydrophilic $-^+NH<$ groups takes place on micellization, but the observed shifts of the protons are found not to be due simply to pH changes in bulk solution.

Many phenothiazine tranquillizers are known to be surface active[2] and to form micelles[3] in aqueous solution. Such properties may or may not be biologically significant,[4] but it is certain that the behavior of the compounds in pharmaceutical formulations is affected as a consequence of them. It is therefore of interest to investigate the surface activity of these drugs, as Zografi and coworkers[5] have done, and to study their behavior in aqueous solution.

The phenothiazines are not just of biological interest. Because of their surface-active properties and their relatively high critical micelle concentrations (cmc), they serve as useful compounds with which to study the phe-

nomenon of micelle formation. In particular, the compounds lend themselves to investigation by nuclear magnetic resonance (nmr) techniques. For example, proton resonance signals of three portions of the pro-

(1) (a) Part I: A. T. Florence and R. T. Parfitt, *J. Pharm. Pharmac.*, **22**, 121S (1970); (b) present address: Chemical Research Dept., Pfizer Ltd., Sandwich, Kent, U. K.

(2) P. M. Seeman and H. S. Bialy, *Biochem. Pharmac.*, **12**, 1181 (1963).

(3) W. Scholtan, *Kolloid Z.*, **142**, 84 (1955).

(4) A. T. Florence, *Advan. Colloid Interface Sci.*, **2**, 115 (1968).

(5) G. Zografi, D. E. Auslander, and P. E. Lytell, *J. Pharm. Sci.*, **53**, 573 (1964); G. Zografi and D. E. Auslander, *ibid.*, **54**, 1313 (1965); G. Zografi and I. Zarenda, *Biochem. Pharmac.*, **15**, 591 (1966).

methazine hydrochloride (I) molecule can be observed, and the chemical shift values can be determined as a function of concentration over a range of concentrations above and below the cmc, without signal enhancement.[1a] The three groups are the $-^+NH(CH_3)_2$ group, the $-CH-CH_3$, and the aromatic region of the molecule. Similarly, with thioridazine (IV) the spectral shifts of the proton lines of the $-SCH_3$ and $^+NH(CH_3)$ groups can be measured. By observation of the direction and magnitude of chemical shift changes one can deduce something about the altered environment experienced by specific proton groups when the monomers enter the micelle.

Investigations of nmr spectral changes occurring on the micellization of a number of surfactants have been reported. Müller and coworkers[6-8] have carried out extensive studies on some fluorinated surfactants and were able to deduce from their results that water was not totally excluded from the micellar interior. Inoue and Nakagawa[9] studied the spectra of ω-phenylalkyl-trimethylammonium bromides, and Eriksson,[10] cetyl pyridinium bromide. Only the latter author observed changes occurring in the spectra of widely separated portions of the surfactant molecule.

In this paper we have studied the behavior of three phenothiazines, namely chlorpromazine (II), promazine (III), and thioridazine (IV) hydrochlorides and present further data on promethazine hydrochloride (I) which was the subject of a preliminary communication.[1a]

On micelle formation the hydrophilic N-methyl groups are concentrated at the surface of the micelle and the bulky phenothiazine rings are arrayed in some manner to form the hydrophobic micellar core. The pH of solutions of the phenothiazine hydrochlorides decreases abruptly at the cmc suggesting increased dissociation of the $^+NH(CH_3)_2$ groups at the micelle surface. As Koch and Doyle[11] have shown that the chemical shift of the N-methyl group of a number of aromatic amines is linearly dependent on the fractional number of free base and salt molecules present, it is likely that any observed shift can be due both to changes in environment *per se* and to changes in the degree of ionization of the monomer. An understanding of both factors is a prerequisite for adequate formulation of a thermodynamic model for micelle formation.

Experimental Section

Materials. Chlorpromazine hydrochloride (Largactil[R]) and promethazine hydrochloride (Phenergan[R]) were commercial samples obtained from May & Baker Ltd. Promazine hydrochloride was a gift from John Wyeth & Brother Ltd., and thioridazine hydrochloride a gift from Sandoz Products Ltd. All drugs were used as received.

Cetomacrogol 1000 B.P.C., a nonionic detergent with the average formula $C_{16}H_{33}(OCH_2CH_2)_{22}OH$, was used as received.

Sodium chloride was AnalaR grade.
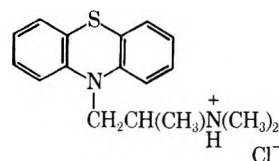
(I)

10-(2-Dimethylaminopropyl)-
phenothiazine hydrochloride
(Promethazine HCl)
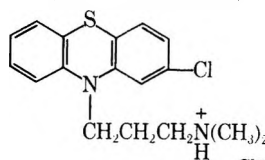
(II)

2-Chloro-10-(3-dimethylaminopropyl)-
phenothiazine hydrochloride
(Chlorpromazine HCl)
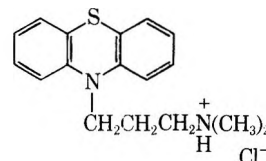
(III)

10-(3-Dimethylaminopropyl)-
phenothiazine hydrochloride
(Promazine HCl)
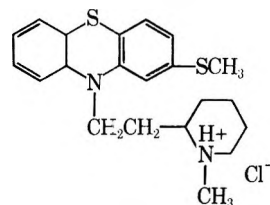
(IV)

10-[2-(1-Methylpiperid-2-yl)ethyl]-2-
methylthiophenothiazine hydrochloride
(Thioridazine HCl)

Methods. Solutions of the drugs in deuterium oxide (D_2O) were prepared just prior to use to minimize photochemical degradation, to which these compounds are susceptible. D_2O was employed to obviate overlap of signals with large H_2O signals and side bands. Micelle formation and hydrophobic bonding in D_2O is not significantly different from that in normal water.[12]

Proton magnetic resonance spectra (60 MHz) were obtained at 34° on a Perkin-Elmer R-12 spectrometer.

(6) N. Müller and R. H. Birkhahn, *J. Phys. Chem.*, **71**, 957 (1967).

(7) N. Müller and R. H. Birkhahn, *ibid.*, **72**, 583 (1968).

(8) N. Müller and T. W. Johnson, *ibid.*, **73**, 2042 (1969).

(9) H. Inoue and T. Nakagawa, *ibid.*, **70**, 1108 (1966).

(10) J. C. Eriksson, *Acta Chem. Scand.*, **17**, 1478 (1963).

(11) S. A. Koch and T. D. Doyle, *Anal. Chem.*, **39**, 1273 (1967).

(12) P. Mukerjee, P. Kapauan, and H. G. Meyer, *J. Phys. Chem.*, **70**, 783 (1966).
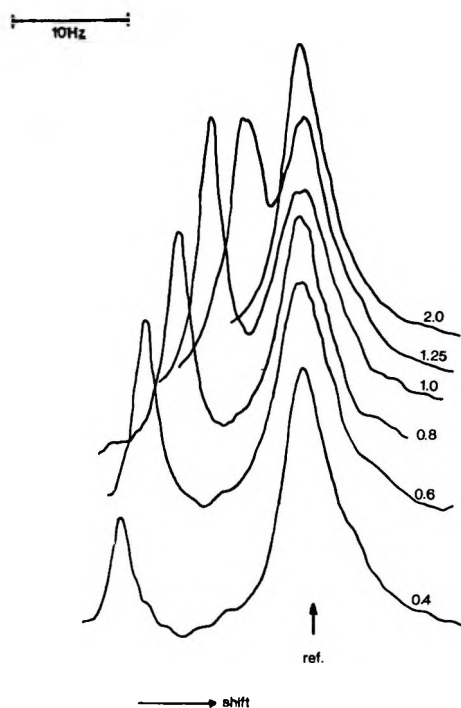
Figure 1. Superimposed scale-expanded spectra of the nmr signal of the $^+N(CH_3)_2$ protons of chlorpromazine hydrochloride in D_2O. The reference solution, contained in the inner capillary (see text) gives rise to the peak marked with the arrow. Solutions of the compound of varying strength (percentage concentrations are given) give the left-hand peaks. This illustrates the shift of the nmr signal with increasing concentration.

Figure 2. Shifts (Hz) plotted against reciprocal molar concentrations of promethazine hydrochloride (M) in D_2O (upper figure) and in 0.154 M NaCl in D_2O. Shifts of the $CHCH_3$ and NMe_2 spectra relative to their position in a 20% solution of promethazine HCl are shown in both diagrams.

Coaxial sample tubes were made by inserting sealed capillary tubes containing the reference solution into accurately centered holes in nylon bushes in standard 5-mm tubes. The reference solution was for promethazine and chlorpromazine a 20% solution of the respective compound and in all other cases an acetone–chloroform–dioxane mixture in carbon tetrachloride.

Chemical shifts of the proton absorptions of ^+NH-$(CH_3)_2$ (singlet) were measured in all cases relative to the corresponding reference resonance line at a sweep width of 100 Hz. All spectra were obtained at least twice; in dilute solutions four sweeps were made and an average shift calculated from the spectra.

The viscosity of micellar solutions was determined in 0.9% NaCl solution and in water using a suspended level dilution viscometer thermostated to 20 ± 0.01° and 34 ± 0.01°.

pH measurements were made with a Pye pH meter (Model 78). A solution of the drug was titrated into its solvent maintained at 20 ± 1° and at 34 ± 1° for comparability with the nmr conditions.

Results and Discussion

The nmr spectra of the phenothiazines obtained had the same characteristics as those published in the compilation of Warren and coworkers[13] and therefore are

not reproduced here. The proton magnetic resonance spectrum of a 20% solution of chlorpromazine hydrochloride in D_2O has as its major feature a 6-proton singlet at τ 7.2 (δ 2.8) corresponding to the $-^+N(CH_3)_2$ group. Figure 1 illustrates a series of scale-expanded spectra in this region, with varying concentrations of chlorpromazine hydrochloride test solution in the presence of an external reference (a 20% chlorpromazine hydrochloride solution in D_2O). An increasing downfield shift relative to the reference is observed on lowering the test solution concentration.

Chemical shifts (hertz) measured from spectra of the hydrochlorides of chlorpromazine, promethazine, promazine, and thioridazine are plotted as a function of reciprocal drug concentration in Figures 2 and 3. (No correction has been made for bulk magnetic susceptibility effects, as these are expected to be small[6,14,15] especially in the experiments where the compound itself acts

(13) R. T. Warren, I. B. Eisdorfer, W. E. Thompson, and J. E. Zarembo, *J. Pharm. Sci.*, **55**, 144 (1966).

(14) R. Haque, *J. Phys. Chem.*, **72**, 3056 (1968).

(15) P. A. Arrington, A. Clouse, D. Doddrell, R. B. Dunlap, and E. H. Cordes, *ibid.*, **74**, 665 (1970).
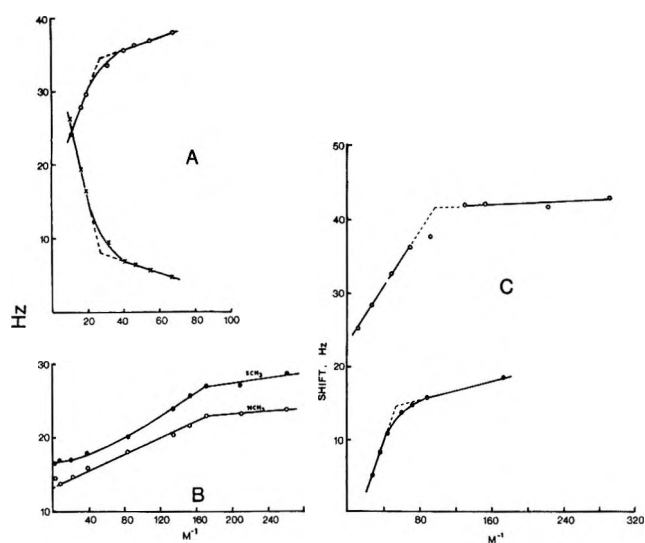
Figure 3. (A) Shifts (Hz) plotted against reciprocal molar concentration for promazine hydrochloride: (O) NMe_2 spectral shifts and (X) shifts of aromatic portions of the spectrum. The reversed order of the aromatic shift is the result of the choice of external reference ($CHCl_3$) and has no special significance. (B) Similar measurements shown for thioridazine hydrochloride. This shows the shifts of both NMe and SMe peaks. The more abrupt change of the position of the latter on micellization is perhaps the result of the more drastic change in its environment as it will be in the core of the micelle. (C) Shifts for promazine hydrochloride in 0.154 M NaCl in D_2O (O) and chlorpromazine hydrochloride in D_2O (●).

as reference.) The plots take the form of two straight lines which intersect at a concentration corresponding to the cmc. Curvature in the region of the cmc is marked in a number of cases, e.g., promethazine in D_2O, whereas with promethazine in the presence of NaCl, where larger micelles are formed, no curvature can be detected. This is indicative of the small micelles formed in the absence of salt.

As the phenothiazine concentration increases, shifts occur to higher fields. Proton resonances of purine, which associates by hydrophobic stacking, show marked movements in the direction of higher fields as its concentration in solution is increased.[16] Shifts of this nature are generally attributed in aromatic systems to the magnetic anisotropy associated with ring currents.[16] Blears and Danyluk,[17] in an investigation of the aggregation of acridine orange, observed that if the rings are stacked parallel to each other a shift of the ring proton resonance to high field should result on increase in solute concentration whereas, if aggregated in a coplanar manner, the opposite trend would be apparent. Their results suggest that the acridine orange molecules are stacked with their planes parallel to each other, the most favored configuration being the stack in which the 1, 9, and NCH_3 protons are located over the center of adjacent rings, rather than the 4, 5, and 6 protons. Catalin models of promazine show that this is a likely configuration for the monomers in phenothiazine mi-

celles. Thyrum and coworkers[18] were able to deduce from nmr data a slightly off-set vertical stacking in procaine–thiamine pyrophosphate complexes.

Attempts to explain the shifts quantitatively are difficult. The application of Johnson–Bovey[19] charts or tables to aromatic systems other than benzene will give only an approximation of the spatial orientation of rings in proximity. Blears and Danyluk[17] have applied these tables, intended for uncomplicated benzene rings, to a π-deficient heterocyclic system, acridine. We do not feel justified in making calculations of this kind for the phenothiazine aggregates. However, application of these tables and chart[20] to the shielding by an adjacent aromatic ring in the SCH_3 group absorption of thioridazine shows that an upfield shift of $+12$ Hz on micellization ($\delta_{mon} - \delta_{mic}$) approximates to a vertical stacking mode in the micelle. This may occur either with the cationic head groups adjacent or alternating, i.e.

adjacent   alternating
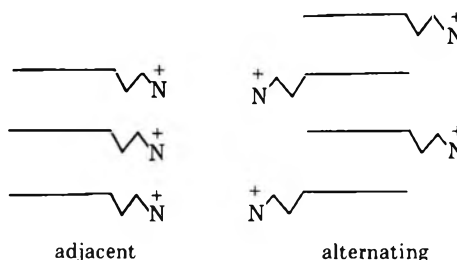
The latter mode is more realistic on steric grounds and on thermodynamic grounds as the hydrophobic regions of the molecule would be better "protected" from water in a three-dimensional micellar array of this construction. It is also possible that in a large enough array a spiral packing in the adjacent model may be achieved. Viscosity results, however, indicate that the micelles are spherical or nearly so, and therefore the micelles are not likely to be large if stacked in either an alternating or adjacent manner. Scholtan's results[3] have shown that at room temperature the micelles of I and II are not large.

The electroviscous correction to the intrinsic viscosity, [η], of the micelles (see Figure 4) is not known at this stage, and hence no attempt is made to calculate the hydration of the micellar species in water. In salt solutions where the micelles are large, the electroviscous correction is negligible and the intercept, [η], is close to the value expected from spherical units, 2.5.

Table I shows cmc values at 20 and 34° from the pH data and nmr plots of shift vs. reciprocal concentration. An insufficient number of compounds have been stud-

(16) P. O. P. Ts'o, Ann. N. Y. Acad. Sci., 153, 785 (1969).

(17) D. J. Blears and S. S. Danyluk, J. Amer. Chem. Soc., 88, 104 (1966); ibid., 89, 21 (1967).

(18) P. T. Thyrum, R. J. Luchi, and E. M. Thyrum, Nature (London), 223, 747 (1969).

(19) C. E. Johnson and F. A. Bovey, J. Chem. Phys., 29, 1012 (1958).

(20) R. H. Bible, "Interpretation of N.M.R. Spectra: An Empirical Approach," Plenum Publishing Co., New York, N. Y., 1967, p 19.
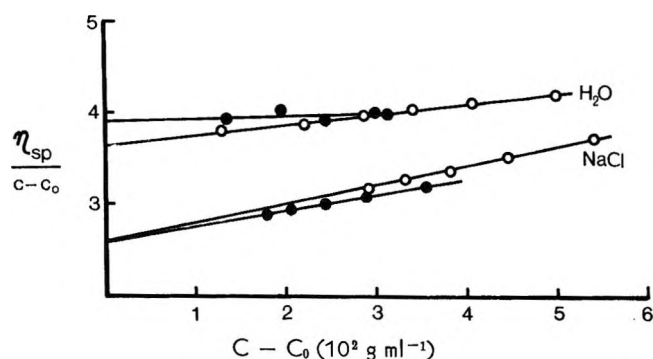
Figure 4. Representative viscosity results showing reduced specific viscosity plotted against micellar concentration (c − c₀) for chlorpromazine (O) and promazine hydrochloride (●). Upper plots show results in water and the lower plots the results obtained in 0.154 M NaCl.

ied to enable us to discuss in detail the effect of the chemical structure of the phenothiazines on their colloidal behavior. However, promazine (III) and chlorpromazine (II) may be directly compared as they differ by only a -Cl group at the 2 position on the phenothiazine ring; the latter has the lower cmc as might be expected from the added hydrophobic group. Promazine (III) and promethazine (I) differ only by the branching of the side chain in the latter. Branching of an aliphatic chain is equivalent to shortening the chain length and hence promethazine has a higher cmc. The most surface-active member of the group is thioridazine hydrochloride (IV) which has a methylthio substituent in the phenothiazine ring. Klotz[21] and Heitmann[22] have both shown that this group can participate in hydrophobic interactions. Némethy and Scheraga[23] assumed that the sulfur atom was equivalent to a CH_2 group and predicted the thermodynamic behavior of cysteine and methionine on this assumption. One can therefore assert that the 2-methylthio group is the main reason for the relatively low cmc of thioridazine.

Table I: Cmc Data from Nmr and pH Results in D_2O and H_2O, Respectively (M)

Compound	Additive	pH (H_2O) 10^2 cmc (20°)	pH (H_2O) 10^2 cmc (34°)	Nmr[a] (D_2O) 10^2 cmc (34°)
Promethazine HCl	. . .	4.35	4.40	4.54
	0.154 M NaCl	1.67	2.48	2.47
Chlorpromazine HCl	. . .	1.79₈	1.88	1.90₅
	0.154 M NaCl	0.45₆	0.555	. . .
Promazine HCl	. . .	3.05	. . .	3.66
	0.154 M NaCl	. . .	1.37₆	1.05
	0.427 M NaCl	0.103		
Thioridazine HCl	. . .	0.654	0.583	0.583

[a] Determined from the inflections of plots of shift against reciprocal concentration by extrapolation of the straight lines above and below the critical concentration.

Information on the changing proportions of monomer and micelle can be obtained from the shift data if some assumptions are made.[24] If the observed chemical shift, δ_{obsd}, is a numerical weight average of the resonance frequencies of the protons of the monomeric and micellar species, and if it is assumed that the monomers have a certain shift, δ_{mon}, and the micellar species have a shift δ_{mic} and that there is rapid equilibration between the two forms we can write

$$\delta_{obsd} = \delta_{mic}x_{mic} + \delta_{mon}x_{mon} \tag{1}$$

where x_{mic} and x_{mon} are the weight fractions of the species, i.e.

$$x_{mic} = 1 - x_{mon} \tag{2}$$

We therefore obtain

$$x_{mic} = \frac{\delta_{obsd} - \delta_{mon}}{\delta_{mic} - \delta_{mon}} \tag{3}$$

δ_{mic} is obtained from plots of chemical shift vs. reciprocal concentration (c^{-1}) by extrapolation of the micellar line to $c^{-1} = 0$. The contribution of the monomers to δ_{obsd} is obtained from points on the extrapolated straight line below the cmc. That this procedure is correct is demonstrated by the close agreement of results for monomer concentrations (Figure 5) obtained from shift values of different portions of the molecule, e.g., the $-SCH_3$ and $-NCH_3$ proton shifts of thioridazine. Examination of the results in Figure 5 show that chlorpromazine and thioridazine monomer concentrations decrease slightly but perceptibly at concentrations three to five times the cmc. Promethazine in the absence of added salt shows almost no change in monomer concentration above the cmc. The plot for promethazine in the presence of 0.9% (0.154 M) NaCl indicates a more sharply rising monomer concentration.

According to the standard treatment of micellar equilibria by the simplified law of mass action[25,26] this would imply that in the presence of such a concentration of salt the micelle was more nonionic in character than in water. The micelles of the phenothiazine hydrochlorides would appear to be less ionic in character than might be expected, as a result of the nature of the dissociation at the micellar surface

$$RNH^{+}(CH_3)_2 \rightleftharpoons RN(CH_3)_2 + H^{+}$$
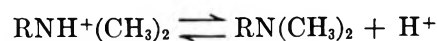
The pH of the phenothiazine solution changes abruptly

(21) I. Klotz, *Brookhaven Symp. Biol.*, **13**, 25 (1960).

(22) P. Heitmann, *Eur. J. Biochem.*, **3**, 346 (1968).

(23) G. Némethy and H. A. Scheraga, *J. Chem. Phys.*, **36**, 3382, 3401 (1962).

(24) J. M. Corkill, J. F. Goodman, T. Walker, and J. Wyer, *Proc. Roy. Soc., Ser. A*, **312**, 243 (1969).

(25) P. H. Elworthy, A. T. Florence, and C. B. Macfarlane, "Solubilization by Surface Active Agents," Chapman and Hall, London, 1968, pp 48–51.

(26) E. W. Anacker in "Cationic Surfactants," E. Jungermann, Ed., Marcel Dekker, New York, N. Y., 1970, pp 210, 211.
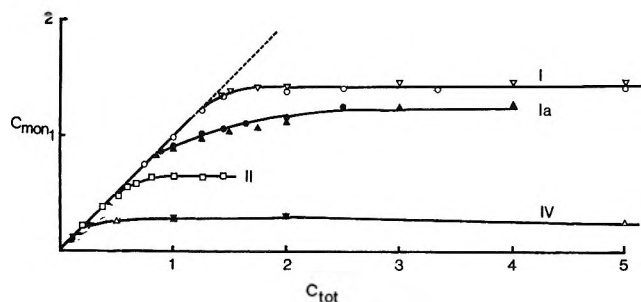
Figure 5. Monomer concentration as a function of total concentration in solutions of promethazine (I) in deuterium oxide and saline solution (Ia), chlorpromazine (II), and thioridazine (IV). The concentrations were determined as described in the text. In the case of promethazine (I and Ia) the $CHCH_3$ shifts and NMe_2 shifts were used to determine the ratio of monomer to total: $\bigcirc$ or $\bullet$, $CHCH_3$; $\triangledown$ or $\blacktriangle$, NMe_2. For IV, $\triangle$ gives value calculated from the NCH_3 spectrum and $\blacktriangledown$ from the SCH_3 spectrum.
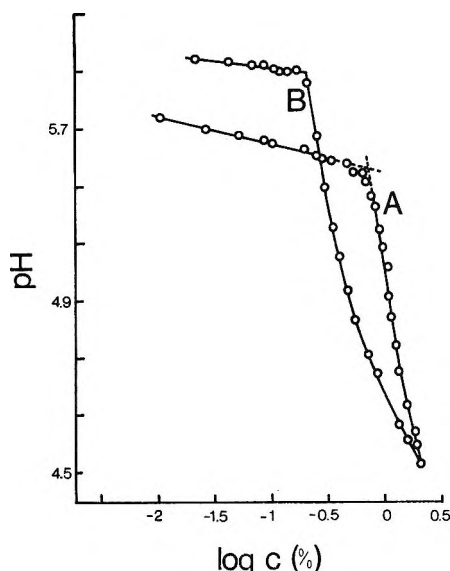
Figure 6. pH vs. log concentration for chlorpromazine hydrochloride in water (A) and 0.154 M NaCl (B) at 34°, showing the sharp break at the critical micellar concentration. Determinations such as these were used to calculate cmc values (see Table II).

at the cmc, as shown by typical results in Figure 6 suggesting that the micellar form of the surfactant is more dissociated than the monomeric species. On dissociation, therefore, the micelle surface becomes less ionic and the micelle behaves more like a nonionic micelle. Because of difficulties in the complete removal of carbon dioxide from the aqueous solutions during pH measurements, the results have not been interpreted further. In addition the measured pH above the cmc may be lower than the true pH of the medium in which the micelles exist, due to the "suspension effect" which has been observed[27] in dispersions of clays, soils, and resins, and which is caused by the development of liquid junction potentials or true membrane potentials
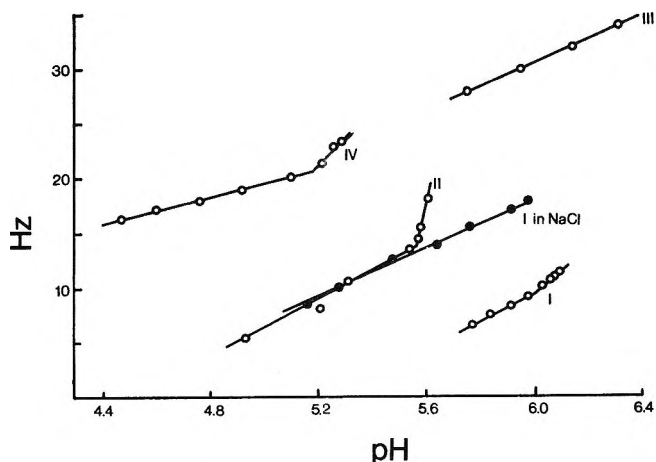
Figure 7. A plot showing the relationship between the chemical shift value and the pH of the solution for the NMe spectrum of I, promethazine; II, chlorpromazine; III, promazine; and IV, thioridazine. Results are also plotted for promethazine in salt.

during measurement. Detailed mass action calculations await further information on the micellar charge and size, now being undertaken by dye electrophoresis and light scattering measurements.[28]

The shifts of the N-methyl groups are plotted as a function of solution pH in Figure 7. As the pH increases, downfield shifts are observed corresponding to an overall decrease in the degree of protonation of the nitrogen atoms. The greater the protonation, the greater is the partial positive charge in the vicinity of the nitrogen atom and hence the greater is the observed deshielding of the N-methyl protons.

Table II: Effect of the Nonionic Surfactant, Cetomacrogol 1000, on the Chemical Shift Values of Thioridazine and Chlorpromazine Hydrochlorides

Compound	Concn of nonionic surfactant, %	Downfield shift, Hz^a
2% thioridazine HCl	0.01	21.10
	0.10	20.33
	1.0	24.0
	2.5	28.5
1% chlorpromazine HCl	0.01	36.4
	0.1	37.43
	1.0	40.0
	2.5	42.4

^{a} Mean of three determinations on $^+NH(CH_3)$ peak; external reference, acetone.

(27) I. Feldman, *Anal. Chem.*, **28**, 1859 (1956). We thank a referee for drawing our attention to the suspension effect and its possible significance in our systems.

(28) D. Attwood and A. T. Florence, to be published.

Addition of the nonionic surfactant cetomacrogol 1000 B.P.C. $(C_{16}H_{33}(OCH_2CH_2)_{22}OH)$ to solutions of the phenothiazine lowers the pH of the solution. This suggests that the phenothiazine is being taken up in the micelles of the nonionic surfactant and that this results in increased dissociation of the drug. However, the chemical shifts are not what would be expected from this type of association. On increasing the concentration of nonionic a shift of the N-methyl proton signal to lower field occurs (see Table II). As stated above, such shifts are normally associated with increased protonation. A possible explanation of the observed direction of shift might be that there is association of the nonionic hydroxyls with the head groups of the phenothiazine, i.e., $CH_2-O-H \cdots : N-(CH_3)$. Hydrogen bonding of this sort would tend to deshield

the $N-CH_3$ protons. The addition of more cetomacrogol could encourage further dissociation of the head groups by a competing hydrogen-bonding interaction, resulting in a net downfield shift. This would also explain the concurrent drop in pH. Precise analogies have not been detected in the literature. Page and Bresler,[29] however, observed a strong downfield shift in the HO-CH_2 signal as a result of interaction between polyalkylene glycol and pyridine. The exact nature of the interaction between nonionic detergent and the phenothiazine molecules is not clear, but it serves to show that the shifts observed in the first part of this study are primary effects and not simply the result of pH changes in the system.

(29)   T. E. Page and W. E. Bresler, *Anal. Chem.*, **36**, 1981 (1964).

Nuclear Magnetic Resonance Study of Interaction between Anionic

and Nonionic Surfactants in Their Mixed Micelles

by Fumikatsu Tokiwa* and Kaoru Tsujii

Industrial Research Laboratories, Kao Soap Company, Wakayama-shi 640-91, Japan   (*Received January 19, 1971*)

The nmr spectra of aqueous solutions of nonionic surfactants, dodecyl polyoxyethylene ethers ($C_{12}POE$) with different number of oxyethylene units, have been measured in the presence of anionic surfactants, sodium dodecyl sulfate ($NaC_{12}S$) and sodium p-octylbenzenesulfonate (NaC_8BS), at different molar ratios of anionic/ nonionic surfactant. When NaC_8BS is added to $C_{12}POE$ solutions, the peak due to protons of the polyoxyethylene chain of $C_{12}POE$ shifts to a higher magnetic field, the extent of the upfield shift depending on the polyoxyethylene chain length of $C_{12}POE$ and the mixing ratio of $NaC_8BS/C_{12}POE$. However, this peak remains at the same position and shows no remarkable change on addition of $NaC_{12}S$. The upfield shift of the polyoxyethylene peak caused by addition of NaC_8BS is ascribed to an interaction between the polyoxyethylene chain of $C_{12}POE$ and the benzene ring of NaC_8BS in their mixed micelle. This interaction has been discussed in relation to the polyoxyethylene chain length of $C_{12}POE$ and the mixing ratio of $NaC_8BS/C_{12}POE$. In the mixed micelle, the number of $C_{12}POE$ molecules influenced by one NaC_8BS molecule was calculated to be 0.6–1.6, depending on the polyoxyethylene chain length and nearly constant for $C_{12}POE$ with oxyethylene units larger than about 9. The number of oxyethylene units influenced by the benzene ring of NaC_8BS was estimated to be about 9.

Introduction

Mixed surfactant systems are of importance from the fundamental and practical points of view. However, a relatively limited number of papers have been reported on the micellar properties of mixed surfactant solutions, probably because of complication of these systems. In previous works, we have studied the colloidal properties of mixed micelles of two different surfactants by means of electrophoresis, light scatter-

ing, vapor pressure depression, and other types of measurements.[1–6] These studies involved the micellar

(1)   F. Tokiwa, *J. Colloid Interface Sci.*, **28**, 145 (1968).

(2)   F. Tokiwa, K. Ohki, and I. Kokubo, *Bull. Chem. Soc. Jap.*, **41**, 2845 (1968).

(3)   F. Tokiwa and N. Moriyama, *J. Colloid Interface Sci.*, **30**, 338 (1969).

(4)   F. Tokiwa and K. Aigami, *Kolloid-Z. Z. Polym.*, **239**, 687 (1970).
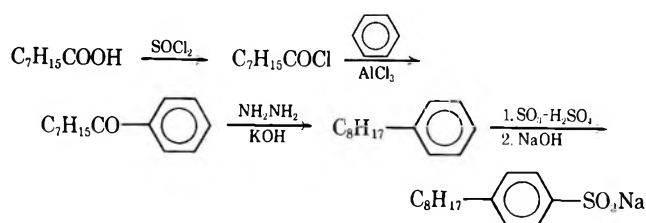
size, electrical nature, and solubilization capacity of mixed micelles and also the degree of ionic dissociation of ionic surfactant in mixed micelles.

During the course of other work of nuclear magnetic resonance spectroscopy (nmr), the present authors observed an interesting aspect of behavior, as will be described below, with respect to the interaction of benzene with polyethylene glycol. The nmr technique is thought to be one of the powerful tools to investigate an intermolecular interaction of two different surfactants in their mixed micelles, and it will give us some information of this interaction which may not be obtained by means of other techniques.

In the present work, an nmr study has been made of the interaction between anionic and nonionic surfactants, sodium p-octylbenzenesulfonate and dodecyl polyoxyethylene ether, in their mixed micelle. Especially, the interaction between the benzene ring of the anionic surfactant and the polyoxyethylene chain of the nonionic surfactant has been discussed in relation to the polyoxyethylene chain length by paying attention to the chemical shift of the polyoxyethylene proton signal.

Experimental Section

Materials. Sodium dodecyl sulfate (abbreviated to $NaC_{12}S$), $C_{12}H_{25}OSO_3Na$, was the same sample as that used in a previous work.[7] Sodium p-octylbenzene-sulfonate (abbreviated to NaC_8BS) was synthesized by the following procedure.

$$C_7H_{15}COOH \xrightarrow{SOCl_2} C_7H_{15}COCl \xrightarrow[AlCl_3]{\bigcirc}$$

$$C_7H_{15}CO-\bigcirc \xrightarrow[KOH]{NH_2NH_2} C_8H_{17}-\bigcirc \xrightarrow[2.\ NaOH]{1.\ SO_3-H_2SO_4}$$

$$C_8H_{17}-\bigcirc-SO_3Na$$

In each step, the reaction product was distilled under reduced pressure or recrystallized from a proper solvent. The product obtained in each step was checked by infrared spectroscopy and element analysis and also by vapor phase chromatography when it was liquid. The final product used for nmr measurement was recrystallized three times from a water–ethanol mixture (20:80) and once from ethanol.

Dodecyl polyoxyethylene ethers (abbreviated to $C_{12}POE$), $C_{12}H_{25}O(CH_2CH_2O)_pH$, with different p were prepared from dodecyl alcohol of a high purity by addition of ethylene oxide in the presence of sodium hydroxide as a catalyst. Polyethylene glycol, a by-product of the reaction, was removed by the following method.

$C_{12}POE$-2.9 (the number written after $C_{12}POE$ denotes the number of oxyethylene units per molecule): This sample was fractionated from the ethylene oxide condensate of dodecyl alcohol (ethylene oxide, ca. 3

mol) at 150–170° under a reduced pressure of 0.03 mm. Paper[8] and vapor phase chromatographies showed the sample to be free of the unreacted alcohol and polyethylene glycol. $C_{12}POE$-4.0, $C_{12}POE$-5.9, $C_{12}POE$-9.1, $C_{12}POE$-11, and $C_{12}POE$-14: each sample was purified by the countercurrent solvent extraction method[9] using butanol-saturated water and water-saturated butanol. Paper chromatography showed the purified samples to be free of polyethylene glycol. $C_{12}POE$-24: This sample was used without purification because the above two methods could not be applied. The sample contained a small amount of polyethylene glycol (less than 1–2%). The average numbers of oxyethylene units per molecule of these samples were determined from their hydroxyl values.

Polyethylene glycol, the molecular weight of which was about 200, was of reagent grade. Benzene was of guaranteed reagent grade. They were used without purification.

Nmr Measurements. A sample solution for nmr measurement was prepared by adding a desired amount of anionic surfactant to 5% (by wt/vol) $C_{12}POE$ solution containing 0.1% 1,4-dioxane[10] as an internal standard. Glass-distilled water was used to make up all sample solutions. The concentrations of sample solutions were sufficiently high as compared to critical micelle concentrations (cmc) and, therefore, most of the surfactant molecules were dissolved in the form of micelles. The cmc values of $C_{12}POE$, NaC_8BS, and $NaC_{12}S$ are 1×10^{-3} to 1×10^{-2}, 3.5×10^{-1}, and 2.3×10^{-1}%, respectively, and those of $C_{12}POE-NaC_8BS$ or $C_{12}POE-NaC_{12}S$ mixtures are probably in an order of 10^{-2}% at the mixing ratios examined. $C_{12}POE$-2.9 and $C_{12}POE$-4.0 were not soluble (but homogeneously dispersive) in water owing to low affinity for water, but soluble in the presence of anionic surfactant. The chemical shift of the polyoxyethylene proton signal, to which attention was paid in the present work, of these two samples in the absence of anionic surfactant was assumed to be the same as the chemical shift for other samples which coincided within the error of measurement. As is easily understood from the chemical structure of C_{12}-

(5) F. Tokiwa and N. Moriyama, Nippon Kagaku Zasshi, 91, 903 (1970).

(6) F. Tokiwa, N. Moriyama, and H. Sugihara, ibid., 90, 449 (1969); 90, 454 (1969); 90, 673 (1969).

(7) F. Tokiwa, J. Phys. Chem., 72, 1214 (1968).

(8) K. Shinoda, T. Nakagawa, B. Tamamushi, and T. Isemura, "Colloidal Surfactants," Academic Press, New York, N. Y., 1963, p 165.

(9) K. Nagase and K. Sakaguchi, Kogyo Kagaku Zasshi, 64, 635 (1961).

(10) Dioxane was also used as an internal standard in aqueous solutions of surfactants in the following papers: e.g., H. Inoue and T. Nakagawa, J. Phys. Chem., 70, 1108 (1966); T. Nakagawa and K. Tori, Kolloid-Z. Z. Polym., 194, 143 (1964); B. R. Donaldson and J. C. P. Schwartz, J. Chem. Soc. B, 395 (1968). It is not possible at this time to apply bulk susceptibility corrections to the observed chemical shifts since the magnetic susceptibilities of the surfactants used have not yet been measured.

POE, all protons of the polyoxyethylene chain are equivalent in nmr spectroscopy except the proton of terminal –OH. This is independent of the polyoxyethylenene chain length. Therefore, it may be assumed that the polyoxyethylene chain of $C_{12}POE$-2.9 and $C_{12}POE$-4.0 surfactants have the same chemical shift as that of their higher homologs.

The nmr spectra were obtained with a Japan Electron Optics JNM-3H-60 spectrometer (60 Mcps) operating at about 22°. Chemical shifts were measured in cycles per second from the dioxane peak.[4,11] The precision of measurements of the distance between the dioxane peak and a peak due to protons of the polyoxyethylene chain of $C_{12}POE$ was ±0.5 cps.

Results and Discussion

When $NaC_{12}S$ is added to $C_{12}POE$ solutions, the peak due to protons of the polyoxyethylene chain of C_{12}-POE shows no change and remains at the same position. On the other hand, this peak shifts to a higher magnetic field and becomes broader on addition of NaC_8BS. Broadening of the polyoxyethylene signal in this case is not owing to an increase in viscosity because of the absence of broadening of other resonance signals of protons. In other signals of $C_{12}POE$ than the polyoxyethylene signal, no appreciable change in chemical shift was observed. The extent of the upfield shift of the polyoxyethylene signal, caused by addition of NaC_8BS, depends on the chain length of polyoxyethylene and the mixing ratio of $NaC_8BS/C_{12}POE$. This upfield shift may be ascribed to an interaction of the polyoxyethylene chain of $C_{12}POE$ with the benzene ring of NaC_8BS in their mixed micelle, since the only difference between the two anionic surfactants is whether they have a benzene ring in the molecule or not. Incidentally, on mixing $C_{12}POE$ with NaC_8BS, the peak due to phenyl protons of NaC_8BS near to the alkyl chain shifts to a lower field to the extent of 3–4 cps.

An evidence of this interaction may be provided by changes in chemical shift of polyethylene glycol by addition of benzene. When polyethylene glycol is mixed with benzene, the polyoxyethylene proton signal shifts to a higher field and the benzene proton signal to a lower field.[12] This is indicative of an interaction of polyethylene glycol and benzene molecules and corresponds to the result for the mixtures of $C_{12}POE$ and NaC_8BS. It also suggests an interaction of the polyoxyethylene chain and the benzene ring in the mixed micelle of $C_{12}POE$ and NaC_8BS.

To discuss quantitatively the interaction in the mixed micelle, it is necessary to evaluate the average chemical shift of the polyoxyethylene proton signal broadened by addition of NaC_8BS. This was done on the nmr chart by calculating the quantity $\int \nu I(\nu)d\nu/\int I(\nu)d\nu$, where ν is the chemical shift in cycles per second and $I(\nu)$ is the absorption intensity at ν.
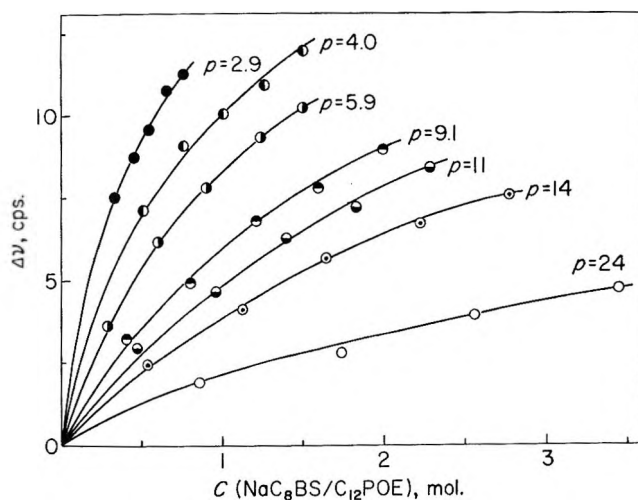
Figure 1. The upfield shift, $\Delta\nu$, of the polyoxyethylene proton signal plotted against the concentration, C, of added NaC_8BS for $C_{12}POE$-p with different p.

In the following discussion, the upfield shift $\Delta\nu$ of the polyoxyethylene proton peak, on addition of NaC_8BS, from the original peak will be expressed by this average value.

Relation between $\Delta\nu$ and p. The curves of upfield shift $\Delta\nu$ vs. concentration C for $C_{12}POE$ with different p are shown in Figure 1 where C is the concentration of NaC_8BS expressed by the molar ratio of $NaC_8BS/C_{12}POE$, the concentration of $C_{12}POE$ being kept constant. When one compares the value of $\Delta\nu$ at a constant C, it decreases with increasing number of p. This suggests that, in the mixed micelle, the influence of the benzene ring of NaC_8BS on the polyoxyethylene protons cannot extend to the whole polyoxyethylene chain when the chain is sufficiently long. Here, if the number of oxyethylene units influenced by the benzene ring is assumed to be l and the dependence of $\Delta\nu$ on C is common to all samples of $C_{12}POE$, then $\Delta\nu$ will be proportional to l/p (where $l < p$) at a definite C. Further, if the extent of influence of the benzene ring on l oxyethylene units is denoted as $\Delta\nu_1$, $\Delta\nu$ is also proportional to $\Delta\nu_1 l/p$ at a definite C. Then, the following equation may be written

$$\Delta\nu = \Delta\nu_1 \cdot \frac{l}{p} f(C), \text{ when } p > l \qquad (1)$$

where $f(C)$ is a function related to the concentration, C.

Here, we have to explain the physical meaning of l in more detail. The $C_{12}POE$ and NaC_8BS molecules form mixed micelles in the form of so-called palisade-

(11) H. Inoue and T. Nakagawa, *J. Phys. Chem.*, **70**, 1108 (1966).
(12) In this case, tetramethylsilane was used as an external standard and, therefore, the difference in magnetic susceptibility between polyethylene glycol and polyethylene glycol–benzene mixture should be taken into account. The magnetic susceptibility correction was made to the chemical shifts observed. However, the extent of correction is insignificantly small.
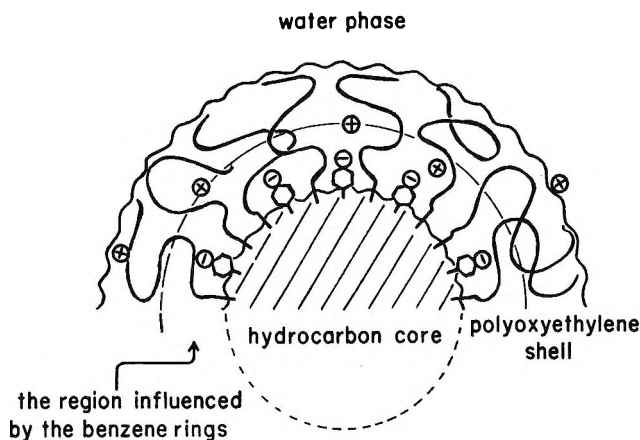
Figure 2. A schematic representation of a part of a mixed micelle of $C_{12}POE$ and NaC_8BS ($p > l$).

Figure 3. The $p \cdot \Delta\nu$ vs. C plots for $C_{12}POE$-p with different p.

type micelles, orientating their hydrocarbon part in side and the ionic head of NaC_8BS and the poly oxyethylene part of $C_{12}POE$ outside. Figure 2 is a schematic representation of this mixed micelle. The benzene rings of the NaC_8BS molecules are probably located in the region between the hydrocarbon core and the polyoxyethylene shell of the micelle. If this is the case, the influence of the benzene rings would be stronger on the oxyethylene units near the hydro-carbon part and weaker on the oxyethylene units re-mote from the hydrocarbon part. This aspect seems to be reflected on the pattern of the polyoxyethylene signal: namely, the width of the signal becomes broader in the presence of NaC_8BS. In the present model we are assuming that, when $p > l$, the benzene rings in the micelle exert an influence of $\Delta\nu_1$ on the oxyethylene units from 1 to l and no influence on the oxyethylene units $(l + 1)$ to p. Then, there would appear two imaginary peaks; one is at the original position and the other at a position corresponding to $\Delta\nu_1$. The relative intensity of the two peaks would depend on the ratio of l/p. The average of the chemical shifts of the two peaks corresponds to the shift $\Delta\nu$ calculated from the spectrum observed.

If the above assumption is reasonable, eq 1 is re-written in the form

$$\Delta\nu \cdot p = \Delta\nu_1 \cdot l \cdot f(C), \text{ when } p > l \qquad (2)$$

According to eq 2, the plots of $\Delta\nu \cdot p$ vs. C will give us a single curve irrespective of p if $f(C)$ is common to all numbers of p, because l and $\Delta\nu_1$ are constants. Figure 3 shows the $\Delta\nu \cdot p$ vs. C plots for $C_{12}POE$ with different p. As expected, these plots can be reduced to a single curve except the plots for $C_{12}POE$ with p of 2.9, 4.0, and 5.9. The reason for deviation from this curve may be easily understood if l is assumed to be larger than 5.9. When $p < l$, eq 1 or 2 has no physical meaning.

Relation between $\Delta\nu$ and C. In the next place, let us determine the function $f(C)$. Consider a micelle consisting of Q $C_{12}POE$ molecules. Divide the micelle surface into small sections, each containing q $C_{12}POE$ molecules $(Q \gg q)$. Assume that if one NaC_8BS molecule enters into a particular small section, all of the q $C_{12}POE$ molecules in this section are influenced to cause the upfield shift of the polyoxyethylene proton signal, and also assume that further entering of NaC_8BS molecules (more than one molecule) into this section exerts no influence upon the upfield shift of the signal. Under this assumption, an increase in upfield shift, $d(\Delta\nu_{mic})$ (the subscript mic refers to one micelle), when dn of NaC_8BS molecules enter into the micelle, will be proportional to the probability, P, of finding the small sections not occupied with even one NaC_8BS molecule in the micelle. Then, we have the following equation
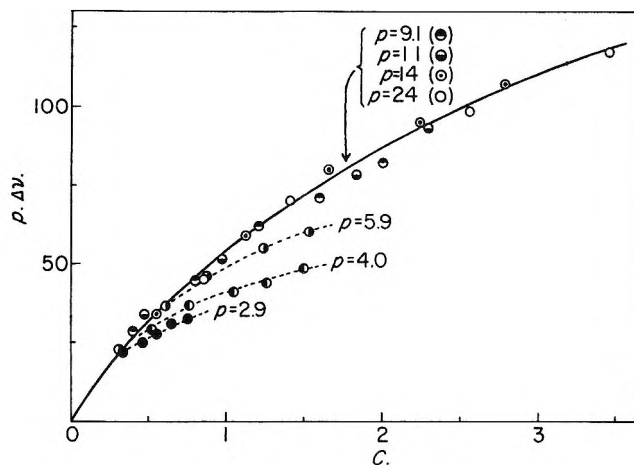
$$\frac{d(\Delta\nu_{mic})}{dn} = kP(n) \qquad (3)$$

where k is a constant.

The $P(n)$ in eq 3 can be calculated as follows. The probability of finding a particular NaC_8BS molecule in a particular small section is q/Q. When n NaC_8BS molecules exist in a micelle being watched, the probability of finding m particular NaC_8BS molecules in the small section and other $(n - m)$ molecules outside the small section is written by

$$\left(\frac{q}{Q}\right)^m \left(1 - \frac{q}{Q}\right)^{n-m}$$

As there are $n!/m!(n - m)!$ ways of selecting m out of n, the probability of finding m arbitrary NaC_8BS molecules in the small section is given by

$$\frac{n!}{m!(n - m)!}\left(\frac{q}{Q}\right)^m \left(1 - \frac{q}{Q}\right)^{n-m}$$

This is equivalent in form to the Poisson's equation for "fluctuation."[13] The probability of finding no

(13) L. Landau and E. Lifshits. "Statistical Physics" (Japanese ed), Vol. II, Iwanami Books Corp., Tokyo, Japan, 1958, p 124.

NaC$_8$BS molecule in the small section being watched is then $\{1 - (q/Q)\}^n$, which can be obtained by putting $m = 0$. This probability, $\{1 - (q/Q)\}^n$, also holds for other arbitrary small sections. Thus, the probability $P(n)$ of finding small sections containing no NaC$_8$BS molecule in the whole of the micelle (Q molecules) is given by

$$P(n) = \left(1 - \frac{q}{Q}\right)^n \tag{4}$$

Substituting eq 4 for eq 3, we obtain

$$\frac{d(\Delta\nu_{mic})}{dn} = k\left(1 - \frac{q}{Q}\right)^n \tag{5}$$

Integration of eq 5 gives

$$\Delta\nu_{mic} = k\int\left(1 - \frac{q}{Q}\right)^n dn + \text{constant} =$$
$$\frac{k}{\ln\{1 - (q/Q)\}}\left(1 - \frac{q}{Q}\right)^n + \text{constant} \tag{6}$$

Here, the boundary conditions are that $\Delta\nu_{mic} = 0$ at $n = 0$, and $\Delta\nu_{mic} \rightarrow \Delta\nu_s$ as $n \rightarrow \infty$ where $\Delta\nu_s$ is the saturation value of the upfield shift. Equation 6 then becomes

$$\Delta\nu_{mic} = \Delta\nu_s\left\{1 - \left(1 - \frac{q}{Q}\right)^n\right\} \tag{7}$$

In the above calculation, only one micelle has been considered. However, this result, i.e., eq 7, holds for all micelles in unit volume because the extent of the upfield shift is irrespective of the number of micelles, although the intensity of the signal is proportional to the number of micelles. Thus, $\Delta\nu_{mic}$ in eq 7 is equal to the upfield shift observed, $\Delta\nu$.

Since $0 < \{1 - (q/Q)\} < 1$, the term $\{1 - (q/Q)\}$ in eq 7 can be expressed as $1 - (q/Q) = e^{-k'}$ ($k' > 0$) for convenience. Then, eq 7 is written in the form

$$\Delta\nu = \Delta\nu_s(1 - e^{-k'n}) \tag{8}$$

The variable n in eq 8 is the number of NaC$_8$BS molecules per micelle, as defined above, and can be convertible to C ($C = M_A/M_N$, where M_A and M_N are the molar concentrations of NaC$_8$BS and C$_{12}$POE, respectively). Then n can be related to M_A by the equation

$$n = \frac{LM_A}{N} \tag{9}$$

where N is the number of micelles in unit volume of solution and L is the Avogadro's number. Since $C = M_A/M_N$, the relation between n and C is then

$$n = \frac{LM_N}{N}C \tag{10}$$

Substituting eq 10 for eq 8, we obtain

$$\Delta\nu = \Delta\nu_s\left\{1 - \exp\left(-\frac{k'LM_N}{N}C\right)\right\} \tag{11}$$

By definition, $e^{-k'} = 1 - (q/Q)$, i.e., $-k' = \ln\{1 - (q/Q)\}$. Further, $k' = q/Q$ since $\ln\{1 - (q/Q)\} \simeq -q/Q$ (q/Q is sufficiently small as compared to unity). Then, eq 11 becomes

$$\Delta\nu = \Delta\nu_s\left\{1 - \exp\left(-\frac{qLM_N}{QN}C\right)\right\} \tag{12}$$

The value of LM_N is equal to QN, both values being the number of C$_{12}$POE molecules in unit volume of solution. Then, (qLM_N/QN) in eq 12 is equal to q and eq 12 is simplified to

$$\Delta\nu = \Delta\nu_s(1 - e^{-qC}) \tag{13}$$

Comparing eq 1 with eq 13

$$\Delta\nu_s = \Delta\nu_l \cdot \frac{l}{p} \tag{14}$$

$$1 - e^{-qC} = f(C) \tag{15}$$

Finally, we have

$$\Delta\nu = \Delta\nu_l\frac{l}{p}(1 - e^{-qC}), l < p \tag{16}$$

Determination of Values of $\Delta\nu_s$, $\Delta\nu_l$, q, and l. As expressed in eq 13, $\Delta\nu$ is a function of C. If h is taken as an arbitrary constant, then

$$\Delta\nu(C) = \Delta\nu_s(1 - e^{-qC}) \tag{17}$$

$$\Delta\nu(C + h) = \Delta\nu_s(1 - e^{-q(C+h)}) \tag{18}$$

Eliminating e^{-qC} from eq 17 and 18, we obtain

$$\Delta\nu(C + h) = e^{-qh}\cdot\Delta\nu(C) + (1 - e^{-qh})\Delta\nu_s \tag{19}$$

According to eq 19, the plot of $\Delta\nu(C + h)$ vs. $\Delta\nu(C)$ should give us a straight line. The values of $\Delta\nu_s$ and q will be then evaluated from the slope and intercept of this straight line. Figure 4 shows the $\Delta\nu(C + h)$ vs. $\Delta\nu(C)$ plots which were obtained from the $\Delta\nu$ vs. C curves shown in Figure 1 by taking $h = 0.1$. The values of $\Delta\nu_s$ and q calculated from the straight lines in Figure 4 are given in Table I. The values of q and $\Delta\nu_s$ are essentially independent of the extent of h since h is arbitrarily chosen so as to obtain an appropri-

Table I: The Values of $\Delta\nu_s$ and q

Samples	$\Delta\nu_s$, cps	q, molecules
C$_{12}$POE-2.9	15.9	1.6
C$_{12}$POE-4.0	14.3	1.2
C$_{12}$POE-5.9	13.5	1.1
C$_{12}$POE-9.1	12.0	0.62
C$_{12}$POE-11	10.9	0.58
C$_{12}$POE-14	8.5	0.54
C$_{12}$POE-24	4.6	0.55
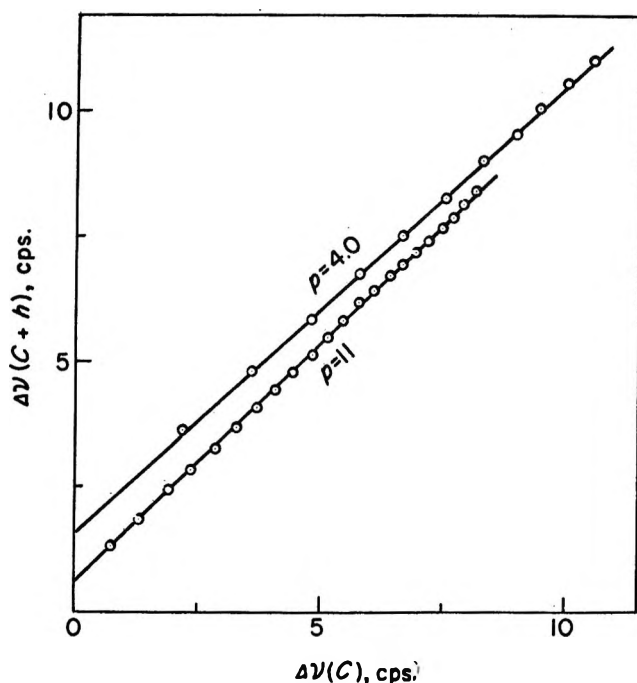
Figure 4. The $\Delta\nu(C + h)$ vs. $\Delta\nu(C)$ plots for $C_{12}POE$-p with p of 4.0 and 11: $h = 0.1$. Straight lines were also obtained for other $C_{12}POE$ with different p although they are not shown here.

Figure 5. The plot of $\Delta\nu_s$ vs. $1/p$.

ate plot of $\Delta\nu(C + h)$ vs. $\Delta\nu(C)$. (In the present case, h is taken as 0.1. Even if h is taken as 0.2 or others, the result is the same.) The value of $\Delta\nu_s$, i.e., the saturation value of the upfield shift, decreases with increasing p, and the value of q, i.e., the number of $C_{12}POE$ molecules influenced by one NaC_8BS molecule, also decreases with increasing p and becomes nearly constant for p larger than 9.1.

The number, l, of the oxyethylene units on which the benzene rings of NaC_8BS exert an influence may be estimated from the plot of $\Delta\nu_s$ vs. $1/p$. This plot should be linear when $l < p$, according to eq 14, and will deviate from the linear relation when $l > p$. Figure 5 shows the plot of $\Delta\nu_s$ vs. $1/p$. The value of l estimated

from the inflection of this plot is about 9, which seems somewhat larger than an expected value. However, this could be interpreted as showing that the polyoxyethylene chains in the mixed micelle of $C_{12}POE$ and NaC_8BS are being in motion, not always stretching straight into the water phase, and even the oxyethylene units remote from the hydrocarbon part of the micelle can approach to the benzene rings of NaC_8BS molecules to interact with each other. From the inflection of the $\Delta\nu_s$ vs. $1/p$ plot, one can also estimate the value of $\Delta\nu_l$, i.e., the upfield shift of the signal for the polyoxyethylene chain with l oxyethylene units. The value estimated is about 12–13 cps.

Heptanol as a Guest Molecule in Dianin's Compound

by J. L. Flippen* and J. Karle

Laboratory for the Structure of Matter, Naval Research Laboratory, Washington, D. C. 20390 (*Received May 19, 1971*)

Publication costs assisted by the Naval Research Laboratory

Dianin's compound (4-p-hydroxyphenyl-2,2,4-trimethylchroman), $C_{18}H_{20}O_2$, forms a crystalline inclusion compound with n-heptyl alcohol. The complex crystallizes in the trigonal space group $R\bar{3}$ with $a = 27.12 \pm 0.03$ Å and $c = 11.02 \pm 0.02$ Å. Almost all the hourglass-shaped cavities which are formed by six molecules of Dianin's compound are occupied with a molecule of the alcohol. The height of the cage is ~ 11 Å. In order for the n-heptyl alcohol to be accommodated in the cavity, the normally extended molecule assumes a gauche configuration. In structures reported earlier it was possible for two guest molecules to reside in one cage. This is the first case in which the included molecule fills the entire cage.

Six molecules of Dianin's compound (I), 4-p-hydroxyphenyl-2,2,4-trimethylchroman, are linked by hydrogen

I
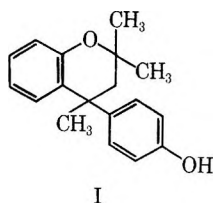
bonding between their hydroxyl groups to become the cage forming entity, Figure 1, in which a large variety of molecules can be entrapped. The formation of the cage, its size and shape, and the inclusion of C_2H_5OH and $CHCl_3$ in the cage have been discussed in a previous publication describing the crystal structure of these adducts.[1] The dotted lines in Figure 2 represent the largest figure of revolution which could be accommodated within the cavity formed by Dianin's compound. The solid lines in Figure 2 show an n-heptyl alcohol molecule in its normal extended configuration surrounded by van der Waals' radii to represent the space occupied by the alcohol molecule. From the illustration, it is obvious that the n-heptyl alcohol can fit through the waist of the cavity but that it appears to be too long to be accommodated within the cage. The purpose of this investigation was to study the occupancy and the configuration of n-heptyl alcohol within the cavity.

The crystal used for the present X-ray analysis was grown by evaporation of a solution of Dianin's compound in n-heptyl alcohol. Intensity data were collected on a four-circle automatic diffractometer using the θ–2θ technique with a $2.0° + 2\theta(\alpha_2) - 2\theta(\alpha_1)$ scan over 2θ. The compound crystallizes in the trigonal space group $R\bar{3}$ with $a = 27.12 \pm 0.03$ Å and $c = 11.02 \pm 0.02$ Å. On the basis of 18 molecules of Dianin's compound and 3 molecules of the alcohol per unit cell the crystallographic density is 1.21 g/cm³. Intensities for 2175 independent reflections were measured. The

data were corrected for Lorentz and polarization factors and structure factor magnitudes $|F|$ were computed.

The coordinates for the C and O atoms of the host molecule, taken from the previous structure determinations of the ethanol and chloroform inclusions, were subjected to a least-squares refinement with the data from the n-heptyl alcohol crystal. The host atoms showed an average shift of 0.06 Å from the ethanol compound in such a way as to indicate a slight enlargement of the cage in the heptanol compound. The largest shift is 0.11 Å for C(16). This probably occurs because the heptanol molecule extends through the center of the cage affecting particularly C(16), at $z \sim 0.5$, which forms the waist of the cage. The positions of the atoms in the n-heptyl alcohol molecule were then deduced from a difference map which also contained all the hydrogen atoms. The space group symmetry requires a threefold rotation axis as well as a center of symmetry. Hence, the one molecule of n-heptyl alcohol (II) in the cavity would be expected to have a

II
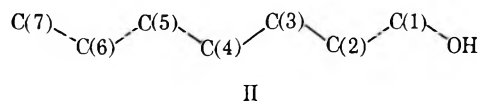
threefold rotational disorder as well as a pseudo center of symmetry between C(3) and C(4). Thus the oxygen atom of the OH group is indistinguishable from the terminal carbon atom. The difference map contained three distinct peaks which could be identified as C(7) or O, C(6) or C(1), and C(5) or C(2). For atoms C(3) or C(4), the three disordered positions about the z axis were close to the z axis, and the difference map indicated only their average position on the z axis.

The coordinates obtained from the difference map show that the n-heptyl alcohol assumes the folded gauche configuration at both ends of the molecule (III)

(1) J. L. Flippen, J. Karle, and I. L. Karle, *J. Amer. Chem. Soc.*, **92**, 3749 (1970).
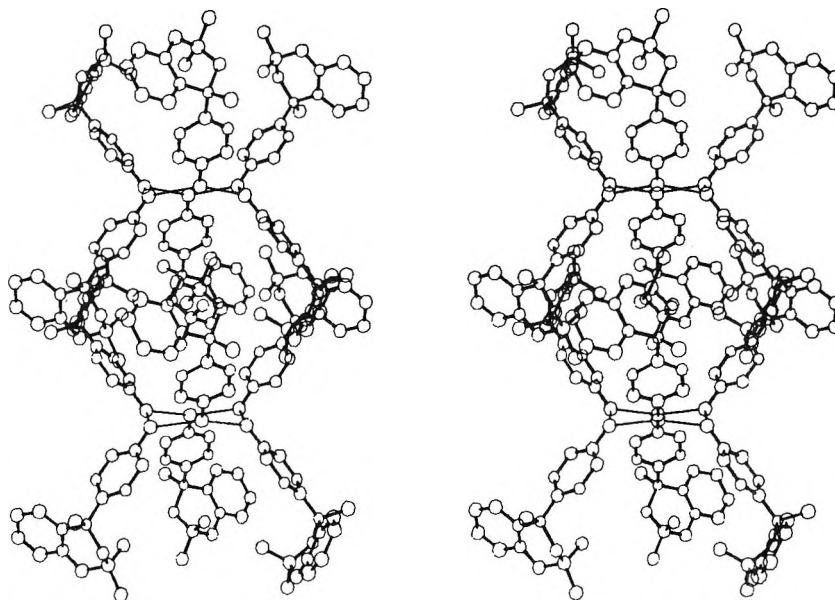
Figure 1. A stereodiagram of the stacking of two complexes along the c axis to form the closed cavities in the crystal. The cavity is bounded at the top and bottom by the rings formed by six hydrogen-bonded hydroxyl groups.
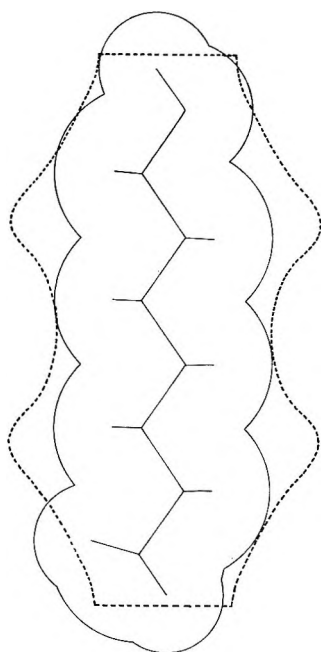
Figure 2. The relative size of an extended n-heptyl alcohol molecule surrounded by its van der Waals' radii (solid line) as compared to the size and shape of the largest figure of revolution (dotted line) which can fit into the cage. The height of the cage is ~11.0 Å.

III
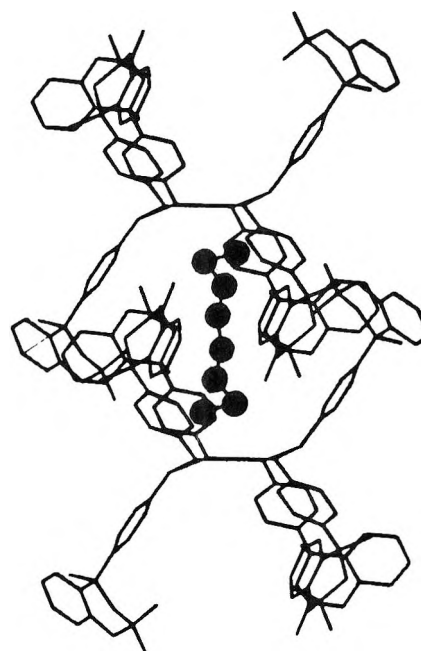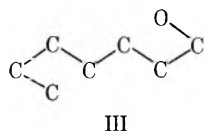
Figure 3. The orientation of the n-heptyl alcohol molecule within the cage.

in order to be included by the clathrate. Figure 3 illustrates the orientation of the alcohol within the cage. Refinement on the atomic positions of the disordered alcohol did not converge. Therefore, guest coordinates were fixed at their difference map values. However, refinement on the occupancy indicated that, for this particular crystal, approximately 95% of the cages were occupied. The final R factor is 8.5%.

An Approximate Equation of State.   I.   A Modified Percus–Yevick

Equation for Argon

by R. M. Gibbons

The Gas Council, London Research Station, Michael Road, London, S.W. 6, England   (*Received December 24, 1970*)

Publication costs assisted by The Gas Council

It is shown how any intermolecular function can be divided exactly into "hard" and "soft" functions.   This approach is used to develop an approximate equation of state for the Lennard-Jones potential, by approximating all the "hard" functions by the "equivalent" hard spheres, using the definition of Barker and Henderson for the diameters, combined with the integral of one "soft" function.   The values obtained from this equation for the properties of argon are compared with experimental data and values obtained from Monte Carlo and Barker–Henderson theory calculations.   The agreement is good at the higher temperatures but depends strongly on the choice of the force constants for the potential at the lower temperatures.   Results are given for two sets of force constants to demonstrate this.

1. Introduction

In principle, the properties of compressed gas and liquids can be obtained from the intermolecular potential by the methods of statistical mechanics.   For realistic potentials the functions involved give rise to intractable integrals which make it impossible to obtain analytical solutions.   Considerable progress, however, has been made in evaluating numerically the complete integrals which occur in the theory.   Numerical results for these integrals have been obtained both directly by Monte Carlo[1-4] and molecular dynamic[5,6] calculations and by solving numerically approximate integral equations for the direct correlation and radial distribution functions.   These results are invaluable for testing approximate theories but are too slow and costly to provide a practical means of calculating the properties of gases and liquids and particularly for mixtures.   For this reason it is useful to have accurate approximate equations of state which are applicable to both pure substances and mixtures.

For the simpler case of mixtures of hard spheres accurate analytical equations have been obtained from solutions of the Percus–Yevick (PY) equation which agree well with the Monte Carlo calculations for hard spheres and their mixtures.   It is natural to seek to extend these results to systems interacting with realistic potentials.   The most successful approach so far is the Barker–Henderson perturbation[7-11] theory which involves a double perturbation expansion about the PY hard sphere results in an inverse steepness parameter and the well depth.   To evaluate this solution involves numerically inverting a Laplace transform and numerical differentiation of the free energy data and requires a large computer program.   The restatement of this approach as a variational problem by Canfield[12,13] and his coworkers similarly involves much computation.

There have been other simpler and more empirical methods of relating the properties of hard spheres to real fluids but these have had only limited success.   Longuet-Higgins and Widom[14] and Guggenheim[15] introduced a van der Waals energy term, a/v, into the PY (compressibility) equation and on determining a from the latent heat of fusion were able to predict some properties of argon with reasonable accuracy.   Henderson and Wertheim[16] similarly empirically added the energy term

$$\frac{-2\pi N}{V}\int^{\infty}(e^{-U_k/T}-1)R^2dR \tag{1}$$

to the PY hard sphere equation but had only limited success.

(1) W. W. Wood, "Physics of Simple Fluids," H. N. V. Temperley, J. S. Rowlinson, and G. S. Rushbrook, Ed., North-Holland Publishing Co., Amsterdam, 1968.

(2) I. R. McDonald and K. Singer, *J. Chem. Phys.*, **47**, 4766 (1967).

(3) I. R. McDonald and K. Singer, *ibid.*, **50**, 2308 (1969).

(4) I. R. McDonald and K. Singer, *Quart. Rev., Chem. Soc.*, **24**, 238 (1970).

(5) B. J. Alder and T. Wainwright, *J. Chem. Phys.*, **31**, 459 (1959).

(6) L. Verlet, *Phys. Rev.*, **36**, 254 (1967).

(7) J. A. Barker and D. H. Henderson, *J. Chem. Phys.*, **47**, 4714 (1967).

(8) J. A. Barker and D. H. Henderson, *ibid.*, **47**, 2856 (1967).

(9) J. A. Barker and D. H. Henderson, Proceedings of the 4th Symposium on Thermodynamic Properties, A.S.M.E., 1968, p 30.

(10) D. Henderson and J. A. Barker, *J. Chem. Phys.*, **52**, 2315 (1970).

(11) G. A. Mansoori, J. A. Provine, and F. B. Canfield, *ibid.*, **51**, 5295 (1969).

(12) G. A. Mansoori, and F. B. Canfield, *ibid.*, **51**, 4958 (1969).

(13) G. A. Mansoori and F. B. Canfield, *ibid.*, **51**, 4967 (1969).

(14) H. C. Longuet-Higgins and B. Widom, *Mol. Phys.*, **8**, 549 (1964).

(15) E. A. Guggenheim, *ibid.*, **9**, 43 (1965).

(16) M. S. Henderson and M. S. Wertheim, *J. Chem. Phys.*, **51**, 5420 (1969).

There are two main problems in relating an equation of state for hard spheres to a system of particles interacting with a realistic potential. The first is how to separate a realistic potential into a hard core and the remainder and the second is how to rearrange the partition function into tractable integrals. The division of the intermolecular potential proposed by Gibbons and Steele[17] solves the first problem essentially exactly. The "equivalent" hard sphere, defined by Barker and Henderson for other reasons, provides another good approximate separation of the intermolecular potential. To separate the partition function into tractable integrals the method of Alder and Pople,[18] as modified by Gibbons and Steele, can be extended to all integrals of a realistic potential. This formal rearrangement of the integrals is exact but is not useful unless it leads to some sets of integrals which can easily be evaluated or approximated.

In this paper it is shown how an equation of state can be obtained by defining intermolecular functions in terms of "hard" and "soft" functions, which allows a separation to be made into terms containing only "hard" functions and terms involving increasing numbers of "soft" functions. A first-order approximation to the equation of state is obtained, and the values for thermodynamic properties calculated from it with the Lennard-Jones potential are compared with experimental data for argon and values obtained from other theories.

2. Rearrangement of the Pair

The effect of perturbing a system of hard spheres with a realistic potential was first considered by Zwanzig[19] and later was developed by a number of authors including Alder and Pople,[18] Smith and Alder,[20] and Frisch, Katz, Praestgaard, and Lebowitz.[21] All these approaches were based on the assumption that the intermolecular forces could be approximated by a temperature-independent hard core for distances less than the collision diameter. For distances greater than the collision diameter the Boltzmann factors in the expression for the partition function were expanded in a series in the reciprocal reduced temperature, normally only as far as second-order terms, since higher terms involve triplet or higher order distribution functions, for which information is not available. It was the development of these approaches that led to the Barker-Henderson theory.[7-11] These authors found a good approximate expression for all second-order terms of the expansions of the Boltzmann factors in terms of an integral of the product of the square of the intermolecular energy with the unperturbed hard sphere radial distribution function, $g(R)$. For distances less than the collision diameter they replaced the actual integrals by "equivalent" hard sphere integrals which are discussed below.

The present approach proceeds somewhat differently.

The method is to divide the intermolecular functions into "hard" and "soft" functions. The expressions for the free energy or $g(R)$ can then be separated into a number of terms which can be identified by the number of "hard" and "soft" functions in each term. The advantage of this approach is it avoids an expansion in the reciprocal temperature and allows full use to be made of the information available on diagram expansions. After discussing the definition of "hard" and "soft" functions this method will be applied to an expression for the compressibility factor in terms of the pair distribution function for the Lennard-Jones potential.

The separation into "hard" and "soft" functions for any function is easily made by defining the "hard" function as equal to the actual function for distances less than an arbitrary value of the intermolecular distance, R, and zero elsewhere; the soft functions are defined in a similar way. As an example, for the Ursell function this separation may be written as

$$f(R) = \exp(-U(R)/kT) - 1.0 = f_H(R) + f_S(R)$$

and

$$
\begin{aligned}
f_H(R) &= f(R) & R &< R(n) \\
f_S(R) &= 0 & R &< R(n) \\
f_H(R) &= 0 & R &> R(n) \\
f_S(R) &= f(R) & R &> R(n)
\end{aligned}
\tag{2}
$$

where $U(R)$ is the intermolecular potential, $R(n)$ is some arbitrary value of R, and the nature of n is specified below. The natural choice of the cut-off point, $R(n)$, is at $R = 1.0$. In this case, the "hard" function cannot be accurately approximated by a hard sphere as $f(R)$ varies from -1.0 to 0.0 in the region $R < 1.0$. The region where the "hard" function can be represented almost exactly by a hard sphere can be found from the expression for $f(R)$, which for the Lennard-Jones potential is

$$f(R) = \exp(-n) - 1.0 \tag{3}$$

where

$$n = 4/T^*(1/R^{*12} - 1/R^{*6}) = U(R)/kT \tag{4}$$

$f(R)$ is equal to -1.0 where $\exp(-n)$ is negligible, and this range of R can be obtained on rearranging eq 4 from the expression, which specifies the nature of n

$$R(n) = (2/(1 + (1 + nT)^{1/2}))^{1/6} \tag{5}$$

Since $\exp(-20) \sim 10^{-8}$, the value of $R(20)$ determines

(17) R. M. Gibbons and W. A. Steele, *Mol. Phys.*, in press.

(18) B. Alder and J. A. Pople, *J. Chem. Phys.*, **26**, 325 (1957).

(19) R. Zwanzig, *ibid.*, **22**, 1420 (1954).

(20) E. B. Smith and B. Alder, *ibid.*, **30**, 1190 (1959).

(21) H. L. Frisch, J. L. Katz, E. Praestgaard, and J. L. Lebowitz, *J. Phys. Chem.*, **70**, 2016 (1966).

the range of R for which the hard sphere approximation is accurate to 1:10.[8]

With the cut-off point at R equal to 1.0 it is necessary to make an additional approximation before the "hard" functions can be approximated by hard sphere functions. This is provided by the "equivalent" hard sphere integrals defined by the Barker–Henderson (BH) diameter. In this it is assumed that the actual integrals of the "hard" functions from 0 to 1 can be approximated by hard sphere functions over the range 0 to d, where d is defined as

$$d = \int_0^1 -f \, dR \tag{6}$$

This d is the BH diameter, and it has been shown[17] that the "equivalent" hard sphere integrals are good approximations for the integrals of "hard" functions in the expressions for the second and third virial coefficients. It is shown below that the "equivalent" hard spheres are also good approximations for some of the integrals in the fourth and fifth virial coefficients. In the development of the equation of state which follows it is assumed that the "hard" functions can be approximated by the "equivalent" "hard" spheres of diameter d.

The same separation as applied to $f(R)$ in eq 2 can be applied to the radial distribution function by writing $f_H(x) + f_S(x)$ for $f(x)$, under the integral signs, in the expression for $g(R)$. The radial distribution function can also be written as a power series in the density and combining the density expansion with the separation into hard and soft functions leads to the expression

$$g(R) = g_H(R) + e_S(R) + \sum_{n=3}^{\infty} \sum_{m=1}^{n(n-1)/2-1} g_{n-2,m}(R) \tag{7}$$

where $e(R) = \exp(-U(R)/kT)$, the subscript m denotes the number of "soft" functions in the integral of $g_{n-2,m}(R)$, and use has been made of the fact that the first term in $g(R)$ is $e(R)$. The terms with m equal to zero consist of "hard" functions only and can be re-summed to give $g_H(R)$, the radial distribution for "hard" functions.

This expression for $g(R)$ can be used to obtain an approximate equation of state. The compressibility factor is related to $g(R)$ by the expression[22]

$$PV/RT = 1 - 2b_0/V \int_0^{\infty} R \frac{\partial U}{\partial R}(R) g(R) R^2 \, dR \tag{8}$$

where V is the molar volume and b_0 is equal to $2\pi \cdot N\sigma^3/3$. Writing $U_H(R) + U_S(R)$ for $U(R)$ and using the expression for $g(R)$ in eq 7 leads to the expression

$$PV/RT = 1 - \frac{b_0}{V}[A_1 + A_2 + A_3] \tag{9}$$

where

$$A_1 = 2 \int R \frac{\partial U_H}{\partial R}(R) g_H(R) R^2 \, dR$$

$$A_2 = 2 \int R \frac{\partial U_S}{\partial R}(R) e_S(R) R^2 \, dR$$

$$A_3 = \sum_{n=3}^{\infty} \rho \sum_{m=1}^{n \, n(n-1)/2-1} 2R^3 \left[\frac{\partial U_H}{\partial R}(R) + \frac{\partial U_S}{\partial R}(R) \right] \times$$
$$g_{n-2,m}(R) \, dR$$

A_1 consists solely of "hard" functions and may be approximated by the equation of Carnahan and Starling,[23] obtained from combining the solutions of the Percus–Yevick equation[24,25] for hard spheres with BH diameters since all $f_H(R)$ have been approximated by "equivalent" hard spheres. A_2 gives the contribution to the second virial coefficient from the "soft" functions, and A_3 contains the contributions to all other virial coefficients, which for a first-order approximation are set equal to zero. Improved approximations can be obtained in two ways. The integrals in A_3 can be summed over all m for fixed n to give all contributions of the "soft" functions to the $(n+1)$th virial coefficient or they can be summed over all n for fixed m to give the contribution to all the virial coefficients for $m = 1, 2 \ldots$, etc. The expansion in powers of the density is not necessary to the development of an equation and in fact can lead to difficulties in the liquid region where the density expansion for $g(R)$ may diverge; a way of avoiding this problem is discussed in the Appendix.

The final form for the first-order equation is

$$PV/RT = (1 + y + y^2 - y^3)/(1 - y)^3 -$$
$$\frac{2\pi N\sigma^3}{V} \int R \frac{\partial U_S}{\partial R}(R) e_S(R) R^2 \, dR \tag{10}$$

where $y = \pi N d^3/6V$. The expressions for the virial coefficients which can be obtained from this equation are of some interest since they provide a justification for taking the cut-off point at R equal to 1.0. The expressions for the virial coefficients, which are obtained on expanding eq 10, are

$$B = b_0 - 2\pi N\sigma^3 \int_1^{\infty} R \frac{\partial U_S}{\partial R}(R) e_S(R) R^2 \, dR$$

$$C = {}^5/_8 b_0{}^2 d^6$$

$$D = {}^{18}/_{64} b_0{}^3 d^9 \tag{11}$$

$$E = {}^{28}/_{256} b_0{}^4 d^{12}$$

Comparisons of these approximate values for the virial coefficients with the exact values are shown in Figures

(22) T. L. Hill, "Statistical Mechanics," McGraw-Hill, New York, N. Y., 1956.

(23) N. F. Carnahan and K. E. Starling, *J. Chem. Phys.*, **51**, 635 (1969).

(24) M. S. Wertheim, *Phys. Rev. Lett.*, **10**, 321 (1963).

(25) E. Thiele, *J. Chem. Phys.*, **39**, 474 (1963).
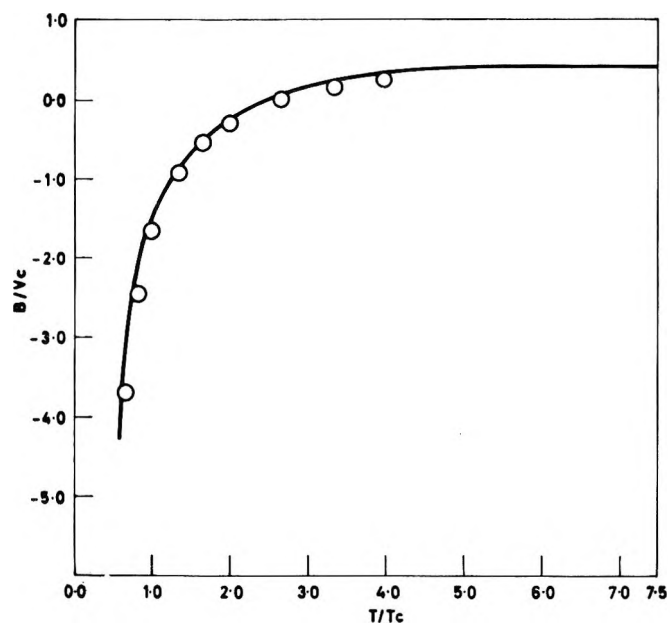
Figure 1. The reduced second virial coefficient. The circles are experimental values from ref 26 and 27; the line is drawn through the values for B obtained from eq 10 with $\epsilon/k = 113.09$ K and $b_0 = 50.06$ cm^3.
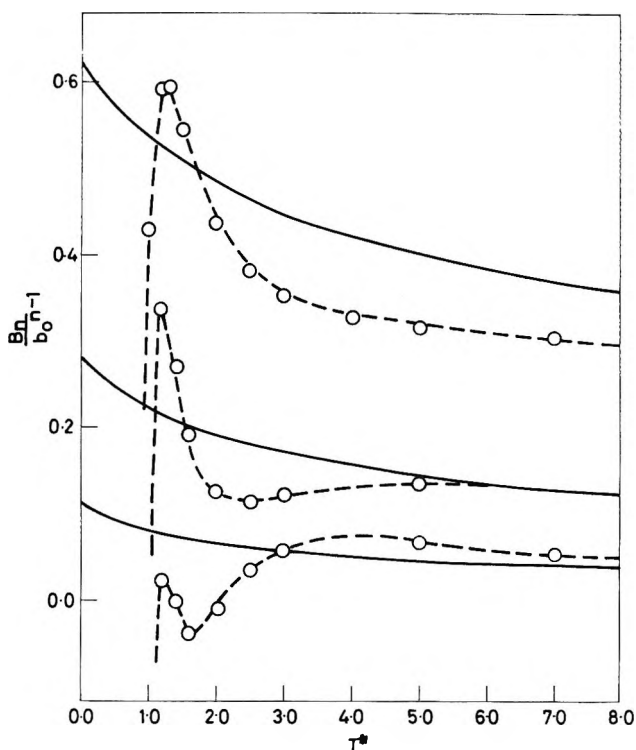
Figure 2. The reduced third, fourth, and fifth virial coefficients as functions of the reduced temperature. The lines are drawn through the values for C, D, and E obtained from eq 10. The circles are exact values from ref 28 and 29.

1 and 2.[26-29] It can be seen that at higher temperatures the approximate values approach the exact values. With other choices of the cut-off point this is not so, and this provides a justification both for taking

the cut-off point at $R = 1.0$ and the use of "equivalent" hard spheres to approximate the "hard" functions.

The values for thermodynamic properties obtained from eq 10 are examined in the following sections where they are compared directly with those obtained from Monte Carlo calculations and the BH theory. Comparisons are also made with experimental data for argon and to do this it is necessary to specify force constants for the Lennard-Jones potential. Before making comparisons of the values obtained from eq 10 with other values the meaning, and ways of obtaining, the force constants for the Lennard-Jones potential will first be discussed.

3. Force Constants for Argon

The force constants for the Lennard-Jones potential, viewed as a pair potential, can be obtained from experimental data for B. However the Lennard-Jones potential cannot describe B exactly, and the values for the force constants depend on the temperature range of the data. Michels[30] and his coworkers obtained values of 119.8 K and 49.8 cm^3 for ϵ/k and b_0 from data in the range 273–473 K while Gosman[31] obtained best agreement with the values 112.4 K and 57.7 cm^3 for the data for argon in the range 90–300 K. The former set of values has been widely used in calculations at low temperatures but there appears to be no rigorous justification for this.

For comparisons with experimental data for argon from ref 31, these values for the force constants are not necessarily appropriate as it is now well established that three-body forces form a significant part of the total interaction energy for dense fluids. Any pair potential used in a theory for dense fluids based on a pairwise potential must be regarded as an "effective" potential which includes the effect of three-body forces. Clearly, the "best" constants for the "effective" potential are not rigorously related to those for the corresponding pair potential and cannot be determined from data for B, since B depends solely on pairwise interactions. The Michels set of constants give good agreement with experimental data when used in Monte Carlo calculations and with the BH theory. This shows these values are good "effective" constants but does not provide a means of obtaining them. There does not appear to be an unambiguous way of obtaining the best "effective" parameters. The best method would be

(26) R. D. Weir, I. Wynne-Jones, J. S. Rowlinson, and G. Saville, Trans. Faraday Soc., 63, 1320 (1967).

(27) E. B. Smith and J. Diamond, "The Virial Coefficients of Gases," Clarendon Press, Oxford, 1969.

(28) D. H. Henderson, G. Kim, and L. Oden, Discuss. Faraday Soc., 43, 26 (1967).

(29) J. A. Barker, P. J. Leonard, and A. Pompe, J. Chem. Phys., 44, 4206 (1966).

(30) J. O. Hirschfelder, C. Curtiss, and R. B. Bird, "Molecular Theory of Gases and Liquids," Wiley, New York, N. Y., 1952.

(31) J. G. Hust, A. L. Gosman, and R. D. McCarty, N.S.R.D.S.-NBS 27, 1969.

based on minimizing the differences between exact calculated (e.g., Monte Carlo) values and experimental data but even in this case the choice of the experimental property is arbitrary. Since such parameters are not available, the alternative is to minimize the difference between the values calculated from eq 10 with some experimental property. This has the inevitable disadvantage that the constants will reflect the inadequacy of the equation as well as errors involved in the assumption of an "effective" potential.

In using this approach to obtain "effective" constants it is desirable to minimize the differences between calculated and experimental values for a property that is sensitive to the choice of the force constants. Results obtained with the Michels constants showed the vapor pressure to be more sensitive to the choice of force constants than other properties. The calculated vapor pressure is obtained from the conditions for vapor-liquid equilibria which are

$$P_1 = P_g$$
$$F_1 = F_g \tag{12}$$

where the subscripts refer to the coexisting phases and F, the free energy, is given by

$$F = \log \left((1 - y)/(yRT)\right) -$$
$$^5/_2 + 3/(2(1 - y)^2) -$$
$$2(2\pi N\sigma^3 \int_1^\infty R\frac{\partial U_s}{\partial R}(R)e_s(R)R^2 dR)/(VRT) +$$
$$PV/RT \tag{12a}$$

In this way, values of 113.09 K and 50.06 cm³ were obtained by adjusting the constants to give the best agreement between the calculated and experimental vapor pressures in the range $T > 0.8T_c$. The lower temperatures were avoided since, as can be seen from Figure 2, the higher virial coefficients are only approximated well for $T > 0.8T_c$. For this reason eq 10 is expected to be applicable only for temperatures greater than $0.8T_c$. The results obtained for both these sets of constants are discussed in the following sections.

4. The Vapor-Liquid Boundary

A severe test of any equation of state is how well it predicts the critical properties of the vapor-liquid boundary. Figure 3 shows a comparison of the vapor pressures obtained from the Barker-Henderson theory, Monte Carlo calculations, and eq 10 with values of 113.09 K and 50.06 cm³ for ϵ/k and b_0. The latter as expected gives excellent agreement since the parameters were obtained from fitting the equation to the vapor pressure curve. For comparison the vapor pressure curve calculated from eq 10 with values for ϵ/k and b_0 of 119.8 K and 49.8 cm³ are also included. These values have large errors of 30% or more and lie close to the Barker-Henderson values. Table I shows the
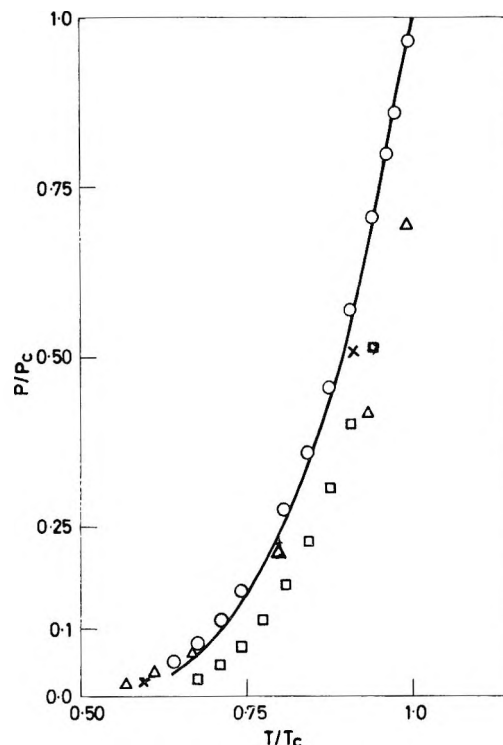
Figure 3. The reduced vapor pressure curve for argon. The line is drawn through the values of the vapor pressure obtained from eq 10 and with ϵ/k = 113.09 K and b_0 = 50.06 cm³. The squares give the results for eq 10 and with ϵ/k = 119.8 and b_0 = 49.8 cm³. The points indicated by O, Δ, and X are the values obtained from experiment,[31] BH theory,[8] and Monte Carlo calculations,[4] respectively.

Table I: The Critical Properties of Argon

| | Reduction factors | | Values of the critical properties | | |
Source	ϵ/k, K	b_0, cm³/mol	P_c, atm	V_c, cm³/mol	T_c, K
Experimental[27]	. . .	. . .	48.34	74.56	150.86
Monte Carlo[6]	119.8	49.8	53.71	74.31–66.05	158.14–162.93
BH theory[7]	119.8	49.8	57.84–74.71	79.26	161.73
Equation 12	113.09	50.06	53.48	84.02	153.45
Equation 12	119.8	49.8	56.946	83.59	162.56

values of the critical properties obtained from Monte Carlo calculations, BH theory, and eq 10 for two sets of reduction parameters. It can be seen that the values for P_c, V_c, and T_c obtained from eq 10 are in as good agreement with the experimental values as either the Monte Carlo or Barker-Henderson values. The reduced molar densities of the two phases are shown in Figure 4. Using 113.09 K and 50.06 cm³ with eq 10 the values calculated agree well with the experimental data while the values obtained using 119.8 K and 49.8 cm³ with eq 10 agree well with the Barker-Henderson values in the range $0.8T_c < T < T_c$.
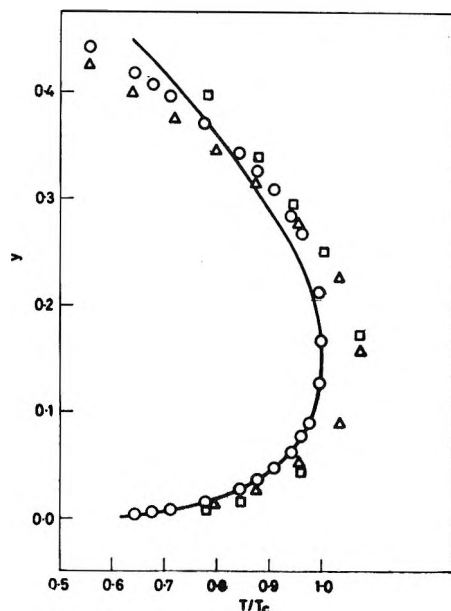
Figure 4. The vapor and liquid densities along the vapor pressure curve. The line is drawn through the values obtained from eq 10 and with $\epsilon/k = 113.09$ K and $b_0 = 50.06$ cm³. The circles give the experimental values,[31] □ give the values obtained from eq 10 with $\epsilon/k = 119.8$ K and $b_0 = 49.8$ cm³, and △ give the Barker–Henderson theory values.

The internal energy can be obtained from eq 10 by standard thermodynamic arguments leading to the expression

$$E = E_0 + E_1$$

where

$$E_0 = 3RTyb_0\frac{\partial}{\partial T}\left\{\int_1^\infty fR^2 dR\right\}_v$$

and

$$E_1 = \left(\frac{\partial y}{\partial T}\right)_v\left\{(1 + y + y^2 - y^3)/(1 - y)^3\right\} \quad (13)$$

The energies of the coexisting phases calculated from eq 13 are shown in Figure 5. The values obtained from eq 13 agree well with the vapor phase experimental data but are somewhat too low for the liquid. The BH theory values for $\Delta U/RT$ which are also shown in the figure are in better agreement with the experimental values for the liquid.

5. The One-Phase Region

The values obtained from eq 10 with both sets of constants were compared with experimental data at 120, 161.73, and 328.25 K and with Monte Carlo and BH theory values. Figure 6 shows the compressibility factor as a function of the reduced density at these temperatures. At the higher temperatures the values calculated from eq 10 with the Michels constants show very good agreement with both the BH theory values and experimental data and are in somewhat better
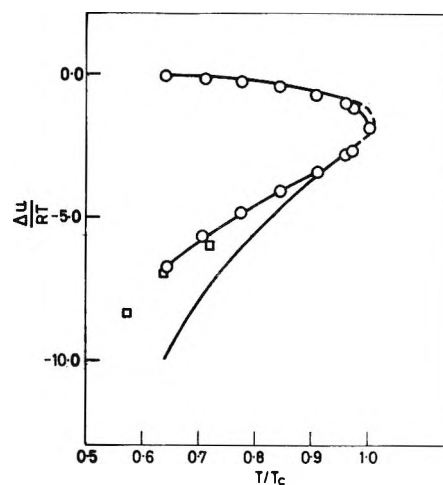
Figure 5. The difference in energy of argon along the vapor–liquid boundary and an ideal gas at the same temperature. The line is drawn through values obtained from eq 10 and 13. The circles represent the values of $\Delta U/RT$ along the experimental vapor–liquid boundary, and the squares represent the values taken from the graph of Barker and Henderson in ref 8.

agreement than the values obtained with the values 113.09 K and 50.06 cm³ for the force constants. At the lowest temperature however the latter are in good agreement with the experimental data and BH theory values while the values obtained with the Michels constants are in poor agreement at high densities.

Figure 7 shows a similar plot for the excess energy at the selected temperatures. For temperatures of 328.25 and 161.73 K the values for U obtained from eq 13 with the values 113.49 K and 50.06 cm³ for the constants agree excellently with the experimental data and the BH theory values at densities up to the critical but become 5–10% too large at higher densities. At lower temperatures the agreement is not good with the calculated energies being 10–25% too low. For the Michels set of constants the calculated values of U are somewhat larger, particularly at the lower temperatures.

6. Discussion

It is perhaps surprising that so simple an equation proves so accurate for the thermodynamic properties of argon. In part this is due to the flexibility in the choice of ϵ/k and b_0. No doubt with optimization of parameters both the BH theory and the Monte Carlo calculations would prove to be in better agreement than this equation with all experimental data for argon. Calculations were also made using the PY (compressibility) equation which led to very similar results except that the compressibility became too large at values of $y > 0.25$. The reason for the success would appear to lie in the accuracy with which B and the higher virial coefficients are represented by the BH "equivalent hard sphere" and the one integral of $f_S(R)$.
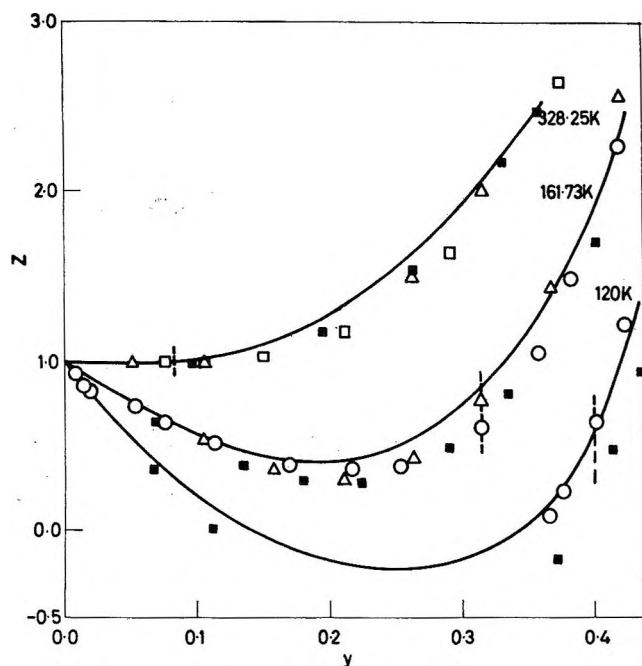
Figure 6. The compressibility of argon as a function of the reduced density. The line is drawn through the values obtained from eq 10 with ϵ/k = 113.09 K and b = 50.06 cm³. The ■ shows the values obtained from eq 10 with ϵ/k = 119.8 K and b_0 = 49.8 cm³. The O and □ represent the experimental and Monte Carlo compressibility values from ref 31 and 4, and the triangles give the values obtained from the graph of Barker and Henderson in ref 8. The vertical dotted lines indicate the density corresponding to 200 atm at each temperature.

Figure 7. The internal energy as a function of the reduced density. The line is drawn through the values for $\Delta U/RT$ obtained from eq 10 with ϵ/k = 113.09 K and b_0 = 50.06 cm³. The ■ show the values obtained from eq 10 with ϵ/k = 119.8 K and b_0 = 49.8 cm³. The circles represent the values obtained from experimental data taken from ref 31 and the triangles give the results taken from the graph of Barker and Henderson in ref 8. The vertical dotted lines indicate the density corresponding to 200 atm at each temperature.

As pointed out previously, at high temperatures the largest terms in the integrals for the virial coefficients arise from the term made up of $f_H(R)$ bonds only with a cut-off at R = 1.0. The other terms depend on higher negative powers of T^* and vanish more rapidly. The accuracy with which the Barker–Henderson "equivalent" hard sphere integral approximates this term can be seen from the comparison in Table II of the exact virial coefficients with the values from the exact hard sphere results using the Barker–Henderson

Table II : Approximation of the Virial Coefficients at High Temperature by the Exact Hard-Sphere Terms with a Barker–Henderson Diameter

T^*	B_2^{-*} (exact)[a]	B_3^* (exact)[a]	B_2^* (BH)	B_3^* (BH)
10.0	0.4609	0.2861	0.7272	0.3349
20.0	0.5254	0.2464	0.65186	0.26558
50.0	0.50836	0.18529	0.55186	0.19034
100.0	0.46407	0.14251	0.4801	0.14406

T^*	B_4^* (exact)[b]	B_5^* (exact)[b]	B_4^* (BH)	B_5^* (BH)
10.0	0.1156	0.0390	0.1103	0.0309
20.0	0.0832	0.0209	0.07955	0.01993

[a] Reference 16.   [b] Reference 31.

diameter. As can be seen from the table at high enough temperatures for all of the first five virial coefficients the BH hard sphere values agree with the exact values within a few per cent which supports this interpretation of the BH diameter.

The present approach uses the same "equivalent" hard sphere diameter as the BH theory. The accuracy of eq 10 for the properties of argon is comparable with the BH theory at high temperatures but is worse in the one-phase region at low temperatures. For the vapor-liquid boundary eq 10 is better for the vapor pressure, while the BH theory gives better values for the latent energy and both approaches have appreciable errors for the liquid densities. However, eq 10 is easier to use since less computation is required. Furthermore, it is open to systematic improvement in a rigorous way by the inclusion of the integrals which contribute to the higher virial coefficients, thus avoiding any consideration, at least for pairwise interactions, of higher order distribution functions.

7. Conclusion

A general method for relating the equations of state for realistic potentials to the equations of state for hard spheres has been presented. This approach has been used to obtain a first-order approximation to the equa-

tion of state for the Lennard-Jones potential, and the values obtained from this equation have been compared with BH theory, Monte Carlo values, and experimental data for argon. For the comparison with experimental data for argon, it was necessary to specify the force constants for the potential, and agreement with the experimental data was found to depend strongly on the choice of the force constants. The meaning of the force constants was discussed but for an "effective" pair potential no unique way could be found to determine the best values for these constants. With force constants obtained from adjusting the calculated vapor pressure to agree with the experimental vapor pressure curve good agreement was obtained for the compressibility factor, critical pressure, and temperature and, at the higher temperatures, for the energy also.

Appendix

The derivation of eq 10 assumes that $g(R)$ can be expanded as a power series in the density, which provides a means of systematically improving the equation but leads to difficulties in the liquid phase since there the expansion in powers of the density may not converge. This difficulty can be avoided by the method outlined below.

Equation 8 of the paper can be written as

$$PV/RT = 1 + 2b_0/V \int \frac{\mathrm{d}}{\mathrm{d}R} e(R)y(R)R^3 \mathrm{d}R$$

where

$$y(12) = \text{constant} \int_{i<j} \pi' e(ij)\mathrm{d}\vec{r}_3 \ldots \mathrm{d}\vec{r}_N$$

is a continuous function, the prime indicates the product

does not include $i = 1$, $j = 2$, and, for brevity, R has been omitted from the argument of e. Substituting $e_H(ij) + e_S(ij)$ for $e(ij)$ in this equation leads to the expression

$$y(12) = y_H(12) + \int e_S(13)\phi_3(1,2,3)\mathrm{d}\vec{r}_3 + \int e_S(34)\phi_4(1,2,3,4)\mathrm{d}\vec{r}_3\mathrm{d}\vec{r}_4 + \ldots$$

where y_H and ϕ_n contain only "hard" functions and

$$\phi_3(1,2,3) = (N - 2) \int_{i<j} \pi'' e_H(ij)\mathrm{d}\vec{r}_4 \ldots \mathrm{d}\vec{r}_N$$

and

$$\phi(1,2,3,4) = \frac{(N - 2)(N - 3)}{2} \int_{i<j} \pi''' e_H(ij)\mathrm{d}\vec{r}_5 \ldots \mathrm{d}\vec{r}_N$$

The $''$ and $'''$ indicate that $i = 1, 2, j = 3$, etc., are excluded from the products. Using this expression for $y(12)$ the equation for the compressibility factor becomes

$$PV/RT = 1 + b_0/V\Bigg[\int R^3 \frac{\mathrm{d}}{\mathrm{d}R} e_H(R)y_H(R)\mathrm{d}R + \int R^3 \frac{\mathrm{d}}{\mathrm{d}R} e_S(R)y_H(R)\mathrm{d}R +$$

terms involving higher order distribution functions $\Bigg]$

Equation 10 is recovered on approximating the first integral in the equation by the Carnahan–Starling equation and setting $y_H(R)$ equal to one in the second integral. The author wishes to thank one of the referees for pointing this out.

The Electronic Spectra of the Heteroaromatics of the Type R₂X.

I. Diphenylamine and *N*-Methyldiphenylamine.

by S. K. Chakrabarti[1]

Department of Chemistry, University of Minnesota, Minneapolis, Minnesota   (*Received June 21, 1971*)

Publication costs borne completely by The Journal of Physical Chemistry

The electronic spectra of diphenylamine and *N*-methyldiphenylamine have been calculated by considering the configuration interaction among the ground, locally excited, and charge-transfer configurations. Satisfactory agreements between the observed and calculated spectra are, however, only obtained with respect to the higher energies. However, the calculations are not diagnostic for the detailed geometry of these compounds. The electronic spectra have been discussed in terms of benzene ring exciton states and charge-transfer states. Furthermore, the calculations do indicate that the charge-transfer configuration plays a relatively insignificant role in both the lowest singlet and triplet states of these molecules.

Introduction

The electronic spectra of diphenylamine and *N*-methyldiphenylamine have been studied theoretically and experimentally by a few workers,[2-5] but these studies were limited to the first two electronic transitions only. However, these studies were qualitative and could not make any real assignments of the bands involved. Furthermore, quantitative theoretical works are not yet available with regard to the energies, the number, and the nature of the electronic transitions. In view of the scanty information available on the electronic spectra of these molecules, the present theoretical work on the calculation of their spectra has been undertaken.

Longuet-Higgins and Murrell[6,7] have established theoretically how the energy levels and wave functions of a composite system R–S are related to those of the separate fragments RH and SH. The same method has also been applied by Nagakura and his coworkers[8,9] to the calculation of the spectra of various monosubstituted benzenes. The results are more or less satisfactory with respect to the experimental findings. In the present study, the above method has been extended for the calculation of energies and wave functions of a composite system like diphenylamine (DPA) and *N*-methyldiphenylamine (MDPA) where the π-electronic system is divided into three fragments: the two benzene rings and the ammonia or methylamine with a pair of nonbonding π electrons on the nitrogen atom.

Method of Calculation

The present method of finding wave functions and energies of DPA and MDPA is essentially based on that presented by Longuet-Higgins and Murrell[6] and, in particular, on that of the calculation for aniline by Murrell.[7] In actual calculation, the interaction between ammonia and the two benzene rings is considered by the

configurational mixing among several electronic configurations consisting of ground state, the locally excited states due to the benzene rings, and the charge-transfer (CT) configurations. The wave functions and energies for the locally excited singlet configurations of the two benzene rings corresponding to the $A_{1g} \rightarrow {}^1B_{2u}$, $A_{1g} \rightarrow {}^1B_{1u}$, and $A_{1g} \rightarrow {}^1E_{1u}$ excitations of benzene and those corresponding to the locally excited triplet configurations were taken from the works of Nagakura, *et al.*[8,9] Since the molecular orbitals θ and ϕ[10] due to the two benzene rings are self-consistent for the separate fragments as well as for the whole molecule (assuming no ring coupling), the ground state will not interact with any of the locally excited configurations. There will, however, be interaction between the locally excited states of the two benzene rings due to electron repulsion.

Taking an electron from the nonbonding π orbital of the amino group (w) and putting it into the lowest vacant orbitals of each benzene ring, the following charge-transfer (CT) configurations are obtained

(1) Address correspondence to this author at the Department of Chemistry, The George Washington University, Washington, D. C. 20006.

(2) W. W. Robertson and F. A. Matsen, *J. Amer. Chem. Soc.*, **72**, 5250 (1950).

(3) P. M. Bugai and V. N. Konelskaya, *Zh. Fiz. Khim.*, **37**, 652 (1963).

(4) A. E. Lutski, *Zh. Obshch. Khim.*, **33**, 1601 (1963).

(5) L. I. Lagutskaya and V. I. Danilova, *Zh. Strukt. Khim.*, **6**, 591 (1965).

(6) H. C. Longuet-Higgins and J. N. Murrell, *Proc. Phys. Soc., London, Sect. A*, **68**, 601 (1955).

(7) J. N. Murrell, *ibid., Sect. A*, **68**, 969 (1955).

(8) K. Kimura, H. Tsubomura, and S. Nagakura, *Bull. Chem. Soc. Jap.*, **37**, 1336 (1964).

(9) K. Kimura and S. Nagakura, *Mol. Phys.*, **9**, 117 (1965).

(10) The six molecular orbitals of benzene are as follows: $\theta_1 = 6^{-1/2}(x_1 + x_2 + x_3 + x_4 + x_5 + x_6)$; $\theta_2 = 12^{-1/2}(2x_1 + x_2 - x_3 - 2x_4 - x_5 + x_6)$; $\theta_3 = 2^{-1}(x_2 + x_3 - x_5 - x_6)$; $\theta_4 = 2^{-1}(x_2 - x_3 + x_5 - x_6)$; $\theta_5 = 12^{-1/2}(-2x_1 + x_2 + x_3 - 2x_4 + x_5 + x_6)$; $\theta_6 = 6^{-1/2}(x_1 - x_2 + x_3 - x_4 + x_5 - x_6)$.

$$\psi\mathrm{CT}_{a_1} = (\mathrm{w}^{-1}\theta_5) \qquad \psi\mathrm{CT}_{a_2} = (\mathrm{w}^{-1}\phi_5)$$
$$\psi\mathrm{CT}_{b_1} = (\mathrm{w}^{-1}\theta_4) \qquad \psi\mathrm{CT}_{b_2} = (\mathrm{w}^{-1}\phi_4) \qquad (1)$$

The two configurations $(\mathrm{w}^{-1}\theta_5)$ and $(\mathrm{w}^{-1}\theta_4)$ are, respectively, symmetric and antisymmetric with respect to the symmetry plane vertical to the molecular plane. The corresponding energies are given by

$$E_{\mathrm{CT}_a} = I - A - Q_1$$
$$E_{\mathrm{CT}_b} = I - A - Q_2 \qquad (2)$$

Here I is the ionization potential of the substituent, A is the electron affinity of benzene, and Q_1 and Q_2 are the electrostatic energies. The values of Q_1 and Q_2 were taken as 5.44 and 5.00 eV, respectively, from ref 8. The $I - A$ values were taken as 11.34 and 11.04 eV,[8] which were found to be the best values for aniline and *N*-methylaniline, respectively, for the calculation of their spectra.[8] The energies of the CT configurations corresponding to the triplet state were assumed to be the same as those for the singlet state.

The exact geometries of DPA and MDPA are still unknown. Models indicate that the two phenyl rings cannot be coplanar with the C–N skeleton, because of steric effect. The situation may, however, be relieved by assuming a nonplanar configuration with the phenyl rings being tilted from a coplanar situation. However, the ring-tilting angle is again unknown, and so we have done a series of calculations to test the models with differing ring inclination angles (which alters the resonance integral $\beta_{\mathrm{C-N}}$) starting, of course, from a planar configuration. The value of $\beta_{\mathrm{C-N}}$ was taken initially as -1.94 eV which was found to be the most suitable value for the spectral calculation of planar aniline by Nagakura, *et al.*[8] All the C–C distances were assumed to be the same as in benzene ($r_{\mathrm{C-C}} = 1.39$ Å), and the C–N distance was taken to be 1.41 Å. Furthermore, in order for the calculated spectra to have a reasonable agreement with the experimental results, it has been found from a series of calculations that the lone-pair orbitals in the nitrogen atom are neither pure sp² nor pure sp³. The most reasonable value for the C–N–C angle was found to lie in the range 114–117°, and the results are reported for a value of 117° for the C–N–C angle in the present paper. The one-center repulsion integrals were evaluated using the methods suggested by Pariser and Parr,[11] while the Nishimoto–Mataga[12] approximation was used for the evaluation of two-center repulsion integrals. The configurations in which more than one electron has been excited were neglected in the present calculation.

The locally excited and charge-transfer configurations are taken in appropriate combinations so as to obtain functions which are, respectively, symmetric and antisymmetric with respect to the symmetry plane passing through the nitrogen atom, and the resulting functions are, therefore, represented by subscripts S and A, respectively, in the tables.

In the approximations of zero-differential overlap and zero overlap, the CT configurations cannot interact with the locally excited states of the benzene fragments through the influence of electron repulsion, but they do so, however, through the influence of the resonance integral $\beta_{\mathrm{C-N}}$ between the two subsystems. The corresponding off-diagonal matrix elements of the total electron Hamiltonian were evaluated by the method of Longuet-Higgins and Murrell.[6] The off-diagonal elements corresponding to the interactions between the locally excited states of the two benzene fragments under the influence of electron repulsion were found to be very small and were, therefore, neglected in the present calculation.

The experimental transition energies were obtained by recording the spectra of these compounds in a Beckman DK-2 spectrophotometer from the near-uv to the vacuum uv region as far as possible. All solutions were deaerated by passing through pure, dry nitrogen gas before measurement.

Results and Discussion

The calculated transition energies of DPA and MDPA for different values of the twisting angle θ of the phenyl rings starting from a planar configuration are shown in Tables I and II, respectively, together with the experimental energies for the first few excited singlet states. It is seen from the tables that the calculated energies are in overall good agreement with the experimental results for $\cos \theta = 1/2$ and $\cos \theta = 1/3$ in DPA and MDPA, respectively, except those for the first two lowest electronic transitions, and that the largest deviation is evident for a planar model. The calculated oscillator strengths for the different transitions were also shown in Tables I and II.

The energies of the low-lying excited states of DPA and MDPA and the way in which the wave functions (whose expansions are given in ref 13) of these states are related to the benzene ring exciton states and charge-transfer states are shown in Tables III and IV. Only the lowest triplet-state energy and the corresponding wave function for DPA are shown in Table III in the last two rows for $\cos \theta = 1/2$.

The first two electronic transitions in the spectra of DPA and MDPA were measured by some workers,[2–4] but they lacked any satisfactory interpretation in absence of any quantitative data. In DPA, the first band is found to be about 4 times more intense experimentally (the intensity is being expressed here in terms of molar

(11) R. Pariser and R. G. Parr, *J. Chem. Phys.*, **21**, 767 (1953).

(12) N. Mataga and K. Nishimoto, *Z. Phys. Chem.* (*Frankfurt am Main*), **13**, 140 (1957).

(13) $\psi_{S_1} = 2^{-1/2}(\psi_{B_{2u_1}} + \psi_{B_{2u_2}})$; $\psi_{A_1} = 2^{-1/2}(\psi_{B_{2u_1}} - \psi_{B_{2u_2}})$; $\psi_{S_2} = 2^{-1/2}(\psi_{B_{1u_1}} + \psi_{B_{1u_2}})$; $\psi_{A_2} = 2^{-1/2}(\psi_{B_{1u_1}} - \psi_{B_{1u_2}})$; $\psi_{S_3} = 2^{-1/2}(\psi_{E_{1u'_1}} + \psi_{E_{1u'_2}})$; $\psi_{A_3} = 2^{-1/2}(\psi_{E_{1u'_1}} - \psi_{E_{1u'_2}})$; $\psi_{S_4} = 2^{-1/2}(\psi_{E_{1u_1}} + \psi_{E_{1u_2}})$; $\psi_{A_4} = 2^{-1/2}(\psi_{E_{1u_1}} - \psi_{E_{1u_2}})$; $\psi_{S_5} = 2^{-1/2}(\psi_{\mathrm{CT}_{a_1}} + \psi_{\mathrm{CT}_{a_2}})$; $\psi_{A_5} = 2^{-1/2} \cdot (\psi_{\mathrm{CT}_{a_1}} - \psi_{\mathrm{CT}_{a_2}})$; $\psi_{S_6} = 2^{-1/2}(\psi_{\mathrm{CT}_{b_1}} + \psi_{\mathrm{CT}_{b_2}})$; $\psi_{A_6} = 2^{-1/2}(\psi_{\mathrm{CT}_{b_1}} - \psi_{\mathrm{CT}_{b_2}})$.

Table I: The Calculated and Experimental Transition Energies ($E - E_0$) of Diphenylamine (eV)

| Calcd energy | | | | | | |
| Cos θ | | | | | | |
1	2/3	1/2	1/3	f_{calcd}	Obsd energy	Log ϵ_{max}[obsd]
5.31 (S)	5.06 (S)	5.00 (S)	4.94 (S)	0.085		
5.23 (A)	5.06 (A)	5.00 (A)	4.94 (A)	0.001	4.38	4.40
5.78 (A)	5.70 (A)	5.70 (A)	5.80 (A)	0.019	5.39	3.80
6.30 (A)	5.97 (A)	5.90 (A)	5.83 (A)	0.105		
6.42 (A)	5.96 (S)	6.08 (S)	5.89 (S)	0.186	6.08	4.91
6.65 (S)	6.45 (S)	6.25 (S)	6.05 (S)	0.249	6.30	4.89
6.81 (A)	6.76 (A)	6.64 (A)	6.69 (A)	0.205		
6.91 (S)	6.86 (S)	6.68 (S)	6.76 (S)	0.261		

Table II: The Calculated and Experimental Transition Energies ($E - E_0$) of N-Methyldiphenylamine (eV)

| Calcd energy | | | | | | |
| Cos θ | | | | | | |
1	2/3	1/2	1/3	f_{calcd}	Obsd energy	Log ϵ_{max}[obsd]
5.25 (S)	5.04 (S)	4.98 (S)	4.93 (S)	0.073		
5.18 (A)	5.02 (A)	4.97 (A)	4.93 (A)	0.003	4.34	4.10
5.61 (A)	5.51 (A)	5.52 (A)	5.54 (A)	0.022		
6.20 (S)	5.83 (S)	5.72 (S)	5.65 (S)	0.045	5.17	4.01
6.31 (A)	5.94 (A)	5.84 (A)	5.81 (A)	0.127		
6.99 (S)	6.49 (S)	6.30 (S)	6.16 (S)	0.175	6.05	4.71
7.20 (A)	6.70 (A)	6.49 (A)	6.30 (A)	0.109		
7.41 (S)	6.87 (S)	6.64 (S)	6.43 (S)	0.112	6.25	4.85
7.74 (A)	6.96 (A)	6.65 (A)	6.37 (A)	0.191		
8.19 (A)	7.50 (A)	7.25 (A)	7.05 (A)	0.214		
8.48 (S)	7.66 (S)	7.39 (S)	7.20 (S)	0.297		

Table III: The Calculated Energy Levels and Wave Functions[a] of Diphenylamine for cos θ = 1/2

Energy, eV	Wave function
$E_0 = -0.20$	$\Psi_0 = 0.985\psi_0 - 0.173\psi_{S_5}$
$E_1 = 4.79$	$\Psi_1 = 0.967\psi_{S_1} - 0.063\psi_{S_2} + 0.248\psi_{S_6}$
$E_2 = 4.79$	$\Psi_2 = 0.965\psi_{A_1} - 0.090\psi_{A_3} + 0.247\psi_{A_6}$
$E_3 = 5.50$	$\Psi_3 = 0.531\psi_{A_2} - 0.227\psi_{A_4} - 0.817\psi_{A_5}$
$E_4 = 5.70$	$\Psi_4 = 0.217\psi_{A_1} + 0.870\psi_{A_3} - 0.444\psi_{A_6}$
$E_5 = 5.88$	$\Psi_5 = 0.712\psi_{S_2} - 0.248\psi_{S_4} - 0.657\psi_{S_6}$
$E_6 = 6.05$	$\Psi_6 = 0.197\psi_{S_1} + 0.209\psi_{S_3} - 0.958\psi_{S_5}$
$E_7 = 6.44$	$\Psi_7 = 0.195\psi_{A_2} - 0.831\psi_{A_4} + 0.521\psi_{A_5}$
$E_8 = 6.48$	$\Psi_8 = 0.185\psi_{S_2} + 0.510\psi_{S_6} - 0.840\psi_{S_4}$
$(E_1 - E_0)_T = 3.60$	$\Psi = 0.975\psi_{S_2} - 0.103\psi_{S_4} - 0.197\psi_{S_6}$
$(E_1 - E_0)_T = 3.59$	$\Psi = 0.975\psi_{A_2} - 0.102\psi_{A_4} - 0.197\psi_{A_6}$

[a] The expansions of ψ_{S_i} and ψ_{A_i} are summarized in ref 13.

Table IV: The Calculated Energy Levels and Wave Functions[a] of N-Methyldiphenylamine for cos θ = 1/3

Energy, eV	Wave function
$E_0 = -0.098$	$\Psi_0 = 0.991\psi_0 - 0.135\psi_{S_6}$
$E_1 = 4.83$	$\Psi_1 = 0.976\psi_{S_1} - 0.023\psi_{S_2} + 0.217\psi_{S_6}$
$E_2 = 4.83$	$\Psi_2 = 0.973\psi_{A_1} - 0.058\psi_{A_3} + 0.224\psi_{A_6}$
$E_3 = 5.44$	$\Psi_3 = 0.369\psi_{A_2} - 0.169\psi_{A_4} - 0.914\psi_{A_5}$
$E_4 = 5.55$	$\Psi_4 = 0.351\psi_{S_2} - 0.204\psi_{S_4} - 0.914\psi_{S_6}$
$E_5 = 5.71$	$\Psi_5 = 0.172\psi_{A_1} + 0.826\psi_{A_3} - 0.527\psi_{A_6}$
$E_6 = 6.06$	$\Psi_6 = 0.217\psi_{S_1} + 0.127\psi_{S_3} - 0.968\psi_{S_6}$
$E_7 = 6.20$	$\Psi_7 = 0.927\psi_{A_2} + 0.132\psi_{A_4} + 0.351\psi_{A_5}$
$E_8 = 6.27$	$\Psi_8 = 0.156\psi_{A_1} - 0.561\psi_{A_3} - 0.813\psi_{A_6}$
$E_9 = 6.33$	$\Psi_9 = 0.935\psi_{S_2} + 0.125\psi_{S_4} + 0.332\psi_{S_6}$
$E_{10} = 6.96$	$\Psi_{10} = 0.071\psi_{A_2} - 0.977\psi_{A_4} + 0.201\psi_{A_5}$
$E_{11} = 7.10$	$\Psi_{11} = 0.069\psi_{S_2} - 0.979\psi_{S_4} + 0.192\psi_{S_6}$

[a] The expansions of ψ_{S_i} and ψ_{A_i} are summarized in ref 13.

extinction coefficient) than the second band, whereas in aniline, the second band (which is regarded as mainly a CT band) is about 6 times more intense than the first band which is taken to be a perturbed $^1B_{2u}$ state of benzene. Accordingly, the lowest electronic transition in each of DPA and MDPA was assumed by previous workers[3,4] to be of mainly charge-transfer character. Their assumptions, however, were based on an apparent belief of increasing conjugation of the amino group with

the phenyl ring as one goes from aniline to DPA or MDPA. This conjugation, however, would involve the lone-pair $p\pi$ electron of the nitrogen atom and would be at a maximum for two coplanar phenyl rings which is sterically impossible for these molecules. Robertson and Matsen,[2] on the other hand, regarded the molecule DPA essentially as a monosubstituted benzene, the aniline (PhN–) substitutent perturbing the benzene system.

However, the present calculation shows (Tables III and IV) that the lowest two excited states arising from both in-phase and out-of-phase arrangements of transition dipoles correspond to the same energy (E_1 and E_2) in both DPA and MDPA whether these molecules are planar or nonplanar. The first excited state incorporates about 94% symmetric combination of the locally excited $^1B_{2u}$ states of the two benzene rings, and the second excited state (E_2) is composed mainly (ca. 94%) of antisymmetric combination of the same $^1B_{2u}$ states. The charge-transfer character in these two states is, however, negligible. The transition moments for electric dipole transitions from the ground state to both these exciton states (E_1 and E_2) are nonvanishing; the resulting transition moment is given by the vector sum of the individual transition dipole moments in the component molecule. The electric dipole vector corresponding to the symmetric (S) state would probably lie in a direction approximately transverse to the N–H axis, and that corresponding to the antisymmetric (A) state would probably lie approximately along the N–H axis. Hence, the resulting electric dipole vector would probably lie approximately along the C–N axis. So the lowest electronic transition in both DPA and MDPA would perhaps be polarized in a direction roughly along the C–N bond. Thus, in both DPA and MDPA the observed lowest singlet–singlet transition arises primarily from both in-phase and out-of-phase combinations of the locally excited $^1B_{2u}$ states of the two benzene rings; consequently, these two allowed states might probably be responsible for such a significant enhancement of the intensity of the observed lowest electronic transition. Although the calculated oscillator strengths (Table I) seem to be small, their relative magnitudes are still significant and further substantiate the present argument. The ratio of the observed molar extinction coefficients for the two lowest electronic transitions also compares favorably well with the corresponding relative magnitudes of the oscillator strengths (Table I).

The third excited state of DPA ($E_3 = 5.50$ eV) which corresponds to the second experimental band is mainly composed of about 65% antisymmetric combination of the CT_a states and about 28% antisymmetric combination of the locally excited $^1B_{1u}$ states of the benzene rings. Accordingly, the resulting electric dipole vector would probably lie in a direction approximately transverse to the N–H axis. So the second electronic transition would probably be polarized in a direc-

tion making an angle of about 30° with the C–N axis. In other words, the electronic transition moment vectors for the observed first two electronic transitions would probably have mixed character. In fact, the unpublished results[14] on the polarized fluorescence spectra of DPA in rigid glass at 77°K agree quite well with this prediction. Details of the polarization of emission of these compounds will be published elsewhere.

The fourth and fifth excited states have energies (E_4 and E_5) very close to each other, and these two together do agree well with the energy of the third absorption band in the experimental spectrum. In other words, the observed third electronic transition would probably contain the overlapping transitions involving these two states. The fourth excited state mainly contains about 75% antisymmetric combination of the locally excited $^1E_{1u'}$ benzene states and about 18% antisymmetric combination of the CT_b states. The fifth excited state is, however, mainly composed of a symmetric combination of the locally excited $^1B_{1u}$ benzene states (ca. 50%) and a symmetric combination of the CT_a states (ca. 42%).

The sixth excited state stems mainly from a symmetric combination of the CT_b states (ca. 92%). The calculated energy of this state corresponds closely to the experimentally observed fourth electronic transition. The seventh and eighth excited states have energies very close to each other. So, they may represent the two overlapping transitions of a given electronic band. The seventh excited state results mainly from an out-of-phase combination (ca. 69%) of the locally excited $^1E_{1u}$ states of the benzene rings as well as of the CT_a states (ca. 27%). On the other hand, the eighth excited state arises primarily from an in-phase combination of the locally excited $^1E_{1u}$ states due to the phenyl rings (ca. 70.5%) and an in-phase combination of the CT_a states (ca. 26%).

In N-methyldiphenylamine (MDPA), except for the first two excited states (E_1 and E_2), the nature of the other excited states (Table IV) responsible for the electronic transitions is, however, somewhat different from those in DPA. In fact, the observed second electronic transition in MDPA is only about 1.24 times less intense than that of the first transition. The relative magnitudes of the oscillator strengths agree fairly well with the present observation. Furthermore, the observed second electronic transition in MDPA is about 3.3 times more intense than that in DPA. It could be observed from Table IV that the third and fourth excited states of MDPA have energies nearly equal to each other, and they correspond approximately to the energy of the second band in the experimental spectrum, although the agreement between the observed and theoretical energies is not very good. Furthermore, it is observed that the third and fourth excited states (E_3 and

(14) S. K. Chakrabarti, unpublished results.

E_4) incorporate about 83% antisymmetric and symmetric combination of the CT_a states, respectively, the contribution of the locally excited states due to the benzene rings being very small relative to the CT_a configurations. The transition moments for electric dipole transitions from the ground state to these excited states (E_3 and E_4) are both finite. Thus, the presence of these two allowed states (instead of one as in DPA) arising primarily from intramolecular charge-transfer transitions might probably be responsible for the observed second electronic transition in MDPA being more intense than that in DPA. The relative magnitudes of oscillator strengths further substantiate this argument. Again considering the individual dipole vectors of the configurations present in significant amount for the third and fourth excited states which constitute the observed second electronic transition, it can be shown as before that the resulting electronic transition moment vector will probably lie in a direction approximately along the C–N bond. In other words, the observed second electronic transition of MDPA will be polarized in the same direction as that of the first electronic transition. In fact, the unpublished results[14] on the polarization of fluorescence spectra do indicate that the 0,0 band of the fluorescence spectra is positively polarized when excited into both the first and second absorption bands of MDPA.

The fifth excited state incorporates ca. 68% antisymmetric combination of the locally excited $^1E_{1u'}$ states of the phenyl rings and about 28% antisymmetric combination of the CT_b states. The sixth excited state is composed mainly of symmetric combination of the CT_b states (ca. 92%). These two states may represent the two close-lying transitions and these two together agree well with the experimentally observed energy of the third electronic transition.

The calculated energies of the seventh, eighth, and ninth excited states are found to lie very close to one another and may, therefore, represent the three overlapping transitions of a given electronic state. Indeed, the observed fourth electronic transition is very close to the energies corresponding to the transitions in these three states (Table II). The seventh and ninth excited states stem mainly from an out-of-phase and in-phase combinations of the locally excited $^1B_{1u}$ benzene states (ca. 86.5%), respectively, while about 65% out-of-phase combination of the CT_b states contributes to the eighth excited state.

The tenth and eleventh excited states of MDPA are found to have nearly equal energy and may, therefore, well represent the two overlapping transitions of a given electronic state. Both these states primarily represent the ring exciton states, corresponding to about 94% of each of the in-phase and out-of-phase combinations of the $^1E_{1u}$ benzene states.

The lowest triplet states of DPA have been calculated for $\cos \theta = {}^1/_2$ which is found to be a suitable value for the calculation of the corresponding singlet states. However, only the data for the lowest triplet state have been shown in Table III for the purpose of comparison with the lowest triplet states of other aromatic compounds. The aromatic hydrocarbons, and the substituted aromatics have their lowest triplet states when extrapolated, correspond to the $^3B_{1u}$ state of benzene.[15,16] The lowest triplet state of DPA in the present calculation is found to be composed of (like the lowest singlet state of DPA) the two separate electronic states of equal energy, arising mainly from symmetric and antisymmetric combinations (ca. 94%) of the locally excited $^3B_{1u}$ benzene states, respectively. Furthermore, it is observed that the calculated wave functions of the lowest triplet state of DPA show a negligible amount of charge-transfer configurations. So, the electron-transfer configurations play an insignificant role in both the lowest singlet and triplet states of DPA. Thus, the lowest triplet state of DPA is a modified $^3B_{1u}$ state of benzene. The agreement between the observed ($\Delta E = 3.2$ eV) and the calculated ($\Delta E = 3.60$) energies of the lowest triplet state is not, however, good.

(15) A. C. Albrecht, *J. Chem. Phys.*, **38**, 354 (1963).
(16) E. C. Lim and S. K. Chakrabarti, *ibid.*, **47**, 4721 (1967).

Modified CNDO Method. IV. Ion–Molecule Interactions in the

Acetone Solutions of Electrolytes

by Joanna Sadlej and Zbigniew Kecki*

*Laboratory of Intermolecular Interactions, Institute of Fundamental Problems of Chemistry,
Warsaw University, Warsaw, Poland* (Received March 1, 1971)

The explanation of the origin of the observed decrease in the CO stretching frequency and also of the intensity changes in the CO infrared band upon the complex formation in the acetone solutions of electrolytes is presented.

Introduction

In part II[1] and part III[2] of this series the modified CNDO method was applied to the study of the ion–molecule interactions in the acetonitrile solutions of electrolytes. It was shown that some fundamental spectral features of the acetonitrile solutions of electrolytes are quite reasonably explained by a simple model of what has been called the acetonitrile–cation complex. The calculations performed for this model allowed for a deeper understanding and even prediction of various spectral properties.

In part II[1] we have presented an explanation of the origin of the observed increase in the CN stretching frequency in the acetonitrile solutions of electrolytes. This explanation was based on the CNDO calculations for appropriate models. It is worth noting that in this case a simple electrostatic consideration of the ion–molecule interaction fails to explain the increase of the CN frequency. We also predicted the intensity increase of the CN absorption band upon the acetonitrile–cation complex formation which afterward was confirmed experimentally by Kecki and Wojtczak.[3] In part III[2] we have calculated ^1H and ^{14}N nuclear magnetic shielding constants in the isolated and complexed acetonitrile. It was predicted that the ^{14}N nmr signal should be shifted to higher field and the ^1H signal to lower field when electrolytes are dissolved in acetonitrile. This result was recently confirmed experimentally by Kecki and Olczak.[4] In part III[2] we also analyzed some previously introduced simplifications. The CNDO calculations reported in part II were performed on a very simplified model with the acetonitrile CH_3 group replaced by a pseudoatom C^* with one sp^3 hybrid orbital. In part III we carried out the CNDO calculations taking into account all the valence shell atomic orbitals. It should be pointed out that both these models, as far as we are interested in changes in the CN bond region, lead to practically the same conclusions.

The present paper deals with the study of a formally similar problem of the ion–molecule interactions in the acetone solutions of electrolytes. Obviously, the complicated problem of the solution structure has to be reduced to the much simpler one of the individual molecule–ion (or ions) interactions. For this reason the available experimental data will be carefully analyzed in the next section.

The Experimental Data and Their Previous Interpretations

The most important experimental data which will provide for a choice of a reasonable model for the acetone–ion (or ions) interaction are listed in Table I. There is a great variety of the acetone band shifts and splittings caused by electrolytes, and this picture is more complicated than that observed for the acetonitrile solutions. For all the investigated electrolytes there is a splitting of B_1 bands of acetone, whereas the A_1 bands are split only in the presence of the Lewis acids.[5] Moreover, the B_1 vibrations do not depend on the nature of anion, while the A_1 bands are influenced by both the cation and the anion. These features are characteristic for the C=O and C—C vibrations.[5] It is evident that in the case of acetone the C=O band is influenced strongly also by anion and, therefore, it should be taken into account when constructing an appropriate model.

A typical decrease of the C=O stretching frequency upon the interaction of acetone with the ions was explained by means of a simple electrostatic model with metal cation bonded to the electron lone pair of oxygen. However, the experimental data indicated that the shift of the C—C stretching frequency is much greater than that of the C=O vibration, al-

(1) J. Sadlej and Z. Kecki, *Rocz. Chem.*, **43**, 2131 (1969).

(2) J. Sadlej and Z. Kecki, *ibid.*, **45**, 445 (1971).

(3) Z. Kecki and J. Wojtczak, *ibid.*, **44**, 847 (1970).

(4) Z. Kecki and M. D. Olczak, to be submitted for publication.

(5) T. Gulik-Krzywicki and Z. Kecki, *Rocz. Chem.*, **39**, 1281 (1965).

Table I: The Experimental Frequency Shifts of the Acetone Solutions of Electrolytes (in cm^{-1}: $\Delta\nu = \nu_{solution} - \nu_{acetone}$[5])

System	$\Delta\nu_{CC}$	$\Delta\nu_{C=O}$	$\Delta\nu_{CH}$
Acetone	0	0	0
Acetone + LiClO$_4$ (2.9 mol/l.)	+8	−3	0
Acetone + LiI (3.1 mol/l.)	+5	−4	−10

though this bond should be only slightly perturbed according to the electrostatic model.

A qualitative interpretation of these experimental data was put forth by Minc, Kecki, and Gulik-Krzywicki.[6] According to these authors, the cation bonded to the lone pairs of oxygen decreases the C=O stretching force constant and also induces a change of the hybridization at the carbonyl carbon atom. Its hybridization becomes more tetrahedral in comparison with that of the isolated molecule. The anion effect makes deeper the changes introduced by the cation. According to this model,[6] the anion interacts with the central carbon atom of the acetone molecule. This model seems to be quite reasonable in view of the chemical properties of acetone.

In the present paper we aim to look for the origin of the C=O frequency shift. If the qualitative interpretation proposed in ref 6 is valid, then one has to explain the difference between the cation–acetonitrile and cation–acetone interaction.

Description of the Model and the Method of Calculation

An introduction of the ionic species into the solvent disturbs its own structure and, therefore, the observed changes of the characteristic properties refer to a change of the solvent–solvent interactions and to the ion–solvent molecule interaction.

Unfortunately, a complete analysis of the experimental data and the interpretation of the relation existing between a set of various physical parameters which describe an isolated solvent molecule, the pure liquid solvent, and the solutions of electrolytes requires a knowledge of both the solution or solvent structure and the electronic structure of their individual components. In practice, nearly all of this information is beyond what is presently known. Therefore, to attain some insight into the problem of ion–molecule interactions we must introduce simplifications.

This is usually done by introducing a model, which resembles as far as possible the most significant features of the real system. Thus, we reduced the real problem to the interaction between the solvent molecule and surrounding ions. Taking into account the most pronounced features suggested by the experimental data, we assumed what follows: the observed effects of the interaction between the solvent and dissolved

electrolyte are mainly due to the solvent molecule-ions interaction.

Although the model is still far from the reality, some further simplifications are desired in order to treat the problem by using the quantum chemical methods. The semiempirical procedure of the CNDO SCF method for obtaining the molecular wave functions has been applied. The description of the modified CNDO SCF method was given in paper.[7]

Apart from the use of the semiempirical approach the model of the acetone molecule interacting with ions has further been simplified. Some of these simplifications were forced by a low speed and small storage of the computer at our disposal; some others were introduced on the basis of qualitative pictures of the acetone–ion interaction. Hence, we assumed what follows. (1) The ions were treated as the point charges. They were placed at the distance from the acetone molecule equal to the sum of the corresponding ionic radius and the van der Waals radius of the nearest acetone atom. (2) The methyl groups were replaced by pseudoatoms C*, each having the core charge equal to +1 and introducing one valence electron at hybrid sp^3 atomic orbital. It was shown in the case of the acetonitrile molecule[1,2] that this simplification does not introduce significant changes in the description of the CN group when compared with results of more elaborate calculations. (3) The lithium cation has been chosen as the representative one for the acetone–cation interaction. It was placed in the plane of the acetone molecule at the oxygen atom. Some ambiguities with respect to the hybridization of the carbonyl oxygen atom do not allow for a sophisticated choice of the most priviledged direction. Therefore, we have performed our calculations for three different geometric arrangements: (i) the lithium cation lying on the CO bond axis ($\phi = 0°$, R), (ii) the lithium cation lying in the direction $\phi = 60°$, K, and (iii) the lithium cation lying in the direction perpendicular to the CO axis ($\phi = 90°$, P). These three geometries of the complex correspond to the sp (cases i and iii) or sp^2 (case ii) hybridization of the lone-pair orbitals at oxygen. For the anions (Cl$^-$ or I$^-$) we assumed them lying in the plane perpendicular to the molecular plane above the carbonyl carbon atom. Such a choice of the geometry corresponds to what is accepted about the polarization of the CO bond. This is also in agreement with organic chemistry concepts of the reactivity of acetone.

In the CNDO calculations the following geometrical parameters were utilized: ionic radii, $r_{Li^+} = 0.68$ Å, $r_{Cl^-} = 1.81$ Å, $r_{I^-} = 2.20$ Å; van der Waals radii, $R_C =$

(6) S. Minc, Z. Kecki, and T. Gulik-Krzywicki, *Spectrochim. Acta,* **19**, 353 (1963).

(7) J. Sadlej, *Acta Phys. Pol.,* **35**, 829 (1969).

1.67 Å, R_O = 1.40 Å;[8] for the C*–C bond lengths the experimental value was assumed (r_{CC} = 1.215 Å).

In the energy minimization process all the bond lengths and bond angles except for the CO distance were kept constant. We thought it rather unreasonable to perform the calculations for different C*–C bond lengths as well as for various anion–carbon atom and cation–oxygen atom distances. The present model seems to be too crude in this respect. For the same reason the calculations were performed for one cation only.

The numerical computations were carried out on GIER computer at the Computational Centre of Warsaw University.

Results

In this section we shall present some selected results. The parameters of the potential energy curve $E(R_{CO})$ for the acetone molecule and its ion complexes are presented in Table II whereas the corresponding dipole moments and their derivatives with respect to the CO bond length are shown in Table III.[9]

Table II: The Parameters of the Potential Energy Curve for the Acetone Molecule and Its Ion Complexes

System	$R_{e,CO}$, au	$K_{e,CO}$, mdyn/Å	$K_{e,CO}^{expt}$, mdyn/Å
C*₂CO	2.693	19.587	11.5[a]
C*₂COLi$_R$⁺	2.645	21.299	
C*₂COLi$_K$⁺	2.631	21.285	
C*₂COLi$_P$⁺	2.639	20.474	
C*₂COCl⁻	2.733	16.815	
C*₂COLi$_R$⁺Cl⁻	2.679	18.450	
C*₂COLi$_R$⁺I⁻	2.670	18.497	
C*₂COLi$_K$⁺I⁻	2.663	19.244	

[a] P. Cosse and J. H. Schachtschneider, *J. Chem. Phys.*, **44**, 97 (1966).

Some comments should be made concerning the calculation of the dipole moment and its derivatives. In the case of charged systems the dipole moment is understood as that one of the adiabatically isolated molecule from the corresponding complex; *i.e.*, this is the dipole moment of the acetone molecule resulting from the electron distribution characteristic for the complex. Because our model does not take into account the charge-transfer effects, this can be done without any further restriction. Considering the interpretation of the change in the ir intensity of the CO stretching band, one needs a knowledge of the dipole moment derivative with respect to the corresponding normal coordinate. In the present calculations we assumed that this derivative is proportional to the dipole moment derivative with respect to the CO bond distance. It seems that this simplifying assumption should not greatly affect the qualitative interpre-

tation of the intensity changes upon the complex formation.

Discussion and Interpretation of the Experimental Data. First of all let us consider some of the results presented in Table II. According to these data, the interaction between the acetone molecule and the cation causes an increase of the C=O bond stretching force constant. This is quite contrary to the experimental decrease of the CO stretching frequency in solutions. However, in the experiments with acetone adsorbed on cationized zeolites[10] there is an increase of CO frequency in the order from Cs⁺ to Li⁺. It also should be recalled that in the case of the acetonitrile complex with cation there was an increase of the CN force constant in agreement with the experimental increase of the CN frequency in solutions as well as on cationized zeolites.[11] In the acetonitrile solutions the experiment suggested strongly an independence of the CN frequency on the anions, whereas in acetone solutions the A₁ mode vibrations were shown to be influenced by cations and anions as well.[5]

Considering the anion interacting with acetone one observes a decrease of the CO stretching force constant much deeper than that required for the interpretation of the lowering of the CO stretching frequency. However, when both the anion and the cation are taken into account, the calculated CO stretching force constant K_{CO} becomes again similar to that calculated for the isolated molecule C*₂CO. This result is in a qualitative agreement with experimental findings.

It is worth noting that different anions and different values of the angle ϕ lead to practically the same result. In the frame of the present calculation it seems to be impossible to decide which of the different cation positions is the most privileged one.

Similarly to the changes noticed for K_{CO}, the CO bond distance is also affected in an opposite fashion by the cation and the anion (Table II).

In view of the data presented in Table II some remarks concerning the previous interpretation by Minc, Kecki, and Gulik-Krzywicki[6] can be put forth. The authors suggested that the changes in CO frequency caused by cation and anion are parallel. It follows from our calculations that the anion and the cation effects are going in the opposite directions, and the observed change in the CO stretching frequency results from the competitive action of both the ions.

A deeper understanding of the difference in the cation and anion action can be obtained by analyzing

(8) M. J. Sienko and R. A. Plane, "Physical Inorganic Chemistry," W. A. Benjamin, New York, N. Y., 1963.

(9) The results of CNDO calculations (the bond order–charge density matrices, the molecular orbitals, and their energies) can be obtained from the authors upon request.

(10) K. T. Gieodakian, A. W. Kisielew, and W. I. Lygin, *Zh. Fiz. Khim.*, **41**, 457 (1967).

(11) K. T. Gieodakian, A. W. Kisielew, and W. I. Lygin, *ibid.*, **40**, 1584 (1966).

Table III: Dipole Moments (in D) and Their Derivatives for the Acetone Molecule and Its Ion Complexes

	C*₂CO	C*₂COLi$_R$⁺	C*₂COCl⁻	C*₂COLi$_R$⁺Cl⁻	C*₂COLi$_R$⁺I⁻
μ_{tot} ($R_{CO} = R_{e,CO}$)	−1.20	−2.04	−1.33	−2.20	−2.19
$\left(\dfrac{\partial \mu_{tot}}{\partial R_{CO}}\right)_{R_{e,CO}}$	−1.61	−2.35	−1.80	−2.55	−2.53
$\left(\dfrac{\partial \mu^{\sigma}}{\partial R_{CO}}\right)_{R_{e,CO}}$	−0.70	−0.54	−0.56	−0.31	−0.40
$\left(\dfrac{\partial \mu^{\pi}}{\partial R_{CO}}\right)_{R_{e,CO}}$	−0.91	−1.81	−1.24	−2.24	−2.13

the changes in the σ- and π-electronic structure of the acetone molecule. It follows from the charge density–bond order matrix that the lithium cation makes the CO bond more polar (for example, for the system C*₂-CO$\cdots$Li$_R$⁺ the net charges are −0.0644 and +0.1184 at C and O, respectively). [In this section the P matrix for C*₂CO system is treated as a reference. Considering the change of P matrix elements the plus sign signifies an increase of the corresponding matrix elements.] This induced polarity is quite similar to that observed in the case of the acetonitrile–cation complex. It should be noticed that the polarity changes become smaller when the angle ϕ increases. Thus, the perturbation acts most effectively if the cation is placed on the CO bond axis. The anion effect on the polarity of the CO bond is much smaller than that of the cation but has the same direction (for the system Cl⁻$\cdots$C*₂CO$\cdots$Li$_R$⁺ the net charges are −0.0220 and +0.0141 at C and O, respectively).

The change in the total electron density at the central carbon atom and at the oxygen atom induced by the ionic perturbation is mainly due to the change of the π-electron component (for example, for C*₂CO$\cdots$Li$_R$⁺ system the σ components are at C −0.0387, at O −0.0152, and the π components are +0.1032 at C and −0.1032 at O). Similarly as in the case of the acetonitrile–cation complex, the σ-charge densities are less influenced than the π-electron ones. Both the anion and the cation affect the π-electron densities in the same direction, but their effects on the σ-electron distribution are opposite.

Some properties of the nondiagonal elements of the bond order–charge density matrices are also worth noting. The $P_{2p\pi C, 2p\pi O}$ bond order are for C*₂CO, 0.9944; C*₂CO$\cdots$Li$_R$⁺, 0.9779; C*₂CO$\cdots$Cl⁻, 0.9925; I⁻$\cdots$C*₂CO$\cdots$Li$_R$⁺, 0.9742. Hence, the $P_{2p\pi C, 2p\pi O}$ bond order is changed in the same direction irrespective of the type (cation or anion) of the perturbation, although the anion has a less pronounced effect. On the other hand, the bond orders $P_{2sC, 2sO}$, $P_{2pxC, 2psO}$, $P_{2sC, 2pxO}$, $P_{2pxC, 2pxO}$ are changed by cation and anion in the opposite directions (for instance, $P_{2sC, 2sO}$ are for C*₂CO, 0.2552; C*₂CO$\cdots$Li$_R$⁺, 0.2630; Cl⁻$\cdots$C*₂CO, 0.2481; I⁻$\cdots$C*₂CO$\cdots$Li$_R$⁺, 0.2557). Therefore, one can con-

clude, that the π-electron structure of acetone perturbed by the anion or cation is changed in the parallel manner, whereas the σ-electron distribution is affected by the anion and cation in opposite directions. This result is different from that found for the acetonitrile complex.[2]

There is also another difference between the present results and those obtained for the acetonitrile complexes. In the case of acetonitrile the changes in the σ-electron bond orders were much greater than those in the π-electron ones. In the acetone complexes they are nearly the same. For the C*₂CO$\cdots$Li⁺ system the bond orders $P_{2sC, 2sO}$ and $P_{2pxC, 2sO}$ increase (to +0.0078 and +0.0093) whereas the matrix elements $P_{2sC, 2pxO}$ and $P_{2pxC, 2pxO}$ decrease (to −0.0057 and −0.0050). There is also a substantial decrease of $P_{2p\pi C, 2p\pi O}$ (to −0.0165). Thus, the increase of the CO stretching force constant is mainly due to the strengthening of the σ part of the CO bond.

In the Cl⁻$\cdots$C*₂CO system the σ-electron bond orders changed in the opposite direction; i.e., the bond orders $P_{2sC, 2sO}$ and $P_{2pxC, 2sO}$ decrease (to −0.0071 and −0.0076), but the $P_{2sC, 2pxO}$ and $P_{2pxC, 2pxO}$ increase (to +0.0014 and +0.0059). This corresponds to the diminished participation of the 2sO atomic orbital in the CO region and also to the larger participation of the 2pxO orbital. The π-electron bond order is only slightly diminished. Thus, the decrease of the CO stretching force constant in the Cl⁻$\cdots$C*₂CO system can be understood in terms of the σ-electron redistribution upon the complex formation.

What has been found for the I⁻$\cdots$C*₂CO$\cdots$Li⁺ system is the result of a competitive action of two ions. Hence, the σ-bond orders are nearly the same as those calculated for the isolated C*₂CO system. (For the following elements the changes are $P_{2sC, 2sO}$, +0.0005; $P_{2pxC, 2sO}$, +0.0017; $P_{2sC, 2pxO}$, −0.0053; $P_{2pxC, 2pxO}$, +0.0017.) However, the π-electron bond order is lowered (to −0.0202). It seems, therefore, that the final decrease of the CO stretching force constant can be ascribed to a slight lowering of the σ-bond strength as well as to the quite remarkable decrease of the π-bond strength.

The calculated values also allow for a qualitative

interpretation of the observed change in the ir intensity of the CO stretching band. It follows from Table III that the derivative of the total dipole moment of the acetone molecule in the $I^- \cdots C^*_2CO \cdots Li^+$ system with respect to the CO bond length is greater than that calculated for the isolated C^*_2CO system. Thus, the intensity of the CO stretching band in the ir spectrum should increase when the electrolyte is dissolved. This result has been recently confirmed experimentally.[12]

When analyzing the changes in the π and σ components of the dipole moment derivatives, one finds that they both contribute significantly. It is quite contrary to what had been noticed for acetonitrile and its complexes.[1,2] In the case of acetonitrile, the change of the σ part of the dipole moment derivative was much smaller than that of the π part.

Conclusions

The following conclusions can be drawn out from the present investigation. (1) All the information obtained from the CNDO calculations for various acetone-ion systems indicates that the cation interacting with the acetone molecule *via* the oxygen electron lone pairs leads to effects quite similar to those found in the case of the acetonitrile–cation complexes. The CO group is influenced by cation in nearly the same way

as the CN group was. This conclusion differs from the commonly accepted views, according to which the electron-accepting species should always weaken the multiple bond.[13] (2) The anion does not make deeper the changes introduced by the cation. The influence is more complicated. The π-electron structure of the system is influenced by both cation and anion in the same direction, whereas the effects on the σ-electronic structure are opposite. (3) The observed change in the CO bond stretching frequency can be attributed to the redistribution of both the σ and π electrons. This electronic redistribution is due to the cation as well as to the anion effect.

Finally, it should be pointed out that the present calculations were carried out within the framework of the semiempirical method. They were also based on a very simplified model of the electrolyte–solvent interaction. A qualitative agreement between the theory and the experimental data allows for the conclusion that the fundamental features of the real system were included in our model. However, one should be careful in extension of these results to other systems.

(12) Z. Kecki and J. Borucka, unpublished data.
(13) K. F. Purcell and R. S. Drago, *J. Amer. Chem. Soc.*, **88**, 919 (1966).

Transport Behavior in Dimethyl Sulfoxide. III. Conductance–Viscosity

Behavior of Tetra-*N*-amylammonium Thiocyanate from Infinite

Dilution to Molten Salt at 55°

by Neng-Ping Yao and Douglas N. Bennion*

*Energy and Kinetics Department, School of Engineering and Applied Science, University of California,
Los Angeles, California 90024 (Received January 19, 1971)*

Publication costs borne completely by The Journal of Physical Chemistry

Conductance, viscosity, and density of tetraamylammonium thiocyanate in dimethyl sulfoxide (DMSO) were determined at 55° over a concentration range from 10^{-3} M to the molten state, *i.e.*, 2.55 M. The (n-C_5H_{11})$_4$NSCN had a limiting equivalent conductance of 64.16 cm^2/ohm equiv in DMSO at 55° and an association constant of 16.2 l./mol in the dilute concentration range. The (n-C_5H_{11})$_4$N$^+$ ion is unsolvated in DMSO and has an effective radius of 5.21 Å. The conductance data in the concentrated region were fitted by the Wishaw–Stokes equation using an ion size $\mathring{a}$ = 3.5 Å. The significance of the fitting is discussed. The results seem to indicate that the molten (n-C_5H_{11})$_4$NSCN is not completely dissociated into its ions. Addition of DMSO molecules into the molten salt increases the Walden product of the solution. The increase appears to be unique to polar solvents and is interpreted as due to an increase in the ion fraction.

Introduction

There are relatively few transport studies in concentrated electrolyte solutions compared to dilute electrolyte solutions. This is, in part, due to low solubility of many inorganic salts. Organic salts generally have lower melting points and are quite soluble in a variety of solvents. Their molten salts are frequently miscible with the solvents. For example, Strong and Kraus[1] studied the conductance of tetraisoamylammonium thiocyanate in benzene from 10^{-4} N to a very concentrated solution of 1.138 M at 25°. Seward[2,3] studied the conductance of tetrabutylammonium picrate (mp 89.4°) in *n*-butyl alcohol (ϵ 9.8), anisole (ϵ 3.60), nitrobenzene (ϵ 24.8), and ethylene carbonate (ϵ 69.4) at 91° from dilute solution to the molten salt.

Some observations on electrolyte conductance over the entire concentration range, *i.e.*, from dilute to molten salt state, showed that the equivalent conductance, Λ, had a minimum or maximum when plotted *vs.* concentration in low dielectric constant solvents.[1,4] In polar solvents, *e.g.*, dielectric constant greater than 10, the equivalent conductance is a continuously decreasing function of concentration.[2,3,5] The Walden product, $\Lambda\eta$, *vs.* concentration generally shows only a minimum. The concentration at which the minimum occurs increases with increasing dielectric constant of the solvent.[4] Similar behavior for the equivalent conductance and the Walden product has also been found in concentrated aqueous solutions[6-9] where Λ is a continuously decreasing function of concentration while $\Lambda\eta$ passes through a minimum. The concentrated region where the Walden product, $\Lambda\eta$, increases,

after passing through the minimum, is of considerable interest, but behavior in this region has not been satisfactorily explained.

The result that the Walden product at infinite dilution, $\Lambda_0\eta_0$, is approximately equal to that of the molten salt, $(\Lambda\eta)_0$, as found by Seward[2,3] for the (n-C_4H_9)$_4$Npic (pic = picrate) salt in some low dielectric constant solvents at 91°, prompted Kenausis, Evers, and Kraus (KEK)[4,10] to suggest that (n-C_5H_{11})$_4$NSCN, just as (n-C_4H_9)$_4$Npic, was completely dissociated in its molten state. KEK[4,10] hypothesized that $\Lambda\eta/(\Lambda\eta)_0$ in the concentrated region might be the high-concentration analog of the Arrhenius fraction of dissociation, α', and have termed $\Lambda\eta/(\Lambda\eta)_0 = F_i$, the ion fraction in concentrated solutions. Furthermore, an equilibrium mechanism between ions and ion pairs was proposed by KEK[4,10] to explain the rising portion of

(1) L. E. Strong and C. A. Kraus, *J. Amer. Chem. Soc.*, **72**, 166 (1950).

(2) R. P. Seward, *ibid.*, **73**, 515 (1951).

(3) R. P. Seward, *J. Phys. Chem.*, **62**, 758 (1958).

(4) L. C. Kenausis, E. C. Evers, and C. A. Kraus, *Proc. Nat. Acad. Sci. U. S.*, **48**, 121 (1962).

(5) F. R. Longo, J. D. Kerstetter, T. F. Lumosniski, and E. C. Evers, *J. Phys. Chem.*, **70**, 431 (1966).

(6) A. N. Campbell, A. P. Gray, and E. M. Kartzmark, *Can. J. Chem.*, **31**, 617 (1953).

(7) R. P. Seward, *J. Amer. Chem. Soc.*, **77**, 905 (1955).

(8) J. F. Chambers, J. M. Stokes, and R. H. Stokes, *J. Phys. Chem.*, **60**, 985 (1956).

(9) M. L. Miller, *ibid.*, **60**, 189 (1956).

(10) L. C. Kenausis, E. C. Evers, and C. A. Kraus, *Proc. Nat. Acad. Sci. U. S.*, **49**, 141 (1963).

Walden product in the concentrated region approaching the molten salt.

The hypothesis and the proposed mechanisms by KEK have been challenged by Longo, et al.,[11] who reported that the Walden product, $\Lambda\eta$, of $(n\text{-}C_5H_{11})_4$-NSCN in nitrobenzene at 52° actually *increased* with addition of nitrobenzene molecules to the molten $(n\text{-}C_5H_{11})_4$NSCN. A maximum value of $\Lambda\eta$, approximately 0.83 cm² P/ohm equiv, was observed at 2.0 N compared to 0.2 cm² P/ohm equiv for the molten salt. In view of the anomalous maximum of the $\Lambda\eta$ product observed by Longo, et al.,[11] for $(n\text{-}C_5H_{11})_4$NSCN in nitrobenzene, the KEK hypothesis of ion fraction, i.e., $\Lambda\eta/(\Lambda\eta)_0$, and the proposed ions and ion-pair equilibrium mechanism must be reexamined, particularly in polar solvents.

In this paper the result of conductance and viscosity studies of $(n\text{-}C_5H_{11})_4$NSCN (mp 50.5°) in dimethyl sulfoxide at 55° is reported. A concentration range of 10^{-3} M to the molten salt, i.e., 2.55 M, was investigated. Limiting equivalent conductance, ionic association constant, and effective ionic size for the salt were obtained in the dilute concentration range. The conductance–viscosity behavior of the $(n\text{-}C_5H_{11})_4$-NSCN–DMSO solutions in the more concentrated region, i.e., 10^{-1} $M < C < 2.55$ M, was examined in the light of the proposed KEK hypothesis and was compared with the result of $(n\text{-}C_5H_{11})_4$NSCN in nitrobenzene by Longo, et al.[11]

Experimental Section

Tetra-n-amylammonium thiocyanate was prepared following the method of O'Malley.[12] The salt was recrystallized twice from 1:1 (v/v) anhydrous ethyl acetate–hexane and was then dried in vacuo at room temperature for 48 hr to constant weight. The salt had a melting point of 50 ± 0.5° which compared favorably with the reported value of 50.1°.[12] The infrared spectrum of the salt showed distinct peaks at 6.84, 4.9, and 3.4 μ which are not yet reported in the literature. The salt was stored in a vacuum desiccator over molecular sieves until used.

Purification of DMSO by vacuum distillation is described elsewhere.[13] Water content in the distilled DMSO was less than 30 ppm as determined by electrometric titration with Karl Fisher reagent. Nmr analysis of distilled DMSO showed no detectable organic impurity peaks. The maximum sensitivity of the nmr analysis is about 0.1%.

Solutions were prepared by weight in a dry nitrogen box and the weights were corrected to weights in vacuo. Volume concentration was obtained by multiplying the weight concentration by the density. Air contamination of the solutions was avoided by sealing the glass cells in the drybox prior to removal.

Density, viscosity, and conductance of the solutions were measured, respectively, with a two-capillary

relative method, modified Cannon–Ubbelohde viscosimeters, and an ac resistance bridge. The apparatus for density, viscosity, and conductance measurements was described previously.[14] The dilute solutions, i.e., $<10^{-1}$ M, were prepared by successive dilution of a 100-ml stock solution, 10^{-1} M. More concentrated solutions were prepared by diluting the molten salt with the purified DMSO. Two separate sequences of runs were made in the concentrated region. The concentrated $(n\text{-}C_5H_{11})_4$NSCN–DMSO solutions were mixed by occasional shaking at 55° in a closed cell. Complete miscibility between the DMSO and the molten $(n\text{-}C_5H_{11})_4$NSCN at 55° required several hours in the extremely concentrated region. The required mixing time decreased with increasing solvent concentration. Equilibrium was assumed to be attained when the DMSO phase disappeared and the resistance value of the solution remained constant after a brief shaking. A sufficient time must be allowed for equilibrium, and occasional shaking is required to minimize the Soret effect and other effects due to concentration and temperature variations in viscous solutions.

Data and Results

The experimental data on density, viscosity, and conductance of $(n\text{-}C_5H_{11})_4$NSCN in DMSO are summarized in Table I.[15]

The Walden product, $\Lambda\eta$, for the molten $(n\text{-}C_5H_{11})_4$-NSCN, $C = 2.549$ M, at 55° is 0.3596 cm² P/ohm equiv which is lower than the value 0.3959 cm² P/ohm equiv obtained from the smoothed equation

$$\log \Lambda\eta = \frac{93.85}{T} - 0.6885 \qquad (1)$$

reported by Kenausis, et al.,[10] for molten $(n\text{-}C_5H_{11})_4$-NSCN over the temperature range 52–110°. The $\Lambda\eta$ value of approximately 0.2 cm² P/ohm equiv reported by Longo, et al.,[11] for molten $(n\text{-}C_5H_{11})_4$NSCN at 52° appears to be low.

The viscosity and the specific conductance for the $(n\text{-}C_5H_{11})_4$NSCN–DMSO solutions at 55° are plotted as shown in Figure 1 as a function of concentration on a log–log scale. The viscosity of the solutions increases by a factor of 75 in going from 1 M to the molten state. The specific conductance increases linearly

(11) F. R. Longo, P. H. Daum, R. Chapman, and W. G. Thomas, J. Phys. Chem., 71, 2755 (1967).

(12) J. A. O'Malley, Dissertation, University of Pennsylvania, 1963.

(13) N. P. Yao, Ph.D. Thesis, University of California, Los Angeles, Calif., June 1969.

(14) (a) Part I: N. P. Yao and D. N. Bennion, J. Electrochem. Soc., 118, 1097 (1971); (b) part II: N. P. Yao and D. N. Bennion, J. Phys. Chem., 75, 1727 (1971).

(15) Table I will appear following these pages in the microfilm edition of this volume of the journal. Single copies may be obtained from the Reprint Department, ACS Publications, 1155 Sixteenth St., N.W., Washington, D. C. 20036, by referring to author, title of article, volume, and page number. Remit check or money order for $3.00 for photocopy or $2.00 for microfiche.
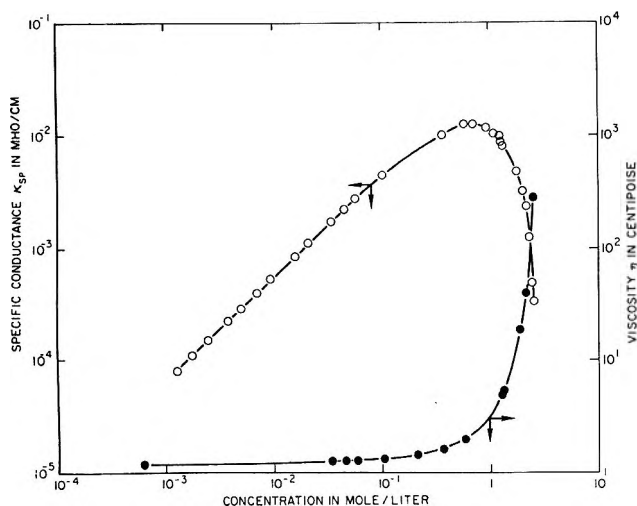
Figure 1. Specific conductance, κ_{sp}, and viscosity, η, of (n-C$_5$H$_{11}$)$_4$NSCN–DMSO solutions at 55° as a function of concentration.

in the dilute concentration region, i.e., $<6 \times 10^{-2}\ M$, and subsequently reaches a maximum $\kappa_{sp} = 1.26 \times 10^{-2}$ mho/cm at $C = 6 \times 10^{-1}\ M$ followed by a rapid decrease to a value 3.32×10^{-4} mho/cm corresponding to the molten salt. The rapid decrease of κ_{sp} in the concentrated region corresponds to the rapid increase of η. Log Λ shows a continuous, rapid decrease above $10^{-1}\ M$. Longo, et al.,[5] observed a similar decrease for the salt in another polar solvent, nitrobenzene, at 25° over the concentration range 7×10^{-5} to $1.83\ N$. Log Λ for similar salts in nonpolar solvents exhibits a different dependence on log C, generally increasing with increasing concentration.[4]

The limiting equivalent conductance, Λ_0, and the association constant, K_A, were obtained for the dilute concentrations following the extrapolation method of Fuoss and Shedlovsky[16] for weak electrolytes. The values of $S(z)$, the Shedlovsky function, were extracted from the table given by Daggett.[17] The mean activity coefficients, $\gamma_\pm$, were calculated from the modified Debye–Hückel law[18] for 1:1 electrolytes. The Fuoss–Shedlovsky plot of $1/\Lambda S(z)$ vs. $C\Lambda S(z)\gamma_\pm^2$ gives $\Lambda_0 = 64.16$ cm^2/ohm equiv and $K_A = 16.2$ l./mol. Longo, et al.,[5] reported that (n-C$_5$H$_{11}$)$_4$NSCN is slightly associated in nitrobenzene at 25° with $K_A = 37.02$ l./mol.

Using the value $\Lambda_0 = 64.16$ for (n-C$_5$H$_{11}$)$_4$NSCN electrolyte and the limiting ionic mobility $\lambda_-^0 = 47.66$ for the SCN$^-$ ion in DMSO at 55°,[14a] the limiting ionic mobility, λ_+^0, and the ionic Walden product, $\lambda_+^0\eta_0$, for the (n-C$_5$H$_{11}$)$_4$N$^+$ ion in DMSO are, respectively, 16.50 cm^2/ohm equiv and 0.1967 cm^2 P/ohm equiv at 55°. The value $\lambda_+^0\eta_0 = 0.1967$ for (n-C$_5$H$_{11}$)$_4$N$^+$ yields a "corrected" Stokes radius of $r_s = 5.21$ Å. This corrected Stokes ionic radius was calculated using procedures outlined in a previous paper.[14a] This ionic radius for (n-C$_5$H$_{11}$)$_4$N$^+$ is in

excellent agreement with the value 5.29 Å[18] estimated from the molecular volume. Thus, (n-C$_5$H$_{11}$)$_4$N$^+$ is unsolvated in DMSO as expected from the consideration of ion–dipole interaction.[13]

The equivalent conductance for (n-C$_5$H$_{11}$)$_4$NSCN–DMSO solutions over the entire concentration range at 55° has been fitted with the semiempirical Wishaw–Stokes equation[19]

$$\Delta = \frac{\eta_0}{\eta}\left(\Lambda_0 - \frac{\beta C^{1/2}}{1 + \kappa\mathring{a}}\right)\left(1 - \frac{\alpha C^{1/2}}{1 + \kappa\mathring{a}}F\right) \qquad (2)$$

where

$$\alpha = 8.204 \times 10^5/(\epsilon_0 T)^{3/2}$$

$$\beta = 82.5/\eta_0(\epsilon_0 T)^{1/2}$$

$$\kappa = 50.29 \times 10^8 C^{1/2}/(\epsilon_0 T)^{1/2}$$

$$F = [\exp(0.2929\kappa\mathring{a}) - 1]/(0.2929\kappa\mathring{a})$$

$\mathring{a}$ is the ion-size fitting parameter in ångströms and η/η_0 is the relative viscosity at concentration C. The values of α and β and the value of κ for DMSO at 55° are, respectively, 0.50886, 59.016, and $0.4289C^{1/2}$. The results of fitting are shown in Figure 2 where the equivalent conductance is plotted vs. $C^{1/2}$. The semiempirical Wishaw–Stokes equation with an ion-size fitting parameter $\mathring{a} = 3.5$ Å (a best fitting value) is shown by the solid line and the experimental points are shown by circles. The fitting is reasonably good in the concentrated range but is not as satisfactory in the dilute concentrations. The bad fit in the dilute region is expected since the empirically introduced factor η_0/η in eq 2 contains a coulombic term which was already included by the theoretical part of the equation; i.e., the Wishaw–Stokes equation overaccounts for the coulombic interactions in the dilute concentrations. The coulombic term is negligible in moderate and higher concentrations and thus the introduction of η_0/η into eq 2 provides a better fit in the concentrated range.

The Walden product, $\Lambda\eta$, is plotted as a function of concentration at 55° over the entire concentration range as shown in Figure 3. The $\Lambda\eta$ product passes through a minimum and a maximum in going from infinite dilution to the molten salt. The rising and the falling portion of the $\Lambda\eta$ product between $1.5\ M$ and the molten state is not predicted by the Wishaw–Stokes equation. Longo, et al.,[11] reported similar anomalous behavior of the $\Lambda\eta$ product for (n-C$_5$H$_{11}$)$_4$-NSCN in nitrobenzene at 52°. Since some of the viscosity or conductance data (shown in the paren-

(16) R. M. Fuoss and T. Shedlovsky, J. Amer. Chem. Soc., 71, 1496 (1949).

(17) H. M. Daggett, Jr., ibid., 73, 4977 (1951).

(18) R. A. Robinson and R. H. Stokes, "Electrolyte Solutions," 2nd ed, Butterworths, London, 1959.

(19) B. F. Wishaw and R. H. Stokes, J. Amer. Chem. Soc., 76, 2065 (1954).

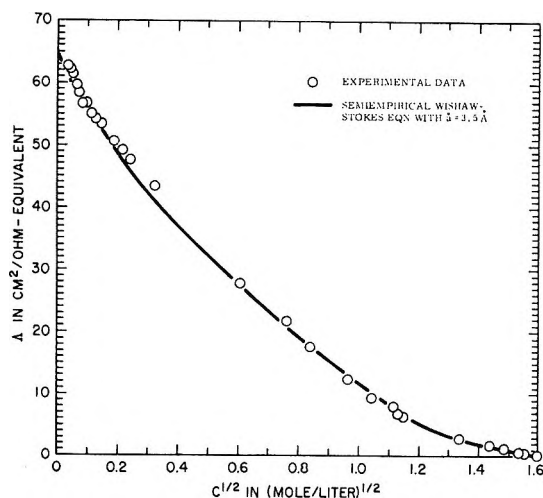Figure 2. Λ vs. $C^{1/2}$ for $(n\text{-}C_5H_{11})_4NSCN\text{-}DMSO$ solutions at 55° as predicted by the Wishaw–Stokes equation.

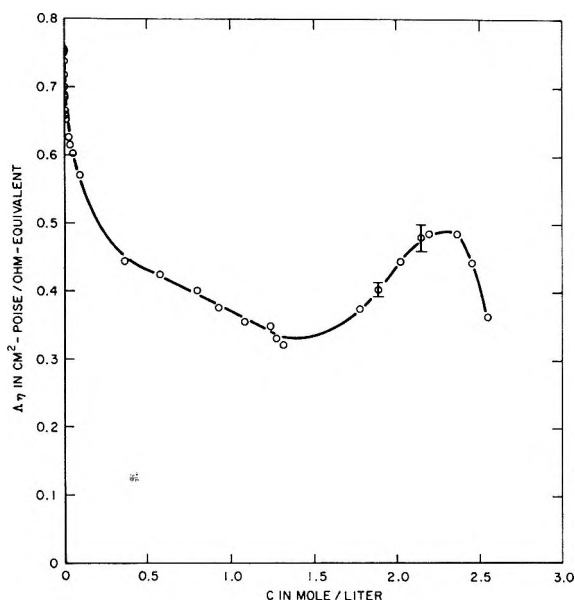Figure 3. Walden product, Λη, for $(n\text{-}C_5H_{11})_4NSCN\text{-}DMSO$ solutions as a function of concentration at 55°.

theses in Table I) in the concentrated region were interpolated from enlarged plots in order to calculate the Λη product at each concentration, the error due to the interpolation must be considered. For example, the Λη products at concentrations 2.154 and 1.893 M have been calculated based on actual experimental viscosity data and the interpolated specific conductance, κ_{sp}. The maximum error in interpolating the specific conductance data is ±0.1 × 10^{-3} mho/cm or less at these concentrations. This gives a maximum uncertainty in the Λη products of about ±0.019 and ±0.01 cm² P/ohm equiv at 2.154 and 1.893 M, respectively. The maximum uncertainties at these concentrations are shown in Figure 3 by the error bars. This indicates that the intermediate maximum portion of the Λη product is well within the experimental

accuracy and not due to error in interpolation of the experimental data.

The Λη product decreases rapidly with increasing concentration in the dilute region followed by a linear decrease between approximately 0.4 and 1.3 M. The minimum occurs at about Λη = 0.33 at 1.4 M and a maximum occurs at about Λη = 0.485 at 2.3 M. It is apparent from Figure 3 that the Walden product at infinite dilution, $\Lambda_0\eta_0$, is not equal to that of the molten salt, $(\Lambda\eta)_0$. $\Lambda_0\eta_0$ is 0.7649 and $(\Lambda\eta)_0$ is 0.3596 cm² P/ohm equiv.

The minimum Λη product occurs at 0.17 mole fraction and a maximum in the Λη product occurs at 0.6 mole fraction of the salt in going from infinite dilution to the molten salt.

Discussion

The Wishaw–Stokes equation, eq 2, with an ion-size fitting parameter $\mathring{a}$ = 3.5 Å has been found to fit the experimental conductance data reasonably well in the concentrated region as shown in Figure 2. Wishaw and Stokes[19] have successfully fitted their conductance data of aqueous ammonium chloride solutions at 25° by eq 2 using $\mathring{a}$ = 4.35 Å for NH₄Cl over the concentration range 0.1–5.0 M. Dunnett and Gasser[20] fitted their conductance data of LiCl in DMSO at 25° by eq 2 using $\mathring{a}$ = 3 Å for LiCl over the concentration range 2 × 10^{-4}–2.6 M with equally good success.

The significance of such fitting using the Wishaw–Stokes equation is not entirely clear. Equation 2 is essentially a theoretical conductance equation for dilute strong electroytes which is multiplied by an empirical factor η_0/η, the reciprocal of the relative viscosity. The theoretical conductance equation, i.e., eq 2 without the factor η_0/η, was based on the consideration of ion–ion interactions and has been successfully applied only in dilute electrolyte solutions, i.e., $C < 10^{-2}$ M. The fact that eq 2 has reproduced the conductance data over a wide concentration range indicates that the factor η_0/η has empirically accounted for other interactions, i.e., ion–solvent and solvent–solvent interactions, which predominate in the more concentrated region. This is expected since the change of viscosity is attributed to the nature of ion–ion, ion–solvent, and solvent–solvent interactions. Ion size, $\mathring{a}$, is a fitting or an adjustable parameter which can absorb the incompleteness of the theory. Thus, the significance of $\mathring{a}$ should not be overrated.

A fit of the conductance data by the Wishaw–Stokes equation over a wide concentration range does not necessarily mean that ion pairing is absent as the theoretical conductance equation implies, as was so interpreted by Dunnett and Gasser.[20] This is because the relative viscosity, η/η_0, itself is a measure of various

(20) J. S. Dunnett and R. P. H. Gasser, Trans. Faraday Soc., 61, 922 (1965).

interactions which are a function of not only the type of ions and solvent but also the concentration of the ionic species. Thus, any ion pairing in the solution may be reflected in the magnitude of η/η_0.

The variation of the $\Lambda\eta$ product as a function of concentration is shown in Figure 3. Clearly the Walden product at infinite dilution, $\Lambda_0\eta_0$, is not equal to that of the molten salt, $(\Lambda\eta)_0$, for $(n\text{-}C_5H_{11})_4NSCN\text{-}$DMSO solutions. This is contrary to the result $\Lambda_0\eta_0 = (\Lambda\eta)_0$ observed for $(C_4H_9)_4Npic$ salt in n-butyl alcohol at 91° by Seward.[2] Thus the KEK hypothesis[4,10] that the molten electrolytes are completely dissociated into their ions, which was based on Seward's results,[2,3] is open to question. The $\Lambda\eta/(\Lambda\eta)_0 > 1$ near the molten state as observed in the present work for $(n\text{-}C_9H_{11})_4NSCN\text{-}$DMSO solutions and in the work by Longo, et al.,[11] for $(n\text{-}C_5H_{11})_4NSCN\text{-}$nitrobenzene solutions implies that the ion fraction is larger than unity applying the KEK hypothesis directly.[4,10] Thus, the KEK hypothesis must be reexamined in view of the present result in DMSO and the result of Longo, et al.,[11] in nitrobenzene, both of which are polar solvents.

Because the magnitude of the specific conductance is low for the molten $(n\text{-}C_5H_{11})_4NSCN$, i.e., $\kappa_{sp} = 3.32 \times 10^{-4}$ mho/cm at 55°, and because $\Lambda_0\eta_0 > (\Lambda\eta)_0$ in DMSO, it appears that the molten salt is not completely dissociated into ions. Assuming that $\Lambda_0\eta_0 = 0.7649$ would be the $(\Lambda\eta)_0$ product if the molten electrolyte were completely dissociated, the ion fraction is approximately 0.47 for the molten electrolyte at 55°. The equation defining the ion fraction as $F_i = \Lambda\eta/\Lambda_0\eta_0$ is still valid providing the above assumption is true.

Examination of the $\Lambda\eta$ product on going from infinite dilution to the molten salt shows that the ion fraction decreases rapidly between 0 and 10^{-1} M, region I. This is followed by a less rapid decrease within 10^{-1} to 1.3 M, region II, until the minimum $\Lambda\eta$ product is reached; i.e., ion fraction at the minimum is about 0.43. Subsequently the ion fraction increases between 1.4 and 2.3 M, region III, reaching a maximum with $F_i = 0.64$ at 2.3 M. This is followed by a rapid decrease to the molten salt, region IV.

Various mechanisms for the equilibrium between the ions and the ion pairs can be used to explain the observed $\Lambda\eta$ product. The rapid decrease of the $\Lambda\eta$ product in region I is approximately a linear function of $C^{1/2}$. The law of mass action for a weakly dissociated electrolyte predicts that the ion fraction is proportional to $1/C^{1/2}$ while the concentration of free ions increases as $C^{1/2}$.

As the concentration of free ions increases, the number of ion pairs also increases with increasing concentration. At moderate concentration, e.g., at 1.0 M, each solute molecule is surrounded by approximately eight DMSO molecules based on the molar ratio at

this concentration. The electrostatic force which holds an ion pair together is substantially reduced due to the presence of a neighboring free ion. Thus, an ion pair in the vicinity of a free ion may be more easily dissociated into its ions upon a collision by a solvent molecule. The occurrence of dissociation by such collisions, therefore, depends on the number of ion pairs and free ions, the dielectric constant of the medium separating the two, and the thermal energy of the solvent, i.e., temperature. It is, therefore, expected that the dissociation increases with increasing concentration at constant temperature. This is essentially the mechanism proposed by KEK[4,10] to explain the rising portion of the $\Lambda\eta$ product with increasing concentration.

In regions II and III there is a dynamic equilibrium between free ions and associated ion pairs where the association is due to coulombic interactions and ionic collisions while the dissociation is due to collisions between energetic solvent molecules and the associated ion pairs. The minimum $\Lambda\eta$ product at 1.4 M corresponds to a point where the dissociation becomes relatively more dominating with increasing concentration. At the minimum $\Lambda\eta$ product, each solute molecule is surrounded by about four solvent molecules. The concentration at which the minimum $\Lambda\eta$ product occurs depends on the solvent and temperature since the occurrence of collisions depends on the number of ion pairs, temperature, etc. In a high dielectric constant medium, the coulombic interaction is weaker and thus there are less associated ion pairs. This means that the minimum will occur at higher concentration compared to that in a low dielectric constant medium. The minimum $\Lambda\eta$ product is at 1.4 M for $(n\text{-}C_5H_{11})_4NSCN$ in DMSO (ϵ_0 41.9 at 55°). This minimum value may be compared with 10^{-5} M for the same salt in p-xylene (ϵ_0 2.22 at 52°) as predicted by Kenausis, et al.,[4] and with 0.6 M for the salt in nitrobenzene (ϵ_0 34.82 at 25°) as determined by Longo, et al.[5]

The ion fraction in region III therefore increases with increasing concentration due to the thermal collisions between the ion pairs and the solvent molecules. As the solution approaches the ultraconcentrated region, e.g., 2.3 M or higher, each solute molecule is now surrounded by less than one solvent molecule and the solution begins to assume the quasilattice structure of the molten salt which is assumed here to be more associated. DMSO is a pyramidal molecule with a dipole moment of 3.9 ± 0.1 D[21] located along the S–O bond and has an effective volume of about 118 Å.[13] It is possible that the addition of DMSO molecules into the molten electrolyte results in the replacement of SCN⁻ ions in an ion pair by DMSO molecules thus increasing the ion fraction as solvent is added to the molten salt.

(21) F. A. Cotton and R. Francis, J. Amer. Chem. Soc., 82, 2989 (1960).

Conclusions

(1) The conductance data were fitted by the semiempirical Wishaw–Stokes equation using $\mathring{a} = 3.5$ Å. A reasonable fit was found in the concentrated region. The significance of such fitting is not fully explained except that the decrease of the conductance with increasing concentration is largely accounted for by the increase of the solution viscosity which has been empirically introduced into the Wishaw–Stokes equation.

(2) The $\Lambda_0\eta_0$ product at infinite dilution for $(n\text{-}C_5H_{11})_4NSCN$ in DMSO is not equal to the $(\Lambda\eta)_0$ product of molten $(n\text{-}C_5H_{11})_4NSCN$ at 55°. The $\Lambda_0\eta_0$ product is found to be 0.765 cm² P/ohm equiv while the $(\Lambda\eta)_0$ product is 0.3596 cm² P/ohm equiv. This result seems to be in disagreement with the KEK hypothesis that the molten salt is completely dissociated into its ions, which was based on the observed result $\Lambda_0\eta_0 = (\Lambda\eta)_0$ for $(C_4H_9)_4$Npic in some nonaqueous solvents.[2,3]

(3) The thermal collision mechanism for ion–ion-pair equilibrium as proposed by KEK[4,10] is adequate in explaining the rising portion of the $\Lambda\eta$ product with increasing concentration which was observed in the intermediate concentration region.

(4) In the dilute concentration region, $(n\text{-}C_5H_{11})_4$-NSCN is slightly associated with an association constant $K_A = 16.2$ l./mol. The "corrected" Stokes radius for $(n\text{-}C_5H_{11})_4N^+$ ion is 5.21 Å indicating that, by comparison to molecular volume data, the ion is unsolvated.

Molecular Association of Hydrogen-Bonding Solutes.   Phenol in

Carbon Tetrachloride

by Earl M. Woolley, John G. Travers, Brian P. Erno, and Loren G. Hepler*

Department of Chemistry, University of Lethbridge, Lethbridge, Alberta, Canada   (Received August 14, 1970)

Publication costs borne completely by The Journal of Physical Chemistry

The intermolecular association of phenol in CCl_4 solution at 25° has been investigated by means of distribution and calorimetric measurements. For the distribution of monomeric phenol between the aqueous and organic phases we obtain $K_d = (P)_o/(P)_a = 0.447$. It is shown that the principal association reaction of phenol in CCl_4 saturated with water is trimerization, for which $K_3 = (P_3)/(P)^3 = 14.9$. Calorimetrically determined heats of dilution of phenol in anhydrous CCl_4 also show that trimerization is the principal association reaction at concentration up to ~2 M. These results lead to $K_3 = (P_3)/(P)^3 = 5.6$ and to $\Delta H_3° = -8.54$ kcal/mol of P_3 in anhydrous CCl_4. Equilibrium constants cited above are expressed in terms of molarities. Heats of solution of phenol in CCl_4 have also been measured and combined with data from the literature in evaluating $\Delta H° = 3.17$ kcal/mol and thence $\Delta G°$ and $\Delta S°$ for transfer of monomeric phenol from water to CCl_4. Calculation of $\Delta H°$ values from equilibrium constants at several temperatures is also discussed in relation to choices of standard states.

Introduction

Many recent investigations have clearly shown that various compounds containing –OH groups (acetic acid, ethanol, and phenol are examples) are associated by way of intermolecular hydrogen bonding when dissolved in "inert" solvents. For some hydrogen-bonding solutes the associated species are sufficiently stable that it has been possible to identify the species (usually as dimers) and to determine their thermodynamic properties in reasonably satisfactory fashion. The situation is considerably different for phenol and some other solutes for which there are disagreements as to the most important species in solution and few reliable thermodynamic data. Although several admirable exceptions can be cited, it is our opinion that many investigations have been based on uncritical acceptance of the idea that all of some measured effect can be attributed to equilibrium between monomers and dimers.

Pimentel and McClellan,[1] Davis,[2] and Whetsel and

Lady[3] have cited a considerable number of investigations of association of phenol in CCl$_4$ solution. There is little agreement as to which associated species (dimers, trimers, etc.) are most important and virtually no agreement on numerical values for equilibrium constants.

Results of several spectroscopic investigations[4-6] have been interpreted in terms of monomer–dimer equilibrium. A number of other investigations present convincing evidence that trimers or other species larger than dimers are present in significant quantities when phenol is dissolved in CCl$_4$, as reviewed briefly below.

Saunders and Hyne[7] have carefully tested the results of their nmr investigations in terms of monomer–dimer, monomer–trimer, and monomer–tetramer equilibria. They found that they could account quantitatively for their results in terms of the monomer–trimer equilibrium but could not do so with either the monomer–dimer or the monomer–tetramer equilibrium.

Extensive measurements by Johnson, Christian, and Affsprung[8] of the distribution of phenol between water and CCl$_4$ and the solubility of water in solutions of phenol in CCl$_4$ have been interpreted in terms of several associated species containing more than one molecule of phenol, with the suggestion that trimeric phenol is a major species in CCl$_4$ solutions that contain some water.

Pimentel and McClellan[1] have cited an unpublished ir investigation by Rea, who also concluded that trimers are the most important associated species of phenol in CCl$_4$. Equilibrium constants (expressed in molarities) have been obtained at several temperatures and used for evaluation of $\Delta H°$ and $\Delta S°$ for the trimerization reaction.

Most recently, Whetsel and Lady[3] have reviewed several earlier investigations, with particular emphasis on results that have been interpreted in terms of one equilibrium constant for dimerization and another equilibrium constant for successive additions of monomeric phenol to form trimers, tetramers, etc. They have also concluded that their own extensive ir data should be similarly interpreted in terms of two equilibrium constants. They have used their equilibrium constants (expressed in molarities) for calculation of $\Delta H°$ and $\Delta S°$ values.

Before turning to our own experimental work and our interpretation in relation to earlier investigations, we consider the general problem of calculating $\Delta H°$ and $\Delta S°$ from K values at several temperatures. A number of recent investigations, particularly of the thermodynamics of ionization of acids, have demonstrated that uncertainties associated with $\Delta H°$ values derived from K values at several temperatures are commonly underestimated.[9,10] There is also a matter of fundamental thermodynamics to be considered in connection with calculation of heats of reaction by

way of the van't Hoff equation

$$d \ln K/dT = \Delta H°/RT^2 \tag{1}$$

Direct application of (1) to K values based on different standard states or expressed in terms of different concentration units can lead to different $\Delta H°$ values, all referring to the enthalpy of reaction with all solute species at infinite dilution. This is incorrect, since the value of $\Delta H°$ at infinite dilution for a particular reaction is independent of how people choose to express concentrations.

The essential thermodynamic requirement for *direct* application of the van't Hoff equation (eq 1) is that the standard states chosen must be independent of temperature, which is a formal way of saying that equilibrium constants to be used in this fashion must be expressed in terms of mole fractions or molalities (or other temperature-independent units) rather than in terms of molarities (or other temperature-dependent units). This is not to suggest that it is thermodynamically incorrect or even undesirable to choose a standard state based on molarity. In practice, such a choice often offers real convenience in terms of experimental procedures or calculations with experimental data. Further, there are sound arguments that comparisons of equilibrium constants, $\Delta G°$, and $\Delta S°$ values for a particular reaction in several solvents are best made in terms of molarities or some other concentration unit based on equal volumes of solution.

One way to use the van't Hoff equation correctly is to convert all equilibrium constants expressed in terms of molarities to new constants expressed in terms of mole fractions or molalities. These calculations require only knowledge of the density of solvent over the temperature range of interest.

It is often more convenient to apply the van't Hoff equation (eq 1) directly to equilibrium constants based on molarities and separately allow for the thermal expansion of the solvent. We consider this calculation for a general association reaction represented by

$$nP = P_n \tag{2}$$

(1) G. C. Pimentel and A. L. McClellan, "The Hydrogen Bond," W. H. Freeman, San Francisco, Calif., 1960.

(2) M. N. Davis, Nat. Bur. Stand. (U. S.), Monogr., No. 105 (1968).

(3) K. B. Whetsel and J. H. Lady, "Spectrometry of Fuels," Plenum Press, New York, N. Y., 1970, pp 259–279.

(4) D. L. Powell and R. West, Spectrochim. Acta, 20, 983 (1964); M. M. Maguire and R. West, ibid., 17, 369 (1961).

(5) M. Ito, Mol. Spectrosc., 4, 125 (1960).

(6) S. Singh and C. N. R. Rao, Can. J. Chem., 44, 2611 (1966).

(7) M. Saunders and J. B. Hyne, J. Chem. Phys., 29, 1319 (1958).

(8) J. R. Johnson, S. D. Christian, and H. E. Affsprung, J. Chem. Soc., 1 (1965).

(9) E. J. King, "Acid-Base Equilibria," Pergamon Press, Oxford, 1965.

(10) J. W. Larson and L. G. Hepler in "Solute-Solvent Interactions," J. F. Coetzee and C. D. Ritchie, Ed., Marcel Dekker, New York, N. Y., 1969.

with equilibrium constants K_M and K_m where subscripts M and m indicate that standard states are based on molarities and molalities, respectively. These equilibrium constants are related to each other and the density ρ of the solvent by

$$K_m = \rho^{n-1} K_M \tag{3}$$

We take logarithms of both sides of (3) and combine with the van't Hoff equation (eq 1) to obtain

$$\Delta H° = RT^2 (d \ln K_M/dT) +$$
$$RT^2 (n - 1)(d \ln \rho/dT) \tag{4}$$

Since coefficients of thermal expansion of liquids are commonly tabulated as

$$\alpha = (1/V)(dV/dT) = d \ln V/dT \tag{5}$$

it is convenient to use (5) in the form

$$\Delta H° = RT^2 (d \ln K_M/dT) + RT^2 (1 - n)\alpha \tag{6}$$

Applications of equations similar to (4) and (6) to ionization of aqueous acids[9] and deuterium oxide[11] have been described previously.

With CCl_4 as solvent for a reaction of type (2) with $n = 3$ at 298°K and $\alpha = 1.23 \times 10^{-3}$ from Rowlinson,[12] $RT^2(1 - n)\alpha = -430$ cal/mol, which is not ordinarily negligible in comparison to $RT^2(d \ln K_M/dT)$. Although several earlier workers (for example, Maguire and West[4]) have converted K_M values expressed in terms of molarities to K_m or K_X values expressed in terms of molalities or mole fractions and then correctly applied the van't Hoff equation (eq 1) to evaluation of $\Delta H°$, random inspection of papers cited by Pimentel and McClellan[1] shows that a majority have calculated $\Delta H°$ values from $RT^2(d \ln K_M/dT)$ without using the required terms involving either density or coefficient of thermal expansion of the solvent as done in our eq 4 and 6.

In an effort to obtain further evidence for or against the variously proposed associated species of phenol in CCl_4, we have made both distribution and calorimetric measurements with results and subsequent calculations that are described in this paper.

Experimental Section

Analytical reagent grade phenol, reagent grade chlorobenzene, and spectroanalyzed carbon tetrachloride were used. Considerable care was taken to make and keep all calorimetric solutions free of water. All distribution and calorimetric measurements were made at 25.0 ± 0.1°.

Distribution measurements were made on solutions containing known total amounts of water, CCl_4, and phenol. After equilibrium was attained by samples in closed flasks placed in a constant-temperature bath, portions of the aqueous layers were analyzed by titration with standard NaOH solutions. These titrations were carried out in a nitrogen atmosphere from

which carbon dioxide was carefully excluded. Titration curves were obtained with a Beckman Research Model 1019 pH meter coupled with a Beckman 39004 pH 0–14 glass electrode and a calomel reference electrode. The pH-measuring system was standardized with pH 10.00 and pH 12.45 buffers. In calculating the equivalence point for each aliquot titrated, we made use of material balance, the electroneutrality relation, and equilibrium constants for ionization of water ($pK_w = 14.00$) and phenol ($pK_a = 9.96$) with activities expressed on the molar scale.[9,10] Activity coefficients for aqueous phenol were taken to be unity and for the ions were calculated from[9]

$$\log y_\pm = \frac{0.5115(I)^{0.5}}{1 + 1.3(I)^{0.5}} \tag{7}$$

All solutions at the equivalence point had ionic strengths I less then 0.1 M. Results of all of our distribution measurements are reported and interpreted in terms of molarities.

Calorimetric titration measurements of heats of dilution of phenol and chlorobenzene in anhydrous CCl_4 solutions were made with the LKB 8700 precision titration calorimetry system and a Metrohm Herisau Dosimat automatic buret to deliver the titrant solution. Heats of solution of solid phenol in CCl_4 were made with the LKB 8700 system and the LKB 100-ml reaction calorimetry vessel, with glass ampoules to contain the phenol. All results of our calorimetric measurements refer to 25.0 ± 0.1° and are reported in terms of the calorie that is defined equal to 4.184 J. All solution compositions are described in terms of molarities.

Results and Calculations

The composition and analytical data from our distribution measurements lead to the molarity of phenol (monomeric) in the aqueous phase and the total molarity of phenol in the organic phase, hereafter represented by $(P)_a$ and C_o, respectively. The distribution constant K_d that refers to the equilibrium

$$P(aq) = P(in \ CCl_4) \tag{8}$$

is written as

$$K_d = (P)/(P)_a \tag{9}$$

in which (P) represents the molarity of monomeric phenol in CCl_4. On the basis of the tentative assumption that association of phenol in CCl_4 can be described in terms of a single equilibrium as in eq 2, we also have

$$K_n = (P_n)/(P)^n \tag{10}$$

where (P_n) and (P) represent molarities of associated P_n molecules and monomeric phenol in CCl_4 solution.

(11) R. N. Goldberg and L. G. Hepler, *J. Phys. Chem.*, **72**, 4654 (1968).

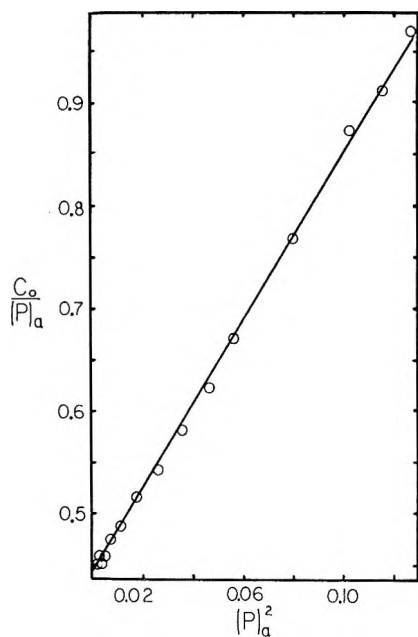(12) J. S. Rowlinson, "Liquids and Liquid Mixtures," Butterworths, London, 1959.

Figure 1. Results of measurements of distribution of phenol between water and carbon tetrachloride, displayed as suggested by eq 14. Every point is the average of two or more duplicate determinations.

The total concentration C_0 of phenol in the organic phase is given by the sum

$$C_0 = (P) + n(P_n) \tag{11}$$

Combination of eq 9–11 leads to

$$C_0/(P)_a = K_d + nK_nK_d{}^n(P)_a{}^{n-1} \tag{12}$$

If we know or can guess the value of n, a graph of $C_0/(P)_a$ against $(P)_a{}^{n-1}$ should yield a straight line with the intercept K_d and slope $(nK_nK_d{}^n)$.

One way to obtain a value for n is to obtain first a value of K_d by extrapolation of $C_0/(P)_a$ to $(P)_a = 0$. Then from (12) we obtain

$$\log \{ [C_0/(P)_a] - K_d \} =$$
$$\log (nK_nK_d{}^n) + (n - 1) \log (P)_a \tag{13}$$

Although use of this equation magnifies experimental uncertainties in C_0 and $(P)_a$ and depends markedly on the value of K_d used in evaluating the left-side term, a graph of $\log \{ [C_0/(P)_a] - K_d \}$ against $\log (P)_a$ leads to slope $\simeq 2$ and thence to $n = 3$. We therefore write eq 12 specifically in terms of $n = 3$ for the monomer–trimer equilibrium in the organic phase as

$$C_0/(P)_a = K_d + 3K_3K_d{}^3(P)_a{}^2 \tag{14}$$

We have used the results of our distribution measurements to construct a graph of $C_0/(P)_a$ against $(P)_a{}^2$ as shown in Figure 1. The intercept of the straight line leads to $K_d = 0.447$ and the slope leads to $K_3 = 14.9$.

The most thorough comparable investigation is that carried out by Johnson, Christian, and Affsp-

rung.[8] Interpretation of their results in terms of the monomer–trimer equilibrium leads to $K_d = 0.467$ and $K_3 = 12.7$, in satisfactory agreement with our values for these quantities.

Although the results of our distribution measurements and similar results from Johnson, Christian, and Affsprung[8] have been shown to be consistent with monomer–trimer equilibrium, it is also important to consider these results in relation to the possibility that other associated species may be present. The calculations reported by Johnson, Christian, and Affsprung[8] rule out dimers as principal species in these solutions. Another way to reach the same conclusion is by consideration of their display of their results on a graph of (our symbols) $C_0/(P)_a$ against $(P)_a$. According to eq 12 with $n = 2$ for monomer–dimer equilibrium, this graph should be a straight line with slope equal to $(2K_2K_d{}^2)$. Both their results and ours lead to distinctly curved lines on this kind of graph. The slopes of the lines at small $(P)_a$ are certainly very small and may be approaching zero as $(P)_a$ approaches zero, which shows that dimeric phenol is not a principal species in these CCl_4 solutions.

Calculations reported by Johnson, Christian, and Affsprung[8] indicate that equilibria involving the combinations monomer–tetramer, monomer–trimer–tetramer, monomer–trimer–pentamer, and monomer–trimer–hexamer are all compatible with their distribution results. They selected the monomer–trimer–hexamer combination as being the most plausible. Our results support their preference for the monomer–trimer interpretation rather than the monomer–tetramer interpretation, since a graph of our $C_0/(P)_a$ against $(P)^3$ leads to a line with steadily decreasing slope at small concentrations that becomes approximately straight at high (P_a). Similar graphs based on $n > 4$ also lead to curved lines rather than the straight lines required by eq 12. Although our results do not definitely rule out simultaneous presence of several P_n species with $n \geq 3$ as proposed by Johnson, Christian, and Affsprung,[8] we can say that our results are adequately interpreted in terms of monomer–trimer equilibrium alone so that there is no need for us to postulate other species.

It is difficult to estimate accurately the uncertainties to be associated with K_d and K_3 values either from our work or from that of Johnson, Christian, and Affsprung[8] for several reasons. First, experimental errors are relatively most important for the most dilute solutions. On the other hand, it is for the most dilute solutions that the implicit but sometimes unstated assumption that activity coefficients are unity is most satisfactory. Further, it is for dilute solutions that we can most confidently interpret experimental results in terms of a single equilibrium rather than in terms of consecutive equilibria and the accompanying increase in number of adjustable parameters. Fi-

nally, for the most concentrated solutions the relatively high concentration of water in the organic phase can have a very large effect on hydrogen-bonding reactions in ways that cannot be understood solely on the basis of distribution data. In spite of these difficulties, we can say that qualitative conclusions concerning the importance of trimers and numerical values of K_d and K_3 reported here and calculated from results of Johnson, Christian, and Affsprung[3] are in good agreement.

Although we may now regard it as well established that trimerization is the principal association reaction of dilute phenol in CCl_4 that is saturated with water, we do not necessarily know from the distribution results that we can properly rule out dimers as important species in anhydrous CCl_4 solvent.

We now set about interpretation of our heat of dilution results, which are reported and used in the form of ϕ_L values. The relative apparent molar enthalpy represented by ϕ_L is equal to the negative of the enthalpy of dilution of 1 mol of phenol from a solution of specified molarity to infinite dilution. In our interpretation, we assume that all differences between actual ϕ_L values and $\phi_L = 0$ for ideal solutions are due to association reactions. In order to test the validity of this assumption, we have measured heats of dilution of chlorobenzene in CCl_4. Chlorobenzene was chosen as a test compound because its molecules have about the same dipole moment and are about the same size and shape as the phenol molecule. The small ϕ_L values we found for chlorobenzene in CCl_4 can be expressed by $\phi_L = AM$ in which $A = -14$ cal l./mol[2]. Thus we see that it is in fact reasonable to attribute nearly all of the much larger heats of dilution of phenol ($\phi_L \cong -1800$ cal/mol for 1 M phenol) to $\Delta H°$ values for association reactions rather than to long-range solute-solute interactions. We have also made density measurements on solutions of chlorobenzene in CCl_4 and have found that the partial molar volumes of chlorobenzene in dilute solutions are nearly identical with the molar volume of liquid chlorobenzene, as required for an ideal solution. On the basis of the calorimetric and volumetric data for chlorobenzene, it is also reasonable to take all (molar) activity coefficients equal to unity for *dilute* solutions of phenol in CCl_4.

Our ϕ_L results for phenol are listed in Table I.[13] These results are based on several separate dilution runs with the calorimetric titration apparatus, in which the starting solutions were independently prepared, having concentrations $M = 1.0970$ mol/l. and $M = 2.0808$ mol/l.

We begin interpretation of the ϕ_L results in terms of the single general association reaction represented by eq 2. Since at any finite concentration there will be both monomeric and associated species present while at infinite dilution all associated species will be dissociated

to monomers, we can express the heat of dilution to infinite dilution in terms of

$$\phi_L = (\alpha/n)\Delta H_n° \qquad (15)$$

in which α and $\Delta H_n°$ represent the fraction of monomers that is associated and the molar enthalpy of reaction 2. We thus have $(P) = M(1 - \alpha)$ and $(P_n) = \alpha M/n$, which we substitute in the defining eq 10 to obtain

$$K_n = (\alpha/n)M^{n-1}(1 - \alpha)^n \qquad (16)$$

We have tested eq 15 and 16 with our ϕ_L results by using a small digital computer to find the value of K_n that leads to the most consistent value of $\Delta H_n°$ over the whole range of concentrations. Standard deviations in $\Delta H_2°$ and $\Delta H_4°$ values calculated in this way are considerably larger than for $\Delta H_3°$ values based on $n = 3$ in eq 15 and 16, corresponding to monomer-trimer equilibrium. Even more convincing evidence that trimers are more important species than either dimers or tetramers in these solutions is the large concentration dependence of the difference between calculated and average $\Delta H_2°$ and $\Delta H_4°$ values. In summary, we can say that all of our ϕ_L results can be accounted for quantitatively in terms of monomer-trimer equilibrium by way of eq 15 and 16, while similar treatments in terms of either dimers or tetramers are unsatisfactory. This analysis of all of our ϕ_L values and also separate analysis of groups of values obtained in single calorimetric runs leads to $\Delta H_3° = -8.55$ kcal/mol of P_3 formed and to $K_3 = 4.8$.

We have also developed another approach to interpretation of ϕ_L results in terms of the general association reaction represented by eq 2. Consider the dilution of a solution containing 1 mol of phenol from its initial concentration M to infinite dilution, for which we write

$$M\phi_L = \Delta H_n°(P_n) \qquad (17)$$

We also have

$$(P_n) = K_n(P)^n \qquad (18)$$

from eq 10. Next we substitute (18) into (17) and rearrange to obtain

$$(P) = (M\phi_L/\Delta H_n°K_n)^{1/n} \qquad (19)$$

Further substitutions of (18) and (19) into the material balance equation

$$M = (P) + n(P_n) \qquad (20)$$

yield

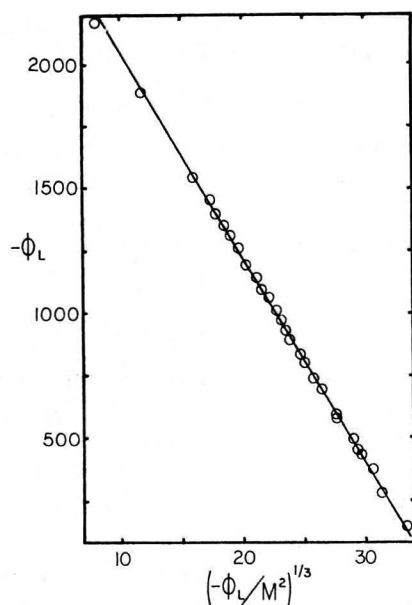$$M = (M\phi_L/\Delta H_n°K_n)^{1/n} + nM\phi_L/\Delta H_n° \qquad (21)$$

Figure 2. Results of heat of dilution measurements displayed as suggested by eq 22 with $n = 3$. Only half of the values given in Table I have been used in constructing this graph, but all of the results were used in obtaining values of K_3 and ΔH_3° reported in this paper.

Finally, we arrange (21) to obtain a linear equation suitable for graphical testing and subsequent evaluation of both K_n and ΔH_n° from the slope and intercept

$$\phi_L = (\Delta H_n^\circ/n) -$$
$$(1/n)(\Delta H_n^\circ)^{(n-1)/n}(1/K_n)^{1/n}(\phi_L/M^{n-1})^{1/n} \quad (22)$$

A graph of $-\phi_L$ against $(\phi_L/M^2)^{1/3}$, corresponding to $n = 3$, is shown in Figure 2. From the slope and intercept we obtain $K_3 = 4.9$ and $\Delta H_3^\circ = -8.57$ kcal/mol of P_3. A similar graph of $-\phi_L$ against $(\phi_L/M)^{1/2}$, corresponding to $n = 2$, exhibits a markedly curved line that has both intercept and limiting slope very close to zero. A graph of $-\phi_L$ against $(\phi_L/M^3)^{1/4}$ shows a line with marked curvature at low concentrations that becomes approximately straight for $M > 0.3$ mol/l. We therefore conclude again that dimers and tetramers of phenol are of little importance compared to trimers in our anhydrous CCl_4 solutions.

Our K_3 and ΔH_3° values obtained by way of eq 15 and 16 and eq 22 differ slightly from each other because these different treatments weight the different experimental results differently.

Our tabulated ϕ_L values are based upon measured heats of dilution from one finite concentration to another finite concentration combined with our extrapolated heat of dilution to zero concentration. Differences in our ϕ_L values are therefore properly regarded as purely experimental quantities, while absolute ϕ_L values are subject to adjustment following any different extrapolation to infinite dilution. It was there-

fore desirable to calculate K and ΔH° values from $\Delta \phi_L$ values as follows. We rewrite eq 15 as

$$\phi_L' = (\alpha'/n)\Delta H_n^\circ \quad (23)$$

for a reference solution of concentration M' with corresponding α' and subtract from eq 15 to obtain

$$\phi_L - \phi_L' = \Delta \phi_L = (\alpha - \alpha')\Delta H_n^\circ/n \quad (24)$$

We have tested eq 24 and 16 and an equation like (16) written in terms of M' and a' by using a digital computer to obtain the values of K_n and ΔH_n° that best account for the $\Delta \phi_L$ values. For these calculations we have chosen our two titrant solutions ($M' = 1.0970$ and 2.0808 mol/l.) as reference solutions and then obtained $K_3 = 6.2$ and 6.3 with $\Delta H_3^\circ = -8.53$ and -8.52 kcal/mol. We were unable to fit our experimental results with $n \neq 3$.

By four slightly different treatments of our heats of dilution we have now obtained $K_3 = 4.8, 4.9, 6.2,$ and 6.3 with $\Delta H_3^\circ = -8.55, -8.57, -8.53,$ and -8.52 kcal/mol. We adopt $K_3 = 5.6$ and $\Delta H_3^\circ = =8.54$ kcal/mol as "best" values for further calculations. From this K_3 we obtain $\Delta G_3^\circ = -1.02$ kcal/mol and combine with ΔH_3° to obtain $\Delta S_3^\circ = -25.2$ cal/deg mol.

Our $K_3 = 14.9$ from distribution data is not directly comparable to our "best" $K_3 = 5.6$ above, because the former applies to CCl_4 solutions that are saturated with water. Johnson, Christian, and Affsprung[8] have combined their distribution and water solubility results to obtain information about the hydration of phenol in wet CCl_4 solutions and thence have calculated $K_3 = 4.1$ for association of nonhydrated monomeric phenol to form nonhydrated trimeric phenol in CCl_4. This K_3 value is in good agreement with our K_3 from heats of dilution. The nmr results of Saunders and Hyne[7] have led them to $K_3 = 4.78$ at 21°, also in good agreement with our work. Interpolation of the K_3 values attributed[1] to Rea leads to $K_3 \cong 11$ at 25°.

To the extent that a single equilibrium such as (2) is a realistic representation of the association of phenol in CCl_4 solutions up to $M \cong 2$ mol/l. we believe that our results and those of earlier investigators[1,7,8] provide convincing support for monomers and trimers as the principal species. However, it is necessary to recognize that it may be possible to fit experimental data with equations derived from unrealistic models. We therefore consider our heats of dilution in relation to stepwise association of monomeric phenol to form dimers and trimers. To do so we write eq 15 in terms of both dimers and trimers as

$$M\phi_L = (P_2)\Delta H_2^\circ + (P_3)\Delta H_3^\circ \quad (25)$$

and combine with a material balance equation similar to (20) and expressions for K_2 and K_3 of the form of eq 10. Since we have already shown that our heats of dilution can be interpreted satisfactorily in terms of

only monomers and trimers, we are not surprised to find that we obtain agreement between calculated and experimental heats only when K_2 is considerably smaller than K_3.

Computer calculations show that we can calculate ϕ_L values in good agreement with experimental values when we combine any very small K_2 with $K_3 \cong 5$ and $\Delta H_3^\circ \cong 8.5$ kcal/mol. Since a small K_2 corresponds to small concentrations of dimer, most of these calculations are insensitive to the value of ΔH_2°. Although we have no unambiguous a priori way to choose any particular small K_2 on the basis of our computer calculations with eq 25, we may make some progress by imposing the additional requirements that ΔH_2° be a few kilocalories per mole exothermic and that ΔS_2° be negative as characteristic of association reactions. On this basis, we can select K_2 of the order of 10^{-2} or 10^{-3} and $\Delta H_2^\circ \cong -2$ kcal/mol. Corresponding ΔH_3° values differ very little from the "best" value given earlier, while corresponding K_3 values are slightly smaller than the "best" 5.6 given earlier.

We now consider an explanation for the relative importance of dimers and trimers in CCl_4 solution. The approximate ΔH_2° value above leads to a reasonable hydrogen-bond strength for the dimer. Since ΔH_3° is considerably more than twice ΔH_2°, we suspect that the principal trimeric species may be cyclic with three hydrogen bonds per molecule. Recent quantum mechanical calculations[14] are consistent with this suggestion and the possibility that the total hydrogen-bond energy in the cyclic trimer is greater than 3 times the hydrogen-bond energy in the dimer. Thus the relative magnitudes of ΔH_2° and ΔH_3° and the corresponding equilibrium constants K_2 and K_3 can be understood in terms of a cyclic trimer.

Our heats of dilution of phenol in CCl_4 and some other solvents are discussed elsewhere[15] in relation to the recent ir investigations of Whetsel and Lady[3] and the stepwise association model they have used.

We have measured heats of solution of solid phenol in CCl_4 and combined the results with our ϕ_L values to obtain $\Delta H^\circ = 6.27 \pm 0.04$ kcal/mol for this heat of solution at infinite dilution where all dissolved phenol is monomeric. The only comparable value we know of is a recently reported[16] $\Delta H = 6.27 \pm 0.07$ kcal/mol "at high dilution." We combine our $\Delta H^\circ = 6.27$ kcal/mol above with $\Delta H^\circ = 3.10$ kcal/mol for the heat of solution of solid phenol in water from earlier calorimetric measurements[17] to obtain $\Delta H^\circ = 3.17$ kcal/mol for the transfer reaction previously represented by eq 8.

Values of K_d obtained in this work and earlier by Johnson, Christian, and Affsprung[8] are not directly useful for our present calculation, since these quantities

refer to transfer of phenol from aqueous solution of CCl_4 that is saturated with water and in which some of the monomeric phenol may be associated with water. As mentioned earlier, Johnson, Christian, and Affsprung[8] have taken hydration of phenol in wet CCl_4 into account to obtain a value of K_3 in good agreement with K_3 values obtained by us and by Saunders and Hyne[7] from investigations of anhydrous solutions. It is therefore reasonable to accept their $K_t = 0.46$ for the transfer reaction corrected for hydration of phenol in CCl_4. This K_t then leads to $\Delta G^\circ = 0.46$ kcal/mol for the transfer reaction. We combine ΔG° and ΔH° values to obtain $\Delta S^\circ = 9.1$ cal/deg mol for the transfer represented by eq 8, with an ideal 1 M solution as the standard state.

The increase in entropy accompanying transfer of 1 mol of phenol from 1 l. of water to 1 l. of CCl_4 may be expressed as

$$\Delta S^\circ = 9.1 \text{ cal/deg mol} = \Delta S_v + \Delta S_{ssi} \quad (26)$$

in which ΔS_v and ΔS_{ssi} refer to entropy effects associated with available or free volumes for solute molecules and to solute–solvent interactions, respectively. We can express ΔS_v in terms of the free volumes associated with 1 l. each of water and organic solvent as $\Delta S_v = R \ln (V_{fo}/V_{fw})$ and substitute in (26) to obtain

$$\Delta S_{ssi} = 9.1 + R \ln (V_{fw}/V_{fo}) \quad (27)$$

Since water is well known to have an unusually open structure, we anticipate that V_{fw} for 1 l. of water is greater than V_{fo} for 1 l. of CCl_4 so that $R \ln (V_{fw}/V_{fo})$ is positive and

$$\Delta S_{ssi} > 9.1 \text{ cal/deg mol} \quad (28)$$

Our conclusion from this positive ΔS_{ssi} is that solute–solvent interactions (hydration) in water lead to a loss of entropy considerably greater than do solute–solvent interactions in CCl_4. This conclusion is consistent with our $\Delta H^\circ = +3.17$ kcal/mol for the transfer of phenol from water to CCl_4, which also indicates stronger attraction of phenol for water than for CCl_4.

(14) L. Del Bene and J. A. Pople, *Chem. Phys. Lett.*, **4**, 426 (1969); *J. Chem. Phys.*, **52**, 4858 (1970).

(15) E. M. Woolley and L. G. Hepler, in preparation.

(16) E. M. Arnett, L. Joris, E. Mitchell, T. S. S. R. Murty, T. M. Gorrie, and P. v. R. Schleyer, *J. Amer. Chem. Soc.*, **92**, 2365 (1970).

(17) L. P. Fernandez and L. G. Hepler, *ibid.*, **81**, 1783 (1959).

Solvation Enthalpies of Hydrocarbons and Normal Alcohols

in Highly Polar Solvents[1]

by C. V. Krishnan and Harold L. Friedman*

Department of Chemistry, State University of New York at Stony Brook, Stony Brook, New York   11790
(Received March 5, 1971)

The heats of solution of the normal alcohols through hexanol, of pentane, hexane, and heptane, and of benzene, toluene, and ethylbenzene have been measured in several of the highly polar solvents and solvent mixtures that are often used for ionic solutions.   The study of the alcohol data leads to an ordering of these solvents in terms of relative base strengths which is compared with some other measures of the solvent basicities.   The study of the chain-length dependence of the heats for the alcohols, together with the heats for the hydrocarbons, shows that these solvents may be ordered in a *lipophilic* series according to their ability to solvate alkyl chains. A crude theory of the effect is described which relates it to molecular properties and "predicts" a difference in the solvation of hexane and benzene by hydrogen-bonded solvents which is also shown by the data.   The results strongly indicate that when alkyl chains (and benzene) dissolve in hydrogen-bonded solvents such as methanol (but not water), they fit between the chains of hydrogen bonds without disrupting the chains.

1. Introduction

In an earlier paper[2] we reported new data for heats of solution of alcohols and some other alkyl derivatives in water, D_2O, propylene carbonate, and dimethyl sulfoxide and discussed their interpretation, especially in terms of additive group contributions to the partial molar enthalpy of the solutes at infinite dilution in the nonaqueous solvents.   The data and interpretation proved to be useful in later studies of the enthalpies of alkylammonium ions in the same solvents.[3,4]

In the present work the study of the nonelectrolytes is extended to a large number of pure solvents, listed in Table I together with some relevant properties, and to several solvent mixtures.   These have all been selected in view of their applicability as solvents for the study of ionic reactions.   The objective is not only to make the nonelectrolyte enthalpy data available to help in the interpretation of the properties of ions with alkyl substituents in these additional solvents but also to see how far the simple behavior of the enthalpies of alkyl chains in PC and in DMSO holds up in other very polar solvents.

2. Experimental Section and Results

The instrumental aspects have been described previously.[5]   The hydrocarbons and alcohols used as solutes were all from earlier preparations.   The various solvents were purified by standard methods,[2,5,6] dried, and vacuum distilled, under nitrogen atmosphere in most cases.   The solute concentrations employed were all well below 10^{-2} M so that solute–solute interactions can be neglected.   The dissolution and mixing processes were practically complete within 2–10 min except for hydrocarbon solutes in formamide.

All the measurements were made at 25.0°.   The results for pure solvents are given in Table II.   The values are averages of two or more measurements agreeing within 0.05 kcal/mol except for hydrocarbons in aprotic solvents and in formamide, in which cases the range is 0.2 kcal/mol.

3. Solvation Enthalpies of Alcohols

The heats of solution of the alcohols in D_2O were measured because of considerable disagreement between the values obtained by Arnett and McKelvey[6] and those of Kresheck, Schneider, and Scheraga[7] which played an important role in our earlier work.[2]   The new results in Table II, when combined with the heats of solution in water reported earlier[2] give enthalpies of transfer to D_2O from H_2O which agree with those first reported[7] within 0.01 kcal/mol for MeOH, EtOH, PrOH, and AmOH and within 0.03 kcal/mol for BuOH.

The heats of solution in the various solvents (Table II) are combined with heats of vaporization[8] to give the desolvation enthalpies $H°(\text{ROH in gas}) - \bar{H}°(\text{ROH}$

(1) Grateful acknowledgment is made of the support of this work by the National Institutes of Health.

(2) C. V. Krishnan and H. L. Friedman, *J. Phys. Chem.*, **73**, 1572 (1969).

(3) C. V. Krishnan and H. L. Friedman, *ibid.*, **73**, 3934 (1969).

(4) C. V. Krishnan and H. L. Friedman, *ibid.*, **74**, 3900 (1970).

(5) H. L. Friedman and Y. C. Wu, *Rev. Sci. Instrum.*, **36**, 1236 (1965).

(6) E. M. Arnett and D. R. McKelvey in "Solute–Solvent Interactions," J. F. Coetzee and C. D. Ritchie, Ed., Interscience, New York, N. Y., 1969.

(7) G. C. Kresheck, H. Schneider, and H. A. Scheraga, *J. Phys. Chem.*, **69**, 3132 (1965).

(8) See Table III of ref 2 for a summary of the data for standard enthalpies of vaporization.   The first entry for each alcohol has been selected for use here.   For hexanol $\Delta H_{\text{vap}} = 15.00$ kcal/mol.

Table I: Properties of Solvents[a]

Solvent S	Abbreviation	Dielectric constant	Kirkwood g factor	Dipole moment, D	Molecular polarizability, Å³	Solubility parameters	Z values, kcal/mol	Desolvation enthalpy of the hydrogen bond.[d] kcal/mol
Nitromethane	MeNO₂	36.7		3.46	4.95	12.60	71.5[c]	5.52 (5.59)
Dimethyl sulfoxide	DMSO	45.0	0.95[g]	3.96	7.97	12.80[i]	71.1	8.13 (8.29)
Acetonitrile	MeCN	36.02		3.97	4.45	11.90	71.3	6.13 (6.05)
Propylene carbonate	PC	65.1	1.18[e]	4.94	8.56	12.30	71.9[c]	6.20 (6.33)
Dimethylformamide	DMF	36.7	1.0[f]	3.86	7.91	11.82[i]	68.5	7.85 (7.83)
3-Methyl sulfolane	3-MS	43.0		4.30	11.38	11.63[i]	77.5[b]	6.15 (6.35)
Dimethylacetamide	DMA	37.8	1.1[f]	3.79	9.65	10.87[i]	66.9	8.18 (8.17)
Formamide	FA	109.5	1.5[f]	3.71	4.22	18.81[i]	83.3	7.58 (7.18)
Methanol	MeOH	31.5	2.94[h]	1.71	3.24	14.37	83.6	7.87 (7.68)
Ethanol	EtOH	24.3	3.04[h]	1.73	5.15	12.76	79.6	7.82 (7.38)
1-Butanol	n-BuOH	17.5	3.21[h]	1.81	8.82	11.43	77.7	7.75 (7.54)
Water	W	78.5	2.7[h]	1.83	1.47	25.0	94.6	7.68

[a] Many of the data are taken from the compilation given by A. J. Parker, *Chem. Rev.*, **69**, 1 (1969). [b] Value for sulfolane. [c] From the linear $E_T(30)$ vs. Z relationship, taken from E. M. Kosower, "An Introduction to Physical Organic Chemistry," Wiley, New York, N. Y., 1968, p 303. [d] The data for $(HO\cdots H)_{g\leftarrow S}$ obtained after correcting for the difference in $(-CH_2-)_{g\leftarrow S}$ and $(CH_3-)_{g\leftarrow S}$ are given within parentheses. [e] L. Simeral and R. L. Amey, *J. Phys. Chem.*, **74**, 1443 (1970). [f] S. J. Bass, W. I. Nathan, R. M. Meighan, and R. H. Cole, *ibid.*, **68**, 509 (1964). [g] R. L. Amey, *ibid.*, **72**, 3358 (1968). [h] G. Oster and J. G. Kirkwood, *J. Chem. Phys.*, **11**, 175 (1943). [i] This is estimated from the boiling point and Trouton's rule and is more uncertain than other values derived from measured heat of vaporization.

Table II: Enthalpies of Solution of Various Solutes at 25° (kcal/mol)[a]

Solute	Propylene carbonate[b]	Dimethyl sulfoxide[b]	Dimethylformamide	Dimethylacetamide	Nitromethane	Acetonitrile	3-Methyl sulfolane	D₂O	Methanol	Ethanol	1-Butanol	Formamide
CH₃OH	1.50	−0.34	−0.14	−0.56	2.27	1.42	1.36	−1.92	...	0.00	0.00	0.20
C₂H₅OH	2.02	0.29	0.30	−0.11	2.84	1.91	1.86	−2.72	0.04	...	0.00	0.51
n-C₃H₇OH	2.27	0.61	0.50	0.10	3.28	2.27	2.16	−2.80	0.13	0.04	0.00	0.73
n-C₄H₉OH	2.53	0.95	0.70	0.25	3.66	2.52	2.38	−2.64	0.24	0.10	...	0.91
n-C₅H₁₁OH	2.77	1.29	0.90	0.45	4.06	2.77	2.56	−2.32	0.40	0.16	0.05	1.07
n-C₆H₁₃OH	3.02	1.62	1.10	0.62	4.31	3.00	2.78		0.51	0.25	0.10	1.37
n-C₅H₁₂	2.19	2.75	1.62	1.50	2.82	2.02	1.98		0.91	0.39	0.25	...
n-C₆H₁₄	2.52	3.18	1.89	1.74	3.28	2.39	2.24		1.12	0.60	0.33	1.23
n-C₇H₁₆	2.84	3.62	2.18	2.00	3.79	2.78	2.51		1.32	0.78	0.42	1.51
C₆H₆	0.37	0.63	0.06	−0.05	1.02	0.62	−0.02		0.37	0.39	0.60	1.12
C₆H₅CH₃	0.56	0.90	0.16	0.09	1.22	0.78	0.12		0.45	0.38	0.51	1.18
C₆H₅C₂H₅	0.76	1.12	0.37	0.25	1.58	0.97	0.23		0.56	0.46	0.54	1.42
C₆H₅Cl	0.41	0.52					−0.15		0.21	0.08		
C₆H₅Br	0.54	0.52					−0.09					
C₆H₅I	0.82	0.31										

[a] The entries are values of the standard enthalpy of solution of the pure solute Y in solvent S; $\Delta H° = \bar{H}°(Y \text{ in } S) - \bar{H}(\text{pure}) \equiv (Y)_{S\leftarrow pure}$. [b] See ref 2.

in solution) shown in Figure 1, where results of earlier studies for the solvents H₂O, DMSO, and PC are also included. It is remarkable that every one of these curves, except that for the solvent water, has a long portion which is accurately linear.

The apparent linearity is retained even when the same data are plotted as enthalpies of transfer to one solvent from another, for example[2,9]

$$(ROH)_{PC\leftarrow DMSO} \equiv \bar{H}°(ROH \text{ in } PC) -$$

$$\bar{H}°(ROH \text{ in } DMSO) \quad (1)$$

as a function of N the number of carbon atoms in the alkyl chain. These linearities are most easily understood if it is assumed that in the gas phase and in all of these solvents, possibly except water, the solute alkyl chains are extended so that in the most probable configurations they do not overlap themselves. Then the effect of adding one more CH₂ group in the chain is additive, and, in fact, the slope of the line for the solvent S is just

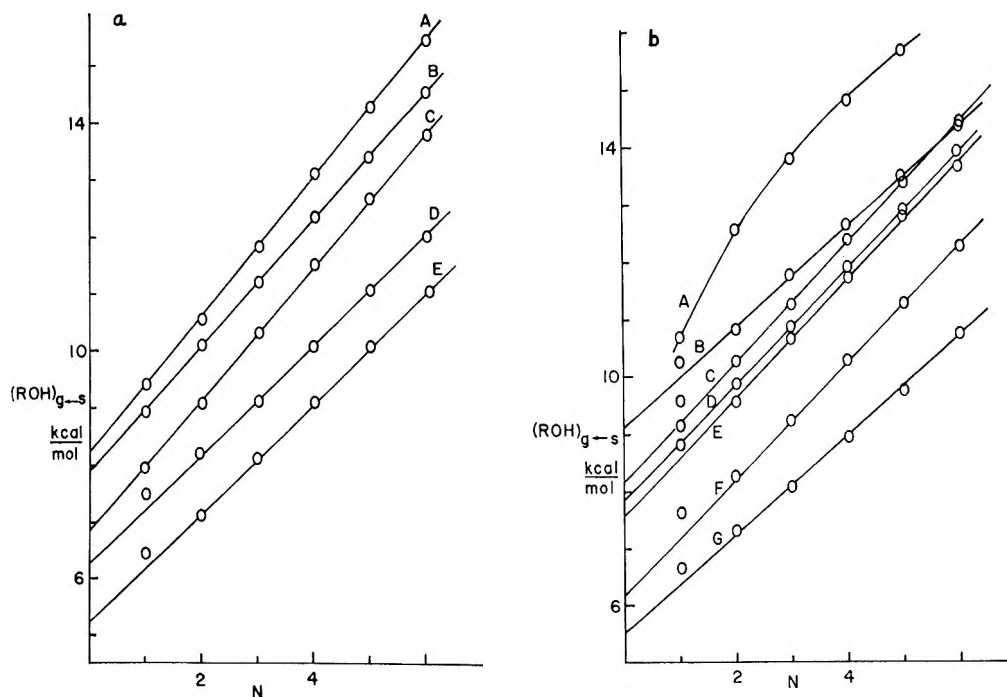(9) This simple notation for enthalpies of transfer is described in detail in ref 2.

Figure 1. (a) Desolvation enthalpy of the normal alcohols $n\text{-}C_NH_{2N+1}OH$ in various solvents as a function of N, the number of carbon atoms. Line A is for n-BuOH; its slope is $s = 1.20$ kcal/methylene group, and $\Delta = 0.5$ kcal/mol has been added to each datum to improve the legibility of the graph. The same information is given for each of the other lines: B, MeOH, $s = 1.10$, $\Delta = 0$; C, EtOH, $s = 1.15$, $\Delta = -1$; D, MeCN, $s = 0.98$, $\Delta = 0$; E, PC, $s = 0.97$, $\Delta = -1$. (b) This is an extension of part (a): A, W, $s = ?$, $\Delta = 0$; B, DMSO, $s = 0.88$, $\Delta = 1$; C, DMA, $s = 1.03$, $\Delta = 0$; D, DMF, $s = 1.01$, $\Delta = 0$; E, FA, $s = 1.02$, $\Delta = 0$; F, 3-MS, $s = 1.00$, $\Delta = 0$; G, MeNO$_2$, $s = 0.86$, $\Delta = 0$.

$$(-CH_2-)_{g \leftarrow s}$$
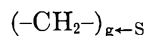
the desolvation enthalpy of the methylene group in the solvent.

While this simple behavior for the aprotic solvents CH_3CN, CH_3NO_2, 3-MS, DMF, and DMA might have been expected on the basis of the experience[2] with PC and DMSO, it is more surprising to find that it holds up for the alcoholic solvents and formamide as well. This behavior sharply distinguishes these hydrogen-bonding solvents from water, where the nonlinear behavior has been used as a basis for estimating the "structural" contribution to the solvation of alkyl chains.[2,3] We shall return in a later section to a deeper discussion of the desolvation effects measured by the slopes in Figure 1.

The $N = 0$ intercepts of the straight-line portions in Figure 1 are listed in Table I. The simplest interpretation of each is[2] that it measures

$$(H\cdots OH)_{g \leftarrow s}$$
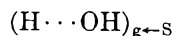
the sum of the desolvation enthalpy of a hydrogen atom H$\cdots$ of the terminal methyl group plus the desolvation enthalpy of the hydroxyl group $\cdots$OH. The latter effect is dominant, of course, and it is not too serious a mistake to neglect the desolvation of the hydrogen atom (the difference in desolvation of a CH_3 group and a CH_2 group[2]) so these intercepts in Figure 1 may be regarded as approximate measures of

the base strengths of the liquid solvents in reaction with the "acid" $\cdots$OH. At any rate various corrections for the hydrogen atom effect have been tried and they do not change the order of solvent base strengths which one may derive from these data, except in the case of pairs of solvents such as DMSO–DMA which are very close in base strength by this measure anyway.

As shown in Figure 2,[10-13] $(H\cdots OH)_{g \leftarrow s}$ as a measure of base strength of highly polar solvents does correlate very well with a number of others involving different acid probes. While this may not be surprising, neither can it be taken for granted because there are a number of clear counter examples.[14,15] Even for a given acid the order of strengths of a series of bases may depend on whether ΔG or ΔH of the interaction is used as a measure.[16] However in the attempt to understand the important chemical concept of solvent

(10) V. Gutmann, "Coordination Chemistry in Nonaqueous Solutions," Springer-Verlag, Vienna, 1968.

(11) R. S. Drago, B. Wayland, and R. L. Carlson, J. Amer. Chem. Soc., 85, 3125 (1963).

(12) R. H. Erlich, E. Roach, and A. I. Popov, ibid., 92, 4989 (1970).

(13) C. V. Krishnan and H. L. Friedman, J. Phys. Chem., 75, 3606 (1971).

(14) E. M. Arnett, R. P. Quirk, and J. J. Burke, J. Amer. Chem. Soc., 92, 1260 (1970).

(15) R. S. Drago and K. F. Purcell, Progr. Inorg. Chem., 6, 271 (1964).

(16) E. M. Arnett, Progr. Phys. Org. Chem., 1, 223 (1963).

Table III: Experimental and Calculated Terms for Lipophilic Series

| Solvent S | Y = n-hexane | | | Y = benzene | | |
	Exptl $(Y)_{g\leftarrow s}$	Calcd $(Y)_{g\leftarrow s}^{el}$	$(Y)_{g\leftarrow s}^{sp}$	Exptl $(Y)_{g\leftarrow s}$	Calcd $(Y)_{g\leftarrow s}^{el}$	$(Y)_{g\leftarrow s}^{sp}$
$MeNO_2$	4.26	1.04	3.33	7.07	0.84	6.39
DMSO	4.36	1.38	3.04	7.46	1.10	6.27
MeCN	5.15	1.38	4.24	7.47	1.10	6.78
PC	5.02	2.14	3.73	7.72	1.70	6.57
DMF	5.65	1.30	4.35	8.03	1.04	6.82
3-MS	5.30	1.60	4.56	8.11	1.28	6.90
DMA	5.80	1.24	5.35	8.14	1.00	7.19
FA	6.31	1.20	−10.45	6.97	0.96	7.36[a]
MeOH	6.42	0.26	0.41	7.72	0.20	7.52[a]
EtOH	6.94	0.26	3.10	7.70	0.20	7.50[a]
n-BuOH	7.21	0.28	4.81	7.49	0.22	7.30[a]

[a] Calculated using an "effective" solubility parameter; see text.
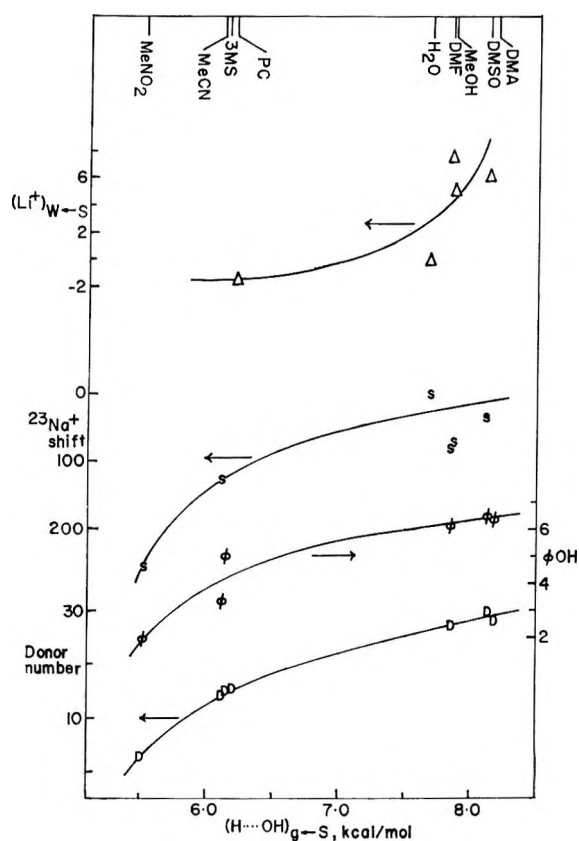
Figure 2. Correlation of various solvent properties with the base strengths measured by the solvation enthalpy of an alcoholic hydroxyl group. The abscissa is the value of $(H\cdots OH)_{g\leftarrow s}$ for the solvent. The solvents are listed at the top of the figure. They are in the same order as in Table I except for H_2O and MeOH. The other alcohols are omitted from this figure. The lines are drawn just to connect the data with simple curves to the extent possible. From the bottom to the top they show the correlation with the donor number of Gutmann,[10] the heat of reaction of the solvent molecules with phenol in dilute solution in CCl_4 as measured by Drago, Wayland, and Carlson,[11] the chemical shift of $^{23}Na^+$ in dilute solution in the solvent measured by Erlich, Roach, and Popov,[12] and the enthalpy of transfer of lithium ion to water from the solvent.[13]

basicity it seems useful to know not only about the exceptions but also about regularities such as those exhibited in Figure 2. Moreover it should be noted that this measure of solvent action correlates poorly with some others, not related uniquely to basicity, such as the dielectric constant, the solubility parameter, and Kosower's Z number, all given in Table I.

4. Solvation Enthalpies of Hydrocarbons

The alkanes below pentane are too volatile to use with the available calorimeter while the alkanes beyond heptane and the alkylbenzenes beyond ethylbenzene dissolve too slowly in many of the solvents of interest, so the present study is restricted to rather small variations in the alkyl chain length. However it seems important to obtain such hydrocarbon data as are accessible in order to see whether the linear behavior shown in Figure 1 may also be found in molecules without the polar head group. Some results, expressed as desolvation enthalpies $(R-H)_{g\leftarrow s}$ or $(R-Ph)_{g\leftarrow s}$, are given in Table III.

Quantities corresponding to the slope in Figure 1 may be examined. There are various estimates of the desolvation enthalpy of a methylene group $(-CH_2-)_{g\leftarrow s}$ which one may derive from the data in Table II. One is the increment $(C_6H_{14})_{g\leftarrow s} - (C_5H_{12})_{g\leftarrow s}$, which we may call R6-5, and the corresponding increment to heptane from hexane, which we may call R7-6. Also we have the toluene–benzene increment AR1-0 and the ethylbenzene–toluene increment AR2-1. One other independent estimate of the desolvation enthalpy of the methylene group which may be derived from these data is $(C_6H_{14})_{g\rightarrow s}/6$. All of these, together with the slopes from Figure 1, are shown in Figure 3.

By comparing Figure 3 and Figure 1 one can see that the linearity in the desolvation enthalpy in the series pentane to heptane is about as good as in the series from propanol to pentanol or hexanol and somewhat better than in the series from benzene to ethylbenzene.
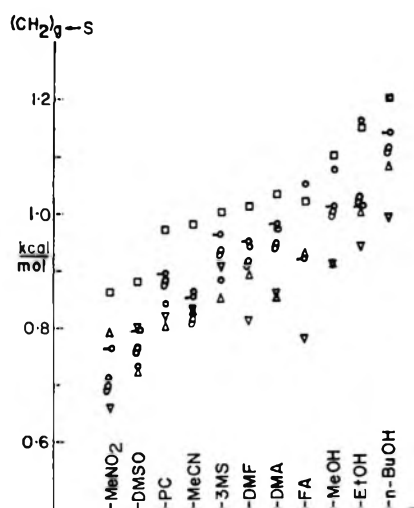
Figure 3. The desolvation enthalpy of methylene groups in various solvents estimated from several kinds of calorimetric data: □, slope from Figure 1; −O, R6-5; θ, R7-6; O, $^1/_6(C_6H_{14})_{g \leftarrow s}$; △, AR1-0; ▽, AR2-1.

It is hard to say more because most of the discrepancies are scarcely larger than might be expected from the errors in the calorimetry, except that there is some systematic trend in the discrepancies from linearity, as though in the hydrocarbon solutes the longest chains were beginning to coil back on themselves.

The data from Figure 1 are mostly appreciably larger than the methylene desolvation enthalpies from the hydrocarbon data. It is hard to find an explanation for this in terms of experimental errors and it would be of interest to inquire about the physical origin of such an effect. It might be traced to the hydroxyl group having an effect on the distribution of conformations of the alkyl chains attached to it, presumably attracting the end of the chain under vacuum (relevant to the gaseous state of the alcohol) and repelling it in solution in a polar solvent. It is hard to say more, especially because such effects, which involve an analysis of electrical fields about solutes in polar solvents, are associated with free energy contributions and enthalpy contributions of opposite sign.

Now by disregarding small inconsistencies among the data one can reach the following conclusions from Figure 3. (1) The dominant features of all these data are consistent with the hypothesis that in all these media in the probable conformations the alkyl chains are extended rather than coiled back on themselves. (2) There is a regular trend in $(-CH_2-)_{g \leftarrow s}$; however it is estimated, which establishes what one might term a *lipophilic series* for these highly polar solvents, with butanol the most lipophilic and nitromethane the least.

It must be remarked that the trend in lipophilic character of these solvents is not very large by this measure, corresponding to less than a twofold change in the desolvation enthalpy of a methylene group.
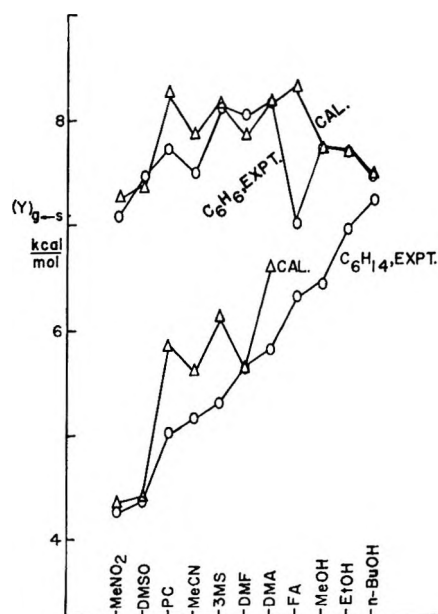
Figure 4. Desolvation enthalpies of hexane and benzene. Experimental data compared with calculation from eq 2. The order of the solvents on the abscissa is the same as in Figure 3: O, experimental; △, calculated.

We next turn to an analysis of the lipophilic series, to see whether it can be understood in terms of the molecular properties of these solvents.

5. On the Molecular Interpretation of the Lipophilic Series

For the purpose of this section it is better to represent the lipophilic series in terms of the desolvation enthalpies of entire molecules such as hexane rather than in terms of methylene group contributions. As is clear from Figure 3, the same series is obtained in either case. The advantage of basing the series on the desolvation of entire molecules is that the data, at least, are more definite than for group contributions. An interesting aspect, which is exploited below, is shown in Figure 4; using benzene rather than hexane as a solute, the series of aprotic solvents is almost the same while the series of hydrogen-bonded solvents is reversed.

We shall explore the applicability of the following approximate equation for the desolvation enthalpy of solute Y in solvent S

$$(Y)_{g \leftarrow S} = (Y)_{g \leftarrow S}{}^{el} + (Y)_{g \leftarrow S}{}^{sp} \qquad (2)$$

Here the electrical contribution derives from the interaction of the electrical dipole μ_S of a solvent molecule with the polarizability α_Y of the solute

$$(Y)_{g \leftarrow S}{}^{el} \cong 2\alpha_Y \mu_S{}^2/r^6 \qquad (3)[17]$$

(17) This equation, with omission of the factor 2, was used in ref 2, Table IX. This hardly makes any difference since an error in this factor can be compensated by a change in r by a factor of $2^{1/6}$ = 1.08 and r is rather uncertain anyway. A more general expression for the quantity of interest is $(Y)_{g \leftarrow S} = 2\alpha_Y \mu_S{}^2 \langle \cos^2 \theta/r^6 \rangle$, where θ is the angle between the dipole and the line of centers of the dipole and polarizable particle, r is the instantaneous separation, and $\langle \ldots \rangle$ specifies an average over an equilibrium ensemble. Essentially in what follows we assume that $\langle (\cos \theta)^2/r^6 \rangle^{-1/6} = 4$Å in every case.

where r is the distance from the center of Y to the center of a solvent molecule in the solution. The solubility parameter contribution to eq 2 is

$$(Y)_{g \leftarrow S}{}^{sp} \equiv V_Y \delta_S (2\delta_Y - \delta_S) \qquad (4)^{18}$$

where V_Y is the molar volume of the solute and the δ_X's are the *solubility parameters* of species X appearing in the regular-solution theory of Scatchard, van Laar, Hildebrand, and Scott[19]

$$\delta_X \equiv \{[(X)_{g \leftarrow liq} - RT]/V_X\}^{1/2} \qquad (5)$$

where $(X)_{g \leftarrow liq}$ is the standard molar enthalpy of vaporization of species X. First we review the basis for these equations.

In an earlier study[2] it was pointed out that the enthalpy of transfer of the groups $-CH_2-$, CH_3-, and $C_6H_5 \cdots H$ to PC from DMSO could be understood if it were assumed that the dominant contribution is $(Y)_{g \leftarrow S}{}^{el}$ with $r = 4$ Å.[20,21] However this term did not account for the solvation enthalpies of hydrocarbon groups in either solvent alone. Moreover, referring to Figure 4, one sees that this term alone does not generally account for differences in lipophilic strength, even qualitatively. For example, PC with a larger dipole moment than DMA is less lipophilic.

To understand these solvation effects in more detail it seems reasonable to try to include a term accounting for the enthalpy associated with the formation of a cavity in the solvent to accommodate the solute particle and a term accounting for the enthalpy of interaction by van der Waals forces (dispersion forces, London forces) of the solute with the solvent molecules next to it in solution. The enthalpy which may be estimated from the regular solution theory seems quite suitable for this purpose. The term $2\delta_Y \delta_S V_Y$ in eq 4 derives from the geometric-mean approximation for estimating the London force between unlike molecules while the term $-V_Y \delta_S{}^2$ accounts for the cavity effect in an elementary way. Moreover the more general equation for mixtures from which eq 4 has been obtained by specialization gives a usefully accurate representation of the free energy properties of mixtures of nonpolar molecules, as shown in detail by Hildebrand and Scott.[19] In the present application one of the assumptions underlying the free energy equation, namely, that the entropy of mixing is ideal in regular solutions, is not required so enthalpy changes are obtained more directly.

While it cannot be assumed that one can add the cavity plus van der Waals contributions to the desolvation enthalpy deduced from regular-solution theory for nonpolar molecules to the electrical term in eq 3 and thereby get an adequate theory for solutions of nonpolar solutes in polar solvents, that is just the approximation which is expressed in eq 2 and which will be tested here. Also it will be assumed that in applying eq 3, $r = 4$ Å is appropriate to each of the

systems considered here,[17] although perhaps one could do somewhat better by estimating it from models in each case.

The experimental desolvation enthalpies and the calculated contributions to them are given for typical solutes in Table III and a comparison of experimental and calculated values is given in Figure 4. The order of the solvents in both cases is chosen as the order of the slopes in Figure 1, except that the aprotic solvents are segregated from the hydrogen-bonded solvents. The results for aprotic solvents will be discussed first.

It seems clear that for the aprotic solvents the desolvation enthalpies calculated by eq 2 give quantitative agreement with the experimental data within 20% and also reproduce the order of the lipophilic series about as well as it is established by any one set of experimental data (of Figure 3). One can see from Table III that the order of the electrical contributions does not give this series but the order of the solubility parameter contributions does very well. In fact the agreement of calculated and experimental values in Figure 4 would not be degraded if we uniformly estimated $(Y)_{g \leftarrow S}{}^{el} = 1$ kcal/mol for the aprotic solvents.

For the hydrogen-bonded solvents one finds that the desolvation enthalpies calculated as described above give very poor agreement with experiment, as may be seen by examining the results for hexane in Table III. The enthalpy calculated in this way is not shown in Figure 4 for the hydrogen-bonded solvents. Now the linearity of the graphs in Figure 1, even for the hydrogen-bonded solvents except water, suggests that a large part of the simply interpreted behavior of the aprotic solvents does carry over to solvents such as MeOH which can be built up from linear chains of hydrogen bonds, rather than branched three-dimensional networks as in the case of water. (Since form-

(18) This equation may be obtained by specializing the equation in footnote 14 of ref 3, or it may be deduced directly from the regular solution theory.[19]

(19) J. H. Hildebrand and R. L. Scott, "The Solubility of Nonelectrolytes," 3rd ed, Reinhold, New York, N. Y., 1950.

(20) As already pointed out[17] there is a factor of 2 error in the earlier work which is not significant. Also, in comparing $(Y)_{g \leftarrow S}{}^{el}$ with experiment one encounters a problem in estimating how many dipoles interact with a given polarizable group Y. However, it can be seen in the following way that this is equivalent to the problem of choosing a value for r, at least for molecules or groups Y which are not too large and compact. Assume that

$$(Y)_{g \leftarrow S}{}^{el} = \sum_{j=1}^{n} 2\alpha_j \mu_j{}^2 / r_j{}^6$$

where the sum is over n dipoles μ_j interacting with Y. Each polarizes a part j of Y having polarizability α_j and mean separation r_j. Now if all these terms are equal, we may write $\alpha_j = \alpha_Y/n$ and $\mu_j = \mu_S$, and we recover eq 3 with $r = r_j$. Of course this approximation leaves out the mutual interaction of the dipoles. However it does not seem that the mutual interaction is necessarily strongly affected by the presence of Y. Moreover, taking the mutual interaction into account is enormously difficult.[21]

(21) D. W. Jepsen, J. Chem. Phys., **44**, 774 (1966); **45**, 709 (1966).

amide, unlike water, exhibits a linear graph in Figure 1, we shall assume that in the liquid at 25° it forms mainly linear chains of hydrogen bonds although structural considerations alone would allow branched networks.)

The topological distinction between the hydrogen-bonded networks in water and methanol suggest a picture of the solvation of oily groups by the latter, namely, that alkyl chains or hydrocarbon molecules which are not too large and compact are accommodated between the chains of hydrogen bonds without the extensive hydrogen-bond disruption or rearrangement which would be required in water. According to this picture, δ_{MeOH} based on the experimental heat of vaporization of MeOH is too large to use in eq 4 because the experimental heat of vaporization accounts for the disruption of hydrogen bonds that do not play a direct role in either the cavity enthalpy term or the van der Waals stabilization term in solvating oily groups.

To test this quantitatively, to the extent possible in the framework of these very elementary considerations, we may use the hexane data to calculate an "effective" solubility parameter δ_S' by assuming that eq 2–4 are valid but that the appropriate δ_S is not independently known for the hydrogen-bonded solvents. These δ_S' values are as follows: FA, 10.50; MeOH, 9.50; EtOH, 8.70; BuOH, 7.60. Then these effective solvent properties are used to calculate the solubility parameter contribution to the solvation enthalpy of a different solute, benzene, with the results shown in Table III and Figure 4. These calculated values even reproduce the trend which is in the opposite direction for C_6H_6 as C_6H_{14}, so it may be concluded that the above picture of solvation of oily groups by these hydrogen-bonded solvents has some predictive value.

The calculations just described have also been carried through for all the other hydrocarbon solutes in Table II. The results parallel those already presented. Furthermore the methylene group contributions R6-5, Ar1-0, etc., which may be obtained by taking differences between calculated solvation enthalpies, fall in the range 1.0 ± 0.3 kcal/mol, which seems quite satisfactory considering the uncertainties. However, if these calculated methylene group contributions were plotted in Figure 3, their scatter would obscure any trend representing the lipophilic series which one might hope to find. In all these calculations the effective solubility parameters derived from the hexane data as described above have been used for the hydrogen-bonded solvents.

It seems important to remark on one other aspect of these calculations, namely, in calculations for heats of solution in hydrogen-bonded solvents using the experimental solubility parameters δ_S rather than the adjusted ones δ_S', the desolvation enthalpy given by

eq 2 is much closer to the experimental one when the solute is benzene than when it is hexane. Perhaps this indicates that benzene does not dissolve in alcohols without disrupting some hydrogen bonds, so that the solvent's experimental solubility parameter is more appropriate to it than to hexane. However, the "calculated" values in Table III fit the data without allowing for this possibility.

6. Mixed Solvents

The following studies in mixed solvents were undertaken to provide additional tests of some of the conclusions reached above as well as to provide data about some mixed solvents that are useful for other purposes.

The new heat of solution data are given in Table IV.

Table IV: Enthalpies of Solution of Various Solutes at 25° (kcal/mol)

Solvent, vol fractions	Solute		
	C_5H_{12}	C_6H_{14}	C_7H_{16}
0.7 MeCN, 0.3 DMA	1.92	2.28	2.64
0.85 DMF, 0.15 MeNO$_2$	1.84	2.13	2.45
0.87 MeCN, 0.13 MeOH	2.06	2.46	2.90
0.55 MeCN, 0.45 MeOH	1.76	2.06	2.42
0.16 MeCN, 0.84 MeOH	1.15	1.41	1.75
0.88 MeCN, 0.12 FA	2.15	2.52	2.97
0.49 MeOH, 0.51 EtOH	0.74	0.93	1.13
0.80 MeOH, 0.20 n-BuOH	0.65	0.87	1.09
0.88 MeOH, 0.12 FA	1.09	1.37	1.65
0.83 MeOH, 0.17 W	2.08	2.57	3.03
0.90 MeOH, 0.10 W	1.53	1.88	2.20
0.93 EtOH, 0.07 W	0.92	1.15	1.38

To compare these results with the predictions of eq 2 one may use the fact that the solubility parameter for a mixture of x volumes of solvent S and $1 - x$ volumes of solvent R is given by[19]

$$\delta(x) = x\delta_S + (1 - x)\delta_R \qquad (6)$$

If this expression for the solubility parameter of the solvent is substituted in eq 4, then one finds that solubility parameter term in the desolvation enthalpy of a solute Y in the mixture depends linearly on the volume fraction x of the mixture as long as $|\delta(R) - \delta(S)| \ll \delta(S)$ which is the case for the systems of interest here. Since the electrical term, eq 3, is relatively small and is also expected to be nearly linear in the volume fraction, it may be concluded that eq 2 predicts that the solvation enthalpy in a mixed solvent is a linear function of the volume fraction.

Comparison with the present data for hexane as solute is made in Figure 5. The data are not extensive but it is clear that for mixtures of two aprotic solvents or two alcohols, the solvation enthalpy is nearly linear in the volume fraction. In these cases one could calculate the solvation enthalpy of hexane in the
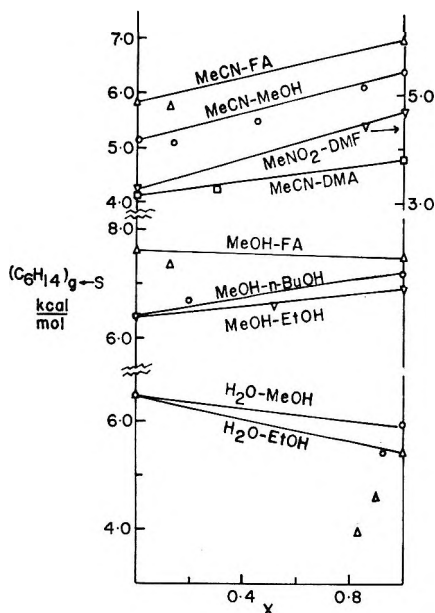
Figure 5. Desolvation enthalpy of hexane in various solvent mixtures as a function of volume fraction x of the mixture. For easy legibility the amount Δ kcal/mol has been added to the data in some cases as follows: MeNO$_2$–DMF, $\Delta = -1$; MeCN–DMA, $\Delta = 0.8$; MeOH–FA, $\Delta = 1.2$.
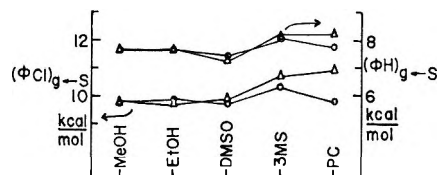

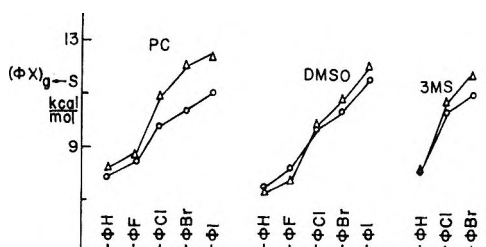Figure 6. Desolvation enthalpies of benzene and chlorobenzene; comparison of experiment and eq 2. The solvents are arranged in order of increasing dipole moment: O, experimental; Δ, calculated.

Figure 7. Comparison of eq 2 with experimental data for desolvation enthalpies of benzene and monohalobenzenes in three solvents: O, experimental; Δ, calculated.

mixture with fair accuracy from eq 2–6, using the experimental solubility parameters δ_S for the pure aprotic solvents and those designated above as δ_S' for the hydrogen-bonding solvents.

It is of course to be expected from the picture of lipophilic solvation in alcohols and formamide described above that mixtures of these solvents with aprotic solvents would not conform to eq 2–6 and the solvation enthalpy would not be a linear function of the volume fraction. Several examples consistent with this are shown in Figure 5. In these solvent mixtures the hydrogen-bond chains characteristic of the pure alcohols or formamide must be largely disrupted so the effective solubility parameter of the mixture is not given by eq 6. This is found even in the formamide–methanol mixture.

Finally, solutions of hexane in mixtures of water with methanol or ethanol also do not conform to eq 6 as one can see from Figure 5. This confirms what one also sees in Figure 1, that, from the point of view of lipophilic solvation, there is a qualitative difference in the hydrogen-bonded structure of water and the alcohols. This is not surprising, but it seems important to have experimental evidence even for obvious points in the study of solvation phenomena, where so many obvious concepts later turn out to be inconsistent with experimental observations.

Using the experimental heats of solution of hexane in the alcohol-rich mixtures with water, the δ_S' derived above for the alcohols, and eq 2–6, one can derive an effective solubility parameter $\delta_S' = 22$ for water in these mixtures. This is close to the experimental

value $\delta_W = 25$ derived from the heat of vaporization and molar volume of pure water but far from the effective solubility parameter $\delta_W' = 7.3$ derived from eq 2–5 by fitting them to the hydration energy of hexane.[22] The latter presumably involves the structural solvation effects which are peculiar to water as a solvent.[2]

The treatment shown in Figure 5 can be extended to the data for pentane and heptane in Table IV, except that for these solutes there are no reliable data for the heat of solution in water. The behavior found is completely analogous to that shown for hexane, so it is not presented here.

7. Halobenzenes

It was reported earlier that, judging from the solvation enthalpies, there was a qualitative difference in solvation of alkylbenzenes and halobenzenes in PC and, possibly, in DMSO as well. It now seems useful to find whether those observations are accounted for when one uses eq 2. To investigate this the enthalpies of solution of some of the halobenzenes were obtained in some additional solvents, as reported in Table I.

The monohalobenzenes all have dipole moments of 1.68 ± 0.03 D so one may expect to find it necessary, in this application, to extend eq 2 by adding a dipole–dipole interaction term

$$(Y)_{g \leftarrow S}^{dd} = \mu_Y \mu_S \langle f(\Omega)/r^3 \rangle \tag{7}$$

where $f(\Omega)$ is a known function depending on the orientations of the dipoles and where the other symbols

(22) D. S. Reid, M. A. J. Quickenden, and F. Franks, Nature (London), 224, 1293 (1969).

are readily identified by comparison with eq 3. To see whether this term is important the experimental desolvation enthalpies are compared with the calculated values obtained by using eq 2 as shown in Figure 6, where the solvents are arranged in order of increasing dipole moment μ_S. In the calculations for hydrogen-bonded solvents the effective solubility parameters δ_S' have been used.

From Figure 6 it may be seen the defect of eq 2 in this application is not correlated with the solvent dipole. In fact, the agreement seems remarkably good, as shown by plotting the calculated and experi-

mental results for benzene in the same way. The effective solubility parameters derived from the hexane data work as well for the halobenzenes as for benzene.

The use of eq 2 enables one to give a useful account of the change in solvation enthalpy in the series Ph–H, Ph–F, Ph–Cl, Ph–Br, and Ph–I, except in PC as shown in Figure 7.

On the other hand, it is troublesome that when eq 2 fails, it tends to give desolvation enthalpies that are too large, even for the halobenzenes where any contribution from the dipole–dipole interaction remains to be accounted for.

Solvation Enthalpies of Electrolytes in Methanol and Dimethylformamide[1]

by C. V. Krishnan and Harold L. Friedman*

Department of Chemistry, State University of New York at Stony Brook, Stony Brook, New York 11790
(Received March 5, 1971)

Literature data for the heats of solution of various 1–1 electrolytes in methanol (MeOH) and dimethylformamide (DMF) have been supplemented by new measurements to enable the construction of extensive tables for single-ion enthalpy of transfer to propylene carbonate (PC) from the other solvents, based on the convention that the single-ion enthalpy of transfer of tetraphenylboride ion equals that of tetraphenylarsonium ion. The PC ← DMF transfers can be analyzed in the way previously reported for PC ← DMSO transfers: the tetraalkylammonium ion data are predictable from data for nonelectrolytes and lead to "real" single-ion enthalpies of transfer in agreement with the conventional ones. The PC ← MeOH transfers show very different behavior and it is concluded that the solvation enthalpy of Ph_4B^- in MeOH is about 7 kcal/mol more negative than that of Ph_4As^+. The implications of this finding for PC ← water transfers are discussed. The alkali metal ion transfers provide a basis for ordering the solvents in basicity series which depend on the ions and are not the same as the series obtained using the hydroxyl group as a probe.

1. Introduction

This work is an extension of earlier studies of ionic solvation enthalpies in propylene carbonate (PC) and dimethyl sulfoxide (DMSO).[2,3] The motivation for this is twofold. The data find application in the interpretation of the properties of solvents as reaction media, and methanol (MeOH) and dimethylformamide (DMF) are often used for this purpose. Also, the earlier work[2,3] led to a number of conclusions regarding single-ion enthalpies of transfer and the interpretation of enthalpies of transfer in terms of properties of the separate solvents and ionic species. It seems important to find whether these conclusions hold up when applied to data in DMF which, unlike DMSO and PC, has two distinct negative centers which may solvate positive ions and data in MeOH which, unlike the other solvents mentioned, has appreciable intermolecular hydrogen bonding.

In the present study it has been possible to use some results of earlier investigations of heats of solution of salts in MeOH[4,5] and DMF[5–8] but not without supplementation by new data. Thus, Slansky's data for the enthalpies of the alkali halides in methanol, which have been used by a whole generation of solution chemists, exhibit a significant internal inconsistency: When expressed as enthalpies of transfer

(1) Grateful acknowledgment is made of the support of this work by the National Institutes of Health.

(2) C. V. Krishnan and H. L. Friedman, *J. Phys. Chem.*, **73**, 3934 (1969).

(3) C. V. Krishnan and H. L. Friedman, *ibid.*, **74**, 3900 (1970).

(4) C. M. Slansky, *J. Amer. Chem. Soc.*, **62**, 2430 (1940).

(5) G. Choux and R. L. Benoit, *ibid.*, **91**, 6221 (1969).

(6) L. Weeda and G. Somsen, *Recl. Trav. Chim. Pays-Bas*, **86**, 893 (1967).

(7) R. P. Held and C. M. Criss, *J. Phys. Chem.*, **71**, 2487 (1967).

(8) O. N. Bhatnagar and C. M. Criss, *ibid.*, **73**, 174 (1969).

of the electrolytes to MeOH from water (W), they fail by as much as 0.5 kcal/mol to exhibit the required additivity in ionic contributions[9,10]

$$(MX)_{MeOH \leftarrow W} = (M^+)_{MeOH \leftarrow W} + (X^-)_{MeOH \leftarrow W} \quad (1)$$

On the basis of our experience[11] and the high degree of consistency of Slansky's data in methanol–water mixtures, the inconsistency in pure methanol may be attributed to calorimetric errors due to the very low rate at which methanol dissolves some alkali halide crystals. This may be circumvented by studying other types of salts.

More recently Choux and Benoit[5] have measured the heats of solution of a number of electrolytes in MeOH and in DMF, but at 30°, whereas most of the data needed for comparison and interpretation are at 25°. Also, in our view, there is an uncertainty in their results because the heats of solution in water of some of the preparations they used, especially NaBPh₄ and Ph₄AsI, are not given among the criteria of purity.

Some of the enthalpies in DMF determined by Held and Criss[7] are not in satisfactory agreement with those of Weeda and Somsen.[6] A resolution of this is obtained in the present work, which also leads to the conclusion that the various calorimetric data are in good agreement with the heat of solution of LiCl in DMF obtained in an emf study by Butler and Synnott.[12]

2. Experimental Section and Results

The instrumental aspects have been described previously.[13] The solutes studied were all preparations from earlier work.[2,14] Spectrograde methanol was distilled from anhydrous calcium sulfate before use. Dimethylformamide was dried over molecular sieves and vacuum distilled before use. The usual pains were taken to exclude water in the process of transferring the solvent to the calorimeter.[13] In the case of RbBPh₄ and CsBPh₄ in MeOH it was not practical to measure the heats of solution directly so heats of precipitation were measured by mixing, in the calorimeter, the trifluoroacetate of Rb or Cs with a very dilute methanolic solution of NaBPh₄ that was already saturated with the appropriate MBPh₄. The dissolution and mixing processes were found to be practically complete within 2–10 min except for alkali and tetramethylammonium halides. All the measurements were made at 25°.

The results are given in Table I where each datum is the average of two or more measurements agreeing mostly within 0.05 kcal/mol. The scatter was somewhat larger for DMF solutions of NaBPh₄ and Ph₄AsCl for which there is a weak concentration dependence of the heats of solution even below 10^{-4} m and the uncertainty in the heat of solution is estimated as 0.2 kcal/mol for NaBPh₄. In fact concentrations below 5 × 10^{-4} m have been avoided in obtaining these data because it

was found in separate experiments that small amounts of water in the solvents produce a large effect on many of the heats of solution in DMF and this source of error is most difficult to control at low electrolyte concentration.

On the basis of this observation it seems advisable to reject the heat of solution data obtained by Held and Criss[7] at the lowest solute concentrations, where they found concentration-dependent heats, but to make use of their data at somewhat higher concentrations ((5–20) × 10^{-4} m) where their data for heats of solution as a function of final concentration have plateaus. These plateau values mostly agree better with the data of Weeda and Somsen[6] than the values selected by Held and Criss. There are conductivity data to show that ion pairing is negligible in this concentration range.[15]

3. Transfers to Propylene Carbonate from Dimethylformamide

The data in Table I may be combined with heats of solution in PC of the same electrolytes to give the enthalpies of transfer in Table II. For electrolytes for which the heat of solution in PC has not been directly determined, it may be estimated using the equation, for example, for LiCl

$$(LiCl)_{PC \leftarrow crystal} = (Li^+)_{PC \leftarrow W} +$$
$$(Cl^-)_{PC \leftarrow W} + (LiCl)_{W \leftarrow crystal} \quad (2)$$

where the transfer enthalpies are taken from ref 2 and the heat of solution in water from the compilation by Parker.[16]

The single-ion enthalpies of transfer in Table II are conventional "best values." They depend on the convention[2,3] that $(Ph_4B^-)_{PC \leftarrow DMF} = (Ph_4As^+)_{PC \leftarrow DMF}$. They are derived from the data for electrolyte transfers after consideration of the probable errors. These single-ion values may be combined to give "calculated" electrolyte values (in parentheses) which, with few exceptions, agree to better than 0.1 kcal/mol with the data from this laboratory. The comparison with data from other laboratories is not uniformly so

(9) $(Y)_{a \leftarrow b} = H°$ of solute Y in solvent a minus $H°$ of solute Y in solvent b is the standard enthalpy of transfer in a notation[10] that is especially convenient for our purpose.

(10) C. V. Krishnan and H. L. Friedman, J. Phys. Chem., 73, 1572 (1969).

(11) C. V. Krishnan and H. L. Friedman, ibid., 75, 388 (1971).

(12) J. N. Butler and J. C. Synnott, J. Amer. Chem. Soc., 92, 2602 (1970).

(13) H. L. Friedman and Y. C. Wu, Rev. Sci. Instrum., 36, 1236 (1965).

(14) Y. C. Wu and H. L. Friedman, J. Phys. Chem., 70, 501, 2020 (1966).

(15) J. W. Vaughn in "The Chemistry of Non-Aqueous Solvents," Vol. II, J. J. Lagowski, Ed., Academic Press, New York, N. Y., 1967, p 246.

(16) V. B. Parker, "Thermal Properties of Aqueous Uni-Univalent Electrolytes," NSRDS-NBS2, National Bureau of Standards, U. S. Government Printing Office, Washington, D. C., 1965.

Table I: Heats of Solution of Pure Substances at 25° (kcal/mol)

Solute	Solvent DMF	CH₃OH	Solute	Solvent DMF	CH₃OH
LiCl	−11.82,[a] −10.7,[b] −11.40[c]	−12.05, −11.50[d]	Me₄NI	2.90, 4.01[g]	9.74, 9.74[l]
LiBr	−18.52,[a] −18.50[c]		Me₄NClO₄	2.23	
LiI	−19.10[a,j]		Et₄NCl	1.66	0.96, 0.82[h]
LiOOCCF₃	−7.68	−9.37[e]	Et₄NBr	2.24	4.91, 4.44[h]
NaCl		−1.90, −2.00[d]	Et₄NI	3.54, 3.42[g]	8.25, 8.11[h]
NaBr	−7.13[c]	−4.05, −4.00[d]	Et₄NClO₄	1.71	8.95
NaI	−13.15,[a] −12.65[c]	−7.14, −7.00[d]	Pr₄NCl	1.93	0.46
NaOOCCF₃	−3.60	−4.78[e]	Pr₄NBr		3.88, 4.04[h]
NaBPh₄	−17.30, −12.05[f]	−10.06, −8.02[f]	Pr₄NI	1.98, 1.996[g]	6.07
KCl		1.57, 1.08[d]	Pr₄NClO₄	3.35	
KBr	−3.65[c]	1.34, 0.87[d]	Bu₄NCl	1.40	
KI	−8.04[a]	−0.15, 0.175[d]	Bu₄NBr		4.19
KOOCCF₃		−1.07[e]	Bu₄NI	4.75	8.57
KBPh₄	−4.68		Bu₄NClO₄	0.80	6.86
RbCl		2.20, 1.28[d]	Am₄NCl	−0.32	−2.37[i]
RbI	−6.64[a]		Am₄NBr	5.74	6.84
RbOOCCF₃	−0.94	0.33[e]	Am₄NI	9.05	12.54
RbBPh₄	−1.99	7.48	Am₄NClO₄	8.57	
CsCl		2.88, 1.85[d]	Hex₄NBr	0.65	1.63
CsI	−4.25,[a] −4.10[c]		Hex₄NClO₄	9.65	15.46
CsOOCCF₃	−1.10	0.41[e]	Ph₄AsCl	−2.20	−0.98[i]
CsBPh₄	−0.92	8.84	Ph₄AsClO₄	3.52	
Me₄NCl		3.38, 3.18[h]	Ph₄PCl	−1.38	−0.12
Me₄NBr		7.35, 7.24[h]			

[a] From Weeda and Somsen.[6] [b] From Butler and Synnott.[12] [c] From Held and Criss.[1] Cf. section 2 of the present paper. [d] From Slansky.[4] [e] From Krishnan and Friedman.[11] [f] From Choux and Benoit.[5] These measurements were made at 30°. [g] From Bhatnagar and Criss.[8] [h] From R. H. Boyd and P. S. Wang, Abstracts, 155th National Meeting of the American Chemical Society, San Francisco, Calif., 1968. [i] From C. V. Krishnan and H. L. Friedman, J. Phys. Chem., 75, 388 (1971). [j] Note Added in Proof. A new determination of the enthalpy of solution of LiI in DMF by C. M. Criss and Y. A. Tsai gives −26.06 kcal/mol, in better ageement with the correlations in Table II. We are grateful to Professor Criss for private communication of this information.

satisfactory, but there are often severe experimental difficulties in getting accurate heats of solution for electrolytes in aprotic solvents.

The data in Table II for enthalpies of transfer of tetraalkylammonium perchlorates may be represented by the equation

$$[(C_N H_{2N+1})_4 NClO_4]_{PC \leftarrow DMF} =$$
$$1.47 + 4N(0.052) \text{ kcal/mol} \quad (3)$$

with an average deviation of 0.03 kcal/mol. The coefficient 0.052 kcal/methylene group, a measure of the degree to which DMF is more lipophilic than PC,[17] may be compared with 0.04 for the same coefficient, derived from the data for alcohols.[17] Just as in the study of the PC ← DMSO transfers,[2,3] the finding of the same methylene group contribution for the alkylammonium ions as for the normal alcohols does strongly imply that the alkyl chains in the former are extended so they are independently solvated rather than coiled up together, even in these highly polar solvents. The relation of the lipophilic strength to other solvent properties has been discussed elsewhere.[17]

Following the argument given in the study of the PC ← DMSO transfers[2,18] the constant term in eq 3 is the single-ion enthalpy of transfer of the common

anion, $(ClO_4^-)_{PC \leftarrow DMF} = 1.47$ kcal/mol. This turns out to be in good agreement with the conventional value in Table II, showing that, for this pair of solvents as for PC–DMSO, the conventional single-ion enthalpies of transfer are close to the real ones.

The conventional single-ion enthalpies of transfer in Table II are shown as a function of ion radius in Figure 1, together with similar data from earlier studies and from the remaining part of the present report. The nearly linear branch for the part of the PC ← DMF curve representing the tetraalkylammonium ions is associated with the linearity exhibited in eq 3 for R₄NClO₄ and by analogous equations for the other tetraalkylammonium salts, although the data are less complete. The slope of this part of the curve is associated with the difference of lipophilic strengths of PC and DMF, as we have seen.

(17) C. V. Krishnan and H. L. Friedman, J. Phys. Chem., 75, 3598 (1971).

(18) If this analysis is made more carefully than in ref 2, an allowance must be made for the difference of the enthalpies of transfer of a methylene group and a methyl group.[10] This difference is (enthalpy of transfer of methylene minus that for methyl) 0.06 kcal/mol for PC ← DMSO transfers,[10] 0.16 kcal/mol for PC ← DMF transfers,[17] and −0.34 kcal/mol for PC ← MeOH transfers.[17] Considering the uncertainties in deducing single-ion enthalpies, it seems negligible for the calculation of single-ion enthalpies of transfer in the first two cases, although not in the last.

Table II: Enthalpies of Transfer to PC from DMF at 25° (kcal/mol)[a]

	Single-ion values	Cl⁻	Br⁻	I⁻	ClO₄⁻	Ph₄B⁻	CF₃CO₂⁻
				—Single-ion values—			
		1.25	2.26	2.16	1.47	1.20	1.60
Li⁺	8.44	10.01[b] 9.59[c] (9.69)	10.82[b] 10.80[c] (10.70)	4.05[b] (10.60)			10.04 (10.04)
Na⁺	5.45		7.79[c] (7.71)	8.11[b] 7.61[c] (7.61)		6.58 (6.65)	6.92 (7.05)
K⁺	4.20		6.40[c] (6.46)	6.88[b] (6.36)		5.42 (5.40)	
Rb⁺	3.16			5.99[b] (5.32)		4.40 (4.36)	4.72 (4.76)
Cs⁺	2.10			5.04[b,c] 4.89[c] (4.36)		3.30 (3.30)	4.14 (3.70)
Me₄N⁺	0.26			2.44 1.33[d] (2.42)	1.67 (1.73)		
Et₄N⁺	0.40	1.64 (1.65)	2.66 (2.66)	2.54 2.66[d] (2.56)	1.87 (1.87)		
Pr₄N⁺	0.58	1.85 (1.83)		2.76 2.74[d] (2.74)	2.02 (2.05)		
Bu₄N⁺	0.81	1.98 (2.06)		3.10 (2.97)	2.23 (2.28)		
Am₄N⁺	1.00	2.24 (2.25)	3.21 (3.26)	3.20 (3.16)	2.56 (2.47)		
Hex₄N⁺	1.24		3.45 (3.50)		2.76 (2.71)		
Ph₄As⁺	1.20	2.45 (2.45)			2.66 (2.67)		
Ph₄P⁺	1.03	2.28 (2.28)					

[a] The values in parentheses are obtained by adding the ionic heats along the margins while the other values in the body of the table are differences between experimental heats of solution in the two solvents. In this table the conventional single-ion enthalpies of transfer are "best values" in view of our estimate of the uncertainties in the various experimental data, rather being selected to give the best agreement with all the experimental data. The propylene carbonate data used in constructing the table are taken from ref 2 and 14. [b] Heat of solution in DMF from ref 6. [c] Heat of solution in DMF from ref 7. [d] Heat of solution in DMF from ref 8.

The branch of the curve representing the alkali metal ions is less well understood but, as in the cases of the ?C ← DMSO and PC ← W transfers, the effect here is an order of magnitude larger than would be predicted from the temperature dependence of the Born-charging free energies of the ions. It may be described as reflecting the difference in basicity of the solvents[19] and it is interesting to compare the order of basicity of the protic solvents in Figure 1 as determined by the alkali metal transfers PC < DMSO < DMF with the series determined by the transfers of alcoholic hydroxyl groups[17] PC < DMF < DMSO. It is suggested that

this difference may arise because DMF has two basic centers, the amide oxygen and the amide nitrogen, one of which may participate more in solvating a lithium ion while the other interacts more strongly in accepting a hydrogen bond from a hydroxyl group. This would be consistent with the observation that the first series above is also obtained from the free energies of transfer of Li⁺.[12] Additional information relevant to this point is summarized elsewhere[17] and it must be concluded that the concept of solvent basicity needs fur-

(19) H. L. Friedman, J. Phys. Chem., 71, 1723 (1967).
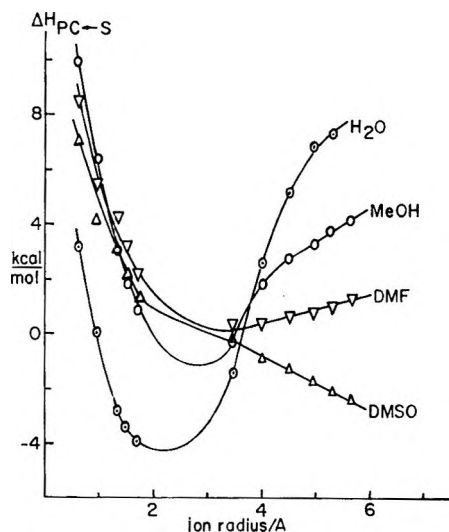
Figure 1. Single-ion enthalpies of transfer to propylene carbonate from various solvents. The data shown here are "real" values estimated as described in the text. For PC ←— DMSO and PC ←— DMF these are the same as the values based on the convention that the enthalpies of transfer of Ph_4As^+ and Ph_4B^- are the same. The data for PC ←— H_2O and PC ←— DMSO transfers are from ref 2. In each case the curves are merely drawn to connect the experimental points. The data points on each curve are, from left to right, Li^+ to Cs^+ and then Me_4N^+ to Hex_4N^+.

Figure 2. Enthalpy of transfer of $(n\text{-}C_NH_{2N+1})_4NBr$ to PC from MeOH as a function of N, the number of carbon atoms in each alkyl chain.

ther refinement and the data need further analysis to separate basicity from other factors, such as those entering into the lipophilic strength,[17] before our understanding of alkali metal cation solvation is good enough to serve as a basis for accurate empirical predictions, let alone for the molecular interpretation of these important but complicated phenomena.

4. Enthalpies of Transfer to Propylene Carbonate from Methanol

The various operations employed in constructing Table III are completely analogous to those described for Table II, including the conventional basis of the single-ion terms. The considerations of consistency of various sets of data are also quite analogous.

The PC ←— MeOH transfers for R_4N^+ salts do not have the simple behavior typified by eq 3, as may be seen in Figure 2. As a result, one cannot obtain single-ion values for the PC ←— MeOH transfers by the extrapolation method with the same assurance as for the PC ←— DMSO and PC ←— DMF transfers. However inspection of Figure 2 shows that no reasonable extrapolation of the R_4NBr data leads to the conventional value of the enthalpy of transfer of Br^-. It must be concluded that in methanol the solvation of Ph_4B^- is very different from that of Ph_4As^+. Only recently there are reports of evidence that the same is true in water[20,21] and further evidence has been obtained in this laboratory.[22]

The behavior shown in Figure 2 is quantitatively similar to that obtained for the other R_4N^+ salts.

Thus if allowance is made for the Br^-,X^- difference, the data for R_4NX agree with those for R_4NBr within 0.04 kcal/mol. Therefore there is an empirical basis for treating the linear portion of the curve in Figure 2 as a real phenomenon. Furthermore the slope of this portion is 0.11 kcal/mol of methylene groups, agreeing closely with 0.13 kcal/mol obtained for the difference in lipophilic strengths from data for the transfers of normal alcohols.[17] This being the case, the extrapolation of the linear part to $N = 0$ provides a measure of the real single-ion value for the enthalpy of transfer of Br^-. However one must also apply a correction for the fact that each of the alkyl chains in the ions is terminated by a methyl group, whose enthalpy of transfer is 0.34 kcal/mol more positive than that of a methylene group, judging by the alkane data.[17,18] The result obtained in this way is $(Br^-)_{PC←MeOH} = -0.28 - 4 \times 0.34 = -1.64$ kcal/mol.

Another, perhaps simpler, way to reach the same conclusion is to assume that for tetrapropyl and larger cations the enthalpies of transfer are made up of additive contributions from the chains, each of which is the same as if the N^+ connecting group were not there. Then Pr_4N^+ is equivalent to two hexane molecules; Bu_4N^+, to two octane molecules, etc. It is also as-

(20) C. Jolicoeur and H. L. Friedman, *J. Phys. Chem.*, **75**, 165 (1971).

(21) F. J. Millero, *ibid.*, **75**, 280 (1971).

(22) C. V. Krishnan and H. L. Friedman, to be submitted for publication.

Table III: Enthalpies of Transfers to PC from CH₃OH at 25° (kcal/mol)[a]

	Single-ion values	Cl⁻ 4.30	Br⁻ 2.14	I⁻ −0.30	ClO₄⁻ −3.36	Ph₄B⁻ −3.07	CF₃CO₂⁻ 5.60
				Single-ion values			
Li⁺	6.04	10.24 9.69[b] (10.34)					11.73 (11.64)
Na⁺	2.48	6.70 6.80[b] (6.78)	4.71 4.66[b] (4.62)	2.10 1.96[b] (2.18)		−0.66 2.7[c] (−0.59)	
K⁺	−0.72	3.62 4.11[b] (3.58)	1.41 1.88[b] (1.42)	−1.01 −1.34[b] (−1.02)			4.80 (4.88)
Rb⁺	−2.16	1.98 3.20[b] (2.14)				−5.07 (−5.23)	3.45 (3.44)
Cs⁺	−3.12	1.18 2.21[b] (1.18)				−6.46 (−6.19)	2.63 (2.48)
Me₄N⁺	−4.17	0.10 0.30[c] (0.13)	−2.08 1.97 (−2.03)	−4.40 −4.40 (−4.47)			
Et₄N⁺	−2.01	2.34 2.48[c] (2.29)	−0.01 0.46[c] (0.13)	−2.17 −2.03[c] (−2.31)	−5.37 (−5.37)		
Pr₄N⁺	−1.03	3.32 (3.27)	1.14 0.98[c] (1.11)	−1.33 (−1.33)			
Bu₄N⁺	−0.53		1.51 (1.61)	−0.72 (−0.83)	−3.83 (−3.89)		
Am₄N⁺	−0.03	4.29 (4.27)	2.11 (2.11)	−0.29 (−0.33)			
Hex₄N⁺	0.32		2.47 (2.46)		−3.05 (−3.04)		
Ph₄As⁺	−3.07	1.23 (1.23)					
Ph₄P⁺	−3.28	1.02 (1.02)					

[a] The values in parentheses are obtained by adding the ionic heats along the margins while the other values in the body of the table are differences between experimental heats of solution in the two solvents. In this table the conventional single-ion enthalpies of transfer are "best values" in view of our estimate of the uncertainties in the various experimental data, rather being selected to give the best agreement with all the experimental data. The propylene carbonate data used in constructing the table are taken from ref 2 and 14. [b] Heats of solution in MeOH from ref 4. [c] Heat of solution in MeOH from ref h of Table I.

Table IV: Comparison of Tetraalkylammonium Ion and Hydrocarbon Enthalpy Changes for the PC ← MeOH Transfer at 25° (kcal/mol)

	Pr₄N⁺	Bu₄N⁺	Am₄N⁺	Hex₄N⁺
		Ion		
Estd from hydrocarbon data	2.80	3.28	3.76	4.24
Conventional	−1.03	−0.53	−0.03	0.32
Diff	3.83	3.81	3.79	3.92

sumed that for normal alkanes larger than hexane we have

$$(C_NH_{2N+2})_{PC \leftarrow MeOH} = (C_6H_{14})_{PC \leftarrow MeOH} + 0.13(N - 6) \quad (4)$$

Then we have the results shown in Table IV showing that the real enthalpy of transfer of Br⁻ is about 3.8 kcal/mol more negative than the conventional one, while the extrapolation method gives a difference of 3.80 kcal/mol.

Table V: Single-Ion Enthalpies of Transfer to PC from MeOH Based on
Comparison with the Data for Hydrocarbons at 25° (kcal/mol)

Li$^+$	Na$^+$	K$^+$	Rb$^+$	Cs$^+$	Cl$^-$	Br$^-$	I$^-$	ClO$_4^-$	CF$_3$CO$_2^-$
9.89	6.35	3.05	1.80	0.79	0.50	−1.66	−4.10	−7.16	1.80

Ph$_4$B$^-$	Me$_4$N$^+$	Et$_4$N$^+$	Pr$_4$N$^+$	Bu$_4$N$^+$	Am$_4$N$^+$	Hex$_4$N$^+$	Ph$_4$As$^+$	Ph$_4$P$^+$
−7.10	−0.37	1.79	2.77	3.27	3.77	4.12	0.73	0.52

Thus, analysis of the data for the tetraalkylammonium ion transfers indicates that the real enthalpies of transfer of the negative ions are 3.80 kcal/mol more negative than the conventional ones, with a corresponding shift in the opposite direction for the positive ions. The resulting values are listed in Table V. While these results must be regarded as tentative, it is interesting to examine several features.

The strongly negative values for the negative ions do suggest that by some mechanism they interfere with methanol's hydrogen-bonded structure which, according to the enthalpy data for alkyl chains and benzene,[17] is relatively undisturbed by neutral solute groups that are not too large. If this is an accurate view, the interference is compensated by the stability of ROH-X$^-$ hydrogen bonds in the case of small anions such as Cl$^-$ but not in the case of larger ones.

The real enthalpy of transfer for Ph$_4$As$^+$ in Table V is not very different from 0.0 kcal/mol which one would expect if this ion, like benzene,[17] dissolves in methanol without disrupting the hydrogen-bonded structure. The figure 0.0 is based on the picture that the solvation of Ph$_4$As$^+$ is like that of four benzene molecules.[17]

Finally, the curve for the "real" single-ion enthalpies for the PC ← MeOH transfers is shown in Figure 1. Apparently methanol is more basic than the aprotic solvents shown, at least by the criterion of lithium ion solvation enthalpies. However for Rb$^+$ and Cs$^+$ as probes the basicity order would be PC < MeOH < DMSO < DMF which is close to the order PC < MeOH < DMF < DMSO determined from the hydroxyl group solvation enthalpy.[17] This may be associated with elementary electrostatic considerations[2] which suggest that Rb$^+$ and the hydroxyl group should be similarly solvated if other effects do not dominate. As one proceeds up the series from Rb$^+$ to Li$^+$ the electric field next to the ion increases greatly and this alone could account for a difference in basicity series according to whether the probe is lithium ion or the hydroxyl group.

5. Enthalpies of Transfer to Propylene Carbonate from Water

The results of the preceding section prompt a reconsideration of our earlier results on PC ← W transfers,[2] even though the conclusions were based on the relative enthalpies of transfer of cations rather than on single-ion values. It should be remarked that the difference between conventional and real enthalpies of transfer to PC from MeOH deduced here does not itself imply a corresponding or even larger difference for PC ← W transfers because in water one has branched three-dimensional hydrogen-bonded networks and it is difficult to guess what will happen in water on the basis of the data in methanol. However, if we make the approximation that[14]

$$(\text{Cs}^+)_{\text{PC}\leftarrow\text{W}} = (\text{I}^-)_{\text{PC}\leftarrow\text{W}} - 0.7 \text{ kcal/mol} \quad (5)$$

for which there is a basis in what is known about the "structural" contributions to the thermodynamic properties of these ions in water, then we have $(\text{Ph}_4\text{As}^+)_{\text{PC}\leftarrow\text{W}} = -1.1$ kcal/mol and $(\text{Ph}_4\text{B}^-)_{\text{PC}\leftarrow\text{W}} = -5.9$ kcal/mol. These figures may be compared with[23] $4(\text{C}_6\text{H}_6)_{\text{PC}\leftarrow\text{W}} = 0.72$ kcal/mol. It follows that in water as in methanol the solvation enthalpy of Ph$_4$As$^+$ is close to that of four benzene molecules while the solvation enthalpy of Ph$_4$B$^-$ shows a very large extra negative contribution.

The enthalpies of transfer to propylene carbonate from water in Figure 1 are not the conventional ones but rather depend on the assumption in eq 5. It seems that the conclusions[2] reached on the basis of the conventional single-ion enthalpies for the PC ← W transfers still are valid. The same is true for the discussion of the enthalpies of the DMSO ← W transfers of the alkylammonium ions[3] although Figure 4 of ref 3 and the numerical values for chain-hydrogen-bond interference effects in water derived therefrom are somewhat different when eq 5 is used as a basis of the single-ion enthalpies rather than $(\text{Ph}_4\text{As}^+)_{\text{PC}\leftarrow\text{W}} = (\text{Ph}_4\text{B}^-)_{\text{PC}\leftarrow\text{W}}$.

(23) The heat of solution of benzene in water was taken from D. S. Reid, M. A. J. Quickenden, and F. Franks, *Nature (London)*, **224**, 1293 (1969).

Bubble Nucleation in n-Pentane, n-Hexane, n-Pentane + Hexadecane Mixtures, and Water

by M. Blander,[*1] **D. Hengstenberg,**

North American Rockwell Science Center, Thousand Oaks, California 91360

and J. L. Katz

Department of Chemical Engineering and Institute for Colloid and Surface Science,
Clarkson College of Technology, Potsdam, New York 13676 *(Received May 17, 1971)*

Publication costs assisted by the Argonne National Laboratory

Bubble nucleation temperatures in pure n-pentane and n-hexane were measured. Both nucleate explosively with most of the small drops of n-pentane (bp 36°) nucleating at 147.8 ± 0.3° and most of the small drops of n-hexane (bp 69°) nucleating at 183.8 ± 0.5°. These temperatures are somewhat higher than previous measurements and are in excellent agreement with calculations from the steady-state Zeldovich–Kagan theory. Addition of the relatively involatile hexadecane to n-pentane raises the nucleation temperature linearly with concentration (weight fraction or mole fraction) to about 197° at 46 wt % hexadecane. The explosive growth phase is slowed in the mixtures because of diffusion control with a high pitched "ping" in the pure n-pentane becoming a lower pitched "pong" with 20 wt % hexadecane and a lower pitched "glub" at 46 wt % hexadecane. The mixtures exhibited a significant spread of nucleation temperatures with volume of the droplets. A modification of theory including an extension to diffusion-controlled nucleation was made. We have superheated water to over 265°; however, this is well below the homogeneous limit.

Introduction

Although bubble nucleation is important in many natural and man-made phenomena, only very limited theoretical or experimental work on this subject has appeared. The early quasi-equilibrium theories of homogeneous nucleation of Becker and Döring[2] and Volmer[3] were followed by the steady-state theory of Zeldovich[4] which was further refined by Kagan.[5] Most of the few reliable experimental data exist for one-component systems.[6] It is the purpose of this paper to check previous work on one-component systems (n-pentane, n-hexane, and water) and to provide new data on a two-component system (n-pentane + n-hexadecane) to serve as a basis for testing and extending the theory of homogeneous bubble nucleation and to gain a better understanding of the details of the phenomenon. We will discuss the theory of multicomponent systems with one volatile component and take into account the influence of diffusion. The experimental measurements will be discussed in the context of the theory.

Theory

The steady-state theory of Zeldovich[4] has been clarified and extended by Kagan.[5] For the case where the influence of viscous and inertial forces is small (which applies to our experiments) Kagan has derived an expression for J, the rate of nucleation, $i.e.$, number of critical size nuclei per unit volume per unit time which continue to grow to macroscopic size.

$$J = \frac{1}{2} N_0 \frac{\beta v_t}{1 + \delta_\lambda} \sqrt{\frac{\sigma}{kT}} e^{-1/3 K} \qquad (1)$$

where β is a condensation coefficient (here taken as 1) and

$$v_t = \sqrt{\frac{8kT}{\pi m}} \qquad (2)$$

is the average thermal velocity of the vapor molecules of mass m, σ is the surface tension of the liquid, and

$$K = \frac{4\pi \sigma r_c^2}{kT} \qquad (3)$$

where r_c is the radius of the critical size bubble given by

$$p_c = p_0 + \frac{2\sigma}{r_c} \qquad (4)$$

where p_0 is the ambient pressure and p_c is the equilibrium vapor pressure of the liquid. p_c is equal to the pressure inside the critical size bubble.

(1) Correspondence should be addressed to Chemical Engineering Division, Argonne National Laboratory, Argonne, Ill. 60439.

(2) (a) R. Becker and W. Döring, *Ann. Phys.*, **24**, 719 (1935); (b) R. Becker, "Theorie der Wärme," Springer, Berlin, 1955.

(3) M. Volmer, "Kinetic der Phasenbildung," Steinkopff, Dresden-Leipzig, 1939.

(4) Ya. B. Zeldovich, *Zh. Eksp. Teor. Fiz.*, **12**, 525 (1942).

(5) Yu. Kagan, *Zh. Fiz. Khim.*, **34**, 92 (1960); *Russ. J. Phys. Chem.*, **34**, 44 (1960).

(6) (a) H. Wakeshima and K. Takata, *J. Phys. Soc. Jap.*, **13**, 678 (1958); (b) V. B. Skripov and G. V. Ermakov, *Zh. Fiz. Khim.*, **38**, 396 (1964); *Russ. J. Phys. Chem.*, **38**, 208 (1964); E. N. Sinitsyn and V. P. Skripov, *Ukr. Fiz. Zh.*, **12**, 99 (1967); (c) G. R. Moore, Ph.D. Thesis, University of Wisconsin 1956 (University Microfilms Publication No. 17,330, Ann Arbor, Mich.).

M. Blander, D. Hengstenberg, and J. L. Katz

The parameter δ_λ is related to the heat flow during the growth of a bubble and involves the enthalpy of vaporization and thermal conductivity of the liquid. In the cases given here δ_λ is small relative to unity. However, for multicomponent systems with one volatile constituent, our calculations indicate a similar factor, δ_D, which takes into account the steady-state diffusion of molecules through the medium into the nuclear bubbles. The result of the calculations[7] includes the factor δ_D

$$\delta_D = \frac{\beta v_t}{2DkT} \frac{\sigma}{p_c - p_0}\left(\frac{dp}{dC}\right)_{p_c} \cong \frac{\beta v_t \sigma}{2(C - C_0)DkT} \qquad (5)$$

where the last expression on the right holds where Henry's law is obeyed and $dp/dC = p/C$. C is the bulk initial concentration of the volatile solute, C_0 is the equilibrium concentration at a vapor pressure equal to the ambient pressure p_0, and D is the diffusion coefficient of the volatile solute in the solvent. The rate of nucleation is lowered from J (eq 1) to J' when diffusion is significant where

$$J' = J/(1 + \delta_D) \qquad (6)$$

If $\delta_D \gg 1$, then where Henry's law is valid

$$J' \cong N_0D(C - C_0)\sqrt{\frac{kT}{\sigma}}e^{-1/_3K} \qquad (7)$$

and the nucleation rate is diffusion controlled.

In addition to the nucleation rate, diffusion will also control the rate of growth of the bubble. As will be seen from the experiment we describe, the rate of growth in a pure material is so rapid that it produces a sharp explosive report. In a dilute multicomponent solution in an involatile solvent, diffusion control slows the rate of growth considerably and changes the character of the growth process. We show below that for bubbles much larger than the critical size, the rate of growth is proportional to the concentration of the volatile constituent in solution and inversely proportional to the radius.

The total number of moles of gas, n, in a bubble of radius $r \gg r_c$ is

$$n \cong \frac{^4/_3\pi r^3 p_0}{RT}$$

and the average thickness, l, of the shell of liquid surrounding the bubble which is partly denuded of the volatile solute for the case where $p_c \gg p_0$ is approximately given by

$$4\pi r^2 l \cong L\frac{n}{C - C_0} = \frac{^4/_3\pi r^3 p_0 L}{(C - C_0)RT} \qquad (8)$$

where L is a proportionality factor of order unity. The rate of diffusion of molecules into the bubble, $\dot{n}$, is proportional to the product of the area of the bubble surface $(4\pi r^2)$ and the concentration gradient which is proportional to $1/l$. Thus the rate of growth of the radius of the bubble

$$\dot{r} \propto \frac{\dot{n}}{4\pi r^2} \propto \frac{C - C_0}{r} \qquad (9)$$

(If the diffusion equation is solved for a stationary boundary and the rate of diffusion per unit area is set equal to $(p_0/RT)\dot{r}$, then $\dot{r} \cong (RT/p_0)((C - C_0)/r)D$ and when $r \gg r_c$ $r \cong \sqrt{(2DRT/p_0)(C - C_0)t}$.) These considerations show that if diffusion is the limiting factor, the rate of growth of bubbles much larger than critical size is proportional to the concentration and inversely proportional to the size of the bubble. At low concentrations growth is slow and increases with increasing concentration. Thus, while bubble growth in a one-component system is explosive, the addition of an involatile diluent slows the rate. The smaller the concentration of the volatile solute the slower the growth. Our measurements demonstrate this change in the character of the growth with dilution.

We also must examine an important correction to the theory first considered by Skripov and coworkers.[6b] Measurements of vapor pressures are made when a substance is under a pressure equal to its own pressure (p_e). Our measurements on these liquids were made while they were metastable at (or close to) ambient atmospheric pressures, which are much lower. Consequently, the actual vapor pressure in our experiments, p_c (i.e., the vapor pressure of the liquid when the ambient pressure is p_0, see eq 4) at a given temperature differs from the measured vapor pressure (p_e). This may be estimated from the relation

$$\left(\frac{\partial \ln f}{\partial p}\right)_T = \frac{v_1}{RT} \qquad (10)$$

where f is the fugacity and v_1 is the molar volume of the liquid.

If v_1 is independent of pressure

$$\ln\frac{f_c}{f_e} \cong \frac{v_1(p_0 - p_e)}{RT} \cong \frac{f_c - f_e}{f_e} \qquad (11)$$

where the expression on the right is valid when f_c/f_e does not differ greatly from unity. By rearrangement we obtain

$$f_c \cong f_e\left(1 - \frac{v_1(p_e - p_0)}{RT}\right) \qquad (12)$$

If the ratios of fugacities do not differ greatly from pressure ratios, then

$$\frac{f_c}{f_e} \cong \frac{p_c}{p_e} \cong 1 - \frac{v_1(p_e - p_0)}{RT} \qquad (13)$$

Activity coefficient data[8] show this approximation to

(7) J. L. Katz and M. Blander, in preparation. (Material in this paper was presented at the 161st National Meeting of the American Chemical Society, Los Angeles, Calif., Spring, 1971, Abstract PHYS 62.)

(8) "Selected Values of Properties of Hydrocarbons and Related Compounds," American Petroleum Institute, Research Project 44, Thermodynamics Research Center, College Station, Texas, 1969.

be valid to within 2.5% for n-pentane and a similar precision probably holds for n-hexane. Equation 13 may be rearranged to obtain $p_e - p_0$ in eq 4

$$p_e - p_0 \cong (p_e - p_0)\left(1 - \frac{v_1 p_e}{RT}\right) =$$

$$(p_e - p_0)\left(1 - \frac{z v_1}{v_g}\right) \quad (14)$$

where z is the compressibility factor $p v_g / RT$. The last expression on the right-hand side with $z = 1$ is the approximate correction factor utilized by Sinitsyn and Skripov. Where data on fugacities vs. pressure are available, eq 11 is preferable. The introduction of this factor leads to a significant increase (1.5–2.0°) in the calculated eruption temperatures and accuracy is needed for a correct estimate.

Another correction which must be considered arises from the fact that the derivation of eq 1 was made assuming that the gas phase is ideal. At the pressures involved the gas phase deviates considerably from ideal behavior, especially gases of strongly interacting molecules. We have calculated the corrections for nonideal gases[7] and find that the exponential term in eq 1 requires no correction and that the only correction is a multiplicative factor which has a negligibly small effect on the temperature we calculate.

Experimental Methods

The method is a modification of the technique of Wakeshima and Takata,[6a] of Skripov, Sinitsyn, and co-workers,[6b] and of Moore.[6c] It consists of the generation of an emulsion of small drops of volatile liquids in an immiscible fluid medium. The individual drops are allowed to rise slowly in a column of the same immiscible medium which is hotter at the top than at the bottom. The drops get hotter as they rise and at high enough temperatures the liquid superheats enough to nucleate and then boils explosively. This boiling can be observed visually and the explosive reports can be clearly heard. For hydrocarbons, sulfuric acid and for water, a silicone oil were used as the immiscible fluid medium in which the droplets rose.

Figure 1 gives a schematic diagram of the Pyrex apparatus used which consisted of a lower vessel 7.5 cm in diameter by 8.5 cm in height connected to an upper column about 5.5 cm in diameter by 46 cm in length with a 1-mm capillary about 3 cm long serving as an opening between the two vessels. The upper column is capped by a Teflon stopper in which is set an L-shaped, thin-walled, small bore thermocouple well, the tip of which can be set at any desired height. The central 28-cm portion of the upper column is wound with 28 turns of nichrome wire, cemented in place with Sauereisen cement and with a total resistance of 45 Ω. The spacing between windings is uneven being about 2 cm at the lower end and about 0.5 cm at the upper end.

Figure 1. Bubble nucleation apparatus.

A side arm is provided in the lower vessel, and a Teflon-coated magnetic stirrer is used to stir the materials in the lower vessel. A 28-gauge copper–constantan thermocouple, calibrated to 0.1° vs. a standard Pt—Pt–10% Rh thermocouple was used for the temperature measurements. The thermocouple was set into the well and was connected through an ice bath to a Leeds & Northrup Type K3 potentiometer standardized vs. an unsaturated Eppley standard cell. The current for the nichrome heater was supplied through a constant voltage regulator and a variable autotransformer set to provide a suitable current for the temperature range of interest.

The operation of the apparatus was quite simple. The vessels were filled to appropriate levels with sulfuric acid, and a fixed voltage was set on the heating wires. After about 2 hr the temperatures in the upper vessel stabilized. Temperature was measured at different horizontal positions at any given level by rotating the thermocouple tip. It differed by less than 0.1° within a given level at any position more than about $^1/_2$ cm away from the walls of the vessel. If the liquid was undisturbed, the temperatures and temperature distribution would remain constant to ±0.1° over the time of the experiment (about 0.5 hr). The temperatures and levels were adjusted so that the temperature gradients in the region where measurements were made were about 2–3°/cm. The nucleation of unusually large drops

would temporarily upset the temperature gradients. Frequent checks of temperature were made, and sufficient time (usually about 0.5 hr) was allowed to permit any such temperature fluctuations to decay.

The volatile liquid to be studied was introduced onto the surface of the sulfuric acid in the lower vessel and partly emulsified by mechanical mixing with a stirring rod followed by rapid stirring with a Teflon-coated magnetic stirrer bar. The sulfuric acid level was about 0.25-1 cm above the bottom of the capillary and by careful manipulation individual drops could be sent through the capillary into the upper tube. These drops floated upward slowly and nucleated when sufficiently superheated.

The liquids used were as follows: n-pentane and n-hexane were Pure grade obtained from the Phillips Petroleum Co. (Special Products Division), 99 mol % minimum with a stated boiling point of 96.9°F (36.0$_6$°) for n-pentane and 155.8°F (68.7$_8$°) for n-hexane. Two grades of n-hexadecane from Matheson Coleman and Bell were used in a separate series of measurements; one grade was ASTM grade olefin free of 99+% purity with a minimum melting point of 18.0°, and the other grade was Practical grade with a melting point range of 17-18°. No significant differences were found between experimental results from these two grades indicating that impurities have little influence on the measurements. Only results from the purer grade are reported here. The sulfuric acid was Du Pont Reagent grade 95-97%, specific gravity 1.84 min. The water was triply distilled, and the silicone oil was Dow Corning No. 710 silicone fluid with a viscosity of 500 cSt at 25°.

Nucleation in Pure n-Pentane and n-Hexane. A small quantity of one of the pure hydrocarbons (about 5 cm^3) was introduced into the side arm of the lower vessel where it floated on the surface of the sulfuric acid in the vessel. Each experiment consisted of several hundred measurements and was repeated at least once using a fresh batch of sulfuric acid in both the upper tube and the lower vessel each time. The organic was emulsified with the sulfuric acid. By a variety of means, including manipulation of the stopper in the side arm or by stopping the stirrer, individual droplets of the organic compound could be made to enter the upper column. The sizes varied from droplets which were so small that they were not visible through the four-power telescope of the cathetometer to some as large as 2 mm. The sizes were estimated by comparison with a scale set in the line of sight of the telescope. The scale served to measure the height at which droplets nucleated and the height of the thermocouple. Any given droplet rose slowly in the cooler lower portion of the tube and accelerated in the hotter upper portion of the tube with large droplets rising more rapidly than small ones. The droplets got hotter as they rose and reached levels where the temperatures were considerably higher than their

boiling points before nucleating to produce sharp high-pitched explosions. Except for the largest droplets (>1.2 mm) and a small number of droplets (<5%) which exploded prematurely, essentially all of the droplets of n-pentane and n-hexane exploded in a narrow range of temperatures (total range of about ±0.3° for n-pentane and ±0.5° for n-hexane). The largest droplets (>1.2 mm) rose very rapidly and probably did not reach the ambient temperature of the medium. They usually nucleated at a higher level where the ambient temperature was higher. Many of the drops which nucleated at lower temperatures appeared to have bubbles attached to them before nucleating and probably did not nucleate homogeneously. The range of temperatures in which the large majority of droplets nucleated was so narrow that when the temperature was stable there was a striking illusion that most of the droplets nucleated close to a single plane. No obvious large differences existed between the smallest drops (which formed 1-2-mm bubbles when they exploded) and those which were 1 mm in size as a liquid. As will be discussed, this is consistent with nucleation theory where J for these one-component fluids is a very steep function of temperature. Calculation of the rate of nucleation in our experiment of droplets of volumes which vary by about three orders of magnitude reveals that nucleation for these pure materials should occur over a narrow range of temperatures ($\sim$0.6°) as observed. Only an occasional small droplet exploded at higher temperatures (0.5-1° higher). The temperatures measured are given in Table I.

Table I: Measured and Calculated Temperatures (°C) for Different Nucleation Rates

	T (measured)	$J = 10^4$ cm^{-3} sec^{-1}	$J = 10^6$ cm^{-3} sec^{-1}
		——— T (calculated) ———	
n-Pentane	147.8 ± 0.3	147.7 (147.2)[a]	148.3 (147.9)
n-Hexane	183.8 ± 0.5	183.6 (183.1)	184.3 (183.8)

[a] Parentheses include compressibility correction.

Nucleation in n-Pentane–Hexadecane Mixtures. The experiments were repeated for the purified n-pentane diluted with the relatively involatile hexadecane. The mixtures were made up by weight. The observations exhibited very significant qualitative and quantitative differences from those on pure n-pentane. Figure 2 gives a plot of the average temperature for the nucleation of these mixtures as a function of weight per cent hexadecane. The nucleation temperature increased with increasing weight per cent of the relatively non-volatile hexadecane. The largest influence on this is probably related to the surface tension of the mixture. Pure n-pentane at 147.8° has a low surface tension (3.3
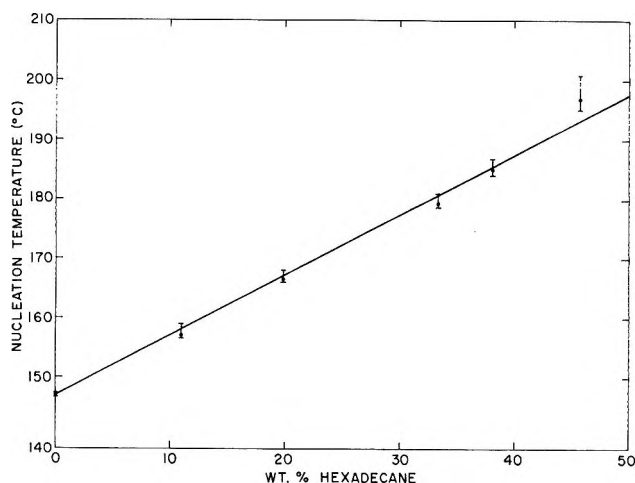
Figure 2. Bubble nucleation temperatures of
n-pentane + n-hexadecane mixtures vs. weight per cent
hexadecane. Bars represent spread of data due to different
size drops and fluctuations in nucleation temperatures.

ergs/cm^2), because it is close to its critical point (196.6°).
Hexadecane, which has a much higher critical tempera-
ture (444°), should have an appreciably higher surface
tension at 147.8° and the mixtures, if they have an
intermediate value, should nucleate at higher tempera-
tures. Another (and probably smaller) influence is that
the vapor pressure of n-pentane is lower in the mix-
tures than in pure n-pentane.

In addition to this, another significant observation
was made on the mixtures. With increasing hexade-
cane content it was observed that there was an increas-
ing tendency for small drops (<0.1 mm) to nucleate at
higher temperatures than large drops. At the highest
concentrations of hexadecane ($\sim$46 wt %) the differ-
ence was about 5°, i.e., drops of about 0.5-mm diameter
usually exploded from 196 to 198° whereas small drops
($\leqslant$0.1 mm) usually exploded from 197 to 201°. This
would result if J were to become less strongly dependent
on temperature with increasing dilution. As will be
discussed, this can probably be ascribed largely to the
relatively weaker dependence of surface tension on tem-
perature of the mixtures as compared with the pure n-
pentane. This wide variance of average nucleation
temperature with volume should be a general feature
for mixtures, especially those dilute in volatile solutes
in a solvent far from its critical temperature. The
points recorded in Figure 2 are those for drops $\sim$0.2
mm. The bars about the points indicate the ranges
where more than 90% of the drops nucleated. Since
the size distribution was not uniform for all composi-
tions, the range does not exhibit a regular change with
composition.

A third observation of significance is on the nature of
the explosive nucleation. For pure n-pentane, the
sharp explosive report was high pitched and could be
best described as a "ping." With dilution, the sound
became lower pitched so that with 20% hexadecane it

might be characterized as a "pong." At the highest dilu-
tions of the n-pentane (35–46% wt % hexadecane) the
rate of growth of bubbles was so slowed that only very
low pitched sounds were produced (characterized as a
"glub"). These differences are related to the process
of bubble growth which is diffusion controlled in the mix-
tures. These characteristic sounds reflect the smaller
rate of growth of a postnuclear bubble with greater di-
lution of the volatile constituent. This is consistent
with the discussion in the Introduction.

Nucleation of Liquid Water. The behavior of water
was not as simple as that of the hydrocarbons, and
nucleation may not have been homogeneous. How-
ever, the nucleation temperatures were quite high, and
our observations seemed to be of sufficient interest to re-
port.

The water utilized was triply distilled, but no special
precautions were taken to degas it. Small amounts of
gases such as CO_2 at the high temperatures and water
fugacities involved probably make little difference in the
nucleation temperature. The ambient fluid was Dow
Corning No. 710 silicone oil. Although the water and
silicone are immiscible at low temperatures, significant
miscibility was observed at high temperatures (>200°).
The miscibility places limitations upon the interpreta-
tion of the results. Droplets were made by emulsifying
water and silicone oil in the lower vessel and a large num-
ber of drops up to 3 mm in diameter were introduced
one at a time into the upper column.

It was quite apparent that water was somewhat solu-
ble in silicone at the higher temperature. Small drop-
lets (<0.1 mm) which rose slowly left a refractive index
contrast trail behind them and disappeared before nu-
cleating. Larger droplets (0.1–0.5 mm) partly dis-
solved in the silicone and silicone appeared to dissolve
in the droplet. These droplets tended to nucleate at
high temperatures 265–280° with fairly sharp explosions.
However, it is questionable whether any of these con-
tained pure water. Some of these drops (as well as
larger ones) appeared to nucleate bubbles at the water-
silicone interface at lower temperatures (200–240°) and
a stream of bubbles rose rapidly from the surface of the
slowly rising droplets. This indicated heterogeneous
nucleation in at least some of the droplets. Most drop-
lets from 0.5 to 1.0 mm nucleated in a range of tempera-
tures from 250 to 275° with occasional droplets explod-
ing at higher temperature up to 280°. These droplets
rose fairly rapidly and from the appearance of the index
of refraction contrast with the silicone probably had a
core of pure water. Droplets from 1 to 3 mm in size
rose rapidly at high temperatures and had little time to
dissolve. The cores had a high index of refraction con-
trast with the silicone and were probably pure water.
Most of these droplets exploded in the range 240–265°
with an occasional explosion at higher temperatures
(270°). These droplets exploded quite sharply and
pushed the vessel against its support with a strong thud.

The wide range of temperatures and the erratic nucleation behavior may be partly the result of heterogeneous nucleation as postulated by Apfel,[9] who has performed similar measurements with water. However, some of our observations do not support this. For example, some large (1 mm) drops evolved a continuous train of bubbles from their surface as they rose until they reached a high temperature where they exploded. Clearly, two separate kinds of nucleation are involved: the train of bubbles coming from a heterogeneous site and the explosive nucleation beginning in an unknown way. (The train of bubbles indicates that the surface tension of the silicone is less than that of the water. A reversal of the relative values of the surface tensions would change the mode of release and nucleation.)

Discussion

In this section we will calculate temperatures where the expected rates of homogeneous nucleation should correspond to our observations. Calculations for n-pentane and n-hexane were made using data from Timmermans,[10] the International Critical Tables,[11] and the API Table.[8] Available data on surface tensions were graphically fit to an equation of the form

$$\sigma = \sigma_0 \left(1 - \frac{T}{T_c}\right)^s$$

The best fits of the data were made with values of σ_0, T_c, and S of 52.72 ergs/cm², 469.77°K, and 1.22 for n-pentane, and 52.40 ergs/cm², 507.85°K, and 1.22 for n-hexane.

Most of the drops recorded in our measurements ranged from about 0.1 to 1.5 mm with a median at about 0.5 mm. The volume of these median sized drops was about 10^{-4} cm³, and they spent about 0.1 sec in the temperature range of about 0.3°. Consequently, a rate of J of about 10^5 cm⁻³ sec⁻¹ is appropriate ($J = 1/vt$, where v = volume and t = time). Since the rise time of a drop is inversely proportional to its radius, the appropriate rate J is proportional to the inverse of the square of the radius. Consequently, the appropriate J for the 1.5-mm drop is about 10^4 and for the 0.1-mm drop about 25×10^5. In Table I our calculated temperatures for $J = 10^4$ and 10^6 are given for n-pentane and n-hexane. The values given in Table I were calculated for values of $Z = 1$ and $Z = 0.74$ (in parentheses). For n-pentane the measured value of Z is 0.74 and it is probably similar for n-hexane. The correction for Z lowers the calculated temperatures about 0.5°, i.e., the factor $(1 - (v_l/v_g))^2$ in eq 14 leads to temperatures about 1.5-2.0° higher than without it, whereas the factor $(1 - (Zv_l/v_g))^2$ leads to temperatures about 1.0-1.5° higher than without it.

The range of temperature for the large change of J in Table I is relatively small and is in excellent agreement with our measurements, both with or without the Z correction. The large change of J with a small change of

temperature (one order of magnitude per 0.3°) explains the very narrow range of measured temperatures despite the range of drop sizes. The variance in the measured values is probably real and probably not related to difficulties in measuring temperatures. The range, though small, stems from the probabilistic nature of each eruption and to the differences in sizes. Of hundreds of drops an occasional small drop might be expected to nucleate as much as 0.5-1° higher than the large majority, as was observed. Our measured and calculated temperatures are significantly higher than those given by previous workers.[6]

One must question whether the homogeneous limit has been reached in these experiments. The surface tension of sulfuric acid is much higher than the small values (~3 ergs/cm²) for the hydrocarbons. Consequently, the interfacial tension between the hydrocarbon and sulfuric acid is likely to be higher than the surface tension of the hydrocarbons. This will lead to a higher probability for homogeneous nucleation than for nucleation at the interface if the hydrocarbons spread on sulfuric acid. Very few drops appeared to nucleate bubbles at the surface and many of these few appeared to have bubbles attached to them before nucleation was initiated. Both n-pentane and n-hexane fit the homogeneous theory at two very different temperatures (and probably at two very different values of the sulfuric acid–hydrocarbon interfacial tensions which govern heterogeneous nucleation). It is very unlikely to be a coincidence and much more likely indicates homogeneous nucleation.

The measurements on the mixtures exhibit a much larger size dependence of the eruption temperature. If we combine eq 3 and 4, we obtain

$$K = \frac{16\pi\sigma^3}{kT(p_c - p_0)^2} \qquad (15)$$

The temperature dependence of K essentially governs the variation of J with temperature since the preexponential factor in eq 1 is essentially independent of temperature. For pure pentane σ decreases and p_c increases relatively rapidly with increasing temperature. Both of these quantities operate to increase J with temperature. For example, between 160 and 170° σ for pentane decreases from 2.34 to 1.59 ergs/cm². Measured surface tensions for hexadecane[8,10] were graphically fit to an equation

$$\sigma = 56.54\left(1 - \frac{T}{T_c}\right)^{1.34} \text{ ergs/cm}^2$$

with $T_c = 717.15°K$. Values of σ calculated from this

(9) R. E. Apfel, J. Chem. Phys., 54, 62 (1971).

(10) J. Timmermans, "Physico-Chemical Constants of Pure Organic Compounds," Elsevier Publishing Co., Amsterdam, Vol. I, 1950; Vol. II, 1965.

(11) E. W. Washburn, et al., Ed., "International Critical Tables," McGraw-Hill, New York, N. Y., 1926-1933.

expression varied from 16.34 ergs/cm² at 160° to 15.57 ergs/cm² at 170°. This relatively small change reflects the fact that hexadecane is far from its critical temperature. Consequently, we see that if the mixtures, as expected, exhibit a behavior intermediate between the two components, then the surface tensions will decrease slower than pure pentane with an increase in temperature and J will have a weaker dependence on temperature. Consequently, a larger spread of nucleation temperatures with size should be expected, as was observed. The higher the concentration of hexadecane the more pronounced this effect should be. In very dilute solutions in solvents far from their critical temperature, the major factor influencing the temperature dependence of J is the variation of vapor pressure with temperature which is generally small relative to the variation in $\sigma^3/(p_c - p_0)^2$ for a one-component liquid. Consequently, nucleation temperatures in very dilute solutions should increase strongly with a decrease in size of the droplets and should have a relatively large scatter for any given size.

The influence of the correction term δ_D in eq 6 may be significant even for the high concentrations considered in our experiments. For a dilution of pentane to $^1/_2N_0$, $\sigma \sim 3$ and $D \sim 10^{-5}\delta_D$ is ~40. This is large enough to make eq 7 valid and leads to a value of J smaller by a factor of ~40. This could raise the calculated nucleation temperature several degrees in the 46 wt % mixture (e.g., about two-thirds of the spread in our measurements of small and large drops where a variation in volume of 10^4 leads to about a 5° spread). For large dilutions this correction term for diffusion can be considerably larger.

Quantitative calculations for the mixtures are not possible because thermodynamic data are not available. Crude estimates of surface tensions and partial pressures of pentane in the mixtures were made by several approximations. The highest estimated nucleation temperatures were obtained when surface tensions were assumed linear in mole fraction[12] and partial pressures linear in volume fraction.[13] Even these led to temperatures lower than measured if the correction term similar to the one represented in eq 14 were not included. This correction analogous to eq 14 is

$$p_c' - p_0 \cong (p_e' - p_0)\left(1 - \frac{p_e' \bar{V}_{C_5H_{12}}}{RT}\right) \quad (16)$$

where $\bar{V}_{C_5H_{12}}$ is the partial molar volume and p_c' and p_e' are the critical and measured partial pressures of n-pentane, respectively. If $\bar{V}_{C_5H_{12}}$ is similar to the molar volume for the pure liquid, then this correction becomes quite large near the critical temperature of n-pentane (e.g., it approaches $(1 - z)$) and the calculated temperatures are relatively close to those which are measured (for the linear approximations considered). An accurate check of the theory requires measurements of surface tensions, partial pressures, and diffusion coefficients in the mixtures.

As an empirical observation, it might be noted that nucleation temperatures for n-pentane and n-hexane are about $0.9T_c$. If this holds for n-hexadecane ($T_c \sim717.15°$K) one would estimate a nucleation temperature of $\sim645°$K in pure hexadecane. A linear plot of temperature vs. mole fraction from the measured temperature for n-pentane ($\sim147.8°$) to that estimated for n-hexadecane ($\sim372°$) goes through the measured data on the mixtures.

In any case, the experiments behave, at least qualitatively, as predicted by theory. Dilution of n-pentane by hexadecane raises the surface tension and lowers the vapor pressure. This requires heating to higher temperatures in order to overcome nucleation barriers. The influence of the factor δ_D is probably important, even in the fairly concentrated mixtures studied here. We hope to investigate more dilute solutions to observe cases where this term is more important and where bubble growth is slowed more by diffusion control.

Conclusions

Nucleation theory appears to provide accurate predictions for the maximum temperature of eruption of pure liquids. The qualitative and quantitative nature of the process of nucleation and growth of binary mixtures differs significantly from one-component systems. Further investigations are needed to quantify the theoretical predictions for binary mixtures.

(12) R. C. Reid and T. K. Sherwood, "The Properties of Gases and Liquids," McGraw-Hill, New York, N. Y., 1966.

(13) J. H. Hildebrand and R. L. Scott, "The Solubility of Nonelectrolytes," Reinhold, New York, N. Y., 1950.

A Correlation of the Excess Molar Volumes of Solutions of

Cadmium and Bismuth in Their Molten Halides

by L. Suski*

Institute of Physical Chemistry of the Polish Academy of Sciences, Cracow, Poland

and J. Moscinski

Institute of Nuclear Techniques, School of Mining and Metallurgy, Cracow, Poland   (Received December 16, 1970)

Publication costs borne completely by The Journal of Physical Chemistry

The excess molar volumes of solutions of cadmium and bismuth in their molten halides exhibit a concentration dependence expressed by the relation $V^E = k x_m (1 - x_m)$. The proportionality constant k is found to be inversely proportional to the molar "free volume" of the salt component for all six systems for which data are available.

In preceding works[1,2] we presented data concerning the molar volumes of solutions of cadmium in its molten chloride, bromide, and iodide, which were obtained by a radiometric measurement method. The densities of analogous solutions of bismuth in its three halides for a wide temperature range had been reported previously by Keneshea and Cubicciotti.[3-5] From their data the excess molar volumes can be calculated. The solutions of cadmium and bismuth in their halides are the only two groups of metal–salt systems for which the excess molar volumes have been determined so far.

It was shown in our previous work[2] that the excess molar volumes of Cd–CdCl$_2$ and Cd–CdI$_2$ solutions at various temperatures fulfill well the dependence

$$V^E = k x_m (1 - x_m) \tag{1}$$

where V^E is the excess molar volume of the solution for the given molar fraction of metal (x_m) and k is a temperature-dependent constant. The results obtained for the Cd–CdBr$_2$ system do not fulfill this relationship; however, with a good approximation, the V^E (and k) values for this case may be considered as nearly zero.

In the preceding work[2] the corresponding state temperature for metals and their salts solutions was defined as

$$T_{cor} = \alpha T_f \tag{2}$$

where T_f is a melting point of the salt and α is a constant. The k values for the solutions of cadmium in its three halides have been reported for the corresponding states temperature equal to $1.2 T_f$.[2]

The respective values of k for solutions of bismuth in its halides may be calculated in the same manner from the experimental data reported by Keneshea and Cubicciotti.[3-5] In Figure 1 the excess molar volumes of these solutions are shown as dependent on $x_m (1 - x_m)$ at temperatures equal to $1.2 T_f$. The experimental

points given in this figure correspond to the molar fractions of bismuth for which Keneshea and Cubicciotti have derived the equations describing the temperature dependence of density of these solutions. In the case of Bi in BiI$_3$ solutions the equations of these authors have been used for the temperatures higher than those at which their measurements were carried out.

It may be seen from Figure 1 that also in this case relation 1 is well fulfilled by solutions of bismuth in chloride and iodide in the whole range of concentrations investigated. The dependence of Bi–BiBr$_3$ system does not show this regularity; however, for comparison it may also be approximated as a linear one in the range of low metal molar fractions. Such limitation of the concentration range seems reasonable since in the case of cadmium systems, for which the solubility of metal is lower, the k values reported by us[2] correspond to the molar fraction of metal not exceeding 0.21. Thus the straight lines drawn in Figure 1 correspond to eq 1 calculated for the molar fractions of bismuth contained in the range 0-0.21.

In Table I the values of k for both groups of systems, calculated for the corresponding state temperatures, are listed.

It seemed of interest to search for empirical correlations between the excess molar volumes of solutions of cadmium and bismuth in their halides and the other properties of these solutions.

The molar volumes of liquid metal (V_m) or liquid salt (V_s) may be regarded as a sum of, respectively,

(1) J. Moscinski and L. Suski, *J. Phys. Chem.*, **72**, 441 (1968).

(2) J. Moscinski, L. Suski, and J. Galka, *J. Chem. Eng. Data*, **16**, 460 (1971).

(3) F. J. Keneshea and D. Cubicciotti, *J. Phys. Chem.*, **62**, 843 (1958).

(4) F. J. Keneshea and D. Cubicciotti, *ibid.*, **63**, 1112 (1959).

(5) F. J. Keneshea and D. Cubicciotti, *ibid.*, **63**, 1472 (1959).

Table I: Values of the Constant $k = V^E/[x_m(1 - x_m)]$ for the Solutions of Cadmium and Bismuth in Their Molten Halides, at Corresponding State Temperatures

System	Temp, °K	k
Cd–CdCl₂	1009	15.3 ± 1.4
Cd–CdBr₂	1009	~ 0
Cd–CdI₂	793	-4.6 ± 1.3
Bi–BiCl₃	604	-12.1 ± 0.2
Bi–BiBr₃	589	-16.1 ± 1.0
Bi–BiI₃	815	-25.5 ± 1.0

atomic (V_m^r) or ionic (V_s^r) "hard spheres" molar volumes and of the remaining part of the liquid molar volume, which we will conventionally call the molar "free volume" of this liquid $(V_m^*$ cr V_s^*, respectively). In first approximation let us assume that atomic and ionic "hard spheres" radii are equal to the respective values in the crystalline state. These values are[6]

	Cd	Bi	Cd²⁺	Bi³⁺	Cl⁻	Br⁻	I⁻
1	1.48	1.46					
2	1.48	1.55	0.97	0.96	1.81	1.95	2.16
3	1.52	1.82					

The radii of ions Cd^{2+}, Cl^-, Br^-, and I^- (in ångström units) are taken from Pauling's data for ionic crystals. The radius of Bi^{3+} cation is given after Ahrens. The choice of the suitable atomic radii for the two metals may present some difficulties. In the first row the values of atomic radii calculated for the covalent bond lengths of cadmium and bismuth are given. In the second row the respective values corresponding to the closest approach in the metallic lattices are reported, and in the third the radii calculated for the structures with the coordination number of 12.[6]

Table II gives the values of the molar "free volumes" for the two metals and six salts, calculated for the $1.2T_f$ temperatures making use of the data of the works cited above. For calculating the "free volumes" of both metals three kinds of atomic radii values have been used.

The comparison of data of Table I with the values of atomic and ionic radii shows a dependence between the radii of anions in the salt and the excess molar volumes of the solutions of both metals in these salts. For both cadmium and bismuth solutions the excess volumes decrease with the increasing radius of anions. In the cadmium solutions their values change from positive for chloride to negative for iodide solutions. In the case of bismuth solutions the contribution of anions to the all ionic "hard spheres" volume is higher and the excess molar volumes are much more negative than in the case of cadmium, but they decrease accordingly.

However, the values of excess molar volumes are determined probably in the first place by the values of
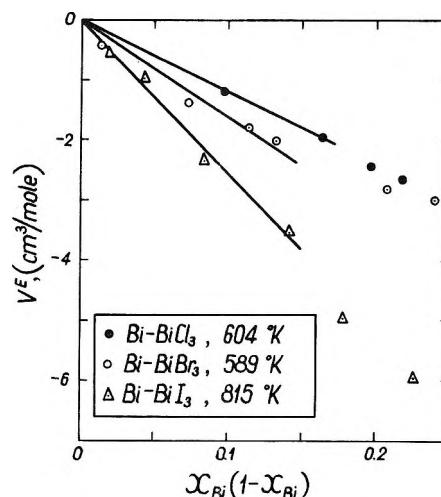
Figure 1. Excess molar volumes of the bismuth–bismuth halide systems vs. the molar fraction product of the components. The points were calculated from the Keneshea and Cubicciotti data (ref 3–5).
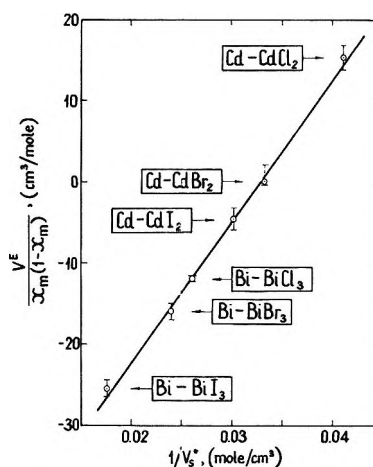
Figure 2. Excess molar volume of the solutions of cadmium and bismuth in their molten halides vs. the inverse of the molar "free volume" of molten halide.

molar "free volumes" of the solution components. It seems to us appropriate to check the correlations between the values of k for the six solutions and the molar "free volumes" of salts, as a sole variable, the more so as the salts are components of solutions in excess to metals. Let us assume that the values of k for solutions investigated are inversely proportional to the "free volumes" of salts. Figure 2 represents the relation

$$k = \frac{A}{V_s^*} + B \qquad (3)$$

(where A and B are empirical constants) for the six solutions under study.

(6) See, for example, R. C. Evans, "An Introduction to Crystal Chemistry," Cambridge University Press, Cambridge, 1964.

Table II: Molar Volumes of Metals (V_m) and Salts (V_s), and Molar "Free Volumes" of Metals (V_m* and Salts V_s*) (in cm³/mol) for Liquid Cadmium, Bismuth, and Their Molten Halides, at the Corresponding State Temperatures[a]

Temp, K	Cd V_m	Cd V_m*	CdCl₂ V_s	CdCl₂ V_s*	CdBr₂ V_s	CdBr₂ V_s*	CdI₂ V_s	CdI₂ V_s*
1009	14.90	a. 6.72	56.57	24.35				
		b. 6.72						
		c. 6.04						
1009	14.90	a. 6.72			69.75	30.05		
		b. 6.72						
		c. 6.04						
793	14.43	a. 6.25					86.23	33.09
		b. 6.25						
		c. 5.57						

	Bi V_m	Bi V_m*	BiCl₃ V_s	BiCl₃ V_s*	BiBr₃ V_s	BiBr₃ V_s*	BiI₃ V_s	BiI₃ V_s*
604	20.98	a. 13.13	85.48	38.37				
		b. 11.58						
		c. 5.77						
589	20.94	a. 13.09			99.94	41.61		
		b. 11.54						
		c. 13.72						
815	21.56	a. 13.72					135.41	56.92
		b. 12.17						
		c. 6.36						

[a] The molar "free volumes" of metals were calculated for various atomic radii: a, covalent radii; b, closest approach radii; and c radii of 12-coordination.

It may be seen that this relation is fulfilled very well. The correlation coefficient is 0.998 and values of the constants are $A = 1740 \pm 50$, $B = -57.2 \pm 1.5$.

In view of such high correlation the attempts to take into account in a relation like (3) the contribution of molar "free volume" of metals cannot improve the result. For the relation

$$k = \frac{A'}{V_s* + V_m*} + B' \tag{4}$$

one obtains constant values (Table III) for the three pairs of values for the atomic radii of cadmium and bismuth, respectively.

These purely empirical relations between the excess molar volume of six systems and the "free volumes" of their components, defined in such a simple manner, are derived without assuming the well-known formation of subions[7] like Cd_2^{2+} and Bi^+.

Table III: The Constants of Eq 4 Calculated for the Three Kinds of Values for Atomic Radii of Cadmium and Bismuth[a]

	A'	B'	Correlation coefficient
a	2100 ± 170	55.2 ± 4.0	0.987
b	2180 ± 150	57.3 ± 3.6	0.990
c	2400 ± 140	65.0 ± 4.0	0.994

[a] a, covalent radii; b, closest approach radii; c, radii of 12-coordination.

(7) See, for example, M. Bredig in "Molten Salt Chemistry," M. Blander, Ed., Interscience, New York, N. Y., 1964, p 307; J. D. Corbett in "Fused Salts," B. R. Sundheim, Ed., McGraw-Hill, New York, N. Y., 1964, p 341.

Size Determination of Sea Water Drops[1]

by H. F. Bezdek

University of California, San Diego, Marine Physical Laboratory of the Scripps Institution of Oceanography, San Diego, California 92152 *(Received May 26, 1971)*

Publication costs assisted by the Office of Naval Research

The fine-scale properties of a liquid surface can be studied by utilizing the drops formed by a bursting bubble. The simple and direct technique is described for measuring the radii of small transparent drops. Results are presented for filtered sea water at room temperature.

If a glass capillary tube is heated and drawn out into a fine hair-like tip, it provides a nozzle that will, upon immersion in a liquid, produce small, uniformly sized bubbles. The rate of production will depend, among other things, on the pressure applied to the tube. When the bubbles reach the surface and burst, a jet of water is thrown into the air that subsequently breaks up into a series of drops.[2] The height and size of each of these drops are quite uniform and reproducible.[3,4] Collection of these drops provides a delicate and sensitive method[5] for investigating the chemical and biological properties of an air–liquid interface.[6,7]

Our recent investigation into the biological structure of a filtered sea water surface using this technique required us to determine the size of the drops. A photographic method was chosen in which a 35-mm still camera was fitted to a variable, low-power microscope. The overall optical gain was adjustable between 2.5 and 10. A slide projector with a 1000-W bulb furnished sufficient illumination while a box lined with black velvet provided a suitable dark background. A measuring scale was obtained by including a picture of a precision micrometer disk (2 mm long with 200 divisions) on the film, this picture being taken through the same optical system as were pictures of the drops.

With the microscope set to view horizontally at a viewing angle of about 20° (see Figure 1) and positioned to observe only the peak of the trajectory of the uppermost jet drop, the pressure was adjusted to produce drops at a rate of 2–3/sec. Ten to fifteen exposures of the drops were taken, the duration of each exposure being from 5 to 20 sec. Of the many tracks obtained in this fashion, only those in sharp focus were chosen for measurement. Each film provided eight to ten such tracks. The speed and graininess of Kodak Tri-X film, in conjunction with Plymouth Ethol UFG developer, yielded negatives that permitted a calibrated microscope to determine the width of the tracks to a precision of 8 μ.

Based upon the height to which the top drop had risen, the first measurements of drop radius yielded results that were different by a factor of 2 or more from

those of previous work[2] (10–15 μ as opposed to 30 μ). However, as we extended our measurements to larger and larger (100-μ radius) drops (and consequently, darker and darker streaks), we began to notice an occasional streak that appeared to be associated with a faint ghost (see Figure 2). A close examination of previous films revealed that a few streaks due to smaller drops were also associated with extremely weak, second images.

This observation resolved the discrepancy. We had overlooked the fact that the drops are transparent. As such, they give rise to a double track, a thick, dark streak resulting from light transmission through the drop and a thin, faint streak due to reflection from its rear surface. The correct diameter for the drop is obtained by measuring the separation of the two streaks.

We computed a ray diagram[8] ($n = 1.36$) and discovered that the apparent diameter of the drop was a function of the viewing angle (see Figure 3). Viewing angles near 60° yield the least apparent change (decrease of about 7%), whereas angles near 90° produce a decrease of about 15% and angles near 15° a decrease of more than 30%. (Correction factors for drops of differing indices of refraction are given in the Appendix.) However, increasing the viewing angle from 20 to 60° in order to minimize this source of error reduces the intensity to the point where the faint streak vanishes completely. Fortunately, the use of a lens to focus the incident beam in the region of the drops removed this

(1) This paper was prepared under the sponsorship of the Office of Naval Research. Contribution from Scripps Institution of Oceanography.

(2) R. Donnelly and W. Glaberson, *Proc. Roy. Soc., Ser. A*, **290**, 547 (1966).

(3) D. C. Blanchard, *Progr. Oceanog.*, **1**, 73 (1963).

(4) O. Stuhlman, Jr., *J. Appl. Phys.*, **2**, 457 (1932).

(5) F. MacIntyre, *J. Phys. Chem.*, **72**, 589 (1968).

(6) D. C. Blanchard and L. Syzdek, *Science*, **170**, 626 (1970).

(7) P. E. Wilkness and D. J. Bresson, *J. Geophys. Res.*, **76**, 736 (1971).

(8) H. C. van de Hulst, "Light Scattering by Small Particles," Wiley, New York, N. Y., 1957, gives a complete and rigorous discussion of the optics of water drops including many references. See especially Chapter 12.
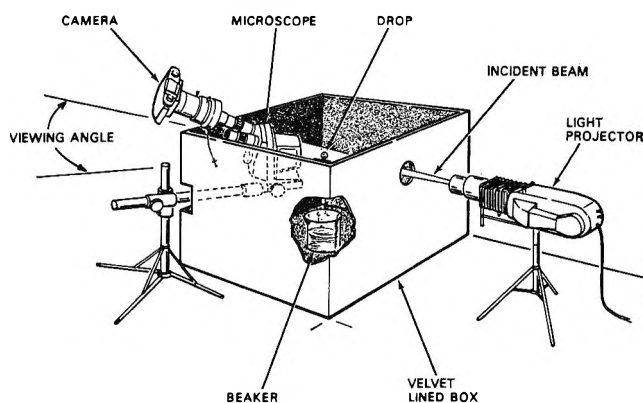
Figure 1. View of the experimental arrangement.
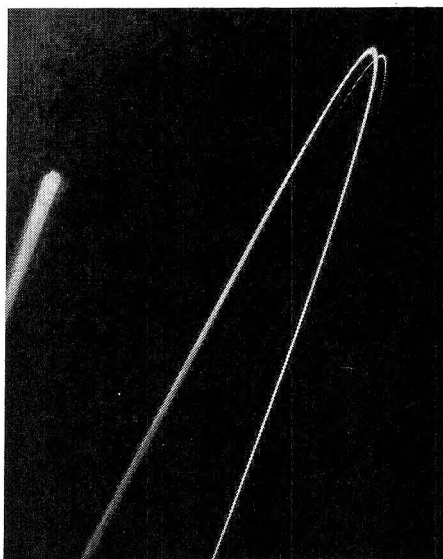
Figure 2. Photograph of the double streak resulting from a drop of sea water with a radius of 100 μ.

difficulty, and pictures taken at viewing angles of greater than 80° produced well defined double streaks.

Photographs of drops taken at angles of 80 and 60° showed little change in the apparent shortening of the diameter (due to the fact that the streaks are not sufficiently sharp to see a change of a few per cent), but those taken at angles of 60 and 20° indicated an apparent decrease in size of 20%. Obviously, drop sizes cannot be obtained from films taken at small viewing angles. Incidentally, the larger viewing angles (>45°) also serve to sharpen the thick streak and reduce its intensity relative to the thin streak. This fact is of importance in improving the resolution of the system.

Since drop height is a convenient and stable indicator[3] of the drop size, we present the results of our measurements (corrected for viewing angle) on filtered (0.45-μ Millipore filter) sea water at room temperature (22°) in the form of a graph where we plot the height of the top jet drop vs. the drop radius (see Figure 4). (The horizontal bar on each of the points represents the magnitude of the error in the radius at that point while
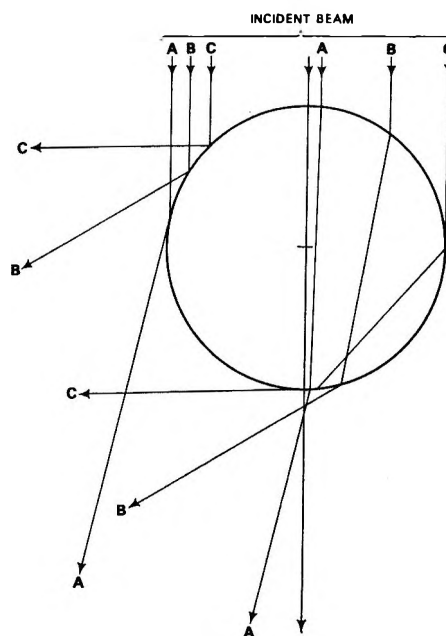
Figure 3. Top view of a ray diagram for a drop of water for $n = 1.36$.
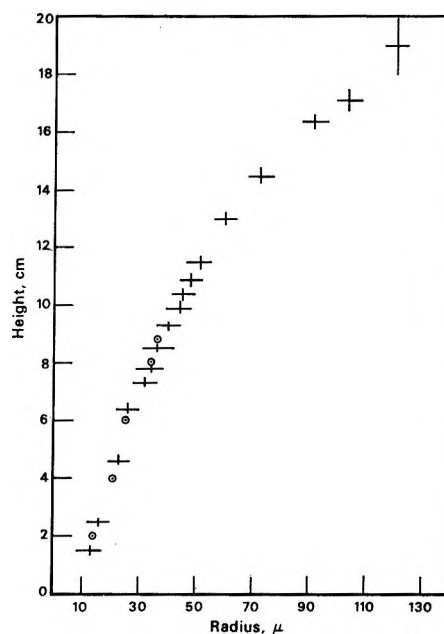
Figure 4. A plot giving the height vs. the radius for a drop of sea water at 22°: ⊙, from Blanchard,[3] +, this work, where the lengths of the bars represent the uncertainty in the measurement of the corresponding quantity.

the vertical bar indicates the observed variation in height.) Also included in the graph are results[3] obtained by using a more indirect method.[3,9]

Although the double streaks have been observed and photographed in the past,[10−12] still the explanation for

(9) D. C. Blanchard and A. H. Woodcock, Tellus, 9, 145 (1957).

(10) J. A. Day, Nature, 216, 1097 (1967).

(11) J. A. Day, Quart. J. Roy. Meteorol. Soc., 90, 72 (1964).

(12) R. D. Cadle and E. J. Wiggins, AMA Arch. Ind. Health, 12, 584 (1955).
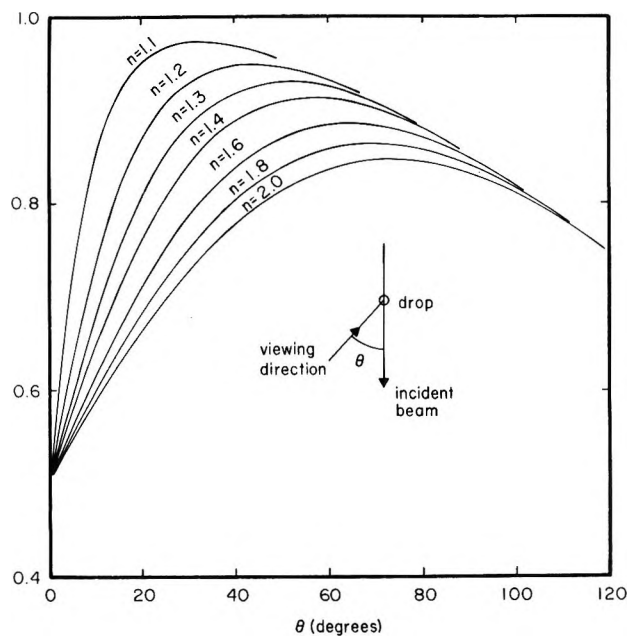
Figure 5. Plots of r (ratio of apparent diameter to actual diameter) as a function of θ with n (index of refraction) as the parameter.

angle θ (angle between the incident beam and the line of sight; see Figure 5). The index of refraction (n) is the parameter. Table I gives values for n, θ_m, and r_m, where θ_m and r_m are the coordinates of the maximum in the curves corresponding to the listed value of n (i.e., for a given value of n, r_m is the maximum value taken by r and this maximum value occurs at the angle θ_m).

Table I: Coordinates (θ_m, r_m) of the Maximum in Curves That Correspond to the Listed Values of n

n, index of refraction	θ_m, deg	r_m, apparent diameter/ actual diameter
1.1	34.2	0.97
1.2	45.4	0.95
1.3	52.6	0.93
1.4	58.4	0.91
1.5	62.4	0.90
1.6	66.6	0.88
1.7	68.4	0.87
1.8	71.0	0.86
1.9	73.0	0.86
2.0	74.6	0.85

their existence seems to have been omitted. In addition, the many excellent discussions[13-18] of methods for the sizing of particles appear to have neglected this simple, inexpensive, and direct technique. However, even in the elementary form described in this note, radii from 13 to 120 μ can be determined to $\pm 4\,\mu$. The precision could be improved with the use of a finer-grained film, but the reduced film speed requires a corresponding increase in the intensity of the light source.

Acknowledgment. I wish to thank J. Sloat for the ray program and Peter Fox for his assistance in the construction and operation of the apparatus.

Appendix

In order that the method described be applicable to transparent liquids other than sea water, calculations were carried out for a series of indices of refraction. The results are presented in Figure 5 as a parametric family of curves, which show r (ratio of apparent diameter to actual diameter) as a function of the viewing

These curves show clearly the effect of neglecting the viewing angle θ and the index of refraction. If proper account is not taken of these variables, errors will occur in the determination of the diameters that can exceed 40%! However, the use of Figure 5 in conjunction with Table I allows the proper correction factors to be ascertained for most situations that are likely to arise during the course of an investigation. More extensive tables can be furnished by the author upon request.

(13) R. C. Kintner, *Advan. Chem. Eng.*, **4**, 51 (1961).

(14) R. C. Kintner, T. J. Horton, R. E. Graumann, and S. Amberkar, *Can. J. Chem. Eng.*, **39**, 235 (1961).

(15) R. D. Cadle, "Particle Size," Reinhold, New York, N. Y., 1965.

(16) T. Allen, "Particle Size Measurements," Chapman and Hall Ltd., London, 1969.

(17) H. L. Green and W. R. Lane, "Particulate Clouds," Spon Ltd., London, 1964.

(18) For a comprehensive review of all phases of bubble and drop phenomena, see B. Gal-or, G E. Klinzing, and L. L. Tavlarides, *Ind. Eng. Chem.*, **61**, 21 (1969); L. L. Tavlarides, C. A. Coulaloglou, M. A. Zeitlin, G. E. Klinzig, and B. Gal-or, *ibid.*, **62**, 6 (1970).

The Competition for e_{aq}^- between Several Scavengers at High Concentrations

and Its Implications on the Relevance of Dry Electrons in the

Radiation Chemistry of Aqueous Solutions

by E. Peled and G. Czapski*

Department of Physical Chemistry, The Hebrew University, Jerusalem, Israel   (Received May 12, 1971)

Publication costs borne completely by The Journal of Physical Chemistry

The relative rate constant for the reactions of e_{aq}^- with H^+ compared to Cd^{2+}, Zn^{2+}, and acetone were measured as a function of concentrations up to 2 M. The results show either that $k_{e_{aq}^-+H^+}/k_{e_{aq}^-+Cd^{2+}}$ and $k_{e_{aq}^-+H^+}/k_{e_{aq}^-+acetone}$ decrease at high concentrations or that alternatively the ratio of rates is constant but the yields of e_{aq}^- ($G(e_{aq}^-)$) decrease in these concentrated solutions. The results are related to the time dependence of the above-mentioned ratios of the rate constants, as postulated by Schwarz, and to the dry-electron concept proposed by Hamill. One cannot, at this stage, make a definite decision with respect to the relative importance of the two alternatives.

In the diffusion model for the radiation chemistry of aqueous solutions it has been assumed[1] that all radicals and ions formed react only after thermalization and solvation of these species have been completed. Recently Hamill[2-7] has suggested a model which includes chemical reactions of e_{dry}^-, thermal electrons without hydration shells, with several e_{aq}^- scavengers such as N_2O, Lewis acids, and acetone. Moreover, Hamill suggests that e_{dry}^- does not react rapidly with H^+. Wolff, Bronskill, and Hunt,[8] using a picosecond pulse radiolysis technique, found that high concentrations of e_{aq}^- scavengers reduced the initial yield of e_{aq}^- and interpreted their results as due to the scavenging of e_{dry}^-.

We have studied the effect of concentrations on the competition reactions for e_{aq}^- between e_{aq}^- scavengers such as H^+–acetone, H^+–Cd^{2+}, Cd^{2+}–acetone, and H^+–Zn^{2+} so as to put to the test Hamill's suggestion that e_{aq}^- scavengers may react with e_{dry}^-.

Experimental Section

Triple-distilled water was used for the preparation of all the solutions. Materials were all of analytical grade. The competition between H^+ and acetone was studied by γ radiolysis in a ^{137}Cs γ source. A Fricke dosimeter was used to determine the dose rate taking $G(Fe^{3+}) = 15.5$. The dose rate was about 2000 rads/min. Total doses used were 14,000–60,000 rads. All solutions were irradiated at 10-cm³ syringes and the gas products were determined by gas chromatography; further details of the technique have been described earlier.[9]

The competitions between H^+ and Cd^{2+}, between Cd^{2+} and acetone, and between Zn^{2+} and H^+ for e_{aq}^- were studied by means of the pulse radiolysis technique. A Varian V-7715 linear accelerator gave 5-MeV electron pulses at a current of 200 mA. The Spectrosil quartz

radiation cell was 4.1 cm long. The analyzing light originated from a 150-W xenon arc passed through the cell three times (optical path 12.3 cm). Details of the experimental assembly are given elsewhere.[10]

The photolysis of 0.03 M iodide solutions with 0.5 M 2-propanol was carried out with a Cd lamp at 226 nm (filtered through 4 cm of H_2O). The solutions were deaerated by bubbling argon through the syringes. During irradiation the solutions were stirred with a magnetic stirrer. Hydrogen was analyzed as described above and yields were found to be linear with time. Hydrogen yields were less than 10 μM and I_3^- formed was less than 1 μM. Under the above conditions the light at 226 nm is almost entirely absorbed by I^- and not by I_3^-, 2-propanol, or acetone (even at 2 M).

Results

(a) *Radiolysis of the H^+ + Acetone System.* Hydrogen yields, $G(H_2)$, have been measured as a function of acid and acetone concentrations: the results are summarized in Table I. In some cases, the ratio $[H^+]/[acetone]$ was kept constant while the absolute

(1) A. Kupperman, "Actions Chimiques et Biologiques des Radiations," M. Haissinsky, Ed., Masson et Cie, Paris, 1961.

(2) W. H. Hamill, *J. Phys. Chem.*, **73**, 1341 (1969).

(3) T. Sawai and W. H. Hamill, *J. Chem. Phys.*, **52**, 3843 (1970).

(4) P. L. T. Bevan and W. H. Hamill, *Trans. Faraday Soc.*, **65**, 2533 (1970).

(5) T. Sawai and W. H. Hamill, *J. Phys. Chem.*, **74**, 3914 (1970).

(6) S. Khorana and W. H. Hamill, *ibid.*, **74**, 2885 (1970).

(7) W. H. Hamill, private communication.

(8) R. K. Wolff, M. J. Bronskill, and J. W. Hunt, *J. Chem. Phys.*, **53**, 4211 (1970).

(9) G. Czapski and E. Peled, *Isr. J. Chem.*, **6**, 421 (1968).

(10) Internal Report of the Accelerator Laboratory, Hebrew University, Jerusalem, Israel.

Table I: Values of $G_{e_{aq}^-}$ and k_6/k_4 According to Different Mechanisms[a]

[Acetone], M	[H+], M	$G(H_2)$	$G_{H_2} + G_H$[c]	$G^0_{e_{aq}^-}$[e]	G_H[e]	k6/k4 f	k6/k4 g	k6/k4 h	$G_{e_{aq}^-}$[f,i]	R[f,i]
0.02	0.01	2.42[b]	1.0[d]	2.8	0.6	0.48	0.43	0.35	...	...
0.3	1.32	3.5	0.9	3.2	0.5	0.94	...	0.5	2.90	0.90
0.4	0.2	2.25	0.85[d]	3.0	0.45	0.48	...	0.4	2.74	0.91
0.6	0.3	2.02	0.75	3.1	0.4	0.63	1.21	0.45	2.66	0.86
0.6	1.32	2.85	0.75	3.2	0.4	0.93	1.47	0.5	2.7	0.84
0.8	0.4	1.78	0.70[d]	3.1	0.4	0.80	1.37	0.5	2.4	0.77
0.8	0.8	2.24	0.70[d]	3.2	0.35	0.90	1.50	0.5	2.55	0.8
0.8	0.2	1.47	0.70[d]	3.0	0.40	0.62	1.22	0.4	2.24	0.75
1.0	0.5	1.46[b]	0.65[d]	3.2	0.35	1.24	1.51	0.5	1.84	0.58
1.0	1.68	2.50	0.65[d]	3.2	0.35	0.93	1.60	0.5	1.65	0.83
2.0	1.0	1.00[b]	0.56	3.2	0.31	2.40	2.00	0.5	1.12	0.35
2.0	1.32	1.15	0.56	3.2	0.3	2.18	1.97	0.5	1.30	0.40

[a] All solutions contained 0.1 M 2-propanol. [b] These solutions contained 0.1 and 0.7 M 2-propanol giving identical results. [c] These values are measured in neutral solutions of acetone concentrations as given in column 1 with 0.1 M 2-propanol. [d] Interpolated values. [e] Estimated values for these solutions. [f] Assuming $k_8/k_5 = 0.0218$ and $(k_7 + k_8)/k_5 = 0.033$ (P. Neta and R. H. Schuler, submitted for publication in *J. Phys. Chem.*) and calculated from eq III and values from columns 1–6. [g] Calculated values by H. A. Schwarz, submitted for publication in *J. Phys. Chem.*, assuming time dependence of k_6/k_4. [h] Values of k_6/k_4 taken from P. Neta and R. H. Schuler, submitted for publication in *J. Phys. Chem.*, and corrected for ionic strength effects of E. Peled and G. Czapski, *ibid.*, **74**, 2903 (1970). [i] Calculated from eq III with values of k_6/k_4 from column 10 and values from columns 1–4 and 6. [j] R defined in eq IV.

concentrations were increased. It was found that with constant $[H^+]/[acetone]$, $G(H_2)$ decreased while the concentrations of H^+ and acetone were increased. The relevant reactions of H_2 formation in this system are the spur reactions

$$e_{aq}^- + e_{aq}^- \longrightarrow H_2 \tag{1}$$

$$e_{aq}^- + H \longrightarrow H_2 \tag{2}$$

$$H + H \longrightarrow H_2 \tag{3}$$
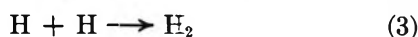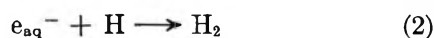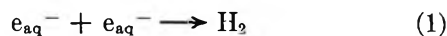
and other reactions, such as

$$e_{aq}^- + H^+ \longrightarrow H \tag{4}$$

$$H + \text{2-propanol} \longrightarrow H_2 \tag{5}$$

$$e_{aq}^- + \text{acetone} \longrightarrow P_1 \tag{6}$$

$$H + \text{acetone} \longrightarrow P_2 \neq H_2 \tag{7}$$

$$H + \text{acetone} \longrightarrow H_2 \tag{8}$$
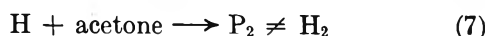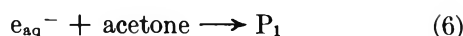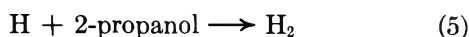
Reactions 1–3 are responsible for the formation of the molecular hydrogen yield, G_{H_2}, while reactions 4, 5, and 8 also contribute to total H_2 formation.

The complications due to reactions 7 and 8 were diminished (though not eliminated) by adding 0.1 M 2-propanol to the irradiated solutions. The rate equation for hydrogen production is

$$G(H_2) = G_{H_2} + \left(G_H + \frac{G_{e_{aq}^-}}{1 + \dfrac{k_6}{k_4}\dfrac{(\text{acetone})}{(H^+)}} \right)\alpha \tag{I}$$

where

$$\alpha = \frac{1 + \dfrac{k_8(\text{acetone})}{k_5(\text{2-propanol})}}{1 + \dfrac{k_7 + k_8}{k_5}\dfrac{(\text{acetone})}{(\text{2-propanol})}} \tag{II}$$

or

$$\frac{k_6}{k_4} = \frac{(H^+)}{(\text{acetone})}\left\{ \frac{G_{e_{aq}^-}}{[G(H_2) - G_{H_2}]/\alpha - G_H} - 1 \right\} \tag{III}$$

where $G(H_2)$ is the observed hydrogen yield and G_{H_2}, G_H, and $G_{e_{aq}^-}$ are the molecular yield of hydrogen (including reactions 1 and 3), hydrogen atoms, and hydrated electrons. The latter three yields are somewhat dependent on the acetone and hydrogen ion concentrations, but reasonable estimates for these effects are available (assuming no role of e_{dry}^-). The rate constant ratio k_8/k_5 is 0.022 and $(k_7 + k_8)/k_5 = 0.033$.[11] The parameter α varies between 1.0 (low acetone concentration) and 0.87 (2 M acetone). Different choices of the yields or rate constant ratios[11,12] affect the value of k_6/k_4 by about $\pm 30\%$ and $G_{e_{aq}^-}$ and R by less than 20% but leave the conclusions unchanged.

Calculation of k_6/k_4, as given in Table I, column 7, shows that this ratio increases with increasing solute concentration up to a factor of 5. Alternatively, k_6/k_4 may be assumed constant (except for a small estimated ionic strength effect, as shown in column 9 Table I) and eq I may be solved for the value of $G_{e_{aq}^-}$ at each concentration. We define R as the ratio of $G_{e_{aq}^-}$ calculated as

(11) P. Neta and R. H. Schuler, submitted for publication in *J. Phys. Chem.*

(12) M. Anbar and P. Neta, *Int. J. Appl. Radiat. Isotop.*, **18**, 493 (1967).
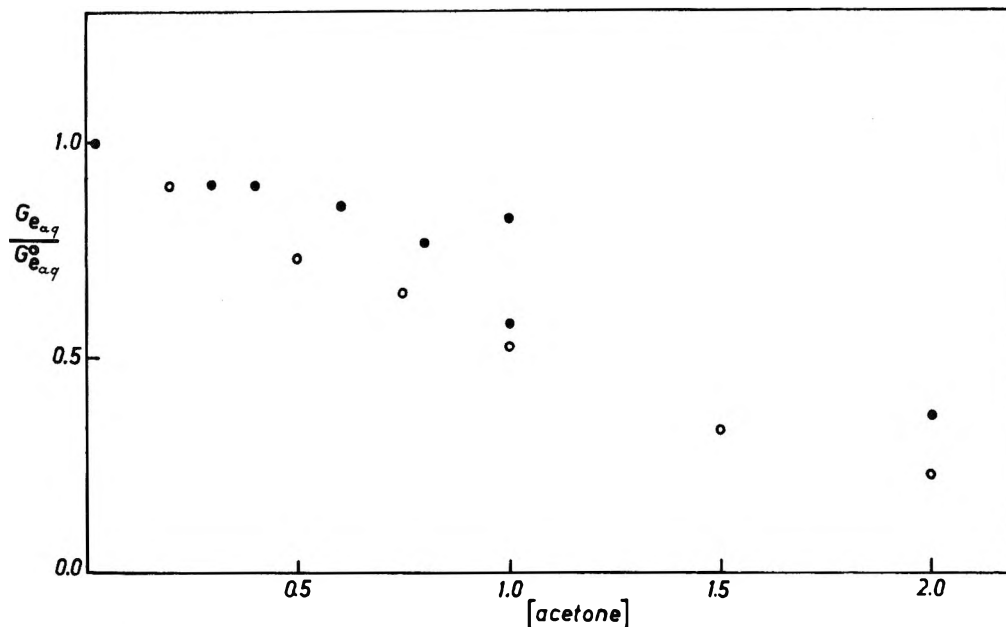
Figure 1. R, the ratio of $G_{e_{aq}^-}$ over $G^0_{e_{aq}^-}$ (at zero concentration of acetone), as a function of the acetone concentration: $\bigcirc$, ref 8; $\bullet$, our results.

described above to the expected value of $G^0_{e_{aq}^-}$ in these solutions, column 5

$$R = \frac{G_{e_{aq}^-}}{G^0_{e_{aq}^-}} \qquad (IV)$$

Values of R are given in Table I, column 11, and, in Figure 1, are compared with values found by Hunt, et al.[8,13]

(b) *Photolysis of Iodide in the Presence of 2-Propanol.* In the photolysis of I^- it was shown that e_{aq}^- is formed through the equation[14]

$$I^- \xrightarrow{h\nu} I + e_{aq}^-$$

In the presence of acetone and H^+, e_{aq}^- competes in reactions 4 and 6. The H atoms formed through reaction 4 yield H_2 by reaction 5.

If we denote by ϕ_0 and ϕ the quantum yields of H_2 in the absence and presence of acetone, respectively, we obtain

$$\frac{k_6}{k_4} = \frac{[H^+]}{[acetone]}\left[\frac{\phi_0}{\phi}\alpha - 1\right] \qquad (V)$$

Values of k_6/k_4 obtained from these experiments at various [H^+] and [acetone] are given in Table II. Equation V assumes a concentration-independent cage effect in the I^- photolysis.

(c) *Cd^{2+} and $H^+ + Cd^{2+}$ System.* The initial yield of Cd^+ from reaction 9 was measured by the pulse

$$e_{aq}^- + Cd^{2+} \longrightarrow Cd^+ \qquad (9)$$
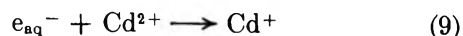
radiolysis technique as a function of H^+ and Cd^{2+} (as $CdSO_4$) concentrations. The effect of [Cd^{2+}] on $G(Cd^+)$ is summarized in Table III. The yield $G(Cd^+)$

Table II: k_6/k_4 Values from Photolysis of I^- [a]

[H+], M	[Acetone], M	[NaClO4], M	$\phi(H_2)/\phi_0(H_2)$	k_6/k_4
1	2	. . .	0.37	0.88 ± 0.05
1	1	. . .	0.53	0.90 ± 0.05
1	0.5	. . .	0.65	1.02 ± 0.05
0.05	0.1	1	0.41	0.72 ± 0.05
0.05	0.1	. . .	0.56	0.42 ± 0.05

[a] 0.03 M I^- + 0.5 M 2-propanol photolyzed at 228 nm.

increases by about 10% ($CdSO_4$) or 20% ($Cd(ClO_4)_2$) as the concentration of cadmium is raised from 0.1 to 0.5 M. The combined effects of H^+ and Cd^{2+} (in the presence of 2-propanol) are shown in Table IV. The percentage increase of $G(Cd^+)$ with cadmium concentration at constant $(H^+)/(Cd^{2+})$ is much greater than that observed in Table III. This increase may result either from the reduction in the lifetime of the reaction $e_{aq}^- + Cd^{2+}$ or from the scavenging of e_{aq}^- precursors by Cd^{2+}.

(d) *$Zn^{2+} + H^+$ System.* The cation Zn^{2+} has relatively low reactivity toward e_{aq}^- ($k_{10} = 1.5 \times 10^9$).[12] It is therefore interesting to find out if this cation can

$$e_{aq}^- + Zn^{2+} \longrightarrow Zn^+ \qquad (10)$$
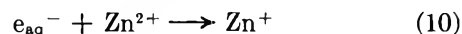
scavenge the e_{aq}^- precursor (e_{dry}^-). The yield of Zn^+ as a function of H^+ and Zn^{2+} concentration was measured by pulse radiolysis techniques following its initial

(13) M. J. Bronskill, R. K. Wolff, and J. W. Hunt, *J. Chem. Phys.*, **53**, 4201 (1970).

(14) J. Jortner, M. Ottolenghi, and G. Stein, *J. Phys. Chem.*, **66**, 2029 (1962).

Table III: The Effect of $[Cd^{2+}]$ on $G(Gd^+)$ at pH >4

[Solute], M	OD_{300}	$G(Cd^+)$
10^{-3} (CdSO$_4$)	0.283	2.70[a]
5×10^{-3} (CdSO$_4$)	0.313	3.00
10^{-2} (CdSO$_4$)	0.325	3.10
3×10^{-2} (CdSO$_4$)	0.329	3.14
0.1 (CdSO$_4$)	0.337	3.21
0.3 (CdSO$_4$)	0.371	3.55
0.5 (CdSO$_4$)	0.375	3.58
10^{-3} (Cd(ClO$_4$)$_2$)	0.283	2.70
0.1 (Cd(ClO$_4$)$_2$)	0.322	3.07
0.5 (Cd(ClO$_4$)$_2$)	0.381	3.64

[a] All yields are relative to this value.

Table IV: The Effect of H^+ and Cd^{2+} Concentration on $G(Cd^+)$

[Cd(ClO$_4$)$_2$] or [CdSO$_4$], M	[HClO$_4$] or [H$_2$SO$_4$], M	[2-Propanol], M	$(OD_{330})_{t=0}$	$(OD_{330}{}^{Cd^+})_{t=0}$
0.05[a]			0.318	
0.05[a]		0.1	0.371	0.356
0.1[a]	2.0	0.1	0.127	0.112
0.3[a]	2.0	0.1	0.225	0.21
0.5[a]	2.0	0.1	0.256	0.241
		0.1	0.015	
0.1[b]	0.2		0.54	
0.25[b]	0.5		0.69	
0.5[b]	1.0		0.84	

[a] HClO$_4$ and Cd(ClO$_4$)$_2$. [b] H$_2$SO$_4$ and CdSO$_4$.

absorption at 330 nm. The results are summarized in Table V. The increase in optical density over 2-propanol alone (due to 2-propanol radical) with Zn^{2+} concentration is within error that which is expected from the competition with H^+ for e_{aq}^-. Hence, zinc ions do not behave like cadmium ions.

Table V: The Effect of Zn^{2+} and H^+ Concentrations on $G(Zn^+)$ (Pulse $\sim$0.5 μsec)

[Zn(ClO$_4$)$_2$], M	[HClO$_4$], M	[2-Propanol], M	$(OD_{330})_{t=0}$
0.2	...	...	0.283
0.5	...	...	0.283
0.1	...	0.1	0.234
0.1	1.0	0.1	0.019
0.3	1.0	0.1	0.022
0.5	1.0	0.1	0.024
...	...	0.1	0.015

(e) Cd^{2+} + Acetone System. The initial yield of Cd^+ was measured as a function of Cd^{2+} and acetone concentrations using pulse radiolysis. The absorption

of Cd^+ was followed at 330 nm at the end of the 1.5-μsec pulse. The results are summarized in Table VI. We found that the yield of Cd^+ increases with the increase of Cd^{2+} and acetone concentrations, while $[Cd^{2+}]/[acetone]$ and the ionic strength were kept constant. This increase of $G(Cd^+)$ may be due to several factors. (1) $G_{e_{aq}^-}$ increases from 3.2 to 3.55 as $[Cd^{2+}]$ is changed from 0.1 to 0.5 M. (2) At high concentrations, Cd^{2+} and acetone may differ in their efficiency of scavenging e_{dry}^-, Cd^{2+} being the better scavenger. (3) At high Cd^{2+} concentrations the short-lived ion radical $(CH_3COCH_3)^-$ or $CH_3\dot{C}OHCH_3$ may react with Cd^{2+} to yield Cd^+. This last possibility was ruled out as $G(Cd^+)$ in 0.4 M CdSO$_4$ was not affected by addition of up to 0.1 M 2-propanol at either pH $\sim$7 or pH 1.7 and in solutions of 2 M acetone + 0.1 M CdSO$_4$ little, if any, Cd^+ could be detected.

Table VI: The Dependence of $G(Cd)^+$ on Cd^{2+} and Acetone Concentrations (Pulse $\sim$1.5 μsec)

Solutes	$(OD_{330})_{t=0}$
5×10^{-3} M CdSO$_4$	0.74
10^{-2} M acetone + 0.1 M 2-propanol	0.039
10^{-2} M acetone + 10^{-2} M CdSO$_4$ + 0.4 M Na$_2$SO$_4$	0.54
0.1 M acetone + 0.1 M CdSO$_4$ + 0.4 M Na$_2$SO$_4$	0.65
0.5 M acetone + 0.5 M CdSO$_4$	0.73

(f) The Effect of Several Solutes on $G_{e_{aq}^-}$. The initial yield of e_{aq}^- was measured in several concentrated solutions of e_{aq}^- scavengers using $\sim$100-nsec pulses. The absorption of e_{aq}^- was followed at wavelengths near the e_{aq}^- peak (when possible) in order to eliminate artifacts due to the movement of the peak at such high ionic strength. The results are summarized in Table VII.

If one assumes that e_{dry}^- is a precursor of e_{aq}^- and reacts with Cd^{2+} and acetone but not with acid or Zn^{2+}, then our results support Hamill's mechanism. The extreme alternative approach assumes that no scavenging of a precursor of e_{aq}^- is necessary if we consider the time dependence of k_4, k_6, k_9, and k_{10} or, in general, the time dependence of $k_{e_{aq}^-+S}$. Schwarz has made calculations on the time dependence of k_6/k_4 assuming no reaction of acetone with any precursor of e_{aq}^-.[15] His results are given in Table I, column 8, and compared to our experimental results given in column 7. The magnitude of the effect of concentration on k_6/k_4 as found experimentally is similar to the computed effect. It is clear that time-dependent rate constant effects must be considered in all work with reactive solutes at high concentration whether or not a precursor of e_{aq}^- exists.

(15) H. A. Schwarz, submitted for publication in *J. Phys. Chem.*

Table VII: The Effect of e_{aq}^- Scavengers on $G_{e_{aq}^-}$ (in Neutral Solutions[a])

Solute	Concn, M	Wavelengths at which OD$_0$'s of e_{aq}^- were measd, nm	$G(e_{aq}^-)_{t=10^{-7} sec}$	$\tau_{1/2}$ of e_{aq}^-,	$k_{e_{aq}^-+S}$, $M^{-1} sec^{-1}$ [c]	k_{H+S}, $M^{-1} sec^{-1}$ [c]	k_{OH+S}, $M^{-1} sec^{-1}$ [c]
Methanol	10^{-2}	625, 650, 675	2.6	>10	$<10^4$	1.6×10^6	$5 + 10^8$
NH$_4$Cl	1.0	625	2.95	~1	1.3×10^6	...	$<10^7$
α-Alanine	1.0	625	2.2 ± 0.25^d	~0.2	$<5 \times 10^6$	...	~10^8
Glycine	1.0	550	1.95 ± 0.25^d	~0.2	8.2×10^6	1.7×10^7	~10^7
Sodium acetate	1.0	625, 650, 675	2.7^b	~7	$<10^6$	2.7×10^5	5×10^7
Sodium formate	1.0	625, 650, 675	2.5^b	~2	$<10^6$	2.5×10^8	2.5×10^9
Sodium citrate	0.5	625, 650, 675	2.6^b	~7	$<10^6$	...	...
2-Propanol	0.3	625	2.85	...	...	5×10^7	1.7×10^9
2-Propanol	1.0	625	2.75	...	...	5×10^7	1.7×10^9

[a] Pulse length 50–100 nsec, OD$_{e_{aq}^-}$ was measured after extrapolation to the middle of the pulse. [b] D. Meisel and E. Peled, unpublished results. [c] Reference 11. [d] Due to uncertainty in extrapolation.

Values of k_6/k_4 obtained from I^- photolysis are greater than the ratio expected from dilute solution (see column 6 of Table I) and parallel those from ^{60}Co radiolysis below 1 M acetone concentration. Above 1 M the values derived from photolysis no longer increase and appear even to decrease slightly with concentration. The meaning of this discrepancy is unclear for the following reasons. (a) The cage effect in these photolysis experiments may depend somewhat on concentration of acetone. (b) The H$^+$ immediately after the photodissociation of I^- may not be randomly distributed around e_{aq}^- since the H$^+$ was in equilibrium with the parent I^-. (The assumption is that in the photolysis of I^- in the CTTS band e_{dry}^- is not even a precursor as e_{aq}^- is formed directly.)

Very recent results of Hamill show that acetate, which is rather unreactive with OH, H, and e_{aq}^-, increases $G_{e_{aq}^-}$ (measured as G_{Cd^+})—such behavior could not be accounted for by time-dependence theory but only assuming the reaction of acetate with a precursor of the OH or e_{aq}^-, such as H$_2$O$_{dry}^+$ or H$_3$O$_{dry}^+$.[7] However in this study, in contrast to Hamill's work, we found that acetate has no effect on $G_{e_{aq}^-}$ (Table VII).

We have studied the effect of several solutes on $G_{e_{aq}^-}$. The solutes were chosen so that their reactivities with e_{aq}^-, H, and OH would be low so that the effect of scavenging these radicals from the spur could be neglected. The results are given in Table VII. The behavior of the amino acids is different from that of the rest of the solutes as they decrease $G_{e_{aq}^-}$ substantially. As glycine and alanine are unreactive with e_{aq}^-, this effect suggests that these amino acids may react with some precursor of the e_{aq}^- (provided that these acids did not contain too much impurities, active toward e_{aq}^-, and that our extrapolation to get $G_{e_{aq}^-}$ did not introduce a too large error).

To summarize this discussion it seems that the time dependence of k_6/k_4 as calculated by Schwarz[15] has to be taken into account in any interpretation of studies in very concentrated solutions. This effect may explain at least to a large extent the effects observed. Nevertheless the possibility of scavenging of e_{dry}^- must also be considered due to the comparison with organic[7] or glassy systems[6] and due to behavior of some of the systems given in Table VII such as the amino acids.

NOTES

Radiation-Induced Oxidation of Liquid Sulfur Dioxide Containing Oxygen and Water[1]

by Siegfried Schönherr,* Helmut Seidel,

Bergakademie Freiberg, Sektion Chemie, Arbeitsgruppe Reaktionsverhalten und Syntheseprinzipien, Freiberg, East Germany

and Walter G. Rothschild*

Department of Chemistry, Scientific Research Staff, Ford Motor Company, Dearborn, Michigan 48121 (*Received February 1, 1971*)

Various recent publications on the radiation chemistry of liquid sulfur dioxide and its solutions make use of a simple radical mechanism to account for the stoichiometry of the products. This mechanism

$$SO_2 \overset{h\nu}{\longrightarrow} SO + O \qquad (1)$$
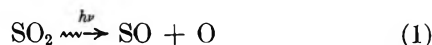
which, as proposed, forms O and SO biradicals in equimolar amounts,[2] has afforded a satisfactory explanation of reaction products and reaction steps in various simple liquid sulfur dioxide systems.[2-5]

It is quite obvious that other mechanisms, which are equally acceptable in describing the product stoichiometry, can be written down. Furthermore, from the nature of liquid SO_2 it is evident that ionic reactions must be considered to fully explain the radiation chemistry of this solvent.[2,3] Yet, remembering that knowledge about the radiation chemistry of this system is still sparse, it seemed more profitable to push instead the proposed radical mechanism to its limits to ascertain where it may fail and where further work—hopefully using more sophisticated techniques than available to us—is indicated.

We have therefore studied, on the basis of eq 1 and some of its logical subsequent steps,[2,4,5] the effect of precisely controlled oxygen atmospheres and of exactly known amounts of water on the ^{60}Co γ-ray induced product formation in the respective liquid sulfur dioxide systems. We expect that initially added oxygen will set up competition mechanisms involving primary (in our mechanism) radicals. Addition of water, on the other hand, would permit us to test whether the complications introduced by active species arising from water decomposition[6,7] can be accounted for in the framework of our simple reaction mechanism.

Experimental Section

Details of the purification, irradiation, identification and analytical procedures have been previously described.[2,5,8] Gas atmospheres and corresponding solution concentrations were precisely controlled by accurate gas mixing, standard analysis, known absorption coefficients,[9] and continuous gas saturation of the solutions. Irradiation temperatures were maintained by using conveniently boiling liquids contained in the cooling jacket of the irradiation vessel ($-40.8°$, Freon 22; $-33°$, ammonia; $-23.7°$, CH_3Cl). The wet liquid SO_2 solutions were analyzed for water using conventional techniques;[10] the measured solubilities agreed well with literature data.[11] Dithionic acid ($H_2S_2O_6$) was determined by a titration method.[12] In all cases we convinced ourselves that the applied analytical techniques were reliable within a few per cent error. The dose rate was measured with the help of the Cu–Fe dosimeter;[13] it amounted to 0.281×10^{17} eV cm^{-3} sec^{-1} in the liquid SO_2 (at $-23.7°$). All yields are reported in milligrams per cubic centimeter or in G values (number of molecules oxidized or reduced per 100 eV absorbed in the solution). Significant amounts of dark reactions were not detected.

Results and Discussion

a. Anhydrous Liquid Sulfur Dioxide–Oxygen System. The points in Figure 1 show the experimental G values of SO_3 formation as a function of dissolved oxygen concentration, $[O_2]$, in liquid SO_2 which was continuously saturated by O_2–Ar mixtures. For relatively low $[O_2]$, the data are seen to extrapolate to $G(SO_3) = G(O) = 1.35$, the radical yield in the deaerated system.[2] For relatively high $[O_2]$, $G(SO_3)$ attains a value of ~2.8,

(1) Taken from the Diploma Dissertation of H. Seidel, 1968–1969.

(2) W. G. Rothschild, *J. Amer. Chem. Soc.*, **86**, 1307 (1964).

(3) W. G. Rothschild, paper 148, Division of Physical Chemistry, 149th National Meeting of the American Chemical Society, Detroit, Mich., April 1965.

(4) W. G. Rothschild, *J. Chem. Phys.*, **45**, 3594 (1966).

(5) S. Schönherr, R. Schrader, and P. Mahlitz, *Z. Anorg. Allg. Chem.*, **365**, 262 (1969).

(6) R. Schrader and S. Schönherr, *Naturwissenschaften*, **48**, 569 (1961).

(7) R. Schrader and S. Schönherr, *Z. Anorg. Allg. Chem.*, **331**, 289, 298 (1964).

(8) P. Mahlitz, Diploma Dissertation, Freiberg, 1968.

(9) M. R. Dean and W. S. Walls, *Ind. Eng. Chem.*, **39**, 1049 (1947).

(10) E. Eberius, *Chem. Rundsch.*, **7**, 337 (1954).

(11) D. Murakami and N. Tokura, *Bull. Chem. Soc. Jap.*, **31**, 431 (1958).

(12) R. Lang and H. Kurtenacker, *Z. Anal. Chem.*, **123**, 81 (1942).

(13) E. J. Hart, *Radiat. Res.*, **2**, 33 (1955).
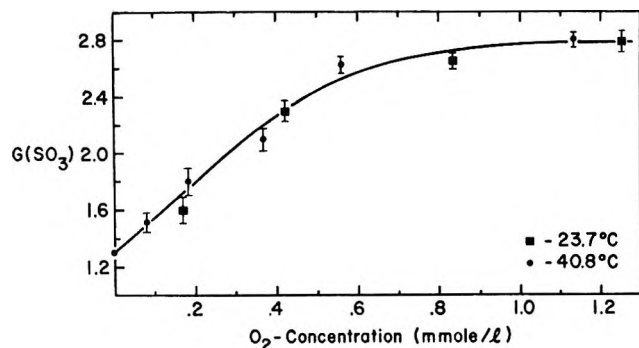
Figure 1. Radiation-induced 100-eV yields of SO_3 formation in anhydrous liquid sulfur dioxide as a function of oxygen concentration. Dose rate: 0.289×10^{17} $(-40.8°)$ and 0.281×10^{17} eV cm^{-3} sec^{-1} $(-23.7°)$. Each point represents the slope of the (linear) plot of mg/cm^3 SO_3 vs. dose at a constant $[O_2]$.

Figure 2. Radiation-induced $H_2S_2O_6$ formation in water-saturated liquid sulfur dioxide. The upper curve shows the $H_2S_2O_6$ formation in a medium which was Ar-saturated prior to irradiation, the lower curve shows this for a medium which was O_2-saturated prior to exposure.

Figure 3. Radiation-induced H_2SO_4 formation in water-saturated liquid SO_2 at $-40.8°$. The solution was continually saturated with pure O_2. The yield during the linear portion corresponds to the highest $G(SO_3)$ in Figure 1.

which is twice the radical yield of the air-free system, since now SO is converted into an oxidizing species[5]

$$O_2 + SO \longrightarrow O + SO_2 \qquad (2)$$

$$O + SO_2 \longrightarrow SO_3 \qquad (3)$$
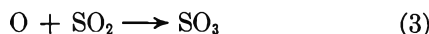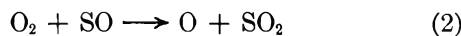
We therefore expect that for intermediate $[O_2]$ a competition mechanism is taking place. On the premise of our radical reaction scheme, the simplest such mechanism is[14]

$$SO + O_2 \longrightarrow SO_2 + O \qquad (2)$$

$$SO + SO \longrightarrow SO_2 + S \qquad (4)$$
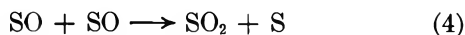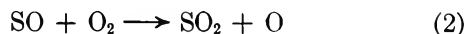
(We always detected elemental sulfur at low $[O_2]$.)

Setting up the corresponding steady-state equations, we obtain[16]

$$d[SO_3]/dt = aG(SO_3)R = aG(O)R +$$

$$k_2[O_2] \left\{ -\frac{k_2}{4k_4}[O_2] + \left(\frac{k_2^2}{16k_4^2}[O_2]^2 + \frac{aG(O)R}{2k_4} \right)^{1/2} \right\} \qquad (5)$$

Developing the expression under the square root into a power series for the cases of low $[O_2]$ and for high $[O_2]$, eq 5 approximates to

$$d[SO_3]/dt \approx aG(O)R + k_2[O_2](aG(O)R/2k_4)^{1/2}$$

$$(\text{low } [O_2]) \quad (6)$$

and

$$d[SO_3]/dt \approx 2aG(O)R \left\{ 1 - \frac{k_4 aG(O)R}{k_2^2[O_2]^2} \right\}$$

$$(\text{high } [O_2]) \quad (7)$$

if the series developments are broken off after the term to first order and second order, respectively.

The rate expressions reproduce satisfactorily the data shown in Figure 1, using a rate constant ratio of

$$k_4^{1/2}/k_2 \sim 0.47 \pm 0.15 \ (\text{mol}^{1/2} \ l.^{-1/2} \ \text{sec}^{1/2}) \qquad (8)$$

(We obtain this value, according to eq 6, from the initial slope of the curve in Figure 1.)

b. Water-Containing System. The principal difference as compared to the reactions in the anhydrous system is (i) appearance of dithionic acid[5] ($H_2S_2O_6$), and (ii) SO_3 formation by an initial short-chain process.[5] Figure 2 shows the rate of $H_2S_2O_6$ formation in wet liquid SO_2 (0.49 wt % H_2O at $-23.7°$, 0.27% at $-40.8°$) which was saturated with wet O_2 and Ar, respectively, prior to irradiation. It is evident that the formation of $H_2S_2O_6$ is suppressed in the presence of O_2. We rationalize this by the steps[16]

$$HSO_3 + HSO_3 \longrightarrow H_2S_2O_6 \qquad (9)$$
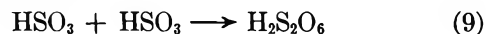
and

(14) In our experiments, $[SO_3]/[SO_2] \sim 0.001$ at the highest dose. In such a case, the back reaction $SO_3 + O \rightarrow SO_2 + O_2$ amounts to less than 1% of the forward step (3); thus $G(SO) \approx G(O) = 1.35$ (see ref 2).

(15) The factor a amounts to $10^{-2}/N$ (N = Avogadro's number) = 0.166×10^{-25}, where dose rate R is in eV l.$^{-1}$ sec^{-1} and concentrations in mol/l.

(16) R. Schrader, S. Schönherr, and B. Fritsche, *Z. Anorg. Allg. Chem.*, **339**, 67 (1965).

$$HSO_3 + O_2 \longrightarrow HSO_5 \quad (10)$$

There are various reaction steps which, together with step 10, could conceivably consume O_2 by a chain mechanism, for instance[5]

$$H + O_2 \longrightarrow HO_2 \quad (11)$$

$$HO_2 + SO_2 \longrightarrow SO_3 + OH \quad (12)$$

$$OH + SO_2 \longrightarrow HSO_3 \quad (13)$$

$$HSO_5 + SO_2 \longrightarrow 2SO_3 + OH \quad (14)$$
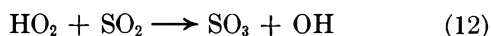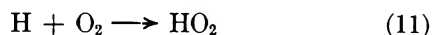
We have observed, as displayed by the data in Figure 3, that this is indeed the case. However, the chain mechanism involves, as is evident from the low chain yield, rather short chains. After an initial rise, $G(SO_3)$ soon drops to a value close to that in the corresponding anhydrous liquid sulfur dioxide–oxygen system (see Figure 1).

It is useful to remark here that the yield of SO_3 in this system is too high to arise by *direct* interaction with oxidizing species from the radiolysis of water (the water absorbs about 0.3% of the total dose). Nor does it turn out that the product formation in wet liquid SO_2 is simply a superposition of that of the anhydrous substance and that derived from the aqueous system—even taking the highest (initial) yield of H_2SO_4 formation reported.[17]

We find that various observations in the water-containing systems are difficult to describe quantitatively or to explain at all on the basis of our simple mechanisms. For instance, we have measured that the yield of $H_2S_2O_6$ formation is 1.6 at $-40.8°$ (see Figure 2) but 2.5 at $-23.7°$. We see no way to rationalize this temperature dependence, which is outside the experimental error (and shows a consistent trend), with the help of the above reaction steps.

Furthermore, we unexpectedly find some initial short-chain oxidation of SO_2 to SO_3 in wet, air-free liquid SO_2 at $+16°$ (vapor pressure 2.9 atm). In fact, the G value of this short-chain oxidation process (~ 17), as well as its duration, were the greatest observed in our experiments.

We are therefore led to the conclusion that the radiation-induced products in anhydrous liquid sulfur dioxide systems can be explained satisfactorily on the basis of a few radical steps involving O and SO, the "primary" decomposition products. On the other hand, in the presence of water the mechanism no longer accounts quantitatively for the reaction products nor (even qualitatively) predicts the observed temperature dependence.

(17) For instance, consider formation of H_2SO_4 in wet, O_2-saturated liquid SO_2 at a dose of 0.25×10^{20} eV cm^{-3}. The observed yield amounts to 0.4 mg/cm^3 (see Figure 3). Regarding the aqueous "part system" (0.42 vol %) as O_2- and SO_2-saturated water, we compute a maximum yield of 0.062 mg/cm^3 H_2SO_4, based on $G(H_2SO_4) = 510$ (see ref 7), for it. For the anhydrous liquid SO_2, we compute a yield of 0.10 mg/cm^3 SO_3, based on $G(SO_3) = 2.6$, for this dose. These individual contributions do not add up to the observed H_2SO_4 yield.

Thermodynamic Data for the Water–Hexamethylenetetramine System

by F. Quadrifoglio, V. Crescenzi,* A. Cesàro, and F. Delben

Istituto di Chimica, Università di Trieste, Trieste, Italy
(Received February 3, 1971)

The physicochemical properties of hexamethylenetetramine (HMT) aqueous solutions have attracted considerable attention.[1-4] In terms of certain features exhibited by these solutions, HMT has been considered as a "structure-maker" solute in water.[5]

The results reported here should help to gain a more complete physicochemical picture of the water–HMT system and hence also to provide additional, though indirect, information on the influence of HMT on the structural organization of the solvent.

Our work has been concerned with measurements of

Table I: Heat of Dilution of HMT Solutions at 25°[a]

$\hat{m}_1$	m_2	q_{obsd}, cal $\times 10^{-3}$	ΔH, cal/mol	$\Delta H/\Delta m$
0.1809	0.1708	2.012	2.655	262.2
0.3118	0.2984	4.602	3.888	290.1
0.3277	0.3120	5.311	4.426	281.9
0.5625	0.5457	8.644	4.886	290.8
0.8509	0.8029	39.84	13.86	288.7
0.9671	0.9078	56.71	16.998	286.6
1.3447	1.2534	117.2	28.36	310.6
1.6824	1.5551	207.0	40.91	321.4
2.0680	1.9486	242.2	38.63	323.6
2.6044	2.4125	457.7	64.65	336.9
2.8076	2.6828	333.1	42.02	336.7
4.4004	4.0973	1252.0	113.3	373.8

[a] All measurements have been carried out using a LKB batch-type microcalorimeter. The purification of HMT has been made as already described.[2a]

(1) J. F. Walker, "Formaldehyde," Reinhold, New York, N. Y., 1944.

(2) (a) V. Crescenzi, F. Quadrifoglio, and V. Vitagliano, *J. Phys. Chem.*, 71, 2313 (1967); (b) *Ric. Sci.*, 37, 529 (1967); (c) L. Costantino, V. Crescenzi, and V. Vitagliano, *J. Phys. Chem.*, 72, 2588 (1968).

(3) J. L. Neal and D. A. I. Goring, *ibid.*, 74, 658 (1970).

(4) O. Nomoto and H. Endo, *Bull. Chem. Soc. Jap.*, 43, 2718 (1970).

(5) G. Barone, V. Crescenzi, A. M. Liquori, and F. Quadrifoglio, *J. Phys. Chem.*, 71, 984 (1967).

Table II: Thermodynamic Characterization of the H_2O-HMT System

t, °C	$m_{sat}{}^a$	φ^b	$\Delta H/\Delta m^c$	ϕ_{L_2}	$\bar{L}_2$	$\bar{L}_1$
25	6.470	$1 + 0.220m$	$273 + 24m$	$273m + 12m^2$	$546m + 36m^2$	$-(4.9m^2 + 0.43m^3)$
30	6.326	. . .	$272 + 24m$	$272m + 12m^2$	$544m + 36m^2$	$-(4.9m^2 + 0.43m^3)$
35	6.150	$1 + 0.196m$	$278 + 21m$	$278m + 10m^2$	$556m + 31m^2$	$-(5.0m^2 + 0.38m^3)$

Integral heat of HMT solution^d (30°): $\Delta H_s = -5.1$ kcal/mol ($m = 0.110$)
Differential heat of HMT solution^e (30°): $\Delta\bar{H} = -3.2$ kcal/mol ($m_{sat} = 6.326$)
Heat of dilution; $m_{sat} \rightarrow 0.110m$ (30°): $\Delta H = -2.2$ kcal/mol (from $\Delta H/\Delta m$)

Enthalpy of melting of the water-HMT clathrate: $\Delta H_m = 9.51$ kcal/mol (at 13°)
(Elemental analysis: HMT·$6H_2O$)

^{a} The concentration of HMT in the saturated solutions was determined *via* HMT decomposition with H_2SO_4 as reported in the literature.[1] ^{b} Isopiestic gravimetric measurements.[2] ^{c} Measurements with a LKB batch-type microcalorimeter. Standard deviation from fit, σ; at 25°, $\sigma = 2.1$; at 30°, $\sigma = 4.7$; at 35°, $\sigma = 4.1$. ^{d} Measurements with an isothermal calorimeter of the type described by Schreiber and Waldman.[6] ^{e} From solubility and activity coefficient data (see text).

(1) the enthalpy of dilution of HMT in a rather wide range of concentrations at three temperatures; (2) the osmotic coefficient of HMT aqueous solutions at 35°; and (3) the differential and the integral heat of solution of HMT in water at 30°. Measurements have been also carried out of the heat of fusion of the crystalline clathrate, HMT·$6H_2O$.

Only the results of the heat of dilution experiments at 25° are reported in Table I, data for 30 and 35° being in fact very close to those for 25°.

In Table II a summary is given of some relevant thermodynamic quantities derived from the experimental heat of dilution data, as well as of other data useful for a physicochemical characterization of the system examined.

These data permit a direct evaluation of the dependence of the excess partial molal entropy of water, ($\bar{S}_1 - S_1^°$), upon HMT concentration. The excess entropy values were calculated according to the equation[7]

$$(\bar{S}_1 - S_1^°) = \bar{L}_1/RT - R\ln(a_1/N_1) \quad (1)$$

where a_1 is the activity of water at the solute mole fraction $N_2 = 1 - N_1$, on the basis of the $\bar{L}_1$-m and φ-m ($\varphi = -(55.51/m)\ln a_1$) relationships reported in Table II, for 30°. For low m values ($m \leq 2$, moles/kilogram of water) the correlation $\Delta\bar{S}_1 = -0.010m^2$ is easily verified. From the magnitude and sign of the relative partial molal heat content of solute and of solvent, i.e., $\bar{L}_2$ and $\bar{L}_1$, respectively, and of the excess partial molal entropy of water, the hypothesis that HMT interacts with water in a way typical of "structure-maker" solutes gains further support.

In Table II, data on the integral and on the differential heat of HMT dissolution in water are also reported. The differential heat of solution, $\Delta\bar{H}$, at 30° was calculated from HMT solubility data (for illustrative purposes rounded off solubility values at only three temperatures have been reported) and the osmotic coefficient data, with the equation

$$\frac{d\ln m}{d(1/T)}\left(1 + \frac{\partial\ln\gamma}{\partial\ln m}\right)R = -\Delta\bar{H} \quad (2)$$

where γ is the activity coefficient of HMT.

The approximate relationship: $\ln\gamma = 0.413m$, immediately derivable from the φ-m data at 25 and 35°, was assumed.

Taking into account the important contribution of the heat of dilution (from the $\Delta H/\Delta m$ data at 30°) it is seen that the experimental integral heat of solution value is reproduced with reasonable accuracy (Table II).

It is worth recalling, finally, that the ability of HMT of interacting with water molecules giving rise to ordered solvent structures is also very clearly demonstrated by the facile formation of a clathrate HMT·$6H_2O$ of well-defined crystal structure[8] and dielectric properties.[9] In our experiments the heat of melting of the HMT clathrate ($\Delta H_m = 9.5$ kcal/mol at 13°, the melting temperature) was determined using small crystals of the clathrate with the aid of a differential scanning calorimeter (Perkin-Elmer, DSC-1B).

A detailed theoretical evaluation of ΔH_m for the $(CH_2)_6N_4\cdot6H_2O$ species, as it has been made in the case of simple gas hydrates,[10] is hampered by various difficulties. It is nevertheless worth pointing out that a rough calculation based on the simple equation

$$\Delta H_m = 6(\Delta H_{ice} + \Delta C_p\Delta T) \quad (3)$$

where $\Delta H_{ice} = 1.436$ kcal/mol is the heat of melting of pure ice I at 0° and 1 atm, and $\Delta T\Delta C_p$ is the heat capacity term for water (for the transition ice → water, with $\Delta C_p = 8.91$ cal/(mol deg) for the transition ice → water, with $\Delta T = 13°$), yields a limit-

(6) H. P. Schreiber and M. H. Waldman, *J. Polym. Sci., Part A-2*, **5**, 555 (1967).

(7) H. S. Frank and A. L. Robinson, *J. Chem. Phys.*, **8**, 933 (1940).

(8) T. C. W. Mak, *ibid.*, **43**, 2799 (1965).

(9) D. W. Davidson, *Can. J. Chem.*, **46**, 1024 (1968).

(10) D. Turnbull, *J. Phys. Chem.*, **66**, 609 (1962).

ing value of *ca.* 9.3 kcal/mol for ΔH_m, which happens to be very close to our experimental figure.

In view of the oversimplified model underlying eq 3 in our case, this coincidence may be somewhat fortuitous.

It is conceivable that at temperatures higher than 13° and at slightly lower concentrations, HMT molecules may induce in water a local order reminiscent of that of the clathrate.

In our opinion, speaking of solvent structure around solute particles would thus mean, in the case of HMT, building of a sphere of solvation whose geometry is strongly influenced by the fourfold symmetry of donating $>$N groups of the solute.

Analysis of Broadly Overlapping Absorption Bands According to a Two-Absorber Model

by T. R. Tuttle, Jr.,* Gabriel Rubinstein,
and Sidney Golden

*Department of Chemistry, Brandeis University,
Waltham, Massachusetts 02154* (*Received April 1, 1971*)

The optical absorption of alkali metal solutions in liquid ammonia consists of a single broad band under a variety of experimental conditions.[1-6] The dependence of the spectrum on composition of the solution is slight.[1,2,5,6] This fact has been cited in support of a one-absorber model of the optical spectra of these solutions.[1,5,7] Nevertheless, the fact that the spectra do depend on composition at all suggests that the observed band may be a composite of broadly overlapping absorbances from two or more distinct absorbers.[8] To test this possibility we have developed a method of analyzing a composite band into two components whose behavior as a function of solution composition provides a test of the validity of the two-absorber model. In addition, possible equilibria between the absorbers may be tested under certain circumstances.

Although the method of analysis was developed with metal–ammonia solutions in mind, it may be applied to any case in which two absorption bands overlap. To suit our purpose it has been assumed in the development which follows that the overlap between the components is great enough so that only one maximum in the spectrum occurs at each composition. The analysis

may easily be modified to accommodate other possibilities.

Suppose that a measured absorption band with a shape function $F(\nu) \leq 1$ at a fixed temperature consists of two overlapping components corresponding to two distinct chemical species. The shape of the composite band may be written as

$$F(\nu) = xf_1(\nu) + yf_2(\nu) \tag{1}$$

in which $f_1(\nu)$ and $f_2(\nu)$ are the characteristic shape functions for the two components and thus depend only on frequency ν, and x and y are coefficients which depend only on composition. Each shape function is normalized so that its maximum value is unity. $F(\nu)$ is thus a function of metal concentration as determined by the magnitudes of the coefficients x and y. It is easy to show that $x = A_1(\nu_{1m})/A(\nu_m)$ and $y = A_2(\nu_{2m})/A(\nu_m)$ in which $A_1(\nu_{1m})$ and $A_2(\nu_{2m})$ are the absorbances due to species 1 and species 2, respectively, at the positions of the maxima of $f_1(\nu)$ and $f_2(\nu)$, respectively, and $A(\nu_m)$ is the total absorbance at the position of the maximum of $F(\nu)$. Because

$$A_1(\nu_{1m}) + A_2(\nu_{2m}) \geq A_1(\nu_m) + A_2(\nu_m) = A(\nu_m) \tag{2}$$

it follows that

$$x + y \geq 1 \tag{3}$$

The equal sign applies when $\nu_{1m} = \nu_{2m}$. When the bands are close together and have comparable widths the sum (3) will be close to unity.

To apply eq 1 to separate $F(\nu)$ into components it is necessary to know at least one of the shape functions $f_1(\nu)$ or $f_2(\nu)$. Suppose $f_1(\nu)$ has been determined by extrapolation to infinite dilution.[6] Then if x is also known $yf_2(\nu)$ and hence $f_2(\nu)$ may be determined through an application of eq 1. If there is a region in the spectrum where $f_2(\nu) = 0$, then $x = F(\nu)/f_1(\nu)$ for frequencies in this region. When no such region exists, as is the case for metal–ammonia solutions, x cannot be determined directly. However, a useful analysis can still be made which under certain circumstances leads to a value of x. Let

$$F(\nu) = x_0 f_1(\nu) + y_0 f_2{}^\circ(\nu) \tag{4}$$

in which $1 \geq f_2{}^\circ(\nu) \geq 0$ and $y_0 \geq 0$; *i.e.*, x_0 is chosen

(1) R. C. Douthit and J. L. Dye, *J. Amer. Chem. Soc.*, **82**, 4472 (1960).

(2) M. Gold and W. L. Jolly, *Inorg. Chem.*, **1**, 818 (1962).

(3) D. F. Burow and J. J. Lagowski, *Advan. Chem. Ser.*, **50**, 125 (1965).

(4) R. K. Quinn and J. J. Lagowski, *J. Phys. Chem.*, **72**, 1374 (1968).

(5) W. H. Koehler and J. J. Lagowski, *ibid.*, **73**, 2329 (1969).

(6) I. Hurley, T. R. Tuttle, Jr., and S. Golden, "Metal Ammonia Solutions," Butterworths, London, 1969, p 503.

(7) M. Gold, W. L. Jolly, and K. S. Pitzer, *J. Amer. Chem. Soc.*, **41**, 3089 (1964).

(8) S. Golden, C. Guttman, and T. R. Tuttle, Jr., *J. Chem. Phys.*, **44**, 3791 (1966).

such that subtracting $x_0 f_1(\nu)$ from $F(\nu)$ gives no negative values. Although $y_0 f_2°(\nu)$ determined in this way is not the true absorption band for the second species the quantity $A_m y_0 f_2°(\nu)$ is proportional to its concentration if the two-absorber model is correct as can be seen from what follows. Since $y_0 f_2°(\nu)$ is positive definite and

$$y_0 f_2°(\nu) = y f_2(\nu) - (x_0 - x) f_1(\nu) \qquad (5)$$

it follows that

$$\frac{f_2(\nu)}{f_1(\nu)} \geq \frac{x_0 - x}{y} \qquad (6)$$

The equal sign applies only at frequencies for which $f_2°(\nu) = 0$. If ν_0 is one such frequency, then

$$\frac{f_2(\nu_0)}{f_1(\nu_0)} = \frac{x_0 - x}{y} \qquad (7)$$

This value is a minimum in the ratio of f_2/f_1. Therefore the frequency ν_0 is fixed by the condition that $y_0 f_2°(\nu) \geq 0$ since a minimum value of f_2/f_1 can only occur at fixed frequency independent of composition. Since ν_0 is independent of composition, it follows that

$$x_0 - x = cy \qquad (8)$$

in which c is a constant independent of frequency and composition. Combining eq 8 with eq 5 yields

$$y_0 = y \left\{ \frac{f_2(\nu) - c f_1(\nu)}{f_2°(\nu)} \right\} = ky \qquad (9)$$

Since k is independent of composition, we obtain the result that $A_m y_0 \propto A_m y$, i.e., the amount of residual absorption extracted is proportional to the concentration of the second species.

A value of x may be determined with the aid of

$$x = x_0 - cy = x_0 - \frac{c}{k} y_0 \qquad (10)$$

by choosing c/k so that the resulting $A_m x f_1(\nu)$ and $A_m y f_2(\nu)$ satisfy a particular equilibrium relationship. Such a fitting procedure is not generally possible when the equilibrium is sensitive to activity corrections, as is the case for ionic equilibria.

A particular value of the present analysis is that certain possible equilibria may be rather easily eliminated from consideration. For example, in the case of sodium solutions in ammonia we were interested to test whether the observed shifts in the optical absorption band could be described in terms of an equilibrium between two species and whether the two species were ions and ion pairs. The analysis of our experimental results yielded residual absorptions, i.e., $y_0 f_2°(\nu)$, for which $f_2°(\nu)$ was independent of metal concentration. Therefore, the assumption of a two-absorber model is justified. In addition, spectra of solutions containing an excess but constant concentration of sodium iodide yielded rela-

tive amounts of residual absorption which depended on metal concentration. For the ion-pairing equilibrium

$$\mathrm{Na^+ \cdot S^-} \rightleftharpoons \mathrm{Na^+ + S^-} \qquad (11)$$
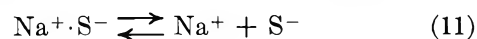
the equilibrium constant relationship yields

$$\frac{[\mathrm{S^-}]}{[\mathrm{Na^+ \cdot S^-}]} = \frac{K_1}{[\mathrm{Na^+}] \gamma_\pm^2} \qquad (12)$$

so that in the presence of the excess NaI at a constant concentration in solution $[\mathrm{Na^+}]$ and $\gamma_\pm^2$ should be practically constant, and hence the ratio of the two absorbers, $[\mathrm{S}]^-/[\mathrm{Na^+ \cdot S^-}]$, should also remain constant. Since the relative amounts of residual absorption did not remain constant on changing metal concentration, we concluded that the residual absorption should not be attributed to the ion pair.

Intermediates in Nucleophilic Aromatic Substitution. VI.[1] Kinetic Evidence of Intramolecular Hydrogen Bonding in Meisenheimer Complexes

by Claude F. Bernasconi[2]

*Max Planck Institut für Physikalische Chemie,
Göttingen, Germany* (*Received May 21, 1971*)

Recently we reported a temperature-jump study on the Meisenheimer complex formation between 1,3,5-trinitrobenzene (TNB) and aliphatic amines in 10% dioxane–90% water,[3] which allowed determination of k_1, k_{-1}, and K_{XH} in eq 1. The data suggested the presence of an intramolecular hydrogen bond to the *o*-nitro group in XH.[3] Inasmuch as XH and X⁻ are models for the intermediate in nucleophilic aromatic substitution reactions by amines, these findings have considerable bearing on the mechanism of such reactions, in particular with regard to the rate-limiting step. This is because intramolecular H bonding will influence the rates of intermediate conversion into products as well as their reversion to reactants, but in different ways, depending on the specific amine.[4] Thus, it seemed highly desirable to obtain more direct evidence for intramolecular hydrogen bonding in these systems.

(1) Part V: C. F. Bernasconi and R. G. Bergstrom, *J. Org. Chem.*, **36**, 1325 (1971).

(2) Address correspondence to the author at the Division of Natural Sciences, University of California, Santa Cruz, Calif. 95060.

(3) C. F. Bernasconi, *J. Amer. Chem. Soc.*, **92**, 129 (1970).

(4) C. F. Bernasconi, in preparation.

$$\text{TNB} + \text{RR'NH} \underset{k_{-1}}{\overset{k_1}{\rightleftharpoons}} \begin{array}{c} \text{XH} \end{array} = K_{\text{XH}} =$$

$$+ \text{H}^+ \quad (1)$$

$$\text{X}^-$$
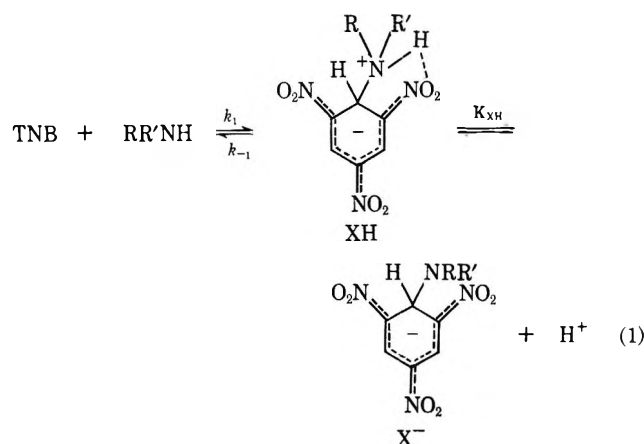
It is well known that rate studies of proton transfers can yield direct information about intramolecular bonds.[5] We now wish to report such a study carried out by means of an improved[6] temperature-jump apparatus.

The mentioned study[3] and some more recent results from our laboratory[7] have shown that in the pH region corresponding approximately to the pK of the respective RR'NH$_2^+$, at concentrations of free amine above 0.002 or 0.005 M and stoichiometric TNB concentrations of 0.005 M,[8] both XH and X$^-$ are present at comparable and spectrophotometrically measurable concentrations when RR'NH is a secondary amine like piperidine, pyrrolidine, or dimethylamine. The following data for the piperidine case[3] are representative: k_1 = 3000 M^{-1} sec^{-1}, k_{-1} = 14,900 sec^{-1}, K_1 = k_1/k_{-1} = 0.201 M^{-1}, K_{XH} = 1.49 × 10^{-11} M, i.e., pK_{XH} = 10.83 wheras p$K_{\text{RR'NH}_2^+}$ ≈ 11.1. Since the visible spectra of XH and X$^-$ differ appreciably between 430 and 450 nm,[9] the system appeared quite suited for a temperature-jump study. In the case of primary amines like n-butylamine[3] and methylamine[7] K_{XH} is relatively greater than for secondary amines. As a consequence the equilibrium between XH and X$^-$ lies very strongly on the side of the anion at all pH values where enough free amine is present to form the complex at appreciable concentrations. This makes unfeasible any reasonably accurate temperature-jump study, and only results on the secondary amines are reported.

Results and Discussion

Relaxation times were determined in amine–amine hydrochloride buffers as a function of pH and of free amine concentration. The concentrations were such that [RR'NH], [RR'NH$_2^+$] ≫ [XH], [X$^-$] in all experiments. Figure 1 shows a representative oscilloscope trace. Since the total lag time, which includes the heating time and the photomultiplier rise time (0.5 μsec) was approximately 1.5 μsec, the section of the relaxation curves covering the first 3 μsec (the first 1.5 horizontal divisions on the photograph) was disregarded for the evaluation of τ.
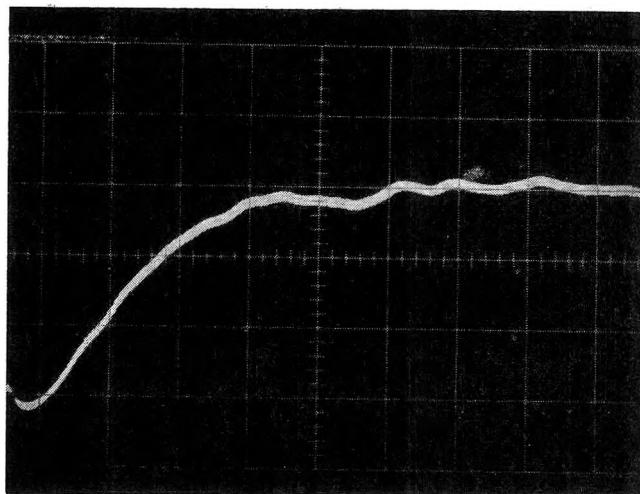
Figure 1. Representative oscilloscope trace at 440 nm: [piperidine]$_0$ = 0.02 M, pH 10.91, [TNB]$_0$ = 2.5 × 10^{-3} M, [NaCl] = 0.49 M; capacitor 1.1 × 10^{-8} F, discharge 50 kV, ΔT = 2°; 2 μsec/horizontal division; multiplier rise time 0.5 μsec, total lag time ≈1.5 μsec (includes heating time).
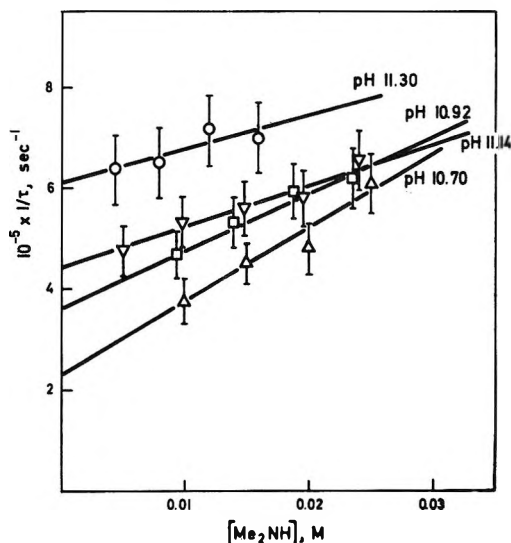
Figure 2. System dimethylamine and TNB at 25°. τ^{-1} as a function of *free* amine concentration and of pH; ionic strength kept at 0.5 M by adding NaCl.

The results for dimethylamine and piperidine are shown in Figures 2 and 3. With pyrrolidine only a few relaxation times at pH 10.98 could be determined with reasonable accuracy ($10^{-5}\tau^{-1}$ = 5.1 ± 0.5, 5.9 ± 0.5, 6.4 ± 0.6, and 7.2 ± 0.6 sec^{-1} at [pyrrolidine] = 0.01, 0.015, 0.02, and 0.025 M, respectively).

(5) M. Eigen, *Angew. Chem.*, **75**, 489 (1963); *Angew. Chem., Int. Ed. Engl.*, **3**, 1 (1964).

(6) Built by L. De Maeyer and C. R. Rabl, Max Planck Institut für Physikalische Chemie, Göttingen, Germany.

(7) C. F. Bernasconi and P. Schmid, unpublished results.

(8) These are about the highest practical concentrations before running into solubility problems.

(9) C. F. Bernasconi, *J. Org. Chem.*, **35**, 1214 (1970).

Table I :   Kinetic Data in 10% Dioxane–90% Water at 25°

	Me₂NH	Piperidine	Pyrrolidine
k_{HO^-}, M^{-1} sec^{-1}	$2.5 \pm 0.25 \times 10^8$	$1.9 \pm 0.2 \times 10^8$	$2.5 \pm 0.7 \times 10^8$
k_{H_2O}, sec^{-1}	$1.2 \pm 0.15 \times 10^5$	$1.7 \pm 0.2 \times 10^5$	
$K_{HO^-} = \dfrac{k_{HO^-}}{k_{H_2O}}$, M^{-1}	$2.1 \pm 0.4 \times 10^3$	$1.1 \pm 0.25 \times 10^3$	
K_{HO^-}, M^{-1}	$2.5 \pm 0.3 \times 10^3$ ^{a}	$1.5 \pm 0.25 \times 10^3$ ^{b}	$2.15 \pm 0.3 \times 10^3$ ^{b}

^{a} C. F. Bernasconi and P. Schmid, unpublished data. ^{b} Reference 3; in ref 3 the equilibrium constant for proton transfer between XH and X⁻ was defined as an acid dissociation constant, K_{XH}.   The relation between K_{HO^-} of this study and K_{XH} is $K_{HO^-} = 10^{14} K_{XH}$.
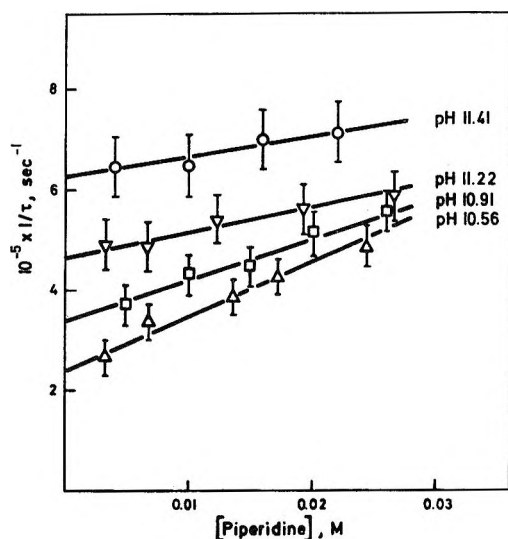
Figure 3.   System piperidine and TNB at 25°. τ^{-1} as a function of *free* amine concentration and of pH; ionic strength kept at 0.5 M by adding NaCl.
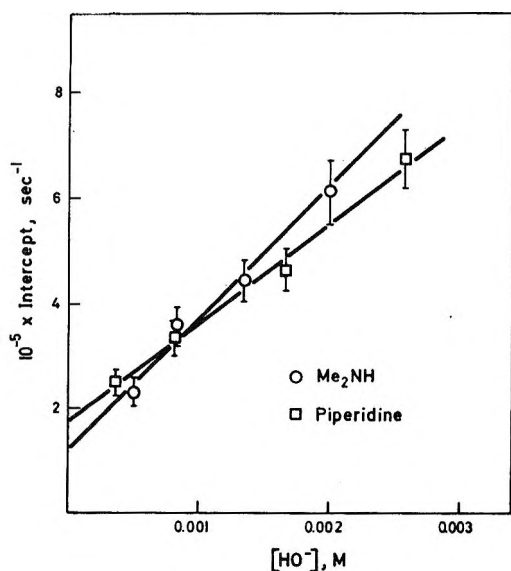
Figure 4.   Intercepts of Figures 2 and 3 as a function of |HO⁻|.

The concentration dependence of τ^{-1} is consistent with Scheme I. This scheme calls for two relaxation times. One for the diffusion-controlled proton transfer between RR′NH₂⁺ and HO⁻—beyond the reach of

Scheme I

$$XH + HO^- + RR'NH \underset{k_{H_2O}}{\overset{k_{HO^-}}{\rightleftharpoons}} X^- + H_2O + RR'NH$$

$$X^- + HO^- + RR'NH_2^+$$
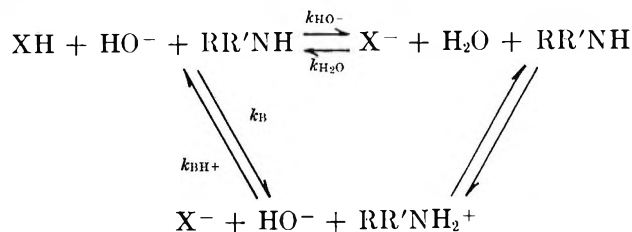
our method—and a second one for the remaining reactions. To derive the analytical expression of this second relaxation time one has to set up a linearized rate equation,[10] *e.g.*

$$\frac{d\delta[X^-]}{dt} = k_{HO^-}[XH]\delta[HO^-] +$$

$$k_{HO^-}[HO^-]\delta[XH] - k_{H_2O}\delta[X^-] +$$

$$k_B[XH]\delta[RR'NH] + k_B[RR'NH]\delta[XH] -$$

$$k_{BH^+}[X^-]\delta[RR'NH_2^+] -$$

$$k_{BH^+}[RR'NH_2^+]\delta[X^-] \quad (2)$$

where the δ terms are small perturbations from the respective equilibrium concentrations.[10] Since chemical relaxation was studied with the amine and amine hydrochloride in large excess over XH and X⁻, and under conditions of pH buffering ($\delta[HO^-] \approx 0$) all terms containing $\delta[RR'NH]$, $\delta[RR'NH_2^+]$, and $\delta[HO^-]$ can be neglected in eq 2. After substituting

$$\delta[XH] = -\delta[X^-] \quad (3)$$

from stoichiometric considerations, eq 2 simplifies to

$$\frac{d\delta[X^-]}{dt} = -\{k_{HO^-}[HO^-] + k_{H_2O} +$$

$$k_B[RR'NH] + k_{BH^+}[RR'NH_2^+]\}\delta[X^-] \quad (4)$$

The term in parentheses is τ^{-1}. Expressing [RR′NH₂⁺] by eq 5

$$[RR'NH_2^+] = [RR'NH]\frac{K_B}{[HO^-]} \quad (5)$$

where K_B is the basicity constant of the amine affords

(10) M. Eigen and L. De Maeyer in "Technique of Organic Chemistry," Vol. VIII, part 2, Interscience, New York, N. Y., 1962, p 895.

$$\frac{1}{\tau} = k_{H_2O} + k_{HO^-}[HO^-] +$$

$$\left(k_B + \frac{k_{BH^+}K_B}{[HO^-]}\right)[RR'NH] \quad (6)$$

By plotting the intercepts of Figures 2 and 3 vs. $[HO^-]$ new straight lines result (Figure 4) with slope k_{HO^-} and intercept k_{H_2O}. All data are summarized in Table I. It can be seen that the values of $K_{HO^-} = k_{HO^-}/k_{H_2O}$ determined in this study agree very well with the ones determined earlier.[3]

The most important finding of this study is that k_{HO^-} in all three cases is around 2×10^8 M^{-1} sec^{-1} which is about a hundredfold lower than the diffusion-controlled limit of a reaction between a tertiary ammonium ion and HO^- in aqueous solution.[5] This allows the inference of an intramolecular hydrogen bond to the o-nitro group in XH with a stability constant of roughly 100.[5]

COMMUNICATIONS TO THE EDITOR

The Behavior of the Solvated Electron in Ethanol-*n*-Hexane Mixtures

Sir: Stabilization of the electron in a polar liquid medium during radiolysis has in recent years come to be recognized as a phenomenon of very general occurrence and importance. Theories[1-4] which have attempted to evaluate the energy states of the solvated electron include as a basic parameter the dielectric constant. Sauer, *et al.*,[5] have shown that the absorption maximum of the solvated electron in alcohols exhibits a red shift with a decreasing static dielectric constant D_s. The dependence of the optical transition energy upon D_s is in agreement with the theoretical approximation of Davydov.[1] For mixtures of two alcohols, only one absorption peak is obtained and the maximum is intermediate between those of the two pure alcohols, as required by the continuum model of Jortner.[2] If the same considerations hold for mixtures of a polar species, such as ethanol ($D_s = 25.7$), and a hydrocarbon of low dielectric constant, the absorption spectrum of the solvated electron would be expected to shift according to the change in dielectric constant.

The yield and decay of the solvated electron has been measured spectrophotometrically for the range of ethanol-*n*-hexane mixtures using 3.5-μsec pulses of 1-MeV electrons. Our results show that dilution of ethanol with *n*-hexane down to $D_s = 1.8$ does not produce an appreciable shift in wavelength for the maximum of solvated electron absorption (Figure 1). There is, however, a decrease in the spectral absorption of the electron, A, with a decrease in ethanol concentration. The overall decrease is due to a decrease in either or both G, the yield of solvated electrons, and ϵ, the molar extinction coefficient, since absorbance is proportional to $G \times \epsilon$. The extinction coefficient was estimated from the correlation[6] between the spectral absorption of e^-_{ROH} and the charge-transfer band of the iodide ion (5×10^{-5} M tetraethylammonium iodide) at 220 nm in the ethanol-*n*-hexane mixtures.

Figure 2 shows the values calculated for G from the expression $(A/k\epsilon_{iod})$, where A is the absorbance by the electron at 585 nm, ϵ_{iod} is the extinction coefficient of iodide, and k is a constant chosen to make $G = 1.1$ in pure ethanol. These points are juxtaposed with values for G which were determined by the analysis of free chloride ion produced during the steady-state radiolysis of solutions containing 5×10^{-3} M 2-chlorobutane.[7] The good agreement between the two sets of values confirms the validity of the spectral correlation. The value of G in pure ethanol was found to be 1.1 ± 0.1, which is in agreement with published values.[8]

(1) A. S. Davydov, *Zh. Eksp. Teor. Fiz.*, **18**, 913 (1948).

(2) J. Jortner, *Radiat. Res. Suppl.*, No. 4, 24 (1964); in "Radiation Chemistry of Aqueous Systems," G. Stein, Ed., Interscience-Wiley, New York, N. Y., 1968, pp 91–107.

(3) G. R. Freeman and J. M. Fayadh, *J. Chem. Phys.*, **43**, 4245 (1967).

(4) For a review, see E. J. Hart and M. Anbar, "The Hydrated Electron," Wiley-Interscience, New York, N. Y., 1970, p 71.

(5) M. C. Sauer, S. Arai, and L. M. Dorfman, *J. Chem. Phys.*, **42**, 708 (1965).

(6) M. Anbar and E. J. Hart, *J. Phys. Chem.*, **69**, 1244 (1965).

(7) (a) W. F. Schmidt and A. O. Allen, *J. Chem. Phys.*, **52**, 2345 (1970); (b) S. J. Rzad and J. H. Fendler, *ibid.*, **52**, 5395 (1970).

(8) For example, see (a) I. A. Taub, D. A. Harter, M. C. Sauer, and L. M. Dorfman, *ibid.*, **41**, 979 (1964); (b) J. J. J. Myron and G. R. Freeman, *Can. J. Chem.*, **43**, 381 (1965).
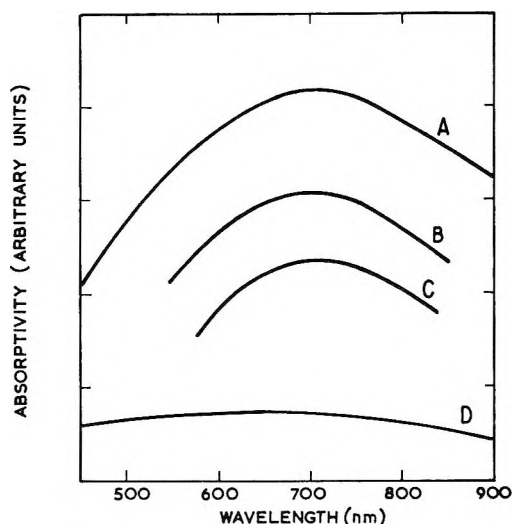
Figure 1. Comparative absorption spectra of (e⁻solv) in ethanol-n-hexane solutions at 22°: A, pure ethanol (D_s = 25.7); B, 60 mole % (D_s = 8.5); C, 31 mole % (D_s = 3.2); D, 5 mole % (D_s = 1.78).
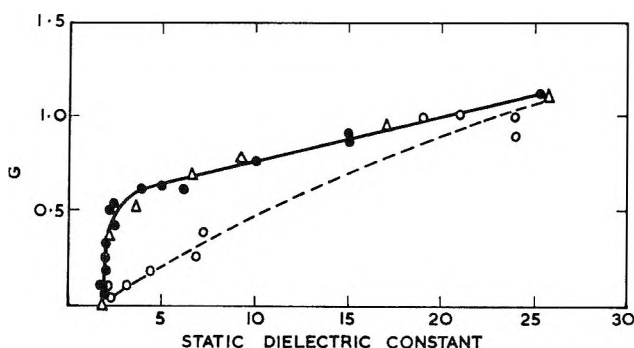
Figure 2. G for solvated electrons as a function of D_s for ethanol-n-hexane solutions: ●, values found under steady-state irradiations; △, values estimated spectrophotometrically by pulse radiolysis ($A/k\epsilon_{iod}$), where A is the spectral absorbance by the electron at 585 nm, k is a proportionality factor, and ϵ_{iod} is the molar extinction coefficient of iodide in the same mixture; ○, values for a number of pure liquids;[3] — — —, theoretical behavior for pure liquids.[3]

The decrease in G with D_s shown in Figure 2 differs from the theoretical trend calculated by Freeman and Fayadh[3] for pure liquids. Electron solvation in ethanol-n-hexane mixtures therefore appears not to be simply a function of the static dielectric constant.

Kemp, Salmon, and Wardman[9] found the lifetime of the solvated electron was unchanged in pure methanol, 67% methanol in tetrahydrofuran, and 4% methanol in cyclohexane. We have found a constant half-life of 3.2 ± 0.3 µsec for the decay over the initial 4 µsec after pulse shut-off for the range of concentrations 2-100 mol % ethanol. This, together with there being no shift in the position of the absorption spectrum maximum, is interpreted to suggest that the electron is trapped in basically the same type of potential well, the

mechanism of reaction remaining virtually independent of the n-hexane concentration. One description of the results is in terms of molecular aggregates of ethanol molecules trapping and stabilizing the electrons.

An infrared spectroscopic study undertaken in conjunction with this work indicates that G varies with the concentration of ethanol tetramer and possibly higher multimers.[10] The presence of these as existing traps is presumably necessary for solvation stabilization of electrons.

(9) T. J. Kemp, G. A. Salmon, and P. Wardman in "Pulse Radiolysis," M. Ebert, J. P. Keene, A. J. Swallow, and J. H. Baxendale, Ed., Academic Press, London, 1965, pp 247-257.

(10) W. C. Coburn, Jr., and E. Grunwald, J. Amer. Chem. Soc., 80, 1318 (1958).

DEPARTMENT OF NUCLEAR AND   BRUCE J. BROWN
  RADIATION CHEMISTRY   NORMAN T. BARKER
UNIVERSITY OF NEW SOUTH WALES
SYDNEY, AUSTRALIA

AUSTRALIAN ATOMIC ENERGY COM-   DAVID F. SANGSTER*
  MISSION RESEARCH ESTABLISHMENT
SUTHERLAND, N.S.W. AUSTRALIA

Reactivity of Hydroxyl Radicals with Olefins

Sir: The rate of conversion of NO to NO₂ in smog chambers has been shown to depend markedly on the particular olefin present.[1,2] The reaction of hydroxyl radicals with olefin has been suggested as an important step in this photooxidation.[3] However, Greiner[4] has suggested the rate of hydroxyl attack on all monoolefins should be approximately constant and equal to the OH-ethylene rate which he has determined. In a recent paper we have shown the rate constant for the reaction of OH with propylene (k = 1.7 × 10⁻¹¹ cm³ molecule⁻¹ sec⁻¹) to be ten times faster than that for ethylene (k = 1.8 × 10⁻¹²).[5] In the present work this series is extended to a number of higher olefins.

The reaction rates were determined in a discharge flow system with mass spectrometric detection as described previously.[5] The concentration of OH and

(1) W. A. Glasson and C. S. Tuesday, Environ. Sci. Technol., 4, 916 (1970).

(2) A. P. Altshuller and I. R. Cohen, Int. J. Air Water Pollut., 7, 787 (1963).

(3) D. H. Stedman, E. D. Morris, Jr., E. E. Daby, H. Niki, and B. Weinstock, 160th National Meeting of the American Chemical Society, Chicago, Ill., 1970, Abstract No. WATR 26.

(4) N. R. Greiner, J. Chem. Phys., 53, 1284 (1970).

(5) E. D. Morris, Jr., and H. Niki, J. Amer. Chem. Soc., 93, 3570 (1971).

olefin was measured simultaneously by monitoring the corresponding parent peaks as a function of the distance between the position of the movable inlet and the sampling pinhole of the mass spectrometer. Hydroxyl radicals were produced by the reaction $H + NO_2 \rightarrow OH + NO$. The olefin and NO_2 were both introduced through the movable inlet to a stream of approximately 10^{13} molecules/cm^3 of H atoms. All of the H atoms were converted to OH in the mixing distance allowed before kinetic measurements were begun. Typical flow conditions were 30 m/sec at 1 Torr pressure of helium diluent at 25°.

In order to keep the ratio of OH to olefin as large as possible, the minimum concentration of olefin was used that could be detected reliably. The exponential decay of each olefin was compared to that of propylene under identical experimental conditions. The relative rate constants were determined from the equation

$$\frac{k_{Ole}}{k_{C_3H_6}} = \frac{\ln\,[(Ole)_{t_2}/(Ole)_{t_1}]}{\ln\,[(C_3H_6)_{t_2}/(C_3H_6)_{t_1}]}\,\frac{\langle OH \rangle_{C_3H_6}}{\langle OH \rangle_{Ole}} \quad (1)$$

The OH concentration was averaged over the reaction time $(t_2 - t_1)$, to correct for decay caused by reaction with olefin and by wall recombination. It should be noted that eq 1 requires the knowledge of only relative concentrations of both OH and olefin. The relative rates determined by this procedure are summarized in Table I. These values represent an average of four independent runs and are reproducible to within 10%. According to eq 1, the rate ratios should be independent of OH concentration. However, because of the extremely

fast rates observed, the OH concentration was subject to severe experimental constraints and could not be varied sufficiently to verify this.

It should be further noted that this method is valid only if the reactant olefin is consumed predominantly by OH radicals. We have previously[5] discussed the advantages of determining rate constants under OH excess conditions to reduce the possibility of secondary reactions. Since the rates of OH reactions are already so fast, it is unlikely that a lower concentration of any other intermediate (such as alkyl[6]) can compete with it for olefin. The reaction $OH + OH \rightarrow H_2O + O$ is a possible source of O atoms. However, the maximum ratio of O/OH can be estimated to be 0.05 because of the rapid reaction $O + OH \rightarrow O_2 + H$.[7] Since the rate constants for reaction of olefins with O atoms are smaller than[8] for reaction with OH, the error is less than 5%. On the time scale used here, reaction with H atoms is slow,[9] and the concentration low because of the NO_2 present.

The experimental results presented in Table I clearly indicate that increasing alkyl substitution of olefinic carbon leads to an enhancement in the reaction rate with OH by two orders of magnitude. The greatest effect is due to the number of alkyl substituents with a smaller effect from size and position. A similar effect of alkyl substitution has been observed by Cvetanović in the electrophilic addition of O atoms to olefins.[8] The reaction of OH with olefins occurs at least in part by addition since transient mass peaks were observed corresponding to the adduct.

Despite the fact that the reactivity scales determined from smog chamber work are a measure of the overall rate of a complicated mechanism, it is interesting to compare this scale with the rate constants for the elementary reactions of O and OH. All three exhibit a general trend toward increasing reactivity with increasing substitution. However, when this comparison is extended to several other classes of compounds, the hydroxyl radical, unlike O atom, continues to show agreement with the reactivity scale.

The extremely fast rate constants observed here, together with the general agreement with the reactivities based on the conversion of NO to NO_2, are consistent with the participation of OH in photochemical smog chemistry.

Table I: Comparison of O and OH Rate Constants to Photochemical Reactivity (Normalized to Propylene)

	OH rate	O atom rate[a]	Reactivity[b]
Olefins			
$CH_2=CH_2$	0.1	0.17	0.4
$CH_3CH=CH_2$	1.0[c]	1.0	1.0
$CD_3CD=CD_2$	1.1	...	...
$CH_3CH_2CH=CH_2$	2.4	1.0	0.9
$CH_3CH_2CH_2CH=CH_2$	2.5	...	0.6
cis-$CH_3CH=CHCH_3$	3.6	4.1	2
trans-$CH_3CH=CHCH_3$	4.2	4.9	3
$(CH_3)_2C=CH_2$	3.8	4.3	1
$CH_3CH_2(CH_3)C=CH_2$	5.3	...	1
$CH_3CH_2CH=CHCH_3$	5.3	3.9	2
$(CH_3)_2C=CHCH_3$	7	13.7	6
$(CH_3)_2C=C(CH_3)_2$	9	17.7	16
Other Compounds			
HCHO	0.9	0.01	0.7
CH_3CHO	0.9	0.01	0.7
CH_3CH_2CHO	1.8	...	2
$CH_3CH_2CH_2CH_3$	0.24	0.008	0.2
Xylene[d]	1.1	<0.01	0.7–1.1

[a] From ref 8. [b] From ref 1 and 2. [c] $k = 1.7 \times 10^{-11}$ cm^3 molecule^{-1} sec^{-1}. [d] Mixture of isomers.

(6) R. J. Cvetanović and R. S. Irwin, J. Chem. Phys., 46, 1694 (1967).

(7) For example, see J. E. Breen and G. P. Glass, ibid., 52, 1082 (1970).

(8) R. J. Cventanović, Advan. Photochem., 1, 115 (1963).

(9) E. E. Daby, H. Niki, and B. Weinstock, J. Phys. Chem., 75, 1601 (1971).

SCIENTIFIC RESEARCH STAFF   E. D. MORRIS, JR.*
FORD MOTOR COMPANY   H. NIKI
DEARBORN, MICHIGAN 48121

Chemical Lasers Produced from O(1D) Atom Reactions. II. A New Hydrogen Fluoride Elimination Laser from the O(1D) + CH_nF_{4-n} (n = 1, 2, and 3) Reactions[1]

Sir: Chemical HF elimination lasers produced from chemically activated CF_3CH_3[2a] and CH_3NF_2[2b] have been discovered recently by Pimentel and coworkers. The vibrationally excited molecules are believed to be principally formed by radical–radical recombination reactions.[3] In this communication, we wish to report a new type of HF elimination laser produced from the decomposition of chemically activated α-fluorinated alcohols, mainly methanols. The vibrationally excited methanol molecule was generated by insertion of an O(1D) atom into a carbon–hydrogen bond of a fluoromethane molecule in a manner similar to the insertion of a $CH_2(^1A_1)$ radical into a C–H bond.[4]

The apparatus employed in this work is essentially the same as that used in our recent study of the O(1D) + C_3O_2 ($^1\Sigma_g^+$) reaction, in which some 40 vibration–rotation transitions in CO laser emission were observed.[5] The concentrations of O_3 to fluoromethanes were adjusted such that the relative probabilities of O(1D) attack on C–H bonds were statistically equal in the three cases. Thus, the mixtures of the following compositions were used: $O_3:CH_nF_{4-n}:He = 1:3:10$, $1:1.5:10$, and $1:1:10$ for $n = 1$, 2, and 3, respectively. Inert gases such as He and Ar were found to be helpful in enhancing the lasing, as was found in the case of the O(1D) + C_3O_2 reaction. This effect is believed to be attributed to the lowering of rotational temperature.[2a,5]

The total emission traces obtained from flashing 30-Torr mixtures of the three fluoromethanes are shown in Figure 1. In all cases, a constant flash energy of 1.5 kJ was employed. No significant increase in laser output was observed when a higher energy was used. A decrease in flash energy to 0.6 kJ, however, pronouncedly reduced the laser intensity and delayed the appearance time to as long as 10 μsec. Among these three systems, CH_2F_2 was found to have the highest output and CHF_3 the lowest. The observed vibration–rotation transitions and their appearance times (in μsec) are listed in Table I. The transitions observed in the CHF_3 and CH_2F_2 systems are similar; both $\Delta v = 2 \rightarrow 1$ and $1 \rightarrow 0$ are present. However, only $1 \rightarrow 0$ transitions were detected in the CH_3F flashes. In all cases, no transitions higher than $2 \rightarrow 1$ were observed. The appearance times given in Table I indicate that in both CHF_3 and CH_2F_2 systems, the $2 \rightarrow 1$ transitions have higher gain than $1 \rightarrow 0$, similar to the F + RH reactions.[6] In the case of CH_3F, however, only the $1 \rightarrow 0$ transition has high enough gain to overcome the threshold. There is a qualitative correlation

Table I: Observed HF Vibration–Rotation Transitions and Their Appearance Times in the CHF_3, CH_2F_2 and CH_3F Systems[a]

Transitions	ν, cm⁻¹	CHF₃	CH₂F₂	CH₃F
$\Delta v = 2 \rightarrow 1$				
P(4)	3622.58[b]	3.0[c]	2.8	
P(5)	3577.52	3.3	3.2	
P(6)	3531.20	5.3	3.2	
$\Delta v = 1 \rightarrow 0$				
P(6)	3693.64	5.2		4.4
P(7)	3644.24	5.4	6.4	4.8
P(8)	3593.89	6.7	6.4	4.8
P(9)	3542.21	7.4	6.8	5.2
P(10)	3489.67		8.0	6.6

[a] Flash energy = 1.5 kJ, P_{total} = 30 Torr, and $O_3:CH_nF_{4-n}:He = 1:3:10$, $1:1.5:10$, and $1:1:10$ for n = 1, 2, and 3, respectively. [b] These values are those reported by D. E. Mann, *et al.*, *J. Chem. Phys.*, **34**, 420 (1961). In the present study, the laser transitions were identified with a 50-cm Model 305 SMP03 monochromator, using 250-μ slits, which provided a resolution of about ±0.5 cm⁻¹ in the spectral region of interest. More details of the detecting system can be found in ref 10. [c] Appearance time of the individual laser pulse in μsec.

between the observed transitions and the exothermicities of these reactions, as will be discussed later.

O_3 was found to be essential to the laser action. No laser oscillation was detected when the three fluoromethane–helium mixtures were flashed in the absence of O_3 under the same conditions; nor was laser emission observed when NO_2 was used instead of O_3. NO_2 was also found to be a less efficient O(1D) atom source than O_3 for the O(1D) + C_3O_2 reaction.[7] Mass spectrometric analyses of the flashed samples indicate the presence of F_2CO, $HFCO$, and H_2CO in the CHF_3, CH_2F_2, and CH_3F systems, respectively. Large amounts of CO and CO_2 were also detected in the last two systems. The following reactions are proposed to account for our present observations

(1) This work is partially supported by the Advanced Research Projects Agency under ARPA Order 660.

(2) (a) M. J. Berry and G. C. Pimentel, *J. Chem. Phys.*, **49**, 5190 (1968); (b) T. D. Padrick and G. C. Pimentel, *ibid.*, **54**, 720 (1971).

(3) M. C. Lin, unpublished work. On the basis of the results recently obtained by Ross and Shaw (*J. Phys. Chem.*, **75**, 1170 (1971)) and by Bumgardner, *et al.* (*Chem. Commun.*, 1079 (1968)), we have calculated the rate constant ratio for $CH_3 + N_2F_4$ and $CH_3 + NF_2$ to be 1.0 × 10^{-2}, at 300°K, with the aid of the RRKM theory. In the same calculations, we also found the critical energy for the elimination of HF from CH_3NF_2 to be 38.0 kcal/mol, which agrees exactly with the value arrived at by employing the RRK theory, assuming S = 9 (see Ross and Shaw). Since the maximum amount of energy the CH_3NF_2 molecule can attain in the $CH_3 + N_2F_4$ reaction is only 40 kcal/mol, the *maximum* rate of decomposition of CH_3NF_2† produced from $CH_3 + N_2F_4$ is about 10^{-2} times as fast as that of CH_3NF_2† produced from $CH_3 + NF_2$. Both factors would make the $CH_3 + N_2F_4$ reaction a less likely laser-pumping reaction.

(4) See, for example, G. Paraskevopoulos and R. J. Cvetanović, *J. Chem. Phys.*, **52**, 5821 (1970).

(5) M. C. Lin and L. E. Brus, *ibid.*, **54**, 5423 (1971), referred to as part I.

(6) W. H. Green and M. C. Lin, *ibid.*, **54**, 3222 (1971).

(7) M. C. Lin and L. E. Brus, unpublished work.

$$O_3 \xrightarrow{h\nu} O(^1D) + O_2(^1\Delta)$$

$$O(^1D) + CHF_3 \longrightarrow CF_3OH^\dagger \longrightarrow HF^\dagger + F_2CO$$
$$(\Delta H_1^\circ = -155 \text{ kcal/mol}) \quad (1)$$

$$O(^1D) + CH_2F_2 \longrightarrow CHF_2OH^\dagger \longrightarrow HF^\dagger + HFCO$$
$$(\Delta H_2^\circ \cong -148 \text{ kcal/mol}) \quad (2)$$

$$O(^1D) + CH_3F \longrightarrow CH_2FOH^\dagger \longrightarrow HF^\dagger + H_2CO$$
$$(\Delta H_3^\circ = -143 \text{ kcal/mol}) \quad (3)$$
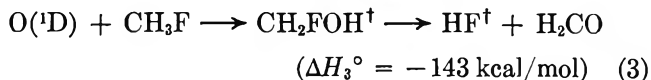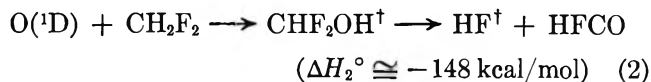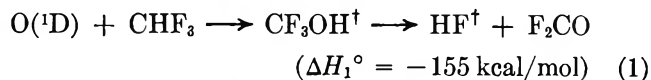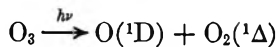
The heats of formation of various species are taken from either Benson's book[8] or from the JANAF tables.[9] The heats of formation of these methanols, however, are not known.

The vibrationally excited methanols formed in the above reactions possess about 130 kcal/mol of excess internal energies. This can be envisaged from the analogous reaction

$$O(^1D) + CH_4 \longrightarrow CH_3OH^\dagger \quad (\Delta H_4^\circ = -135 \text{ kcal/mol})$$
$$(4)$$
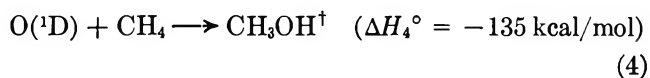
Thus, the newly born excited fluoromethanol molecule has at least 100 kcal/mol of excess energy above the critical barrier for the four-centered elimination reaction, which is probably much less than 30 kcal/mol because of the instability of the α-fluorinated alcohols. The lifetime of the excited methanol is expected to be of the order of 10^{-11} sec. In view of this high excess energy and short lifetime, the deactivation of excited molecules cannot occur within the period of laser oscillation under our present conditions. The early appearance of laser pulses, in comparison with that of the F-atom abstraction laser produced in the flash photolysis of N_2F_4–RH mixtures,[10] also indicates that the $O(^1D)$ insertion–elimination reaction is very fast; it is probably much faster than the insertion of $CH_2(^1A_1)$ into a C–H bond, which is known to have a rate constant of about $1 \times 10^{12} \text{ cm}^3/\text{mol sec.}$[11] An attempt to make an HF elimination laser from the $CH_2(^1A_1)$ + CH_nF_{4-n} reactions failed. Both CH_2N_2 and CH_2CO were used as the CH_2 radical source in these experiments.[12] CO_2 laser emission was not detected when either CH_2N_2 or CH_2CO was flash-photolyzed in the presence of CO_2 and He. A similar attempt to use $C_2O(^1\Delta)$ instead of $CH_2(^1A_1)$ by flashing the mixture of C_3O_2 and CHF_3 with He as a diluent also failed to produce laser oscillation.[12]

Our present results given in Table I also allow us to estimate the initial relative population, N_v/N_{v-1}, for the transition that has the highest gain. Assuming HF deactivation is negligible and that the rotational-translational temperature is about $300°K$, the observation that $P_{21}(4)$ reaches threshold first (see Table I), in both CHF_3 and CH_2F_2 systems, implies that $N_2/N_1 \approx 0.8 \pm 0.2$, according to our gain calculations. Similarly, for the HF molecule produced in reaction 3, a value of $N_1/N_0 \approx 0.35 \pm 0.1$ can be deduced.
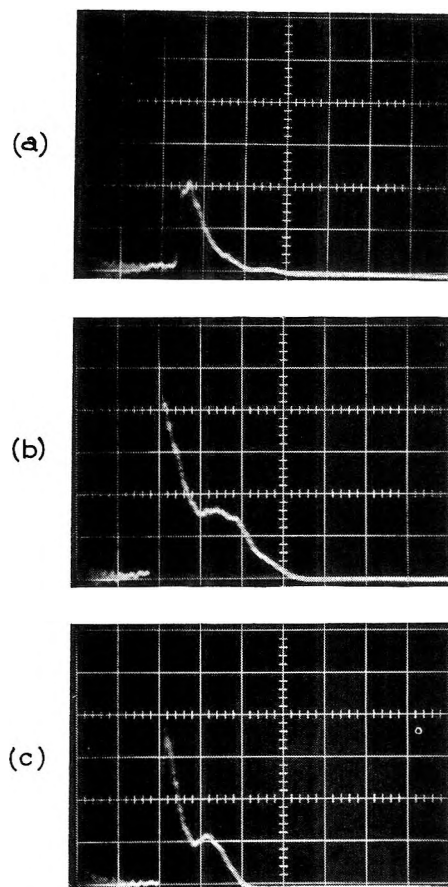
Figure 1. The total emission traces. Ordinate: emission intensity (0.5 V/division); abscissa: time (2 μsec/division): a, CHF_3 mixture ($O_3:CHF_3:He = 1:3:10$); b, CH_2F_2 mixture ($O_3:CH_2F_2:He = 1:1.5:10$); and c, CH_3F mixture ($O_3:CH_3F:He = 1:1:10$). In all cases, flash energy = 1.5 kJ and $P_{total} = 30$ Torr.

Recently, Clough, Polanyi, and Taguchi[13] measured the relative populations of HF produced in the following reactions

$$CH_3 + CF_3 \longrightarrow CH_3CF_3^\dagger \longrightarrow HF^\dagger + CH_2CF_2$$
$$(\Delta H_5^\circ \approx -69 \text{ kcal/mol}) \quad (5)$$

$$Hg^*(^3P) + CH_2CF_2 \longrightarrow Hg + CH_2CF_2^\dagger \longrightarrow Hg + HF^\dagger + CHCF \quad (\Delta H_6^\circ \approx -64 \text{ kcal/mol}) \quad (6)$$
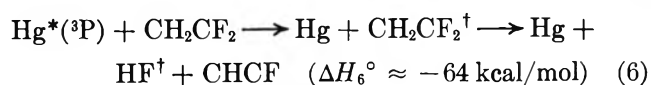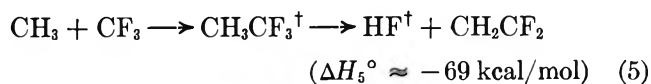
N_2/N_1 ratios were determined to be 0.39 and 0.36 for reactions 5 and 6, respectively. These values are about a factor of 2 lower than our estimate of $\sim 0.8 \pm 0.2$ for

(8) S. W. Benson, "Thermochemical Kinetics," Wiley, New York, N. Y., 1968.

(9) D. R. Stull, Ed., "JANAF Thermochemical Tables," The Dow Chemical Co., Midland, Mich., 1960.

(10) L. E. Brus and M. C. Lin, J. Phys. Chem., 75, 2546 (1971).

(11) W. Braun, A. M. Bass, and M. Pilling, J. Chem. Phys., 52, 5131 (1970).

(12) These experiments were carried out with the cooperation of Dr. L. E. Brus.

(13) P. N. Clough, J. C. Polanyi, and R. T. Taguchi, Can. J. Chem., 48, 2919 (1970).

reactions 1 and 2. It is to be noted that the exothermicities of reactions 5 and 6 are also about half as much as those of reactions 1 and 2. In contrast to reaction 5, in which the $1 \rightarrow 0$ transition has the highest gain,[2a,13] we observed a higher gain for $2 \rightarrow 1$ than for $1 \rightarrow 0$ in both reactions 1 and 2.

Our estimated value of $N_1/N_0 \approx 0.35 \pm 0.1$ for reaction 3 compares closely with the ratio $N_1/N_0 = 0.35 \pm 0.02$ determined by Padrick and Pimentel[2b] for HF produced from the $CH_3NF_2^\dagger$ elimination reaction. If our conclusion[3] is correct, then the exothermicity of the reaction,

$$CH_3 + NF_2 \longrightarrow CH_3NF_2^\dagger \longrightarrow 2HF^\dagger + HCN$$
$$(\Delta H_7{}^\circ = -141 \text{ kcal/mol}) \quad (7)$$
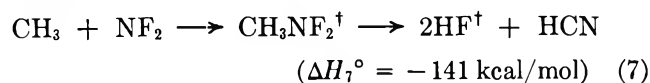
is comparable to $\Delta H_3{}^\circ$. The main difference between the two reactions is that reaction 7 produces two HF molecules, probably in a consecutive manner.

Another interesting aspect of our present results is the observation of both CO and CO_2 in the flashed mixtures of $O_3 + CH_2F_2$ and $O_3 + CH_3F$. They were, however, absent in the flashed $O_3 + CHF_3$ samples. CO may be formed by the decomposition of vibrationally excited formaldehydes, which possess large fractions of exothermicity in reactions 2 and 3 because of their greater numbers of degrees of freedom.[2b,13,14]

$$HFCO \longrightarrow HF + CO \quad (\Delta H_{8a}{}^\circ \approx 0 \text{ kcal/mol}) \quad (8a)$$
$$\longrightarrow H + FCO \quad (\Delta H_{8b}{}^\circ \approx 87 \text{ kcal/mol}) \quad (8b)$$
$$H_2CO \longrightarrow H_2 + CO \quad (\Delta H_{9a}{}^\circ = 1.3 \text{ kcal/mol}) \quad (9a)$$
$$\longrightarrow H + HCO \quad (\Delta H_{9b}{}^\circ = 87 \text{ kcal/mol}) \quad (9b)$$
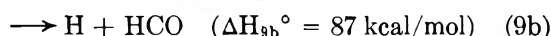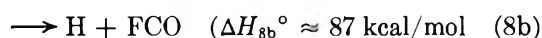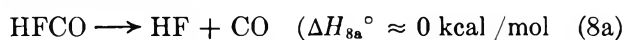
Both FCO and HCO may undergo further decomposition into CO. Other possibilities such as a radical-induced decomposition cannot be ruled out, however. CO_2 is probably formed by the secondary reactions such

as $O + CO + M \rightarrow CO_2 + M$ and $O_2{}^\dagger(^1\Delta) + CO \rightarrow CO_2 + O$. No CO or CO_2 laser emission was detected in these systems. The fact that no significant amount of CO or CO_2 appeared in the flashed $O_3 + CHF_3$ sample is consistent with the extraordinarily high stability of F_2CO; the first C–F bond dissociation energy of F_2CO is known to be as high as ~ 137 kcal/mol.[15]

The elimination reaction (8a) has been shown to take place rather readily at low temperatures;[16] its occurrence may account for the comparatively stronger laser output observed in the CH_2F_2 system (Figure 1). It would be worthwhile to flash-photolyze the HFCO molecule in the vacuum-uv region to further substantiate this conclusion.

We are currently extending the investigation of $O(^1D)$ atom reactions in the following ways: (1) further study of hydrogen halide elimination reactions of many other vibrationally excited α and β halogenated alcohols, including the simultaneous, competitive elimination of different hydrogen halide molecules from an excited molecule; (2) detailed study of both pressure and temperature effects by employing the "equal-gain technique"[2] to determine the exact population ratios; and (3) construction of a low-pressure, fast-flow setup to study the ir chemiluminescence of various ir-active products formed in the $O(^1D)$ atom reactions.

(14) H. W. Chang, D. W. Setser, and M. J. Perona, *J. Phys. Chem.*, 75, 2070 (1971).

(15) The value $D(FCO-F) \simeq 137$ kcal/mol was arrived at by taking $\Delta H_b{}^\circ(FCO) \simeq -34 \pm 5$ kcal/mol reported by H. Henrici, M. C. Lin, and S. H. Bauer, *J. Chem. Phys.*, 52, 5834 (1970).

(16) G. Fisher and A. S. Buchanan, *Trans. Faraday Soc.*, 60, 378 (1964).

PHYSICAL CHEMISTRY BRANCH   M. C. LIN
NAVAL RESEARCH LABORATORY
WASHINGTON, D. C. 20390

Journal of Chemical and Engineering Data

OCTOBER 1971, Vol. 16, No. 4

TABLE OF CONTENTS